Component Development to Accelerate Commercial Implementation of Ultra-Low Emissions Catalytic Combustion

Final Report

For Period October 1, 2000 – September 29, 2002

by
Jon McCarty
Brian Berry
Kare Lundberg
Orris Anson

Catalytica Energy Systems, Inc.
430 Ferguson Drive
Mountain View, CA, 94043

March 31, 2003

Prepared for

U.S. Department of Energy
Contract No. DE-SC02-00CH11052

Legal Notice

Table of Contents

List of Figures

List of Tables

Abstract

Catalytica Energy Systems, Inc. (formerly known as Catalytica Combustion Systems, Inc.) is commercializing catalytic combustion technology for gas turbines to achieve nitrogen oxides (NOx) concentrations in the turbine exhaust of 2.5 ppm or lower. This technology, incorporated in the Xonon Combustion System, is operating in a 1.5 MW industrial gas turbine engine connected to the electric power grid at Silicon Valley Power in Santa Clara, California. Achieving NOx emissions at these levels in the combustion system (rather than through cleanup of the exhaust gas), without compromising gas turbine performance, will reduce the cost and potential environmental impact of ultra-low emissions in gas turbine installations and make ultra-low emissions performance available in more gas turbine applications.

In view of the value of catalytic combustion in gas turbines, the current DOE-sponsored program is directed at overcoming the remaining risks and barriers that inhibit widespread commercial adoption of catalytic combustion technology. These barriers lie in the technical challenge of adapting catalytic combustion technology to gas turbines having different cycles and/or operating requirements. Of course, reducing the cost of the technology also can accelerate its market acceptance. Catalytica is engaged in an effort to develop an expanded technology base for catalytic combustion to facilitate its application in the engines of a broad set of manufacturers and applications, and to reduce its cost. The broad range of work completed under the current program constitutes a part of this larger effort. The program addressed and successfully exploited opportunities in three categories to facilitate market acceptance of catalytic combustion: 1) cost reduction, 2) broadened operating range and 3) extension to backup diesel fuel.

To reduce the cost of catalytic combustion applied to gas turbines, significant progress was made to extend catalyst life from the current 8,000 hours to 12,000 hours. This has a direct bearing on life-cycle costs and provides a catalytic module component with a life span that supports current gas turbine industry trends toward longer inspection intervals. Under this task, new hot stage catalysts (palladium-based PI-PS catalysts) were developed and tested and found to have the potential to increase catalyst life two-fold. These materials have been adopted for commercial use. Other promising non platinum group metal (and lower cost) catalyst materials with the potential to extend life to 24,000-hr also were identified, characterized, and successfully tested in this effort. These materials were not chosen for commercial implementation because their long-term durability has not been fully established, because their use would require significant hardware modifications, and because the easily implemented PI-PS catalyst was successfully developed. A second task to reduce lifecycle cost was the successful design and evaluation of a lower cost catalyst container. This container provides mechanical support and peripheral sealing for the catalyst in the commercial application.

To enhance its potential penetration of the gas turbine market, a new technology must be adaptable to a wide range of operating environments, both in terms of ambient conditions and in terms of the degree to which the turbine must follow load variations. For a catalytic combustor, one way to accommodate such variations in the operating environment is via a preburner that can adjust the gas temperature entering the catalyst. Existing preburners typically have two shortcomings in this context: they produce undesirably high levels of NOx and they operate over a relatively narrow range of fuel-air ratios. A solution to this problem is the use of a catalyst in the preburner. The technical operability of a catalytic preburner was successfully tested in sub-

scale rigs using current catalyst materials. The design and operation of a catalytic preburner for the KHI M1A-13X turbine was evaluated in this effort. The catalytic preburner provides a wider range of operation than homogenous burners and emits essentially no NOx. Instabilities typical of lean burners are minimized because the catalyst operates over a wide range of fuel/air ratios.

A primary factor that generally limits the operation of a lean-premix burner on the fuel-lean side of its operating window is the tendency of the flame to blow out as the fuel-air ratio approaches the lower limit. A catalytic "pilot" for stabilizing lean-premix burners has been designed, fabricated, and tested and tested at full-scale to successfully demonstrate this concept.

Some fraction of the industrial gas turbine market requires the ability to use a backup fuel stored on-site. The traditional and most available backup fuel is diesel oil. A series of engineering economic analyses were conducted to evaluate the investment costs of upstream fuel processing to convert diesel fuel into compatible gaseous turbine fuel. However, costs remained above a target deemed economically viable. An innovative hydrothermal fuel processing reaction with potential for significant cost reduction was then investigated and found technically feasible.

This program included cooperative efforts with Solar Turbines, Inc. of San Diego, the Combustion Laboratory of the University of California at Irvine, and SRI International of Menlo Park.

I. Executive Summary

1.1 Proposed Approach to Program Objectives

The stated intent of the DOE solicitation is to advance the state of development of "durable, cost-effective, low-emission technologies for integration into Advanced Industrial Gas Turbine Systems without sacrificing efficiency." Catalytica Energy Systems, Inc (formerly known as Catalytic Combustion Systems, Inc. and shortened to "CESI" hereinafter) has completed a co-funded program with the DOE to continue development of technologies with all of those desirable characteristics. CESI's "Xonon" technology uses catalytic combustion to achieve nitrogen oxides (NOx) concentrations below 2.5 parts per million (ppmv) in the turbine exhaust. To reach similar levels, other combustion technologies require add-on units such as selective catalytic reduction (SCR) or SCONOX to chemically treat the exhaust stream to remove the NOx produced in the combustor. The CESI technology has been under development for more than a decade with the active participation of several gas turbine manufacturers, including General Electric Company, Solar Turbines, Rolls Royce Allison Engine Company, and Pratt & Whitney Canada. In an ongoing demonstration, a Xonon unit on a 1.5 MW gas turbine has recently passed the 8,000-hour mark in power generation service connected to the electrical grid, with emissions levels well below the targeted values of 2.5 ppmv NOx, 10 ppmv carbon monoxide (CO), and 10 ppmv unburned hydrocarbons (UHC).

Achieving NOx emissions at these levels in the combustion system (rather than through cleanup of the exhaust gas), without compromising gas turbine performance, reduces the cost and potential environmental impact of ultra-low emissions in gas turbine installations and makes ultra-low emissions performance available in more gas turbine applications.

In addition to its ultra-low emissions profile, another demonstrated advantage of CESI's approach over many lean-premix systems is the absence of noise and potentially damaging vibrations that occur when a lean-premix flame is operated near its stability limit. The catalytic combustor also has a very uniform temperature profile at the combustor exit, reducing the potential for "hot spots" that can cause thermal fatigue of the downstream components, vanes and turbine blades.

There are economic advantages of the new technology as well. Capital and operating costs are attractive relative to the alternative of installing a cleanup unit for the exhaust, especially for small gas turbines. The ultra-low NOx production in CESI's technology can reduce emissions offset requirements, generate Emission Reduction Credits, and shorten the permit timetable for a gas turbine project. Barriers to the widespread adoption of catalytic combustion for gas turbines lie in the technical challenge of adapting the technology to gas turbines having different cycles and/or operating requirements. In particular, overlapping, parallel efforts with several engine manufacturers to expand the engine cycle and operating range of the technology, though oriented to each manufacturer's specific requirements, may increase the total cost and time to market for the technology. Also, reducing the total cost of the technology can accelerate its acceptance.
In light of these barriers, CESI has, in this DOE co funded program, completed an effort developing an expanded technology base for catalytic combustion to facilitate its application in the engines of a broad set of manufacturers and applications, and to reduce its cost. The program proposed in this application constitutes a part of this larger effort. The Gas Research Institute

(GRI) and the California Energy Commission (CEC) has contributed to engine field testing of this technology and to some earlier work in components development.

1.2 Problems and Solutions

In view of the attractive features of catalytic combustion in addressing the DOE goals, this co-funded program is a major step in overcoming remaining risks and barriers that inhibit widespread commercial adoption of the CESI technology. The opportunities for facilitating market acceptance are placed in three categories:

1. Cost reduction
2. Broadened operating range
3. Extension to backup diesel fuel

A summary of the results of accomplishment in each of the three areas is described below.

1.2.1 Cost Reduction

The choice of low-emissions technology for any particular gas turbine installation will ultimately be governed by the total cost of the technology over the life of the project. Two aspects of the overall cost of Xonon were addressed in this program: (1) catalyst replacement cost and (2) module cost. The former cost is directly related to the length of time the catalyst can remain in service before it must be replaced. The latter is dependent in large part upon the manufacturing cost of the catalyst container. The program accomplishments for both aspects are as follows:

- Task 1.1 – Catalyst life extension
  The initial work in this task was focused on validating the mathematical models developed at CESI to predict catalyst performance and any changes expected to occur with operating time. This mathematical model is used in the design of catalyst systems for specific gas turbines, for prediction of performance and for prediction catalyst life under specific gas turbine operating conditions. At the same time, investigations began with the objective of generating new materials with improved long-term performance. Promising new formulations were converted into prototype catalyst systems for validation testing using CESI's extensive facilities for evaluating both catalytic and physical properties of materials.

- Task 1.2 – Module Cost Reduction
  Mechanical systems for providing axial support for Xonon catalysts in their container represent a significant fraction of the overall cost of the catalyst module. As part of this task, the impact of various lower-cost support designs at the contact points with the catalyst were studied analytically and experimentally. The selected design was incorporated into computer models of the complete container and added to the commercial container. The computer model was subjected to finite element analysis to predict its functional characteristics under turbine operating conditions. The outcome is a lower-cost container with all the necessary performance attributes for gas turbine combustor service. This design is applicable to any OEM Xonon system design.

1.2.2 Broadened Operating Range

To enhance its potential penetration of the gas turbine market, a new technology must be adaptable to a wide range of operating environments, both in terms of ambient conditions and in terms of the degree to which the turbine must follow load variations. For a catalytic combustor, one way to accommodate such variations in the operating environment is via a preburner that can adjust the gas temperature entering the catalyst. Existing preburner designs typically have two shortcomings in this context: they produce undesirably high levels of NOx and/or they only operate over a relatively narrow range of fuel-air ratios. Thus the limited range of preburner performance represents a limitation on widespread adoption of catalytic combustion in certain user situations. A remedy for this barrier is the catalytic secondary burner. A summary of the accomplishment for this task is:

- Task 2.1 – Catalytic Secondary Burner
  The approach in this task was to develop an appropriate catalyst to extend the preburner operating range by improving the combustion efficiency in the secondary stage of the burner. This system allows the preburner to deliver a larger temperature rise without generating the higher NOx levels that would normally accompany an increase in preburner temperature. The system design was incorporated into the existing KHI M1A-13X Xonon combustor with the goal of minimum change to existing hardware. Although the plan was to fabricate test hardware for system validation testing, more work was required than initially thought to complete the design. An extensive amount of CFD was required to define the flow path and fuel injection design.

  The preliminary design was completed and is ready for fabrication of test hardware for a follow-on program. A reasonable amount of structural analysis was accomplished to assure that the design was rig-test ready and did not have any analytically predictable structural issues. Final system performance analysis indicated the design to be ready for rig testing and optimization.

Although lean premix low emission combustion systems are currently installed and in operation of a large number of gas turbines, their stable operating range limits the engines operating range with respect to emissions regulation compliance. A catalytic pilot to replace the conventional pilot was the focus of this program task. A summary of the accomplishment for this task is:

- Task 2.2 – Catalytic Pilot for Lean Premix Burner
  The factor that generally limits the operation of a lean-premix burner on the fuel-lean side of its operating window is the tendency of the flame to blow out as the fuel-air ratio approaches the lower limit. The design for extending the operating range in this situation is to introduce a catalytic "pilot" unit into the lean-premix burner. It has been well established that a diffusion pilot can widen the operating range of a lean premix burner. If a catalytic pilot, with substantially reduce NOx can similarly widen the operating range, another preburner technology would be demonstrated. The design accomplished a stable flame, reduction in NOx and a low acoustic signature. The design was successfully tested (with support from other programs) in the atmospheric rig at UCI and in the Solar Turbines full pressure combustion rig with a Taurus 60 fuel injector at Taurus 60 operating conditions.

1.2.3 Extension to Back-up Diesel Fuel

In certain situations, gas turbine users occasionally need to operate on economical diesel fuel rather than the natural gas used for normal operations. Liquid fuels (except propane or liquid petroleum gas) are not workable back-up fuel for a Xonon catalyst system. Task 3 was included in the current program to explore the feasibility of converting back-up diesel fuel on-site into a gaseous fuel suitable use in a Xonon-equipped gas turbine and thereby address this market demand.

Preliminary economic analysis of investment costs for on-stream processing diesel to combustion gases using modifications of commercial processes were significantly above an economically viable target ($250/kW vs. $40/kW). As a result, further in-house and contracted engineering economic evaluations focused on the potential for greatly reduced capital investment costs in the processing of diesel into substitute natural gas. A summary of the accomplishment for this economic evaluation subtask is:

- Task 3.1 – Diesel to Gas Process Economic Evaluation
  The in-house effort to analyze capital costs for a base-case diesel fuel conversion process was launched at the end of November 2001. Process specifications were defined and the preliminary equipment sizing and cost estimates were concluded in January 2002. The baseline direct fixed costs (DFC) at a 40-MW scale were determined to be $110/kW and again well above target values, but significantly below the vendor's estimates. Several modifications were made to reduce investment costs and an optimized case showed reduced DFC at $79/kW. In work contracted to Aurora Engineering in March 2002, further reductions in temperature and pressure were presumed feasible for short-term SNG processing and the best case DFC was reduced to $60/kW ($63/kW with product gas polishing to SNG).

Because these capital cost estimates were well above target levels, alternative processing concepts with the potential to greatly reduced fuel conversion investment costs were initiated in April 2002. Adiabatic catalytic hydrothermal processing was examined as a promising process approach because a large air compressor would not be required, heat exchange sizes would be significantly reduced, and reactor temperatures would be lowered (although at significantly increased pressure). From May through July 2002, SRI International conducted preliminary high-pressure hydrothermal reaction tests with dodecane/water mixtures over a variety conditions using catalyst and materials supplied by CESI. A summary of the accomplishments for this feasibility subtask follows:

- Task 3.2 – Hydrothermal Diesel to Gas Process Evaluation
  Results of the subcontracted diesel gasification process development work to improve economics of high-pressure steam cracking were promising. The process concept is thermal and catalytic reaction of diesel fuel components with super- or near-critical water into a mixture of methane and carbon dioxide. Three catalysts representing a variety of materials were prepared at CESI and tested in pressurized autoclave reactors by SRI International. Two catalysts showed high conversion of liquid to gaseous fuel with

reasonable processing conditions. Very rough cost estimates showed direct fixed costs between $45 to $55/kW.

1.3 Key Accomplishments

Key project findings and major accomplishments are highlighted as follows:

- Task 1.1 – A new preconditioned (PI-PS) catalyst was developed under the current program and subsequently qualified and adapted for use in second (hot) stage catalyst foil packs of CESI's commercial combustion models. A prototype combustion module using this catalyst material has been installed in the KHI M1A-13X combustion module at Silicon Valley Power, Santa Clara, CA in preparation for an 8000-hr demonstration run;
- Task 1.1 – CESI's catalyst performance and life models were significantly extended by new measurements of mass (and heat) transfer correlations foil pack friction factor correlations, specific combustion kinetic rates for both oxide and metal active-phase catalysts, and sintering rates for the preconditioned catalysts. The updated models are now in use for catalyst design and the evaluation of engine test data over extended operating periods;
- Task 1.2 – A more durable, lower cost catalyst retaining structure was successfully designed and tested under the current program and immediately adopted for commercial applications;
- Task 2.1 – A catalytic preburner concept was successfully demonstrated to be feasible, full-scale designs were worked up and prepared for submission as a patent application;
- Task 2.2 – A catalytic pilot concept for stabilizing lean burners was demonstrated as feasible in full-scale testing with a prototype. The design and operability of the catalytic pilot was reported for submission of a patent application;
- Task 1.1 – Two novel candidate catalyst materials were developed and found technically promising for longer-term (24,000-hr) use as the (third) hot stage in a three-stage catalyst system.
- Task 3.2 – Diesel fuel conversion for back-up gaseous fuel was found not economically feasible, but a promising new process approach was identified and found technically feasible.

Recommended work for follow-on development and implementation of the findings not already adopted for commercial use include:

- Fabricate and further test in sub-scale rigs new catalyst designs to utilize the more economical and thermally stable oxide catalyst materials; this work would include long-term thermal stability tests;
- Implement preburner concepts in higher pressure (16-atm) engine design and development;
- Implement and demonstrate capabilities of a catalytic pilot in an annular multi-can lean-burn combustion system on a gas turbine engine;
- Further investigate the technical and economic feasibility of high-pressure catalytic hydrothermal processing of diesel fuel into compatible SNG fuels.

II. Cost Reduction - Task 1.1 – Catalyst Life Extension

2.1 Summary

Two materials development approaches for extending hot stage catalyst life were investigated and candidate materials tested for stability and performance under the DOE program. These approaches were: 1) pre-age supported palladium (pre-coarsened or pre-sintered, PS catalyst materials), and 2) preparation of non-platinum group metal catalyst formulations (NPGM catalyst materials) with lower specific activity but the potential for greater stability. For the first approach (PS catalysts) the current catalyst structure and flow patterns, would be used but the geometric design parameters (e.g., channel size, coating thickness, etc.) would be adjusted to accommodate the lower activity of the pre-aged catalyst materials. For the second approach (NPGM catalysts) a substantial change in the design of the module (e.g., a separate third catalyst stage) would be required to accommodate the significantly lower activity of these candidate materials at temperatures below 800°C. Subscale tests with a pre-aged palladium-based catalyst (PS-8) under the DOE program were successful and CESI anticipates incorporating this material or variations of it depending on manufacturing scale-up into our current (KHI-13X) and future commercial products.

About a dozen NPGM materials were screened for high temperature combustion activity and two base oxides were selected for additional screening. A multiple-catalyst test reactor was successfully developed and utilized for screening NPGM candidate catalyst formulations under realistic combustion conditions at 16-atm. The multi-channel reactor uses optical imaging to determine the catalyst temperature of up to 10 candidate materials in parallel given identical combustion conditions of gas composition, pressure and inlet temperature. A thermal and chemically stable supporting oxide and an oxide promoter were found for a promising NPGM catalytic material but the active phase in one candidate showed rapid grain growth in preliminary accelerated aging tests. Another NPGM material with good high temperature activity appeared to have good thermal stability but showed evidence of reaction with candidate supporting oxides in 4000-hr accelerated aging tests. The further screening and materials development required to bring these two NPGM catalyst formulations to commercial status was judged well beyond the scope of the DOE program.

Experiments were conducted in the CESI high-pressure rig in order to gather data for pressure drop, fuel conversion, and temperature rise through Xonon catalyst modules. Nine different modules were considered and flow conditions were chosen to span a range of Reynolds numbers typical of intended operation. The data were used to develop correlations for friction factor, Colburn factor for mass transfer, and flow splits between catalytic and non-catalytic channels. Individual friction factor correlations were developed for each module and good agreement was attained between predicted and experimental values. Results for mass transfer correlations are in good agreement with those published for Camet® metal monoliths.

Analysis of data for fuel conversion indicates that the flow distribution between catalytic and non-catalytic channels is consistently lower than the corresponding cross-sectional areas. The primary factor for the reduced catalytic channel flow is the reduction of hydraulic diameter by compression of the porous ceramic catalyst coating at crossover contact points with the opposing herringbone (15° off axial) foils. Other factors in flow resistance and heat/mass transfer, such as

coating roughness and channel height to pitch, did not vary sufficiently to discern their influence with the limited range of parameters in this investigation.

A moderate-pressure microreactor test system was fabricated and used to determine specific combustion rates at temperatures and residence times relevant to commercial conditions. Several commercial and developmental catalysts were analyzed for specific methane combustion activity using a microreactor and for exposed PGM (platinum group metal) by hydrogen chemisorption. The results extend CESI's previous low temperature, atmospheric-pressure kinetic measurement results. The measure value of the apparent activation energy for methane combustion on metallic Pd was much greater than expected and the effect of water on activity under 10-atm pressure extended to much higher temperatures than expected. These results both suggest that an aged catalyst approaching end-of-life will show much greater sensitivity to operating conditions (fluctuations) than that the fresh catalysts examined in CESI's test rigs. The kinetic results will be incorporated into our predictive catalyst design tool for thermal aging, the Catalyst Performance and Life Model (CPLM).

2.2 Background and Objectives

2.2.1 Development of Stable Hot Stage Materials – Presintered Palladium-Based Catalysts

Background: Initial tests of second (hot) stage monolith performance were conducted from 1994 to 1999 using the very active catalysts developed for the inlet (cooler) stage. These catalyst monoliths showed excellent stability with fuel conversion limited by mass transport to the catalytic surfaces rather than the kinetics of the combustion reactions by the catalyst materials, and development continued to focus on improving the activity and stability on inlet stage catalysts. By 1999, long-term rig tests and 1000-hr and 4000-hr in-engine tests using these inlet stage materials for the hot stage showed significant loss of activity with the result that hot stage fuel conversion dropped below acceptable limits. Parallel investigation of thermal sintering (or more correctly expressed, thermal coarsening) in pressurized aging furnaces (HPARs) when combined with a kinetics-based model of monolith performance projected that hot stage conversion could not be sustained over the target life of 8000-hr. By combining catalyst aging rates with the performance model, CESI developed a tool, the Catalyst Performance and Life Model (CPLM), to predict performance for design work and to estimate combustion module life. Because the coarsening rate of our PGM-based catalysts slow significantly as the metal crystallites grow larger, and because design changes can be made to accommodate reduced activity catalyst materials, stability of hot stage conversion can be enhanced by using materials with low metal dispersion (fraction of surface to bulk metal atoms in the average sized supported particle). New supporting oxides than those used for inlet stage catalysts also would be needed because those higher surface area oxides show grain growth exceeding a factor of 10 over 4000-hr under outlet hot stage conditions. This degree of support sintering probably enhances PGM coarsening and causes those of mechanical strength of the washcoat to unacceptable levels.

Objectives: The overall objective of this subtask is to develop a commercially accessible Pd-based combustion catalyst with a narrow distribution of relatively large Pd particles to reduce extent of thermal aging under hot stage conditions. Specific objectives of PS catalyst development effort include the following:

.

Assess two approaches for production of pre-sintered catalysts – Determine which of two approaches provides the greatest degree of thermal stability:

1) conventional salt impregnation rapid drying and very high temperature calcination; and

2) physical mixtures of sub-micron supporting oxides and Pd metal powders

Modify washcoat for enhanced mechanical stability – Identify and utilize commercially available low-area, dense, supporting oxides tailored to accommodate low-area palladium and increase washcoat cohesion

Produce and test hot stage PS catalyst in sub-scale test rig – After choosing a production approach with a candidate PS catalyst, design, fabricate, and evaluate the initial performance of the new hot stage.

2.2.2 Development of Stable Hot Stage Materials – Non-Platinum Group Metal Catalysts

Background: Pre-sintered Pd-based catalysts while increasing stability of stage conversion have several serious disadvantages: 1) they generally require more catalyst material (and associated initial costs) for the same stage conversion, 2) for practical amounts of PS catalyst, the performance of the stage is much more strongly influenced by temperature and fuel composition because reaction kinetics and not fuel mass transport have the greater impact on conversion, and 3) since the KHI M1A-13X turbine operates at 9.4-atm, some portion of the hot stage must be present as metallic Pd and not the more active oxide, PdO, leading to decreased activity, faster coarsening kinetics, and phase transition kinetics can lead to instability of the stage (this is something that the XONON IHE technology was specifically designed to avoid and successfully does so with high activity catalysts). Thus the PS catalysts, while allowing valuable life extension of the current implementations of XONON catalysts, are not viewed as the most economical and desirable materials.

A view of the thermochemical stability of gaseous metal oxides, hydroxides, and oxyhydroxides, suggest two non-platinum group metal (NPGM) active phase components that should be investigated for activity and thermochemical stability, ceria and . Two problems immediately apparent:

1) Pure phase components have much lower specific activity than even pre-sintered PdO and Pd; therefore, promoters must be sought to increase specific activity even if relatively higher component loading per unit area of foil substrate is used.

2) Neither of the active phase candidates is a refractory oxide, and thus both would rapidly and continuously sinter under composition conditions; therefore a compatible (non-reactive, dispersing) supporting oxide must be found for each of the two candidate active NPGM components.

This means that the investigation of NPGM necessarily is far more exploratory in nature than the investigation of PS catalysts.

Typically, new catalyst material concepts go through a rigorous screening process that includes preparation of multiple materials with subsequent physical and kinetic characterization to narrow down to a few catalysts for further optimization. These identified catalyst are then prepared in large approximately 100 gram batches for 2-inch metal monolith combustion rig testing. The entire process to perform tests of this magnitude is time consuming, labor intensive, and expensive (due to labor charges). A new and innovative catalyst screening system that

incorporates much of the same screening protocol with much less catalyst preparation amount and catalyst preparation time and testing was sought. The main requirement of this new test system is that multiple catalysts be tested at the same time using simulated turbine conditions in one of the catalyst monolith combustion test rigs. This new screening system was designated the multiple catalysts screening reactor (MCSR).

Objective: The overall objective of this subtask is to determine if a candidate NPGM catalyst formulation can be found with sufficient activity and stability to warrant further development of an ancillary third hot stage. Sub-scale testing would not be performed unless one of both of the candidate active phase material can be dispersed over refractory supporting oxides and promoted for acceptable specific composition activity. Specific objectives of this subtask are:

1) Prepare and evaluate the thermal stability of candidate non-reactive supporting oxides for each active phase candidate material;
2) Prepare and evaluate the thermal stability of sets of catalysts using the two active components;
3) Design, fabricate, and use a multi-channel screening reactor to evaluate activity of candidate NPGM oxide catalysts relative to a Pd-based reference catalyst;
4) Identify and optimize concentration of promoter oxides for each base active-phase material using the MCSR;
5) Use HPAR aging furnaces to evaluate the hydrothermal stability of those formulations with promising activity;
6) Perform a rig test of hot stage performance with one or more candidate formulations with good activity and good thermal stability relative to PS Pd-based catalysts.

These objectives are ambitious and it was recognized that no NPGM catalyst could be developed through sub-scale combustion testing.

2.2.3 Validation of Catalyst Performance Models – Measurement of Flow Distribution and Mass Transfer in Xonon Modules

Background: Xonon catalyst modules are based on metal foils that are corrugated according to detailed specifications. Typically, one side of each foil is spray coated with catalyst and two foils are rolled together (with their coated sides facing each other) to form a module containing an array of catalytic and non-catalytic channels. When the fuel-air mixture enters the module, a fraction enters the catalytic channels with the remainder flowing through the non-catalytic channels. A portion of the fuel in the catalytic channel reacts to form combustion products (depending on the catalyst activity and mass transfer in the channels), while the fuel in the non-catalytic channels passes through the module unreacted. The heat generated by the reaction on the catalyst-coated side of each foil is carried off by the gases flowing in both the catalytic and non-catalytic channels. Such an approach allows catalytic combustion to be conducted at temperatures low enough to prevent the formation of more than trace levels (< 2.5 ppmv) of NOx.

The need for predictable and reliable performance of Xonon catalyst modules translates into a need to possess detailed quantitative knowledge regarding the flow and transport characteristics in these devices. The development of detailed correlations of flow and transport properties could be beneficial for 1) optimizing the performance of existing Xonon modules, 2) aiding the development of detailed computer simulations of our catalytic combustion systems, and 3)

designing Xonon modules with specific performance objectives. For instance, semi-empirical equations for pressure drop, Colburn factors for heat and mass transfer, and flow splits between catalytic and non-catalytic channels could suggest a set of optimal operating conditions. In practice, estimates of pressure drop can be useful for determining compressor requirements, while values of heat and mass transfer coefficients can lead to estimates of peak wall temperatures and catalyst stability. An understanding of flow splits is crucial for predicting fuel conversion and temperature profiles because one would expect the flow distribution between catalytic and non-catalytic channels to depend on corrugation specifications and washcoat properties, such as thickness and roughness.

Objective: The specific objective of this work is to generate experimental data for nine different Xonon modules and develop correlations to predict friction factor, mass transfer behavior, and flow splits over a wider range of Reynolds numbers than had been previously investigated.

2.2.4 Validation of Catalyst Performance Models – Measurement of Specific Combustion Rates of Xonon Catalyst Materials

Background: The essential component of a catalyst module is, of course, the catalytic material and its performance is limited by the ability of this material to sustain minimum activity for fuel combustion over the guaranteed life of the module. The hydrothermal conditions to which the catalyst materials are exposed under combustion are unusually severe – 1- to 2-atm steam and oxygen partial pressure at temperatures approaching 1000°C for periods up to 8000-hr. No catalyst can sustain high activity under these conditions for such long periods. CESI addresses this problem in several ways, 1) using proprietary technology to limit temperature of the catalyst at the inlet and middle regions of catalyst structure; 2) over-designing the catalyst so that fuel conversion within structure does not depend on catalyst activity to the greatest extent possible; and 3) developing a predictive model (the CPLM) of thermal aging and the influence of catalyst aging on fuel conversion for use in the design of commercial modules. Thermal aging rates for the coarsening of supported Pd and PGM catalysts have been measured extensively by CESI over the past several years in quasi-static pressurized reactors but the direct measurement of catalytic activity under relevant conditions had not been performed prior to the DOE Program. Knowing these rates is not essential for the fresh (over-designed) catalysts but it is important for determining the wall temperature profile along the foil over time and for predicting performance when the aged catalyst approaches end of life.

Objective*:* Measure specific combustion rates for supported metallic Pd and supported oxidized PGM catalysts with methane fuel as functions of temperature, water vapor pressure, and total pressure. Derive kinetic expressions from the data and incorporate those expressions into the CPLM.

2.3 Experimental Methods

2.3.1 Development of Stable Hot Stage Materials – Presintered Palladium-Based Catalysts

Preparation of pre-sintered catalyst materials.

Selection and characterization of thermally stable refractory oxide supporting materials – Only refractory low-area zirconia supports were considered for PS catalyst development. Three moderate to low area zirconia powders produced by Daiichi Kigenso Kagaku Kogyo Co., Ltd.

(DKK) were evaluated for desired pore volume distribution and hydrothermal stability. Pore volume distribution of fresh (as received) and treated powders were measured from ~10- to >10,000-nm using a Micromeritics 9220 Autopore Mercury Porosimeter instrument. BET (N_2) total surface area properties of the powders were also measured using a Micromeritics 2010 ASAP instrument. The candidate powders (listed in Table 2-1) were treated by 10-hr calcination in ambient air and by steaming in ~8-atm H_2O with ~2-vol% O_2 for 20-hr. The steam treatment aggressively simulates hydrothermal stability under combustion conditions since the latter has lower catalyst temperature (>50°C) and lower steam concentration (X3). Although steam treatment did not significantly change the meso- and macro-pore cumulative volumes (10- to 3,000-nm), the total surface area of the DK-1 decreased significantly from 29- to 8.4-m2/gm with a significant increase in mean pore size (Fig. 2-1). The low area DK-2 powder showed much less change for the same treatment and given its desirable pore distribution, DK-2 was chosen as the supporting oxide for the development of PS catalysts.

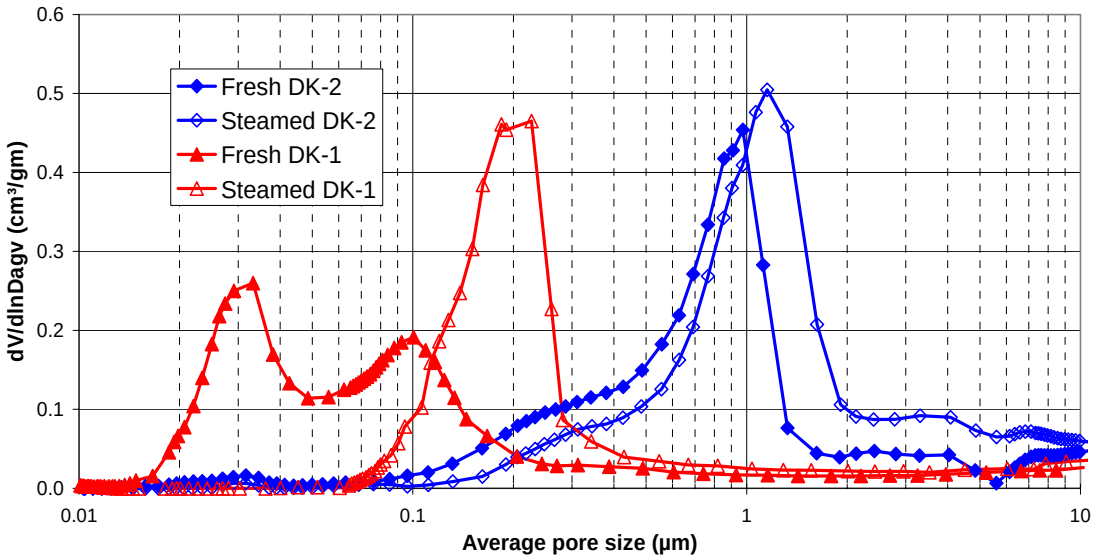

Figure 2-1. Hg porosimeter pore volume distributions for DK-1 and DK-2 zirconia powders
Fresh – as received; steamed – after 20-hr exposure to 8-atm H_2O and 0.4-atm O_2 at 950°C.

Preparation of pre-impregnated PS catalysts – Impregnation of fresh DK-2 powder using highly acidic 25-wt% $Pd(NO_3)_2$ salt solution was readily accomplished in a single step given the high interstitial volume (~1.2-mL/gm) of the powder (mean particle size ~2.0-µm). Low temperature drying was selected as desirable to grow large nitrate salt grains, and several temperatures from 25°C (vacuum drying) to 100°C were examined for the effect on Pd metal dispersion after drying and calcining to 950°C in ambient air for 10-hr. The range from 45 to 55°C was found optimal for producing low specific area Pd catalysts because lower temperatures required very long (days) drying time and left concentration gradients (color gradation) in the dried beads. Calcination conditions were determined to have the greatest effect on Pd dispersion; air calcination at 1050°C for 10-hr produced a PS catalyst powder, designated PI-1, with the target value of exposed Pd metal. Further steam-treatment (~80% water vapor and 20-vol% air at 10-atm) and this powder produced a lower dispersion catalyst, designated PI-2. These two powders were chosen for further examination of sintering resistance.

Preparation of physically mixed PS catalyst powders – Many commercially available pure Pd-black powders are available with the very low dispersion (<1%) targeted for the pre-sintered hot stage material. We chose a Johnson Matthey Inc. (JMI) 100-nm Pd black powder for preparation of two PS materials. Two DKK low area powders (DK-2 at ~2-µm particle size and low BET area F-1312 at ~0.5-µm) were combined with ~10-wt% Pd powder and milled 16-hr in distilled water to form a uniform paste. Two physically mixed powders (PB-1 and PB-2) with high and lower metal content were dried at 100°C for 4-hr; then calcined in air at 950°C for 10-hr and selected for further examination of sintering resistance in the high pressure aging reactors.

High pressure aging reactor (HPAR) system and aging condition.

The high pressure aging reactors (HPAR) were used to collect aging data over selected range of time and conditions that simulated catalyst environment in a turbine including short high temperature excursions. A picture of the opened reactors in a test cell is shown in Figure 2-2 and a schematic diagram of the HPAR flow system is shown in Figure 2-3. The gas composition was set to simulate gas turbine base load conditions assuming 100% conversion at the catalyst wall. This condition is perhaps more severe than may be expected for PS and NPGM catalysts, since their lower kinetic rates would leave unreactive fuel at the outer layer of the catalyst. The nominal gas composition was: 14-vol% O_2, 4-vol% CO_2, 0.5-ppmv SO_2, and N_2 balance. The volumetric gas flow rate through the reactors was approximately 300- mL(STP)/min and was adjusted to match liquid pumping rates and settings to achieve a target (typically 10-vol%) water concentration. The thermal stability tests were performed at 9.4-atm and 950°C. Catalyst powders were placed in trays on shelves of a ceramic sample holder. Finally, the set of the catalysts were placed inside the reactors.

Figure 2-2. Interior of a high-pressure test cell containing two high-pressure aging reactors

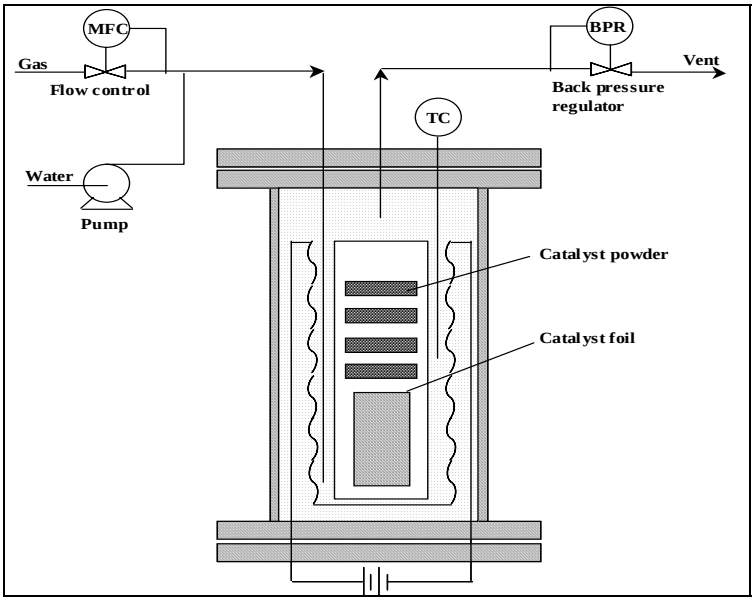

Figure 2-3. Schematic diagram of the High Pressure Aging Reactor (HPAR) system

After each thermal aging time interval, the powdered materials were removed from the reactors, a sufficient amount of samples were taken for characterization and the remaining portions of catalysts were returned to continue the tests. The samples were taken from the reactor at progressive intervals after 100-, 510-, 1000-, and 2000-hr of cumulative aging for the PI-1 and PI-2 and 100-, 410-, 910-, and 1910-hr for PB-1.

Reduced active-catalyst surface area measurement (via H_2 chemisorption).

Hydrogen titration method was used for measurements of surface area of Pd metal. This method was performed on Micromeritics AutoChem 2910 using the pulsed hydrogen titration method. Catalyst amounts from 30 to 250 mg were used for analysis depending on expected catalyst surface area. The PS catalysts were reduced at 400°C for 60 min in flowing pure hydrogen. After flushing for 15 minutes with pure argon, the samples were cooling to 100°C and exposed to a mixture of 5-vol% oxygen, balance helium, for a few minutes. Then the powder samples were flushed with argon before injecting hydrogen. Typically six pulses of a mix of 5-vol% hydrogen with balance argon were used for the titration measurement. The amount of adsorbed pulsed gas depended on loaded catalyst weight and if necessary the sample size was adjusted to hold significant adsorption between one and three pulses. The chemisorption measurements were calibrated by using three reference peaks of hydrogen with the sample by-passed. The integrated of the hydrogen areas represent amount of hydrogen reacted with active-catalyst surface area Pd metal.

Low-pressure rig testing of PS catalyst performance.

Testing was conducted in the CESI low-pressure rig (schematically illustrated in Fig. 2-4) and existing thermocouple assemblies and gas sampling instruments for data collection and the analysis of performance. In order to prepare each module, the metal foil (River Lite US-5 by Kawasaki Steel) was corrugated, cleaned, and calcined at 900°C for 16 hours to generate a thin protective layer of aluminum oxide that also assists in adhesion of the washcoat and provides oxidation resistance during long-term exposure to combustion conditions. Next, the calcined foil

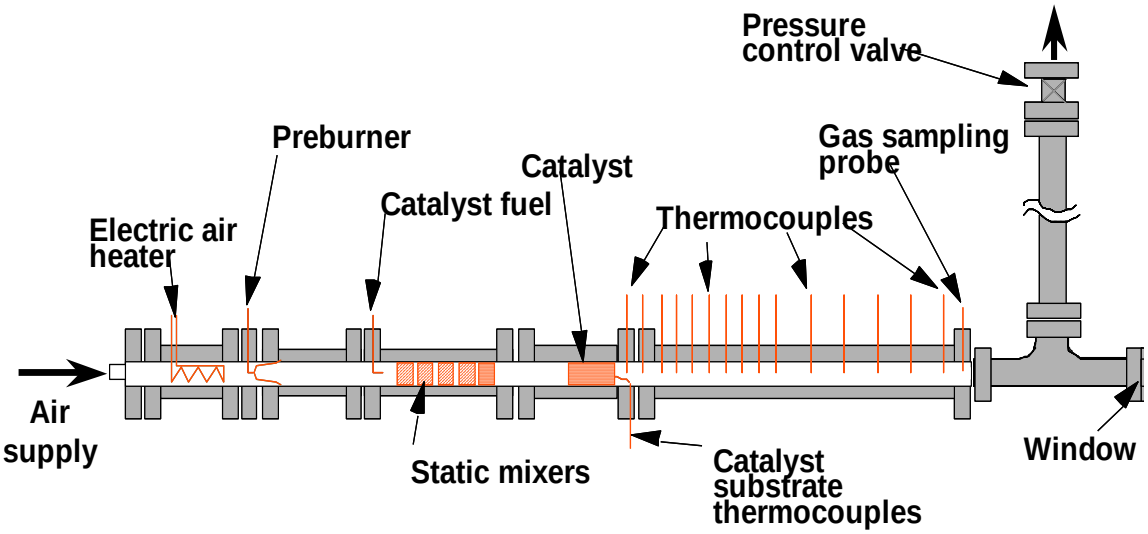

Figure 2-4. Schematic diagram of a subscale (2-in) catalyst module test reactor

was coated with PS catalyst slurries and rapidly dried. The slurries were composed of ~30-wt% ball-milled PS powder and suspended using a surfactant, methanol (to lower surface tension), ZA-20 (colloidal zirconia) binder, and nitric acid for pH control. The dried foil was calcined at 950°C for 16-hr before assembly into a ~2-in coiled foil pack for hot stage performance testing. A standard commercial inlet stage foil (for the KHI M1A-13X) was used as the inlet stage. Performance was determined by measuring the average of two thermocouples located between the first and second stages (interstage temperature) and the average of four outlet stage thermocouples. The fuel to air ratio is determined from the measure peak temperature of the fully combusted mixture downstream of the catalyst, which is designed as the adiabatic temperature (Tad). Performance was typically measured under standard KHI testing protocols for the PI-1, PI-2, PB-1, and PB-2 candidate PS catalysts following 24-hr operation under simulated full load conditions.

2.3.2 Development of Stable Hot Stage Materials – Non-Platinum Group Metal Catalysts

2.3.2.1 Multi-channel screening reactor test system: Exploratory screening of < 1-gm quantities of new NPGM catalyst materials requires rapid performance testing under high temperature and commercial pressures, gas composition, and flow rates. While the sub-scale rigs (Fig. 2-4) provide reliable testing, they also test only one NPGM catalyst candidate over the course of at least 24-hr and require preparation of some 25-gm of novel material. The combustion test rigs can only monitor a maximum of ten thermocouples for a catalyst test section. Due to this limitation, a method of measuring catalyst temperature was sought so that we could mount several catalysts in the 2-in test section. Optical pyrometry (thermal imaging) was chosen as the method to perform catalyst performance measurements simultaneously for several channel clusters of candidate catalyst materials in our multi-channel screening reactor (MCSR). Thermal imaging incorporates the use of a charge-coupled device (CCD) optical video monitoring camera with computer software to turn light intensity into temperature with the use of a look up table generated from black-body calibration curves. San Francisco Industrial Software was selected for this development effort because of their expertise in LabView software

development and strong technical background in adapting imaging methods to PC-data acquisition. Features and specifications of the thermal imaging data acquisition system are described below (Table 2-1) and a typical displace screen image of the IMAC data acquisition control system is shown below (Figure 2-5)

Hardware and software

- Pulnix CCD black and white camera.
- National Instruments IMAC video input board, with interface for the Pulnix camera.
- National Instruments analog input and output board.
- National Instruments Lab View data acquisition program.

Temperature measurement

- CCD pixel image intensity information is converted to a temperature within ±5°C.
- Temperature range will vary from 600 to 1200°C.
- Camera sensitivity adjusted automatically to cover this temperature range by changing the shutter speed using a timing signal and trigger sent to the camera by the computer.
- Calibrate temperature range using a black body radiator in the LPR test system.
- Temperature of entire image continuously updated within 1-second.
- Captures light intensity of up to 20 fixed previously defined regions within the camera image.
- Prior to the experiment, we will identify these regions, assign them a code identifier and then the LabView program will follow the image intensity/temperature of each of these regions.
- Software scans each region, determines a representative temperature maximum by the average of specified higher number of intensity readings, e.g., highest 10% or highest 25% for each region, displaces the value along with highest and lowest readings, and saves these values to a log file.

Software program custom features

- Set-up multichannel template is pulled up and overlays the camera image. Circles or ellipses are created (default patterns are accessible) to overlap the outlet face of cluster of channels representing a specific catalyst. The template as a whole can be moved and/or rotated to align the location spots.
- Circles on up to 20 regions in the template selected to represent the regions that will be monitored. Each selected region is given an identification number and a catalyst descriptor.
- Temperature representing each region is recorded to a file in separate columns along with external thermocouple data from the LPT controller and data acquisition system.
- User selects data recording cycle time appropriate to file size for the experiment.
- Start/stop button used to synchronize data record between parent LPR Lab View data acquisition computer and the IMAQ computer. Input boxes used for file title, test duration, and sampling rate.
- The screen should display (but should not be limited to) the following items:
- Screen display contains image (~30% of screen area) with image of the templated region generated by the user with temperature readout displayed in a column next to the image. This screen is full size for initial template set up.
- Screen display also shows chart of inlet gas temperature, selected region maximum temperatures vs. run time.

Table 2-1 - Features and specifications of the MCSR data acquisition system

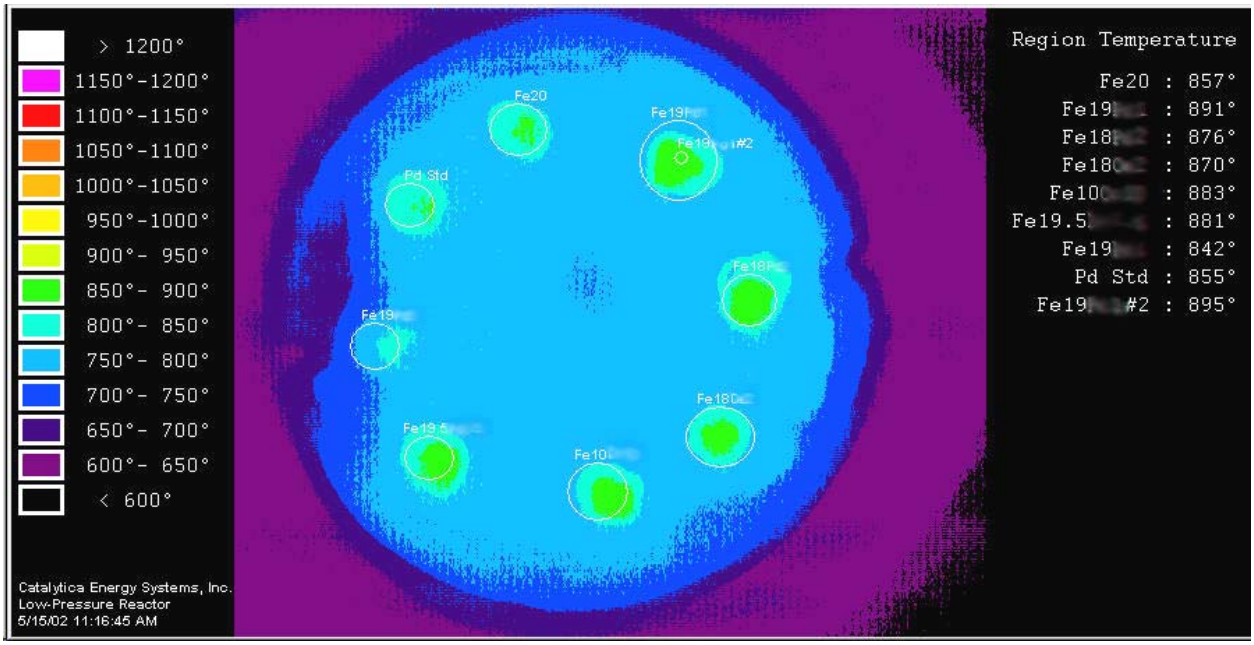

Figure 2-5. Typical MCSR temperature data acquisition image (monolith #7) The control screen shows the camera image, color code conversion to temperature, location of recording template circles, and a list of catalyst regions and average of highest temperature readings for each catalyst.

2.3.2.2 MCSR monolith preparation - Prior to the start of the DOE project, CESI instigated numerous materials as potential refractory materials for dispersing (supporting) active combustion catalyst components. Such refractory oxides must have two critical properties: 1) they must have great resistance to sintering and coarsening in the humid high temperature combustion environment; and 2) they must not be reactive with the target active component. For example, moderate surface area zirconia and high surface area alumina when stabilized with surface coatings of rare-earth oxides can withstand the severe hydrothermal combustion environment for thousands of hours, but these materials also react with most all transition metal oxides that have combustion activity. Some oxide compounds, e.g., $LaAlO_3$, a perovskite, are refractory and potentially have low reactivity, but they are difficult to prepare as high specific surface area pure phase powders suitable for use as a supporting oxide. Based on known specific activity 2-3] and considerations of the need for low volatility of active phase oxides and oxyhydroxides, two base components, ceria (CeO_2) [see Zarur and Ying (2000), and McCarty (2000)] and hematite (Fe_2O_3) [see McCarty, et. al. (1988)] were selected for development of NPGM catalysts. If unsupported, these components sintering rapidly under combustion conditions, and if unpromoted, their specific activity will not be acceptable. . Based on prior experience, we selected and synthesized large batches of two refractory complex oxide powders as our supporting oxides (designated as supports, K and L) for the effort to develop stable NPGM catalysts. Therefore, the focus of the NPGM hot stage catalyst development effort was to find effective promoters or co-catalysts and determine which of the supporting oxides was most compatible with each base active phase catalyst component.

Cordierite™ honeycomb monolith material with either 100 or 200 cells per square inch (cpsi) was chosen as the structural support for the screening and development of NPGM catalyst materials. Cordierite has excellent strength and thermal shock resistance, and its maximum allowable working temperature is ~ 1250ºC, well above expected target levels. The monolith diameter is fixed at 2-in, the diameter of the combustion test rig flow path, and a length of 1-in was chosen to minimize the heat and mass transfer entrance region. After experimentation imaging with single, two (adjacent), four (square), five (cross) clusters of channels coated with a Pd-based reference hot-stage catalyst, a cluster of four channels was deemed most effective for screening purposes. Target channel wall loadings were a relatively thick ~10-mg/cm^2 to provide good "light-off" performance of even low activity catalysts.

The standard procedure for preparing the catalysts and impregnating monolith is as follows:

- **Powder impregnation –** Hand impregnate powders with salt solutions, target preparation is 1-gm supporting oxide with ~250±100-mg NPGM active component on a dry basis. Salts are combined if compatible, otherwise sequential impregnation and drying steps are used.
- **Powder drying temperature –** The impregnated powders are flash dried in a 300°C oven for at least 30 minutes between impregnations (if multiple impregnation steps are necessary).
- **Powder calcination** – The dried NPGM powders are calcined at 1000°C for 10-hr in ambient static air.
- **Preparation of individual slurries of candidate materials –** Slurry solids targets are ~20 wt%. A capped 4-ml polyethylene vial is used with 1-mm zirconia beads to homogenize the slurry in a high speed shaker for ~15-min. Typical amounts of material used for slurry preparation are ~0.75 grams of calcined catalyst material, 3-ml solvent, 10µL of cationic surfactant, and 4-gm ZrO_2 milling beads.
- **Alcohol wetting –** Methanol or methanol de-ionized water solutions are used to suspend catalyst precursor powders. Both cationic surfactant and nitric acid (pH control of particle charge) are used as necessary to stabilize the slurry. Binder can be added, but is rarely needed to provide adequate adhesion and cohesion of the coatings.
- **Preparation of a multichannel monolith** - Use a 200-cpsi (typical) Cordierite monolith, target 10 mg/cm^2 loading, fill a square block of four adjacent cells by sealing one side of the monolith with parafilm, and inject an amount of slurry via a syringe to fill the channels completely (85µL of catalyst sol is a typical amount of sol injected per channel). After a few minutes, excess slurry is pulled through the selected channel array by placing the monolith a parafilm mask over a vacuum flask. The next catalyst channel is then prepared until all materials and a palladium catalyst standard (PI-1) are placed in the monolith.
- **Final calcination –** After the desired number and pattern of catalyst channel arrays are filled, the monolith is given a final calcine at 1000ºC in ambient static air for 10-h.

Table 2-2 lists the catalyst compositions prepared and examined in eight tested MCSR monoliths under the DOE program. The 66 compositions included the two supporting oxides, two active phase base components which were sometimes used as co-catalysts, and six different promoters. The results of the early MCSR tests guided the preparation of subsequent tests. Several of those catalysts with more than acceptable MCSR performance relative to a standard PS Pd-based catalyst (typically PI-1) were selected for aging in the HPAR and characterization by BET total

surface area measurements and analysis of phase stability and grain growth using x-ray diffraction.

Mono-lith#	Sample Position	Catalyst Support	Base Component	Base Ld (wt%)	Co-cat Component	Co-cat Ld (wt%)	Prmtr Aa Ld (wt%)	Prmtr Dd Ld (wt%)	Other Prmr Ld (wt%)	Temp(°C) Perf-50%	Temp(°C) Perf-80%
MCSR-1	1	K	CeO_2	20	--	--	2	--	--	730	--
	2	K	CeO_2	20	--	--	5	--	--	782	--
	3	K	CeO_2	20	--	--	10	--	--	716	--
	4	K	CeO_2	20	--	--	--	--	2 (Bb)	782	--
	5	K	--	--	Fe_2O_3	20	--	--	--	745	--
	6	K	CeO_2	5	Fe_2O_3	20	--	--	--	755	--
MCSR-2	1	L	CeO_2	20	--	--	2	--	--	758	**785**
	2	L	CeO_2	20	--	--	5	--	--	<700	**733**
	3	L	CeO_2	20	--	--	10	--	--	710	**785**
	4	L	CeO_2	20	--	--	--	--	2 (Bb)	775	>800
	5	L	CeO_2	20	--	--	--	--	5 (Bb)	780	>800
	6	L	CeO_2	20	Fe_2O_3	10	--	--	--	>800	>800
	7	L	CeO_2	20	Fe_2O_3	20	--	--	--	>800	>800
	8	L	--	--	Fe_2O_3	20	--	--	--	790	>800
	9	L	CeO_2	20	Fe_2O_3	40	5	--	--	780	>800
MCSR-3	1	K	CeO_2	20	Fe_2O_3	10	--	--	--	770	>800
	2	K	CeO_2	20	Fe_2O_3	20	--	--	--	775	>800
	3	K	CeO_2	20	Fe_2O_3	40	--	--	--	770	>800
	4	K	--	--	Fe_2O_3	40	--	--	--	770	>800
	5	K	CeO_2	20	Fe_2O_3	40	10	--	--	775	>800
	6	K	CeO_2	5	Fe_2O_3	20	5	--	--	775	>800
MCSR-4	1	L	--	--	--	--	20	--	--	>820	>820
	2	L	CeO_2	2	--	--	20	--	--	770	>820
	3	L	CeO_2	10	--	--	20	--	--	735	805
	4	L	CeO_2	20	--	--	--	--	--	740	>820
	5	K	--	--	Fe_2O_3	20	10	--	--	755	>820
	6	K	--	--	Fe_2O_3	20	2	--	--	730	**780**
	7	K	--	--	Fe_2O_3	20	--	--	2 (Co)	770	>820
	8	K	--	--	Fe_2O_3	20	--	--	10 (Co)	775	>820
MCSR-5	1	L	CeO_2	18	--	--	2	--	--	750	810
	2	L	CeO_2	16	--	--	4	--	--	740	**765**
	3	L	CeO_2	14	--	--	6	--	--	<735	**755**
	4	L	CeO_2	12	--	--	8	--	--	735	**755**
	5	L	CeO_2	10	--	--	10	--	--	740	**760**
	6	L	CeO_2	8	--	--	12	--	--	<735	**750**
	7	L	CeO_2	6	--	--	14	--	--	735	**745**
	8	L	CeO_2	4	--	--	16	--	--	<735	**755**
	9	L	CeO_2	2	--	--	18	--	--	735	**755**
	10	L	CeO_2	20	--	--	0	--	--	775	>825
	11	L	--	--	--	--	20	--	--	750	**765**
MCSR-6	1	K	Fe_2O_3	18	CeO_2	2	--	--	--	755	**780**
	2	K	Fe_2O_3	15	CeO_2	5	--	--	--	765	**800**
	3	K	CeO_2	15	Fe_2O_3	5	--	--	--	765	805
	4	K	CeO_2	18	Fe_2O_3	2	--	--	--	805	835
	5	K	Fe_2O_3	18	--	--	2	--	--	765	**790**
	6	K	Fe_2O_3	15	--	--	5	--	--	755	**780**
	7	K	Fe_2O_3	18	--	--	--	--	2 (Co)	775	825
	8	K	Fe_2O_3	15	--	--	--	--	5 (Co)	755	**775**
	9	K	Fe_2O_3	18	--	--	--	2	--	735	**760**
	10	K	Fe_2O_3	15	--	--	--	5	--	750	**770**
MCSR-7	1	L	CeO_2	18	--	--	--	--	2 (Ee)	760	>820
	2	L	CeO_2	15	--	--	--	--	5 (Ee)	730	805
	3	L	CeO_2	18	--	--	--	2	--	<700	**770**
	4	L	CeO_2	15	--	--	--	5	--	700	**745**
	5	L	CeO_2	18	--	--	--	--	2 (Ff)	>820	>820
	6	L	CeO_2	15	--	--	--	--	5 (Ff)	>820	>820
MCSR-9	1	K	Fe_2O_3	20	--	--	--	--	--	<735	**780**
	2	K	Fe_2O_3	19	--	--	--	1	--	<735	**760**
	3	K	Fe_2O_3	18	--	--	--	2	--	<735	**765**
	4	K	Fe_2O_3	18	CeO_2	2	--	--	--	<735	**780**
	5	K	Fe_2O_3	10	--	--	--	--	10 (Co)	<735	**765**
	6	K	Fe_2O_3	19.5	--	--	--	0.5	--	<735	**770**
	7	K	Fe_2O_3	19	--	--	--	5	--	<735	**800**

Table 2-2 - Catalyst prepared and examined in MCSR monoliths 1-4

Two supporting oxides were designated as powders K and L. Component loadings are on a metals weight basis, e.g., weight of metallic Ce per unit weight catalyst x100%. Performance is indicated by the (interpolated) interstage

(monolith inlet) temperature for which the optically measure catalyst temperature rise was 50% or 80% of the Pd standard catalyst.

MCSR test conditions in the LPR, low pressure rig:

Each of the monoliths described above were tested using the MCSR test system. As discussed above, the test system uses a thermal imaging system and the LPR combustion test rig for relatively high through-put screening of 1-gm quantities of candidate catalyst materials. The LPR was configured for MCSR testing, a standard KHI M1A-13X stage 1 catalyst was installed with pass-through thermocouples for monitoring interstage gas temperature, and the MCSR monolith and retaining rods were installed typically with catalyst #1 at the 12 o'clock position. The LPR test conditions and test protocol were as follows:

- **Base Test Conditions** – Air flow 4200-slpm air, monolith diameter 2-in, pressure 123-psig, initial preheat temperature 450 or 500°C at the inlet of stage 1.
- **Test Protocol** – Tad (F/A) step-up test at 450ºC and 500ºC with 50ºC Tad steps from at 1050- and 1250ºC. Test typically completed within 2-hr; occasionally ~30-min hold and ~800°C monolith inlet gas temperature with Tad step-down.
- **Catalyst and reactor constraints** – Catalyst false color image <1100ºC, interstage gas <850ºC, test terminated upon initiation of homogeneous combustion.

The MCSR operated successfully through the end of the DOE program contract and additional follow-up tests continued until the end of 2002. Additional work with the MCSR/LPR system for screening and optimizing NPGM catalysts was planned throughout the year 2003.

2.3.3 Validation of Catalyst Performance Models – Measurement of Flow Distribution and Mass Transfer in Xonon Modules

2.3.3.1 Test system

Testing was conducted in the CESI high-pressure rig (similar to the LPR which is schematically illustrated in Fig. 2-4 above) and existing instrumentation was used for data collection. In order to prepare each module, the metal foil (River Lite US-5 by Kawasaki Steel) was corrugated, cleaned, and calcined at 900°C for 16 hours to generate a thin protective layer of aluminum oxide that also assists in adhesion of the washcoat and provides oxidation resistance during long-term exposure to combustion conditions. Next, the calcined foil was coated with catalyst layers containing active highly-dispersed precious metals of CESI's proprietary inlet stage formulation. Two washcoat loadings were used and washcoat thickness fell within the range of 40- to 100-μm.

To form each module, two processed foils were wound around a core rod to form a unit with a 2 inch diameter and 3 inch length. The properties of the catalyst modules used in the testing are given in Table 2-1.

For 100% IHE† cases, each of the foils was coated with catalyst on both sides so that all of the channels formed upon rolling were catalytically active. In 50% IHE cases, only the two foil sides facing each other were coated with catalyst, allowing gases to pass through 50% of the channels in the module without reacting. It should be noted that modules in which all of the channels are catalytic do not represent actual Xonon systems but are included as reference systems without flow split effects. In each of the first eight modules listed in Table 2-1, both

	Foil 1	Foil 1	Foil 2	Foil 2		nominal
Module	Channel height	Corrugation	Channel height	Corrugation	Loading [2])	IHE
1	0.5	Hb	0.5	Hb	lo	50
2	0.5	Hb	0.5	Hb	lo	100
3	0.8	Hb	0.8	Hb	lo	50
4	0.8	Hb	0.8	Hb	lo	100
5	0.8	Hb	0.8	Hb	hi	50
6	0.8	Hb	0.8	Hb	hi	100
7	1.1	Hb	1.1	Hb	hi	50
8	1.1	Hb	1.1	Hb	hi	100
9	0.8	Hb	1.3	RA	hi	34

Table 2-3. Foil Properties, Catalyst Loading, and Flow IHE for Catalyst Modules tested

foils had herringbone corrugation (HbC) with a pitch angle of 15º and a segment length of 15-mm. Only the last module was based on an HbC/RAD configuration, where RAD is a proprietary corrugation specification intended to have improved structural properties. Each module was configured with three thermocouples for measuring the inlet foil temperature, three for outlet foil temperature, three for outlet gas temperature, and one for inlet gas temperature.

Methane and propane were used as fuels and fuel/air mixture flow rates were 2000, 5000, 7500, and 9600 slpm with vessel pressures of 5, 10, and 15 atmospheres considered. In each case, the inlet gas temperature, Tin, was 450°C with the fuel level chosen to yield an adiabatic temperature, Tad, of 1000°C for single-sided foils and 750°C for double-sided foils. Once steady operation was attained, the temperatures of the ten thermocouples, pressure drop across the module, and levels of UHC, O2, and CO2 were monitored. For each set of conditions, twenty data points were collected at time increments of four seconds.

2.3.3.2 Dimensionless Groups.

The experimental data were cast in terms of dimensionless groups in order to facilitate the analysis and make the results more general. Data for pressure drop and mass transport were described by the non-dimensional Fanning friction factor and Colburn factor, respectively. The flow was characterized by the Reynolds number, Re, which represents the ratio of inertial forces to viscous forces in the flow.

Flow - The Reynolds number is defined by Equation 1:

$$\mathrm{Re} = \frac{G * \mathrm{d_h}}{\varepsilon * \mu} \qquad \text{Eq. 1}$$

Here, G is the mass flux, ε is the module porosity, $\mathrm{d_h}$ is the hydraulic diameter, and μ is the gas viscosity estimated at the outlet gas temperature. The mass flux is simply the product of the inlet channel velocity and gas density. For the gas viscosity, we use the air viscosity relation obtained from the DIPPR database, as shown in Equation 2:

$$\mu = \frac{1.425*10^{-6}\left(\mathrm{T(K)}\right)^{0.5039}}{1+108.3/\mathrm{T(K)}}\ \mathrm{Pa*s} \qquad \text{Eq. 2}$$

$\mathrm{T(K)}$ is the average value from the three thermocouples recording outlet gas-phase temperature. The porosity is the bulk void fraction computed from the total reactor volume, core rod volume, bulk catalyst volume, and foil volume, as shown in Equation 3:

$$\varepsilon = \frac{\frac{\pi * L}{4} * \left(\mathrm{D}^2_{\mathrm{reactor}} - \mathrm{D}^2_{\mathrm{rod}}\right) - m_{cat} / \rho_{cat} - \mathrm{A_f} * \mathrm{t}_f}{\frac{\pi * L * \mathrm{D}^2_{\mathrm{reactor}}}{4}} \qquad \text{Eq. 3}$$

Here, L is the reactor length (3 inches), $\mathrm{D}_{\mathrm{reactor}}$ is the reactor diameter (2 inches), $\mathrm{D}_{\mathrm{rod}}$ is the core diameter (¼ inch), m_{cat} is the total mass of catalyst deposited on the foils, ρ_{cat} is the catalyst bulk density, $\mathrm{A_f}$ is the one-side corrugated foil surface area, and t_f is the foil thickness. The corrugated foil area is the product of the measured length and width and a corrugation factor, f_c, that is computed according to Equation 4:

$$f_c = \frac{2}{CHP}\sqrt{\left(CHH\right)^2 + \left(\frac{CHP}{2}\right)^2} \qquad \text{Eq. 4}$$

Here, CHP is the channel period and CHH is the channel height. The corrugation factor is used to take into account the extra surface area due to the presence of the corrugations. The hydraulic diameter is defined by Equation 5:

$$\mathrm{d_h} = \frac{4*\varepsilon}{\alpha} \qquad \text{Eq. 5}$$

where ε is the previously described porosity and α is given by Equation 6:

$$\alpha = \frac{2*\mathrm{A_f}}{\frac{\pi * \mathrm{D}^2_{\mathrm{reactor}}}{4} * L} \qquad \text{Eq. 6}$$

Friction Factor - The Fanning friction factor, f, represents the non-dimensional ratio of the wall shear stress to the kinetic energy of the flow and is defined by Equation 7:

$$f = \frac{\varepsilon^2}{4}\left(\frac{\mathrm{d_h}}{L}\right)\left(\frac{\Delta \mathrm{P}}{\rho \mathrm{v}^2/2}\right) \qquad \text{Eq. 7}$$

Here, $\Delta\mathrm{P}$ is the pressure drop across the module and $\rho\mathrm{v}^2/2$ is the kinetic energy of the gas evaluated at outlet conditions. For a given module length, it would be expected theoretically that the friction factor for an isothermal system would be a function of Reynolds number, corrugation

specifications (channel height, angle, segment length), and washcoat properties (thickness, roughness).

Mass Transfer - Because the catalytic combustion of methane is fast, external mass transport effects play a significant role in the performance of Xonon modules. It is therefore important to understand the influence of the operating conditions and module design on mass transfer behavior. Specifically, we investigate the variation of Colburn factor, j_D, with Reynolds number, vessel pressure, and module design. The Colburn factor is defined as:

$$j_D = Sh * Re^{-1} * Sc^{-1/3} \qquad \text{Eq. 8}$$

That is, the dimensionless Colburn factor is a combination of three other dimensionless groups: Sherwood number (which characterizes effect of mass transfer relative to diffusion), Reynolds number (which is the ratio of inertial to viscous forces, as previously explained), and Schmidt number (which is the ratio of momentum diffusivity to mass diffusivity).

The Schmidt number, Sc , is given by:

$$Sc = \frac{\mu}{\rho * D_{AB}} \qquad \text{Eq. 9}$$

where ρ is the outlet gas density and μ is the outlet gas viscosity that was used in calculating the Reynolds number. D_{AB} is the diffusivity of the fuel in air under the outlet gas conditions. The expression for D_{AB} [Perry's Chemical Engineers Handbook (Equation 3-133)] is given by:

$$D_{AB} = \frac{10^{-3} * (T(K))^{1.75} * \sqrt{\left(\frac{mw_{air} + mw_{fuel}}{mw_{air} * mw_{fuel}}\right)}}{P(atm) * \left((\Sigma\nu)_{air}^{1/3} + (\Sigma\nu)_{fuel}^{1/3}\right)} \frac{cm^2}{s} \qquad \text{Eq. 10}$$

In this expression, P is the absolute pressure, mw_{air} and mw_{fuel} are the air and fuel molecular weights, respectively, and the $(\Sigma\nu)_{air}$ and $(\Sigma\nu)_{fuel}$ terms correspond to diffusion volumes. The diffusion volume for air is 20.1 and values for our nonpolar fuels are obtained by summing the atomic diffusion volumes for their component atoms. $(\Sigma\nu)_{CH4}$ is 24.42 and $(\Sigma\nu)_{C3H8}$ is 65.34.

The Sherwood number, or Nusselt number for mass transfer, is given by Equation 11:

$$Sh = \frac{d_h * k_m}{D_{AB}} \qquad \text{Eq. 11}$$

In this case, the value of the diffusion coefficient used is the average of those calculated from inlet and outlet conditions. The mass transfer coefficient, k_m , can be calculated from data obtained with 100% IHE modules according to Equation 12:

$$k_m = -\frac{s}{\alpha} * \ln(1 - X) \qquad \text{Eq. 12}$$

where X is the fuel conversion and s is the space-velocity, which is based on the arithmetic mean of the inlet and outlet channel velocities. The space velocity is equal to the mean channel velocity multiplied by the porosity and divided by the module length. Equation 12 was easily obtained by doing a shell balance for the quantity of fuel in an axial slice of the reactor assuming zero surface concentration of fuel (since mass transfer is limiting).

2.3.4 Validation of Catalyst Performance Models – Measurement of Specific Combustion Rates of Xonon Catalyst Materials

2.3.4.1 Catalyst materials tested

The kinetics tests included samples of outlet and inlet stage foils, scraped inlet stage foil (powders) and some new materials (powders) with medium and high levels of exposed palladium (surface area) that potentially useful for inlet-stage catalysts. Table 2-2 summarizes the catalyst materials tested under Task 1 and a brief description of each. Catalyst materials were analyzed for reduced active-catalyst surface area and for methane combustion activity in a microreactor.

2.3.4.2 Catalyst characterization – active metal surface area

The pulsed-chemisorption hydrogen titration method was used to measure of the specific surface area of reduced Pd metal in each aged catalyst sample using a Micromeritics AutoChem 2910 instrument. Depending on initial catalyst surface area and aging conditions, samples from 30 to 250 mg were used for the titration measurements. Catalyst samples were loaded in a tapered tube reactor and held in place by glass wool at the top and the bottom. First, a catalyst sample was reduced in flowing hydrogen for 60 min at 400°C, flushed with pure argon gas for 15-minutes, and cooled to 100°C. At 100°C, a temperature too low to grow bulk palladium oxide, the catalyst sample was held for 15-minutes in a flowing mixture of 5-vol% oxygen and helium balance, and finally flushed with argon gas before injecting aliquots of hydrogen for the titration and chemisorption. Six 1.04-mL aliquots of a mixture of 5-vol% hydrogen and argon balance were injected into an argon carrier and passed through the catalyst bed at 100°C. The number of adsorbed aliquots was between one and three pulses.

Samples	Description	Exposed PGM Surface Area (µmol_H_2/gm)
Low SA		
PI1-E2	Extruded pre-impregnated PdO-based catalyst on a low-area zirconia support	9.6 fresh 10.2 aged 1200-hr
High SA		
Gen2-Stage1	Commercial production catalyst – scraped inlet stage foil; P01-5-028 + P01-5-029	103.7 fresh 35.7 aged 1200-hr
Com 22	Pre-impregnated PGM-based developmental catalyst on a stabilized zirconia support	159.8 fresh 32.5 aged 1200-hr

Table 2-4 - Catalyst materials used for kinetic measurements

Finally, titration ended by measuring the detector response for three reference peaks of 5-vol% hydrogen while by-passing the catalyst sample using a switching valve. The obtained data was used to calculate areas of the absorbed picks. The detector response signal area (time-integrated) represents the amount of hydrogen that did not react or with or adsorb on the surfaces of oxygen-covered reduced Pd or other noble metal particles within the sample powder. The amount of hydrogen that reacted or adsorbed then determines the surface area of reduced Pd metal via a stoichiometric value of 0.6667-moles H_2 titrated per mole of surface palladium metal. This key catalyst property was (or will be) measured and used to compare HPAR-aged samples.

2.3.4.3 Catalyst characterization – microreactor test of specific activity

The specific activity of a catalyst for methane (or any fuel component) combustion has been assumed to vary in proportion to surface area of palladium metal measured by pulsed-chemisorption hydrogen titration. This assumption rests on a series of measurements of activity with freshly prepared catalyst with varying surface area of reduced Pd metal. It has not been examined previously for HPAR aged catalysts. Therefore, selected aged catalysts were examined for specific activity for methane combustion in a pressurized flow microreactor.

The microreactor sample bed (Figure 2-6) is confined by a quartz tube (OD=6.35mm and ID=3.96mm). This quartz tube is placed inside a furnace that has a heating zone slightly longer than the height of a catalyst bed. The catalyst sample is diluted with high-thermal-conductivity silicon carbide granules (0.15- to 0.18-mm) mixed in the proportion 1 to 150 by weight for the catalyst to diluent. The diluted catalyst bed was supported by quartz wool and two thermocouples from the top and the bottom. The combustion gas mixture flowed downward through the catalyst bed at a volumetric flow rate of 600-mL(STP)/min. The nominal dry gas composition was 0.5-vol% CH_4, 25-vol% O_2, varying amounts of water vapor (0-, 2-, and 8-vol%), with high-thermal-conductivity helium making up the balance. Water was introduced by

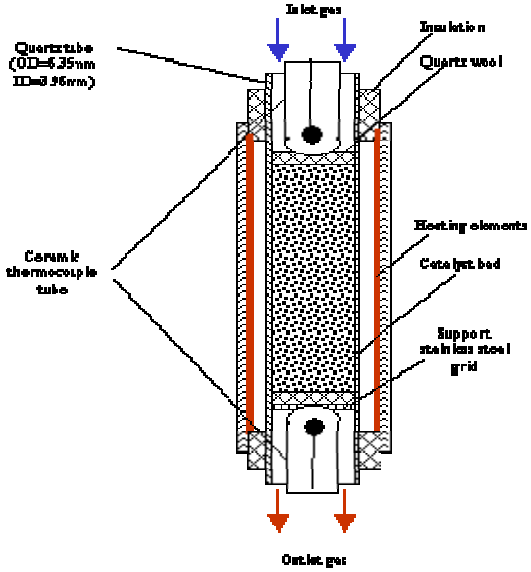

Figure 2-6 - Schematic diagram of the microreactor vessel and catalyst bed

adding pure hydrogen gas to the oxygen-helium mixture and reacting it at 100°C in a catalyst bed upstream of the mixing point for the methane reactant. The pressure inside the reactor was

~6-atm and the temperature ranged from 600°C to 800°C. The pressure drop through the nominally 300-mg catalyst bed was approximately 0.2 atm. The methane combustion rate was determined by on-line measurement of the methane and carbon dioxide concentration downstream of the reactor catalyst bed using a mass spectrometer (QMS - Balzers Quadstar 422). The microreactor data (see Figure 2-7 for a typical result) was analyzed to determine the amount of methane converted on a tested catalyst. Analysis includes: subtracting QMS intensity background signals, normalizing of CO_2 and CH_4 intensities to that of helium to correct for signal drift over the several hour time of the analysis, forcing a carbon balance to determine CO_2

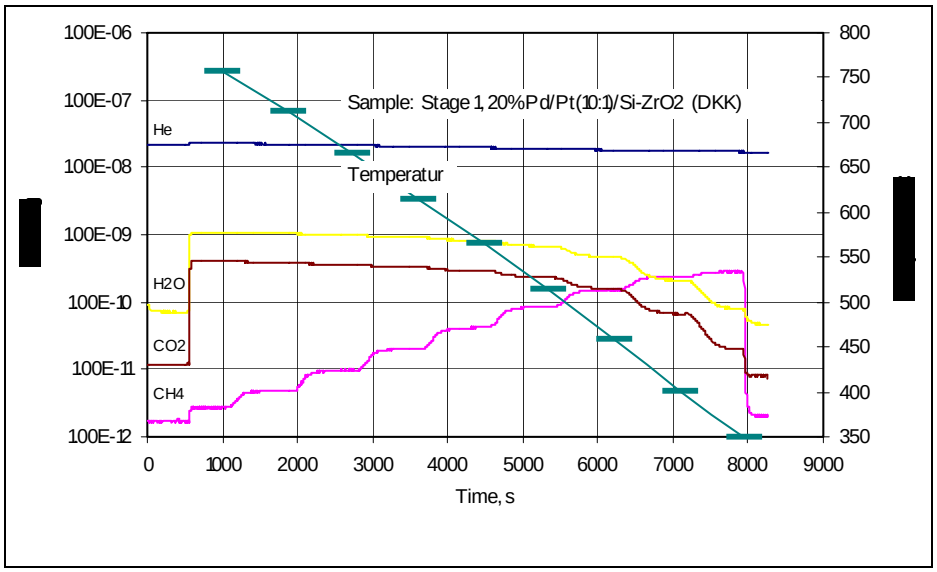

Figure 2-7 - Typical microreactor mass spectrometer data for a catalyst activity test

sensitivity relative to methane, determining microreactor outlet (exit) CH_4 concentration, and finally calculating first-order (CH_4) rate constants and activation energy for a series of measurements over a range of temperatures.

2.4 Experimental Results and Discussion

2.4.1 Development of Stable Hot Stage Materials – Presintered Palladium-Based Catalysts

2.4.1.1 Hydrothermal Aging

Powders of the four candidate PS catalysts were loaded into the HPAR reactor and exposed to simulated combustion gas at 9.4-atm pressure for 2200-hr at an accelerated temperature, 950°C. Because these conditions were in the metallic region of Pd, i.e., PdO would have been completed decomposed despite the high oxygen partial pressure (~1.4-atm), the aging furnaces were purged with dry N_2 during cool-down to avoid oxidizing the supported Pd. The key measurement was the value of reduced exposed Pd metal. The aging data (Table 2-5 and Figure 2-8) were the primary factor used to choose the PS formulation for commercial use following acceptable sub-scale rig tests. The PI-1 catalyst showed very good resistance to thermal aging relative to the PB-1 (mixed powder) formulation and the expectations of aging from the former higher activity material (Gen 2 catalyst). The rate of sintering for the PB materials generally followed

expectations based on the Gen2 formulation, but reasons for the slower sintering of the PI-1 and especially PI-2 is not understood. The heavily pre-sintered PI-2 catalyst actually showed a slight increase in exposed metal values with exposure time, but this material and the lower activity PB-2 catalyst had significantly lower activity, inferior stage conversion (see following subsection) and because they showed some tendency to kinetic instability, the PI-1 material was chosen as the PS catalyst.

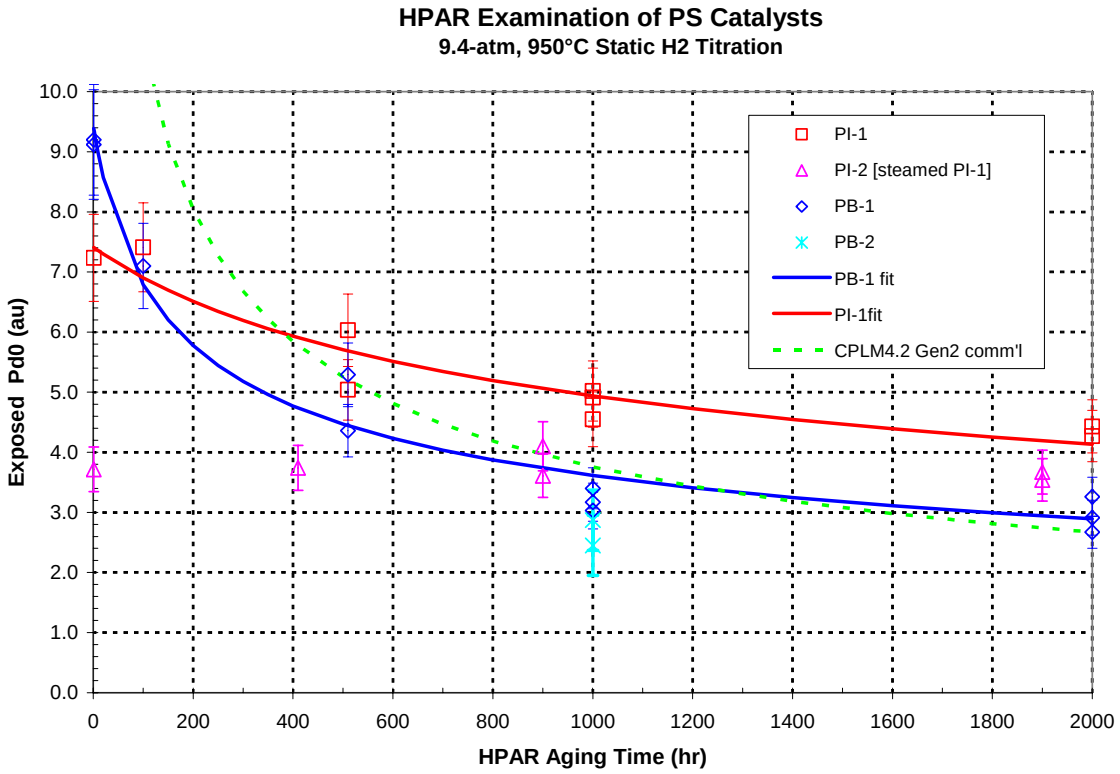

Figure 2-8. PI catalyst materials show significantly lower sintering rates relative to original Xonon catalysts and the PB materials. PB (physically mixed) catalysts show sintering rates similar to the Gen2 catalyst.

2.4.1.2 Subscale Catalyst Test Performance

Herringbone corrugated stage 2 foils of identical geometer were coated with each of the four PS candidate materials and tested in the sub-scale test facility. Performance of the PS catalysts (with the exception of PB-2) fell within the range of two Gen 2 hot stage catalysts (Figure 2-9) for interstage gas temperatures above 600°C. The PB-1 catalyst equally or outperformed the Gen 2 catalysts over the entire temperature range (570 to 660°C) examined. The fresh PI-1 catalyst performed as well as the best Gen 2 material at and above 650°C, which is the lower end of the expected range of interstage gas temperatures (650 to 700°C). However, below 600°C both PI catalysts showed lower conversion because of a more pronounced fall-off in activity (higher activity energy) than the other catalysts, both Gen2 and PB. The cause of this discrepancy and the nearly identical performance of PI-1 and PI-2 despite a factor of two in exposed metal are not clear. It should be noted that the scale of Figure 2-9 is very fine,

reproducibility (standard deviation) of this test is typically ±0.5% stage conversion for identical foils. On this note, only PB-2 would appear to significantly differ from the other materials over the commercial temperature range. Further investigation of the kinetics of PI materials is warranted because of their conversion performance at low temperature.

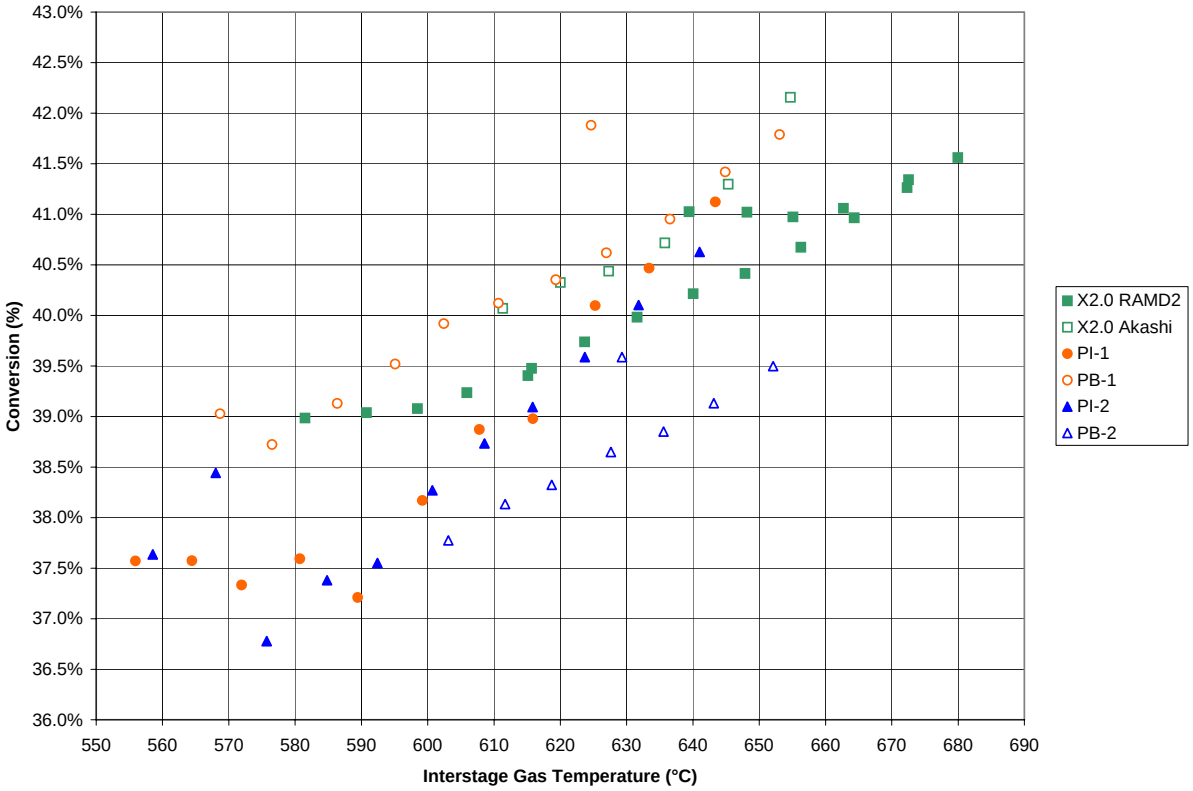

Figure 2-9. Subscale LPR pre-heat step-down test results for PS candidate catalyst materials. In this test, Tad is held at 1200°C while inlet (stage 1) gas temperature increased.

2.4.2 Development of Stable Hot Stage Materials – Non-Platinum Group Metal Catalysts

2.4.2.1 MCSR Test Results and Discussion:

Most of the MCSR monoliths (#5-#9) were tested with both 450ºC and 500º inlet gas (stage 1) to the monolith system while varying the fuel concentration to achieve the calculated and measured range of adiabatic temperature from 1050 to 1200°C. The first four runs of the MCSR tests (monoliths #1-#4) used a single inlet gas temperature and the adiabatic temperature was not as carefully controlled as during the subsequent tests. The performance results from these early tests (shown in Table 2-2) were determined by comparing temperature rise (interstage thermocouple to the average of the highest 5 image temperatures in the optical image) of a particular catalyst channel cluster with that of the reference low-area palladium catalyst (e.g., PI-1) under the came conditions. Performance is listed in the table as interpolated temperatures where the temperature rise was 50% and 80% of the temperature rise for of the reference catalyst. These early tests established the supporting oxide "L" was superior to oxide "K" primarily because promoter "A" was not effective when used with support "K". Subsequent aging work with powders using CRD showed that the promoter was being consumed by support

"K". On the contrary, support "K" was found superior for the hematite-based catalysts since iron reaction with support "L" was observed in aged powders by XRD. The early tests showed that combinations of the two base active phase components as co-catalysts were not effect on either support. The MCSR runs following #4 represent a systematic search for promoters or co-catalysts for the two heavily loaded active phase-support combinations: CeO_2/L and Fe_2O_3/K.

The test results for MCSR monolith #5 at two different adiabatic temperatures demonstrate the methodology of the MCSR approach (Fig 2-10a, 2-10b). The variation in relative loadings of Ce

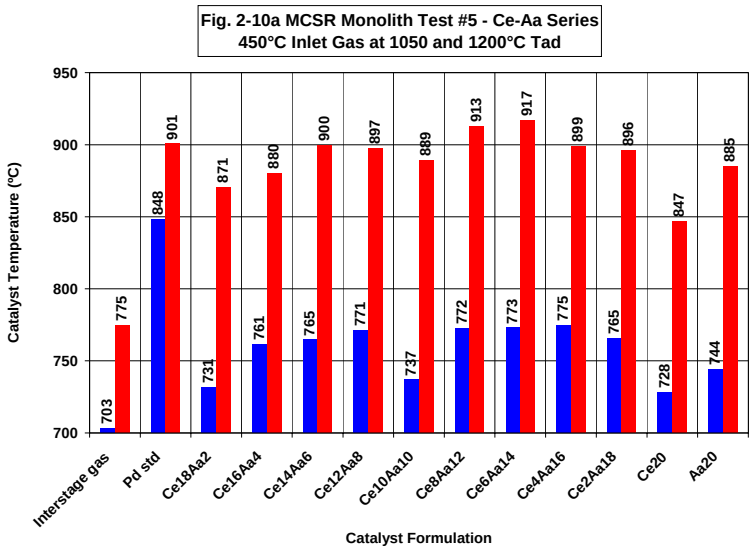

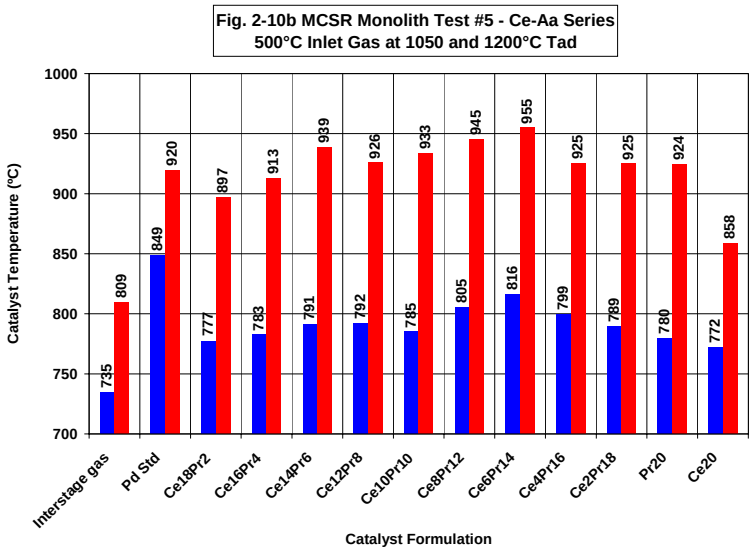

Figure 2-10. Tad step-up test results for MCSR #5 at 450ºC (2-10a) and 500ºC (2-10b) inlet gas temperature and 1050ºC and 1200ºC Tad

and promoter "Aa" are displayed on the X-axis versus catalyst spot temperature as measured by the thermal imaging system. Two wide-ranging test conditions (1050 and 1200°C Tad) contrast activity among the series of catalysts. The effect of methane concentration (presumed first order) on the reaction kinetics is seen at the lower (1050ºC) adiabatic temperature. A trend in the

500º, 1050ºC test data appears as the concentration of promoter Aa is increased. The catalyst temperature rise levels off when promoter Aa concentration reaches 4-wt% (Ce16Aa4); similarly when Aa is used as catalyst a small amount of CeO_2 in turn "promotes" with as little as 2-wt% CeO_2. Both components show minimum activity when unpromoted. The data with 500°C inlet gas shows similar results, increasing promoter Aa concentration improves ceria activity while Aa requires only a small amount of ceria for promotion. Equal mixtures and pure phases showed minimal activity, although the accuracy of the method makes it difficult to precisely optimize promoter levels. The small variation in fuel concentration (slightly higher) and water vapor concentration (slightly lower) caused by the difference in inlet gas temperature, 450º versus 500ºC, does not appear to a significant effect on the catalyst activity when comparing data trends in Figure 2-10. Only on the 450ºC Tad step-test will be presented for remaining MCSR tests.

At the higher 1200ºC adiabatic set point, the hotter wall temperatures cause kinetic rates to begin competing with mass transfer. The trend in the data for the 1200ºC Tad test point is still apparent with the pair of Ce14Aa6 and Ce6Aa14 catalysts producing the hottest temperature rise, in both cases well above that of the palladium reference catalyst.

An alternative method for measuring activity of these advanced materials is to ratio the temperature rise produced by these catalyst against the known highly active standard palladium catalyst. This method is performed by calculating the temperature rise from interstage gas to measured catalyst temperature for all catalyst tested including the palladium catalyst at each test point then dividing by the palladium delta temperature rise to obtain a percent catalyst temperature rise relative to palladium catalyst delta temperature. Data presented in this manner (Figure 2-11)

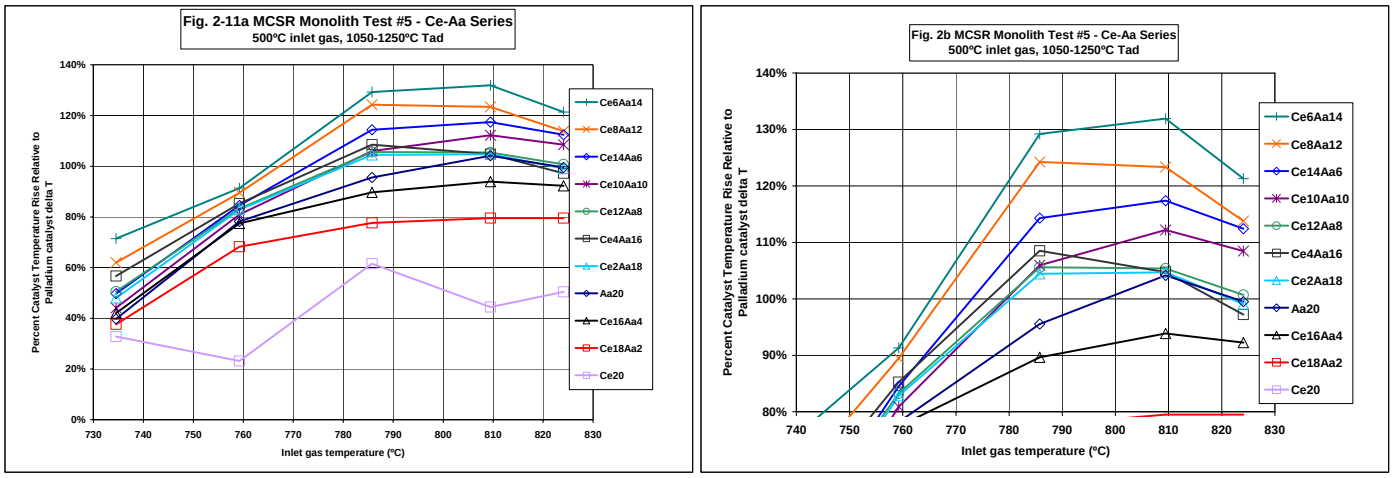

Figure 2-11. Relative temperature rise for ceria-based NPGM catalyst materials in MCSR#5 vs. interstage gas temperature with 1250°C adiabatic temperature and 500°C inlet gas temperature; a) full y-axis scale (0 to 140%), b) y-axis scale highlighting those materials with superior performance (80 to 140%).

aids in illustrating relative catalyst activities. Catalyst activities greater than 80 percent of PI-1 for interstage gas temperatures at or below 800°C are considered to be candidate hot stage type catalysts. Displayed in Figure 2-11 is the Tad turn-up data at 450ºC inlet temperature for the Ce-Aa/K catalyst series presented relative to palladium catalyst activity. Figure 2-11b displays the same data as in Figure 2-11a but magnified to focus on the catalysts with greater than 80 percent activity relative to PI-1. The significant increase in performance of the CeO_2-Aa/L relative to PI-

1 confirms expectations that the activation energy for methane combustion by these active phase components is much greater than PdO/Pd, and that the concentration of active sites in the NPGM catalyst is also much greater than the pre-sintered Pd catalyst.

Between approximately 740-760ºC interstage gas temperature, the more active catalyst formulations in the MCSR#5 series show relative temperature rises above the 80 percent target. One should keep in mind however that the PI-1 reference catalyst is an aged catalysts designed to perform stably over 8000-hr, while the NPGM candidates have seen only 950°C calcination for 10-hr. Given the relatively good performance of both components when un-promoted, and the potential for complex oxide formation, a more extensive investigation into morphology and microreactor kinetics will be needed to determine if there is an optimum for this catalyst system. It should also be noted that component Aa is considerably more expensive than ceria and certainly hematite which is examined in other MCSR runs.

The Tad turn-up results at 500ºC inlet gas for MCSR monolith #6 (see Table 2.2b and Figure 2-12) show significant activity of the promoted hematite and ceria-hematite co-catalyst formulations. Again the steep slop in the relative temperature rise with increasing fuel concentration (each step in Tad) is apparently associated with larger activation energies expected for the Fe based catalyst formulations relative to Pd catalysts.

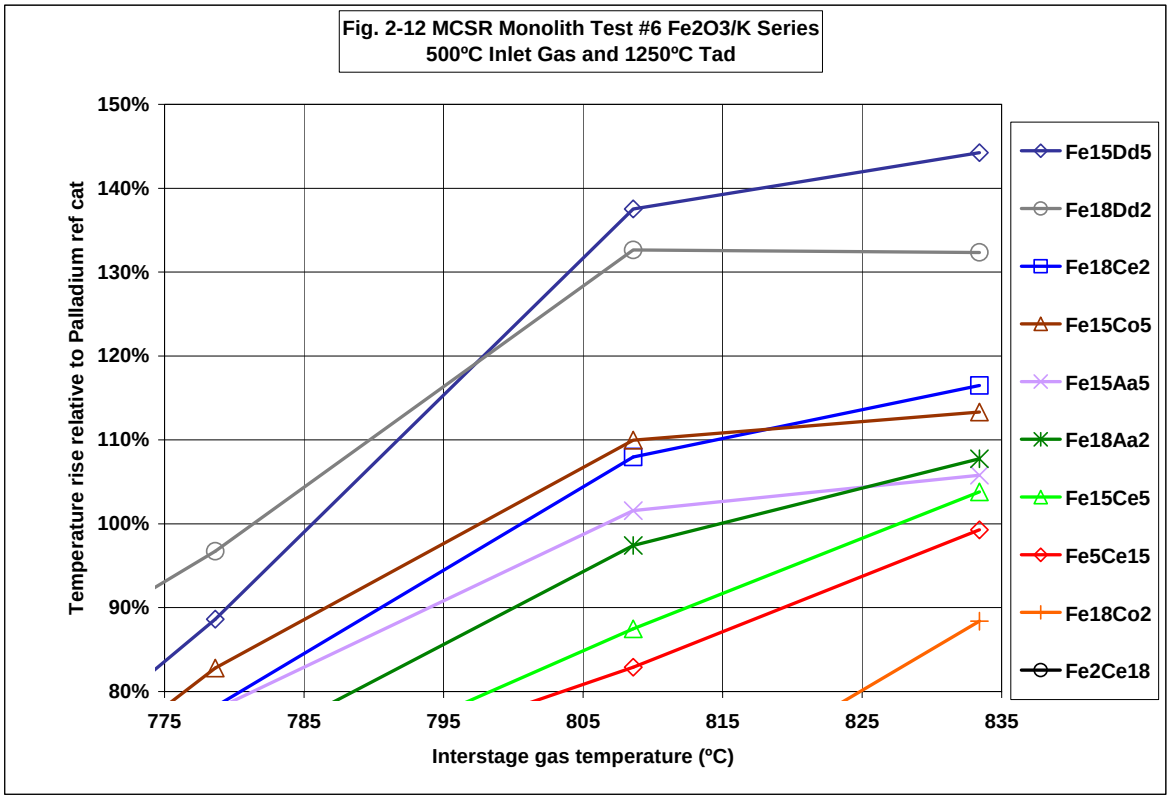

Figure 2-12. Relative temperature rise for hematite-based NPGM catalyst materials in MCSR#6 vs. interstage gas temperature with 1250°C adiabatic temperature and 500°C inlet gas temperature, highlighting those materials with superior performance (>80%).

A minimum amount of Ce is required to enhance the activity of Fe with the Fe18Ce2 catalyst being the more active. The Fe18Ce2 catalyst reaches the 80% target compared with PI-1 palladium catalyst temperature rises at ~780°C and out performs the palladium catalyst above

800ºC. Increasing the ceria concentration has a negative effect, and Fe seems clearly detrimental to the activity of ceria catalysts. Unlike the situation with ceria-based catalysts, promoter Aa has little effect on hematite activity. Likewise, Cc is not a good promoter for iron. Another promoter, Dd, was very effective at increasing hematite activity and was chosen to be examined further in the subsequent MCSR tests (monolith #9).

Additional investigation of the promoted CeO_2/L catalyst system showed two good promoters, Dd and Ee, and a very poor promoter, Ff (see Figure 2-13 and Table 2-2b). Promoter Dd continued to enhance ceria activity with increasing levels from 2- to 5-wt%, unlike the promotion of hematite, where increased concentration had relatively little effect (Figure 2-13). Promoter Ee was expected to behave similarly to promoter Aa, and this was shown to be the case (Figure 2-14). Because Ee is chemically similar but even more expensive than Aa, this result only serves to confirm the utility of Aa in promoting supported ceria for methane combustion.

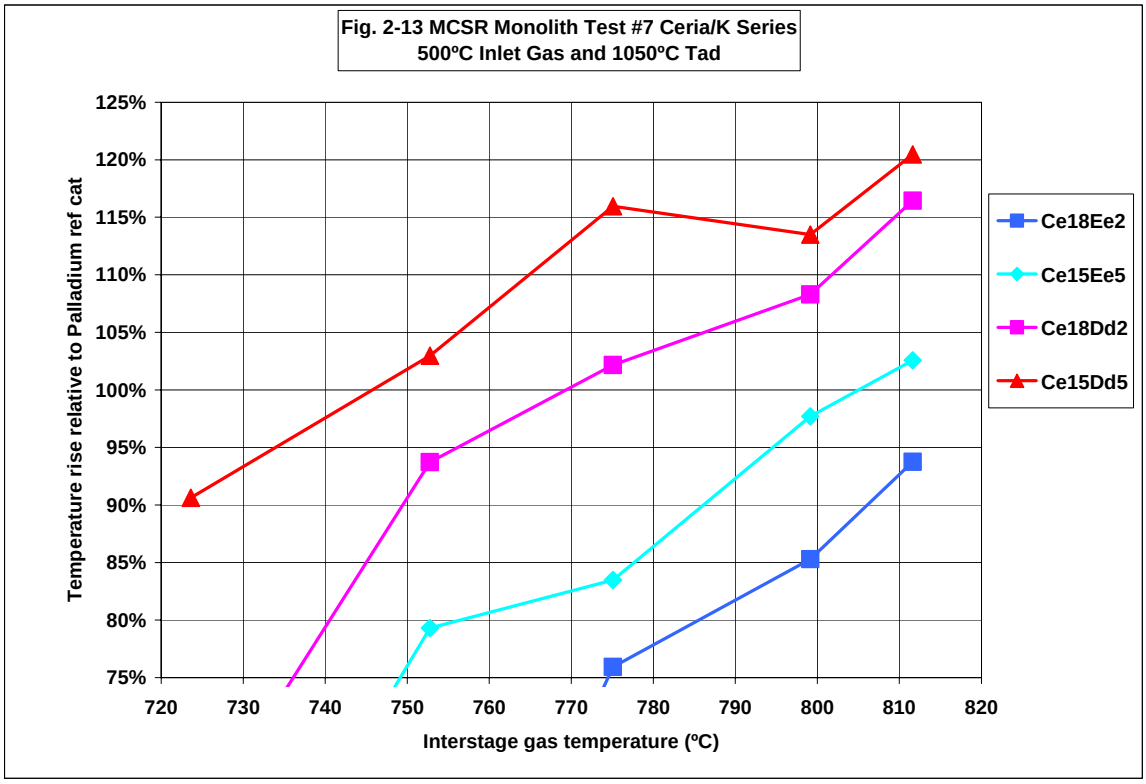

Figure 2-13. Relative temperature rise for promoted ceria-based NPGM catalyst materials in MCSR#7 vs. interstage gas temperature with 1050°C adiabatic temperature and 500°C inlet gas temperature.

The final MCSR test (run #9 – monolith #8 was prepared but damaged during testing so no results were obtained for MCSR#8) focused on fine-tuning promoters for the Fe_2O_3/support-K catalyst system (Fig. 2-15). Contrary to a previous run (MCSR#6) small amounts of ceria and promoter Dd, were not so effective in promoting hematite, not was a co-catalyst with promoter Cc. But significant levels of Ee continued to show promise, not only reaching the 80% relative temperature target at ~750°C with 450°C inlet gas conditions, but exceeding PI-1 performance

above 765°C. Like the Ce14Aa6/support-L, the Fe15Ee5/support-K catalyst was chosen for future development work including XRD examination and HPAR aging tests.

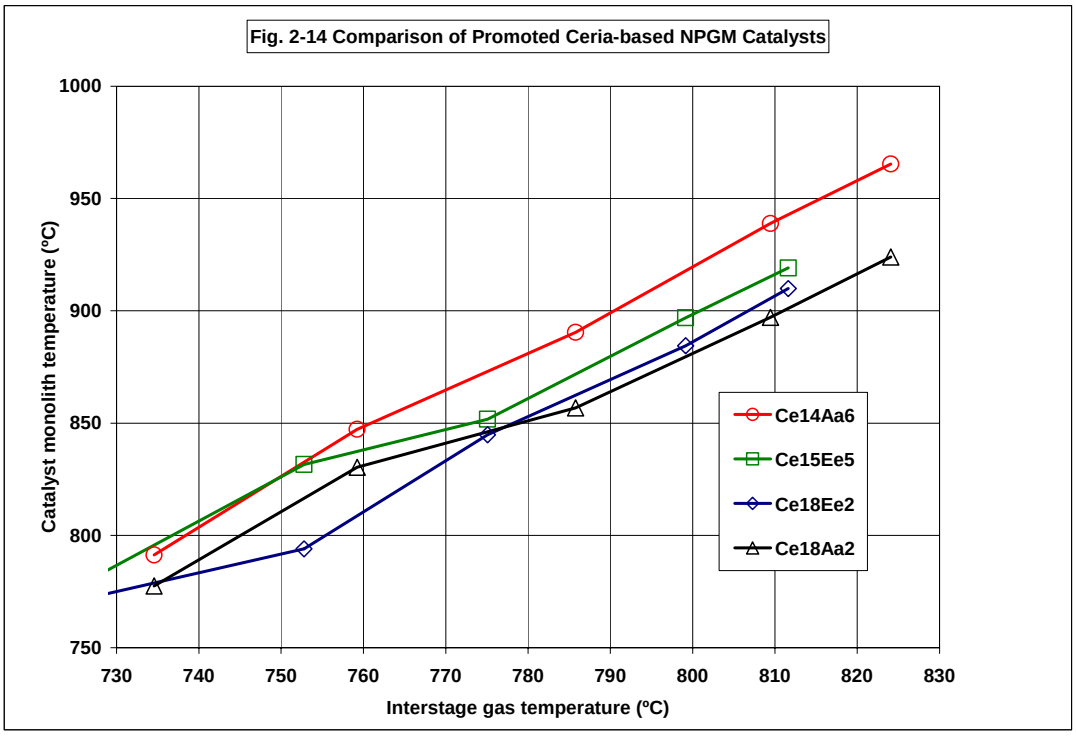

Figure 2-14. Comparison of channel-cluster peak outlet temperature vs. interstage gas temperature for ceria-based NPGM catalyst materials with Aa & Ee promoter components.

2.4.2.2 HPAR Aging Results for Selected NPGM Catalysts:

Selected NPGM catalysts (ceria base active phase only) and supporting oxide powders were examined in the HPAR furnaces as described above. Aging conditions were as described for the PS materials (9.4-atm, 950°C, 10% H_2O and 14% O_2) for increasing exposure periods up to 1000-hr. The BET total surface area of the refractory supporting oxides (without catalyst) was very stable although addition of the active and promoter components decreased the initial value for the catalyst using support-K (Figure 2-16). Both the support and catalyst prepared from support-K were very stable for 1000-hr at 950°C with almost 1-atm water vapor partial pressure. Power law fits to the sintering rate data showed a typical <-0.2 dependence, and projections of the two Ce20Aa2 catalysts with support-L and support-K extrapolated to 8000-hr showed both to stabilize at about 15-m^2/gm, far better than zirconia (typically ~1-2-m^2/gm)under these conditions.

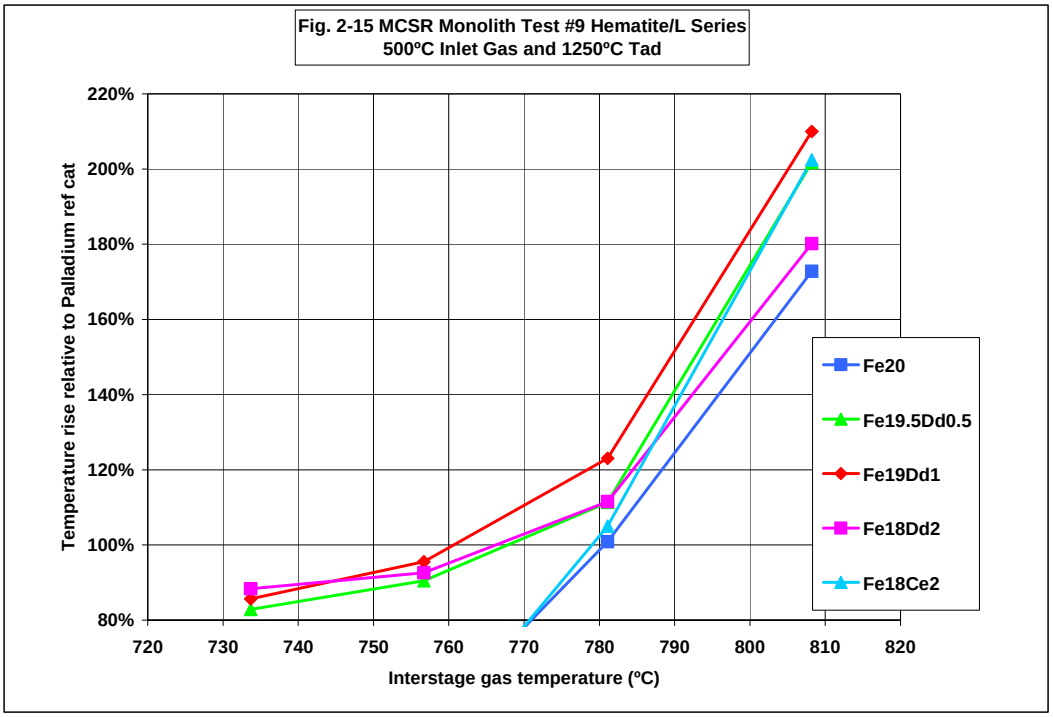

Figure 2-15. Relative temperature rise for promoted hematite-based NPGM catalyst materials in MCSR#9 vs. interstage gas temperature with 1250°C adiabatic temperature and 500°C inlet gas temperature.

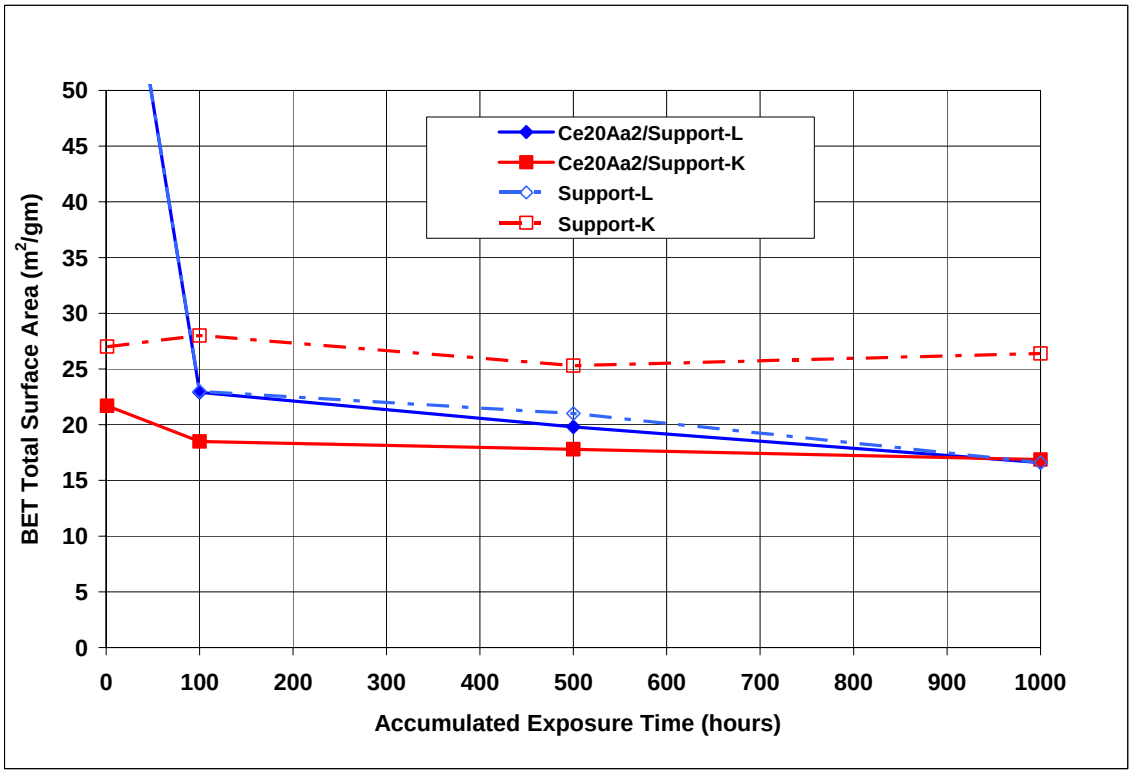

Figure 2-16. BET Surface area of ceria-based NPGM catalysts and their corresponding supporting oxides under simulated combustion aging at 950°C.

Because no surface-specific titrant gases were known for the NPGM active phase components, we used grain size growth rates measured by XRD line broadening to estimate coarsening rates of the supported and promoted ceria-based formulations (Figure 2-17). The estimated ceria grain size with support-L doubled from 15-nm as calcined to 30-nm after the first 100-hr of exposure to simulated combustion conditions at 950°C. After 100-hr the growth rate slowed significantly and the estimated grain size at 1000-hr under these accelerated aging conditions was ~38-nm. For support-L the initial grain size was larger (25-nm) but the rate of growth smaller increasing to 35-nm at 100-hr and ~43-nm at 1000-hr.

The slightly better aging resistance of support-L and other observations that promoter Aa was reactive with this supporting material lead to the choice of support-L for the ceria-based catalysts. Extrapolation of both surface area and ceria grain size to 10,000-hr exposure (~50-nm) is very encouraging because the anticipated activation energy for both coarsening and methane combustion is expected to be high. Rough estimated 200-kJ/mol for the sintering rate would give extremely good stability at 800°C, the point where the performance of the Ce14Aa6/support-L catalyst exceeded that of PI-1 and the lower range of temperatures expected of a third hot stage catalyst. Likewise, using a modest 100-kJ/mol for the activation energy of the ceria catalysts for methane combustion would increase combustion rates about 4 times the rate at 800°C more than compensating for the decreased surface area extrapolated for 100- to 1000-hr aging. Additional aging work needs to be performed for the more active formulation (e.g., Ce14Aa6 vs. the Ce20Aa2 aged in the current work) with a full 2-in subscale monolith as part of a preliminary third hot stage design. Such a monolith could be aged for 8000-hr and tested in the LPR for stage conversion performance and stability. The stability of support-K with active component added is reassuring for the stability of the Fe20Dd5/Support-K system, although this of similar catalysts should be given HPAR aging to at least 1000-hr to check stability before proceeding with sub-scale design and long-term performance testing

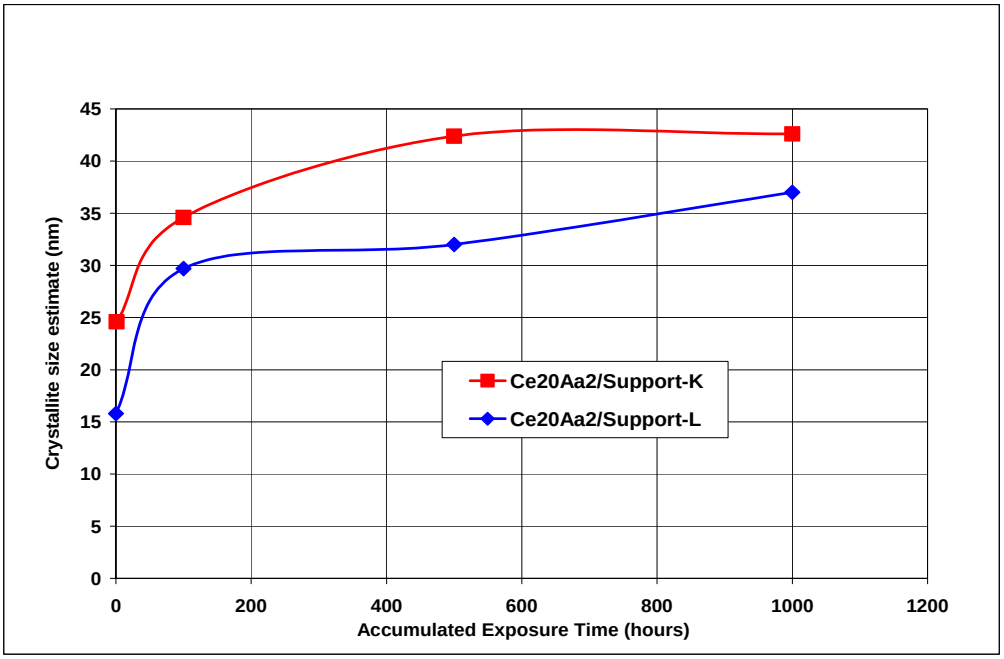

Figure 2-17. Estimated grain-size (via XRD line broadening) of ceria-based NPGM catalysts under simulated combustion aging - Conditions: 950°C, 9.4-atm, 8-vol% H_2O, 14-vol% O_2, 0.5-ppmw SO_2.

2.4.3 Validation of Catalyst Performance Models – Measurement of Flow Distribution and Mass Transfer in Xonon Modules

2.4.3.1 Friction Factor

After all of the pressure drop data were collected, it was discovered that the filters on the legs of the pressure transducer were introducing some noise, which resulted in scatter in the data, particularly at low Reynolds numbers. Experiments for the 50% IHE modules were repeated without the resulting data were further refined by subtracting out the baseline value (up to 0.07 psi) of pressure drop transducer. Figure 2-18 shows friction factor data as a function of Reynolds number for 1) the original 50% IHE data with the filter in place, 2) 50% IHE runs repeated without the filter installed, and 3) repeated 50% IHE data corrected for the baseline reading of the pressure drop transducer. The data collected without the filter installed and with being corrected by the baseline reading of the pressure transducer certainly exhibit reduced scatter. It should be noted that experiments with the 100% IHE modules were not repeated, so the correlations were developed using data collected under two sets of conditions (i.e. the filter was in place when the 100% IHE data were collected but were not in place when the data were collected for the 50% IHE modules).

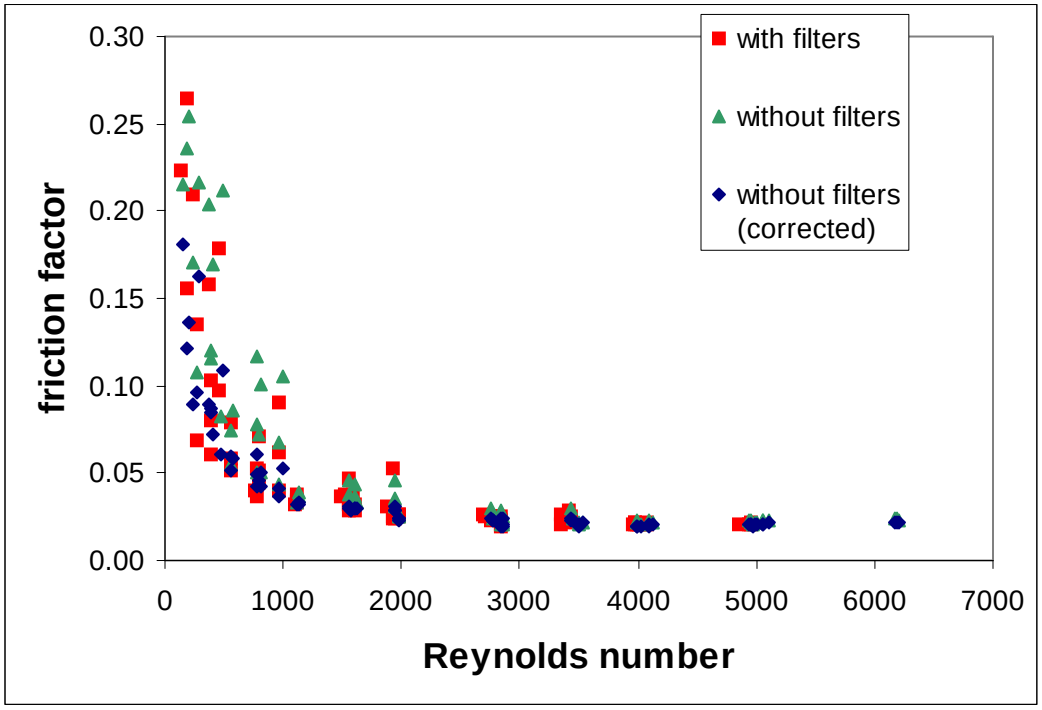

Figure 2-18 - Friction factor data for 50% IHE modules are shown as a function of Reynolds number. Results are shown for data collected with filters on the legs of the pressure transducer, without filters in place, and data (collected without filters in place) adjusted for baseline reading of the pressure transducer

All of the data points for friction factor in the HbC/HbC modules are shown in Figure 2-19. The data points are separated according to module. The 50% IHE modules are shown as blue symbols and the 100% IHE modules are given as red symbols. The data reveal a strong dependence of friction factor on Reynolds number for less than around 2000. Based on our

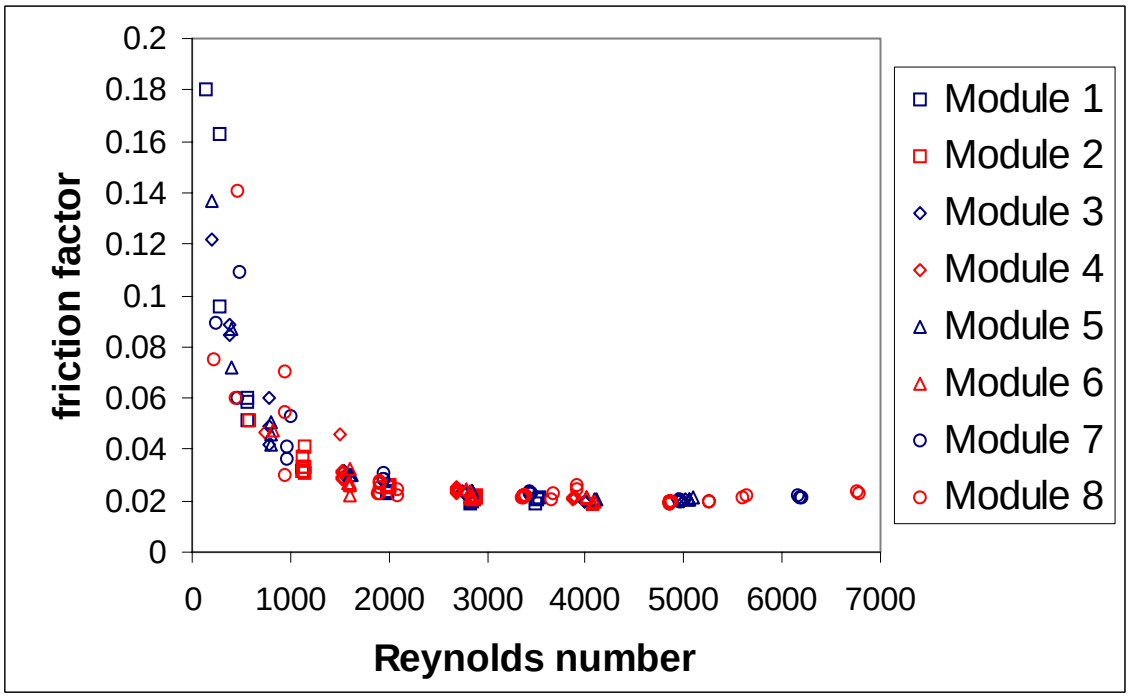

Figure 2-19: Friction factor data for all HbC/HbC modules are shown as a function of Reynolds number and separated by module

data, for low Reynolds numbers; this behavior is similar to what one would expect for fully developed laminar flow. Gulian et al. (1991) investigated herringbone metal monoliths and found that friction factor was proportional to . In the limit of high Reynolds number, tends to a constant value for each module.

So we can write a correlation, as shown in Equation 5, which incorporates these limiting conditions:

$$f_{fit} = \frac{A}{Re} + B \qquad \text{Eq. 13}$$

where A and B are determined from a linear fit of the quantity f_{fit}*Re versus Re. This variable, rather than simply the friction factor itself, is used in developing the correlations because it prevents the low Reynolds number data from dominating the fit. Values of A and B were chosen to minimize the average absolute deviation, *e*rr , between experimental and computed values, as shown in Equation 14:

$$err = \frac{1}{n}\sum_{i=1}^{n}\left(\left(f_{fit} * Re\right)_i - \left(f * Re\right)_i\right) \qquad \text{Eq. 14}$$

where n is the number of data points used. Results for the global correlation are shown in Figure 2-20.

The correlation gives a reasonable fit of the data with roughly equal numbers of data points above and below the correlation curve. Modules 7 and 8 seem to yield the greatest deviation from the correlation. For the global correlation, A = 20.83, B = 0.0159, and *e*rr = 5.31. Next,

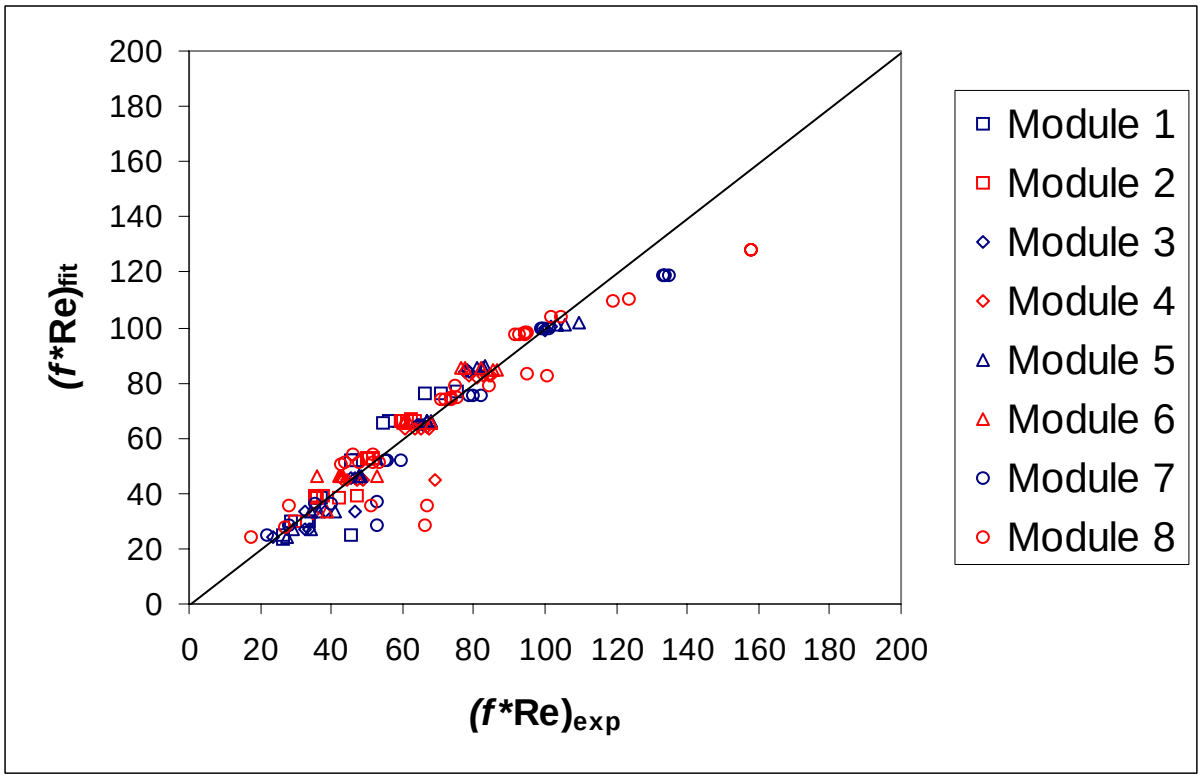

Figure 2-20 - Comparison between experimental and predicted values of *fRe is shown for a global correlation involving a single value of A and a single value of B. Here, A = 20.83, B = 0.0159, and err = 5.31**

we will determine the benefit obtained by using a single value of A for all of the modules, while allowing each module to take on its own value of B. Results of this exercise are given in Figure 2-21.

The values of A and B for this correlation are summarized in Table 2-5 below.

Module	A	Bi	IHE	Channel Height (mm)
1	22.49	0.012504	50%	0.56
2	22.49	0.013760	100%	0.56
3	22.49	0.015519	50%	0.86
4	22.49	0.015899	100%	0.86
5	22.49	0.015942	50%	0.86
6	22.49	0.013796	100%	0.86
7	22.49	0.016881	50%	1.16
8	22.49	0.015157	100%	1.16

Table 2-5 - Correlation parameters for the HbC/HbC modules

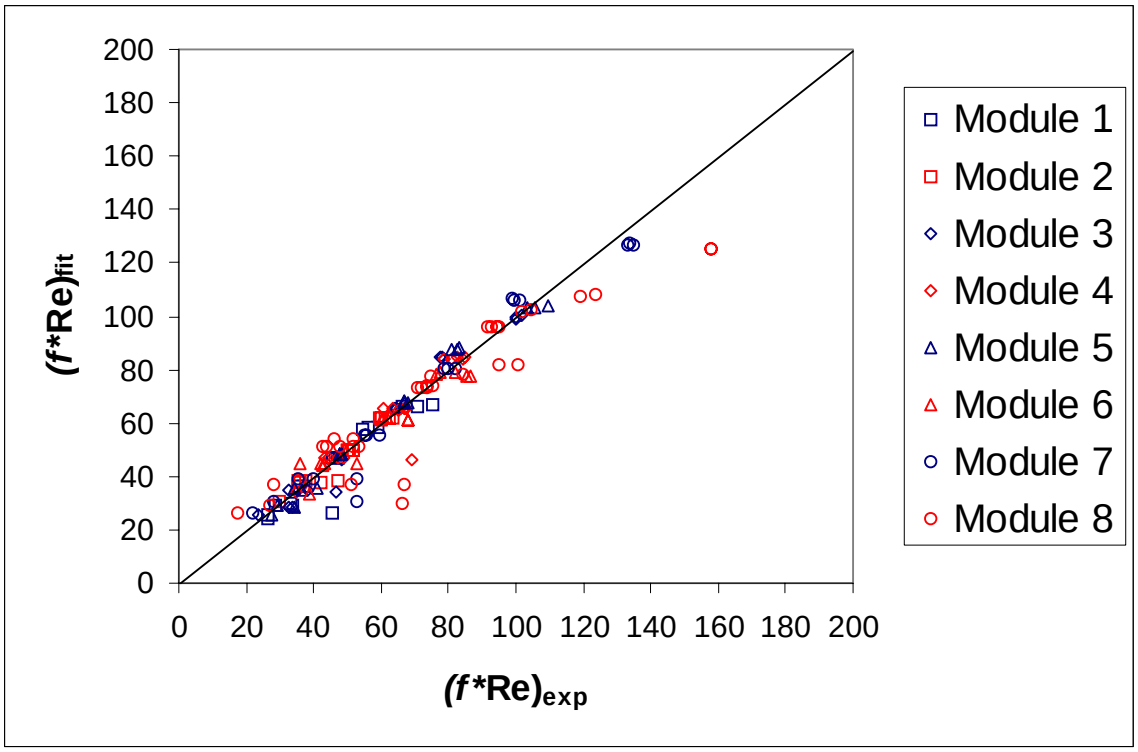

Figure 2-21: A comparison between experimental and predicted values of f*Re is shown for a correlation involving a single value of A for all the modules, while each module is allowed a distinct value of B. For this case, A = 22.49 and err = 4.48. The values of B for the different modules are given in Table 2-5.

Recall that the value of *e*rr had been 5.31 using the global correlation and that its value is 4.48 when a single A but distinct B values are used. In our case, going from a two-parameter model to a nine-parameter model yields a 15.6% reduction in the mean absolute deviation between experimental and predicted values of f*Re. Using a sixteen-parameter model, in which each module is allowed a distinct A and a distinct B value, results in *e*rr = 4.30, which represents a 19.0% advantage over the global two-parameter model. However, using a sixteen-parameter model to describe 157 data points that contain quite a bit of scatter may not yield very statistically meaningful values of the coefficients in the correlation. At best, using a global value of A and distinct B values for the modules is viable. It makes sense to allow an individual value of B for each module because each B is related to the surface roughness of the corresponding Xonon module. Trends of B with respect to channel height, catalyst loading, etc. could not be discerned because of experimental uncertainty and the lack of a large number of data points.

2.4.3.2 Mass Transport

For the following results, values of jD based on experiments with methane were used because significant differences were observed for the propane data. Recall that for 100% IHE modules, the standard inlet temperature is 450°C with a fuel fraction adjusted to yield an adiabatic temperature of 750°C. Under these conditions, the values of jD based on propane as the fuel were up to 50% higher than those based on methane. Propane results at a Tad of 600°C were closer to the methane results; data collected with propane at an inlet temperature of 425°C and Tad of 500°C fell within about 10 to 15% of the methane data collected with an inlet temperature of 450°C and Tad of 750°C. Because the difference between the methane and propane jD values decreases as we decrease the adiabatic temperature in the propane runs, it is suspected that contributions of homogeneous oxidation of propane may be playing at role at the higher temperatures. It is for this reason that the following correlations are based on methane data. Figure 2-22 shows values of the Colburn factor for mass transfer based on methane runs in the 100% IHE modules:

The data are separated by module and good linearity is displayed on the log-log plot of jD versus Reynolds number. There is some scatter at the higher Reynolds numbers, which is partially due to the higher number of data points in that region. Comparison of the results in Figure 2-22 with the module specifications in Table 2-1 reveals no obvious, significant pattern with respect to loading level or channel height, although the values of jD for Re > 1000 are slightly higher in module 8 (1.16 mm channel height) than in the other three modules with smaller channel heights. Similar observations can be made when the data are separated by vessel pressure, as shown in Figure 2-23. Here, the data acquired at 15 atm. are slightly higher than for the other two operating pressures, but statistically meaningful differences in the various data sets cannot be discerned due to experimental uncertainties and the limited number of data points.

A global correlation was developed using all of the data (46 points) based on methane. Since the previous plots of jD versus Reynolds number appeared linear, we can assume a correlation of the form, $jD = A*ReB$ and determine the values of A and B from the slope and intercept of the best-fit line for log10(jD) versus log10(Re). Linear regression results indicate a slope of –0.470 and an intercept of –0.4259, with a correlation coefficient of 0.89. These values of slope and intercept translate into A = 0.375 and B = -0.47. This result agrees very well with results presented by Pereira and Plumlee [2], who observed a Reynolds number exponent of –0.45 for Camet metal monoliths.

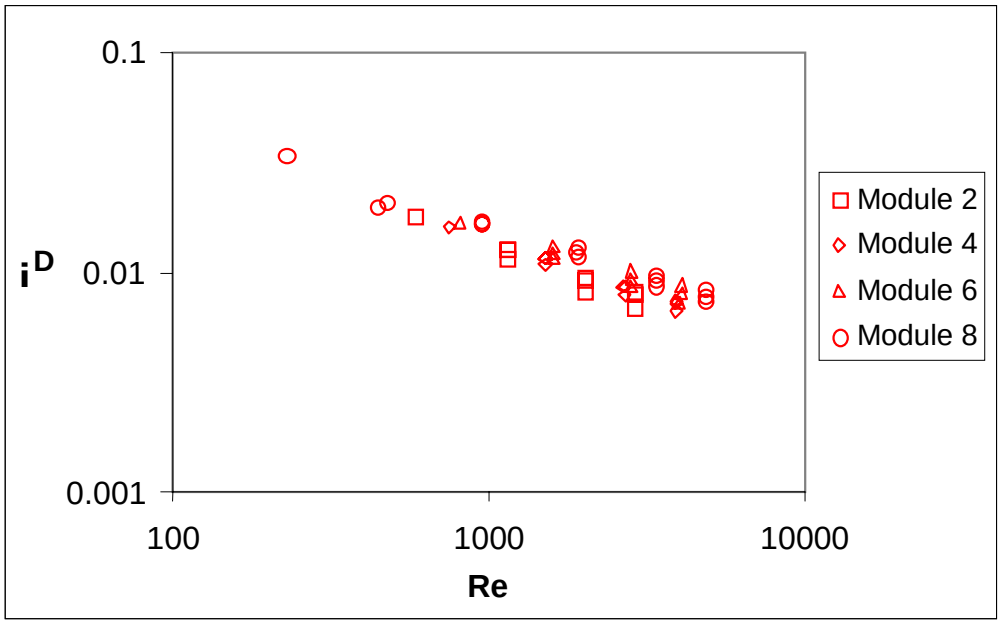

Figure 2-22 - Values of j_D versus Re are shown for methane runs in the 100% IHE modules. The data are separated by module.

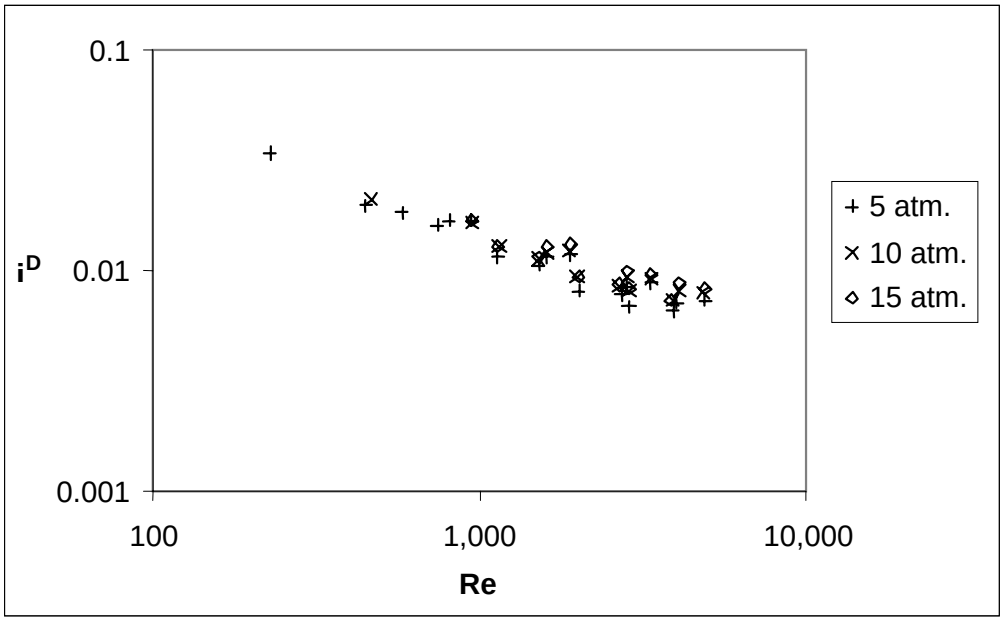

Figure 2-23 - Values of j_D versus Re are shown for methane runs in the 100% IHE modules. The data are separated by vessel pressure.

Figures 2-24 and 2-25 show linear-linear and log-log plots that compare results of the global correlation for Colburn factor with the experimental data:

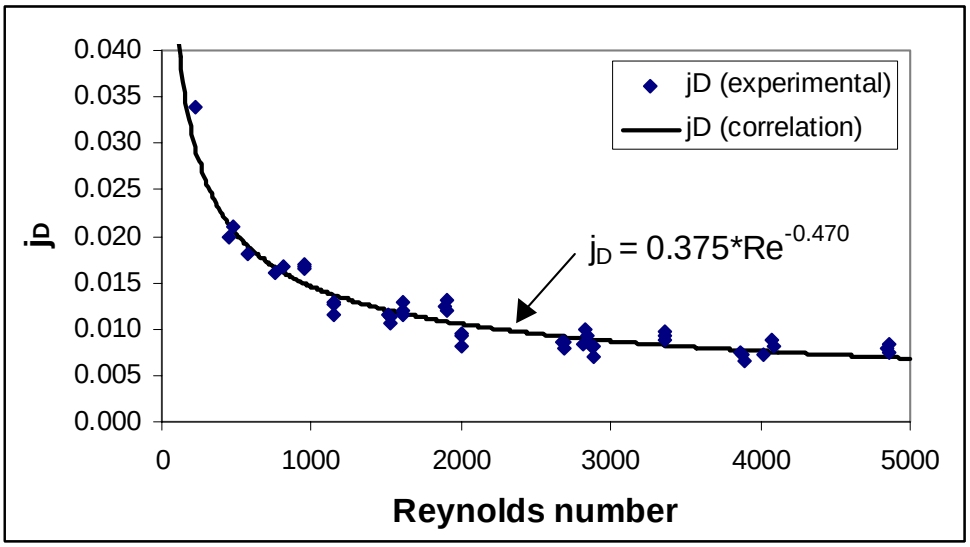

Figure 2-24 - Experimental results and a global correlation are shown for Colburn factor for mass transfer as a function of Reynolds number. (Linear-linear plot)

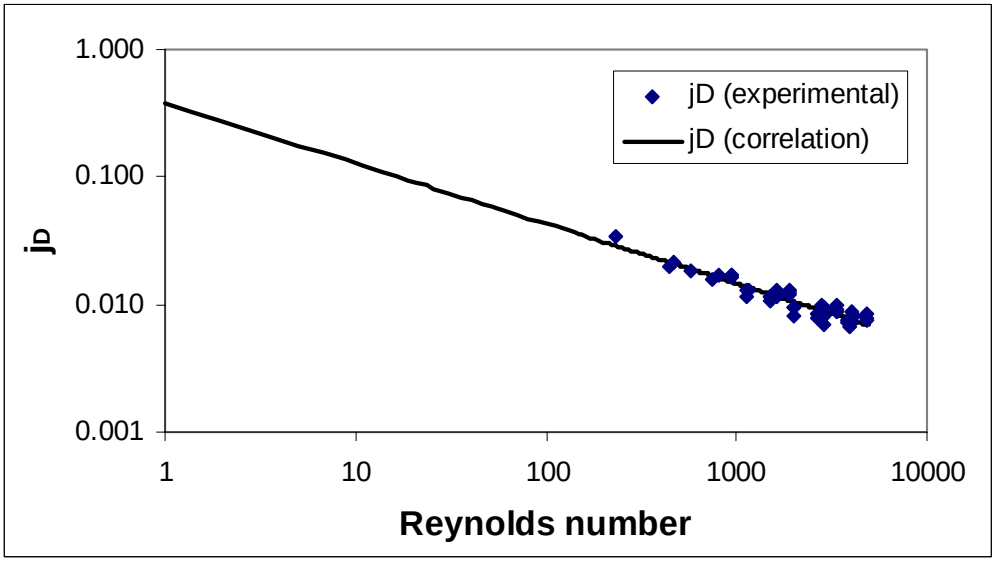

Figure 2-25 - Experimental results and a global correlation are shown for Colburn factor for mass transfer as a function of Reynolds number. (Log-log plot)

The correlation fits the data well, with the greatest variations exhibited for data at Reynolds numbers between around 1000 and 3000. This feature is not surprising since this is the regime in which we would expect inertial effects and transients in the flow‡.

2.4.3.3 Flow Splits

Because Xonon performance is influenced by the flow split between catalytic and non-catalytic channels, quantitative knowledge of this behavior is imperative for design and modeling considerations. Obviously, the area fractions and surface roughness of each type of channel contribute to determining the flow split. Indeed, earlier modeling work performed at CESI has been based on flow splits estimated from area fraction or from equating pressure drops across catalytic and non-catalytic channels. The purpose of the current research is to determine flow splits from data for fuel conversion in the modules.

Methane conversions were computed based on unburned hydrocarbons or temperature rise. When using temperature rise, for instance, the conversion, is computed as:

$$X = 100\% * \frac{T_{out} - T_{in}}{T_{ad} - T_{in}}$$

Eq. 10

Although temperature losses in the apparatus could lead to underestimating the fuel conversion, good agreement has been exhibited between the different methods for computing conversion. Figure 2-26 illustrates the percentage of fuel conversion as a function of Reynolds number for the 100% IHE modules.

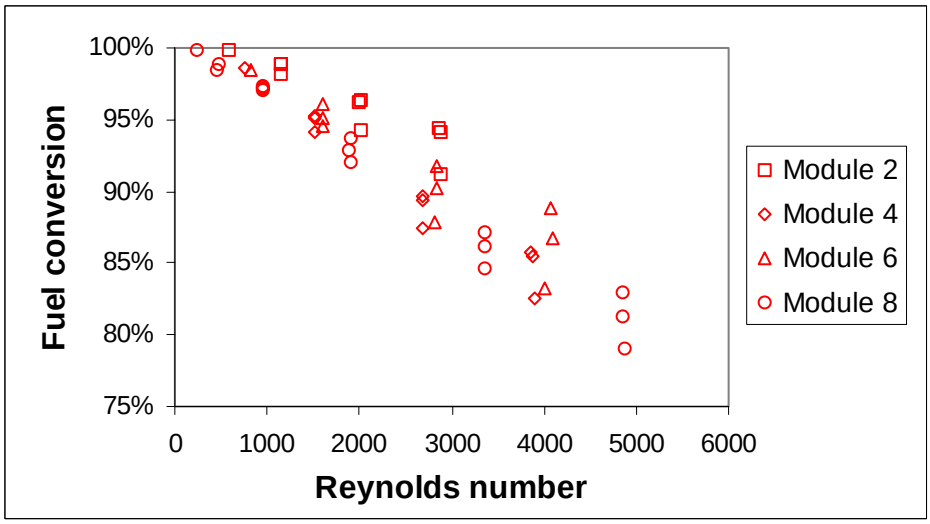

Figure 2-26 - Methane conversion is shown as a function of Reynolds number for the 100% IHE modules.

Methane conversions close to 100% are obtained for Reynolds numbers up to about 1000, beyond which significant external mass transport limitations result in hydrocarbon slip. Of course, the Reynolds number at which a decrease in conversion begins depends on the inlet fuel concentration. However, these results for the 100% modules provide further confidence in our conversion calculations and illustrate the impact of the flow on the extent of the combustion reaction. Results for 50% IHE modules are shown in Figure 2-27.

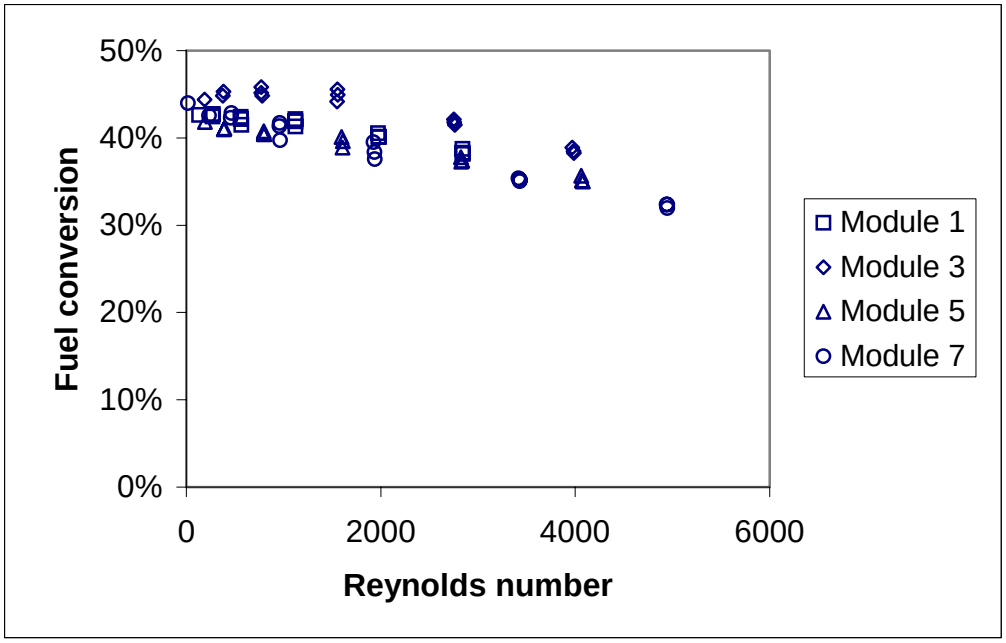

Figure 2-27 - Methane conversion is shown as a function of Reynolds number for 50% IHE Xonon modules.

For modules 1, 5, and 7, fuel conversion drops slightly with increasing Re for Reynolds numbers up to approximately 1000. This observation suggests that the fuel conversion in the 50% IHE modules for Re below 1000 should be the fraction of flow going through the catalytic channels. At higher Reynolds numbers, the decrease in conversion becomes more pronounced. Conversion data for module 3 exhibit a slightly different trend by increasing slightly up to a Reynolds number of 1000 before beginning to drop. Methane conversions at low Reynolds numbers in all of the HbC/HbC modules tend toward a limiting value that is less than 50%. Table 2-6 compares values of flow IHE (low Re) and exact area IHE for the 50% IHE modules:

Module	Type	Flow IHE	Exact area IHE
1	HbC/HbC	42.3%	45.4%
3	HbC/HbC	45.1%	47.8%
5	HbC/HbC	40.9%	44.3%
7	HbC/HbC	42.6%	46.0%

Table 2-6 - A summary of flow IHE and exact area IHE for 50% IHE Xonon modules is given

2.4.3.4 Results for HbC/RAD Module

Only one HbC/RAD module was tested, so the data analysis is quite brief. With respect to friction factor, data analysis yields A = 17.58 and B = 0.0092, indicating that the values of the friction factor are generally lower in the HbC/RAD module than in the HbC/HbC modules. Figure 2-28 shows methane conversion as a function of Reynolds number for the HbC/RAD module.

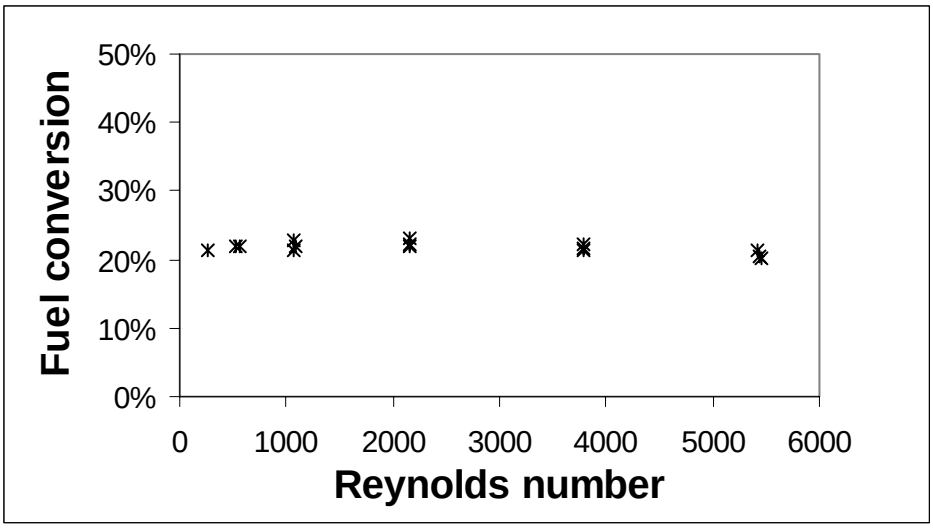

Figure 2-28 - Methane conversion is shown as a function of Reynolds number for the single HbC/RAD module tested.

The observation that the methane conversions in the HbC/RAD configuration (module 9) are roughly uniform for the entire range of Reynolds numbers considered suggest that transport characteristics in the HbC/RAD configuration are different than in the HbC/HbC systems, in which fuel conversion dropped with increasing Re. For this module, the flow IHE is 21.9% and the area IHE is 25.0%. As with the HbC/HbC modules, the flow IHE is lower than the area IHE, indicating that flow resistances (mostly due to washcoat roughness) are higher in the catalytic channels than in non-catalytic channels.

2.4.4 Validation of Catalyst Performance Models – Measurement of Specific Combustion Rates of Xonon Catalyst Materials

2.4.4.1 Methane combustion rates by metallic and oxide supported palladium

Microreactor activity tests were performed on Gen2.5-stage 2 and Gen2-stage1 catalysts both fresh and after 1200 hours aging. These measurements were typically conducted in a sequence of decreasing temperature steps of ~30-min duration from 900 to 800°C for the metallic phase and from ~800 to 500°C for the oxide phase with fixed gas composition and volumetric flow rate. Microreactor activity test results for the Gen2.5 prototype catalyst, shown in Figure 2-29, produced surprisingly high apparent activation energy for first-order methane combustion (0.5-vol% CH_4). Reproducibility for the microreactor activity tests was only about ±50% and may have been caused by several experimental factors: 1) the difficulty measuring temperature precisely (±8°C) because of thermal gradients near the catalyst bed and the lack of a direct thermocouple reading mid-bed; 2) errors in the extreme dilution of the bed (typically 2.0±0.1-mg powdered catalyst dispersed into 100-mg quartz or SiC granules); 3) a pressure gradient (5.5±1.0-atm) across the bed; and 4) drift in the flows of reactant gas vs. carrier for the mass spectrometer sampling gas.

Activation energies were reproducible (Table 2.7) for several metallic and oxide phase catalysts. These first-order rate constants differ significantly for the values used in the CLPM rate expressions

Catalyst Description	Exposed PGM, µmol/gm	Water vapor pressure, atm	Activation energy metal, kJ/mol	Pre-exponential fact metal, AU
Metallic Phase				
Gen2.5-Stage2 (PI-1)	9.6	0 to 0.44	255±16	$8.6*10^{15}$
Oxide Phase				
Gen2-Stage1 scraped foil		0		
Gen2.5-Stage2 (PI-1)	9.6	0	47.6±2.4	$1.7*10^{6}$

Table 2-7 - Oxide phase catalyst activation energies

(see Figure 2-29) although the average value of the model rate constant agreed well with the microreactor results through the key temperature range of 650 to 900°C. The new rate parameters and the effect of water vapor pressure on the methane combustion rate are incorporated into a revised CPLM version, 4.5.

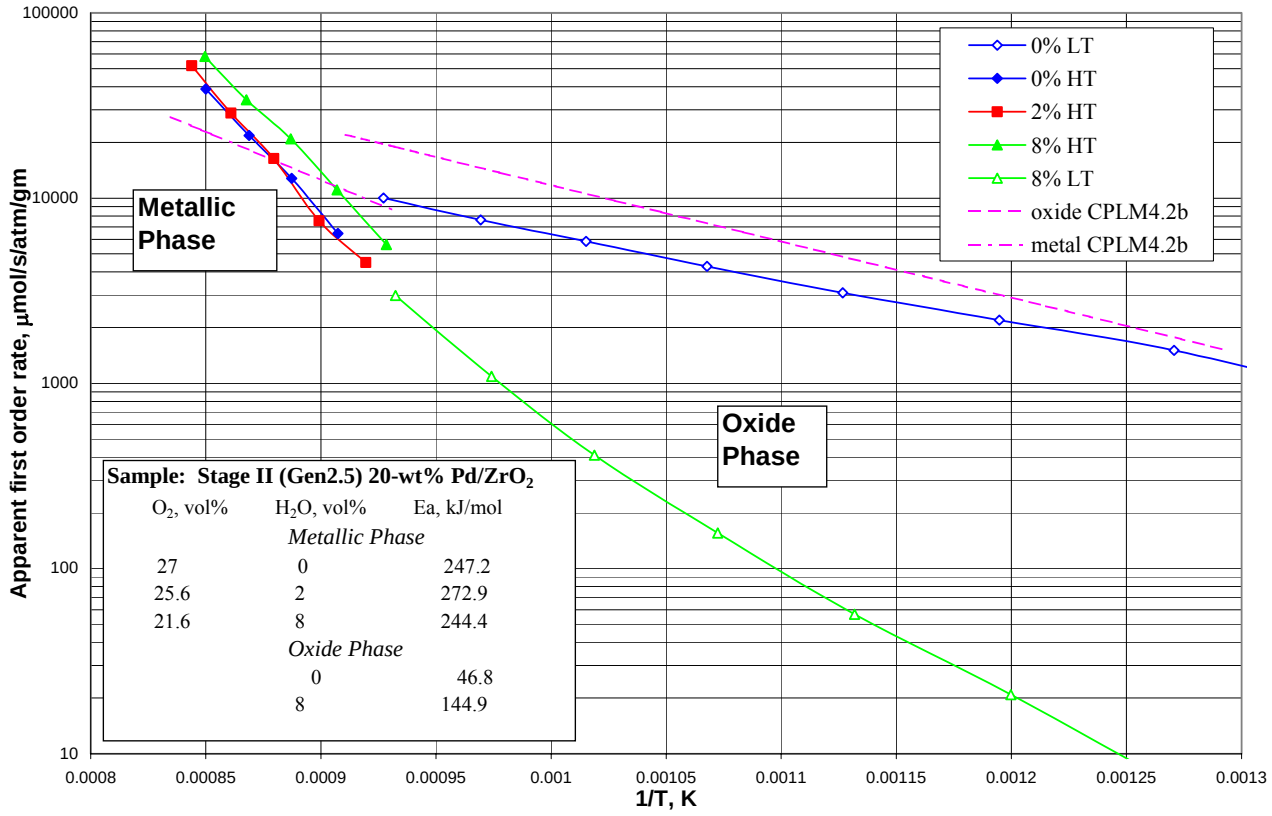

Figure 2-29 - Microreactor apparent first-order rate constants vs. reciprocal temperature for a fresh Gen2.5-Stage 2 catalyst in the metallic and oxide phase.

2.4.4.2 Effect of water vapor

As seen in Figure 11, increased concentrations of water vapor did not significantly affect the apparent first-order rate constant for the metallic phase but had a significant effect of the rate of methane combustion on the oxide phase. Fresh and aged commercial Gen2 catalyst powders were tested in the microreactor at three different levels of added water vapor in reactant gas stream, as shown in Figures 2-30 and 2-31 for the aged Gen2-Stage1 catalyst and in Figures 2-32 and 2-33 for a fresh developmental, high surface area catalyst (COM22).

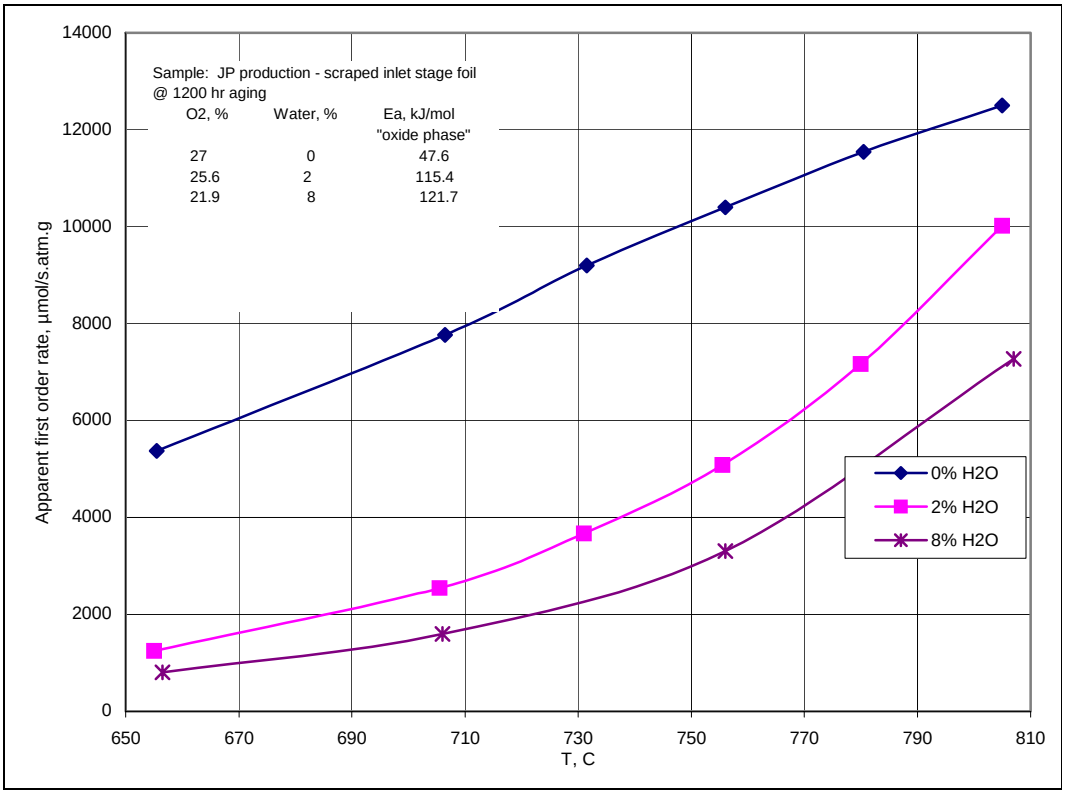

Figure 2-30 - Apparent first order rate constant for 1200-hr aged Gen2-Stage1 catalyst (linear scale)

The apparent activation energy for the aged catalyst increases from 47.6 kJ/mol to 121.7 kJ/mol for 0% and 8%-vol% water vapor, respectively.

Simple oxide vacancy substitution descriptions for water adsorption kinetics on the oxide surface could not be fitted to the data and a weakly adsorbing ensemble description (4th order in water partial pressure) seemed to work well over a wider temperature range with partial pressures ranging from near zero (no added water, only product water) to about 0.45-atm., as shown in Figure 2-34. The validity of the water inhibition kinetics can be tested with adsorption/desorption measurements, but these difficult tests are beyond the scope of the current work. The degree of water inhibition was influenced by the temperature and time held in higher

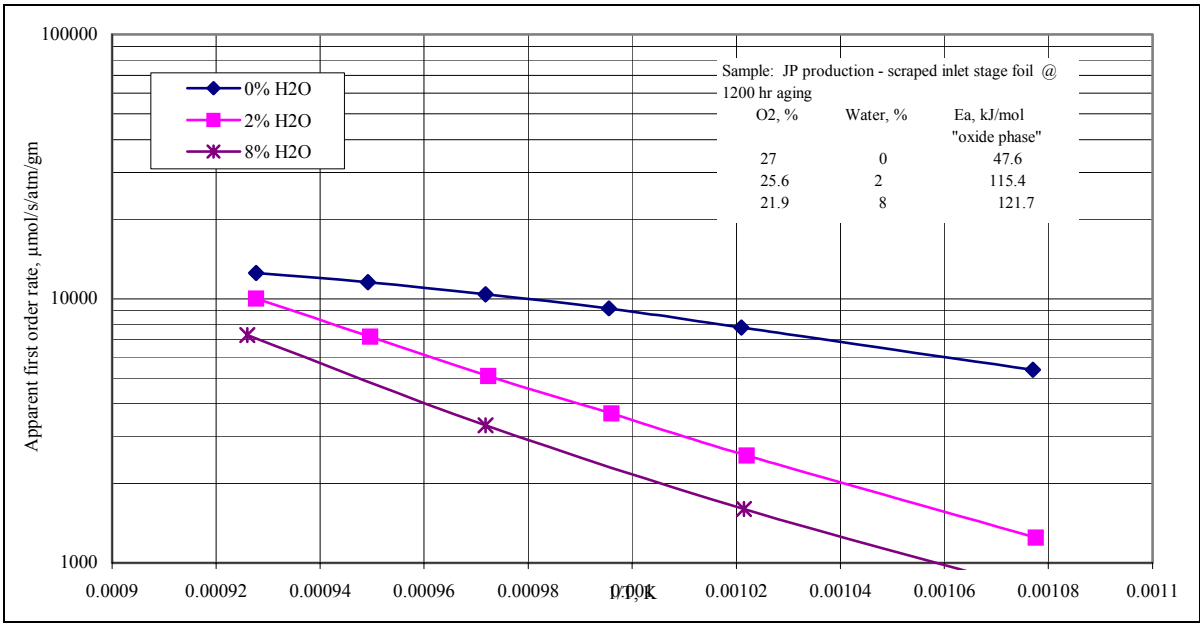

Figure 2-31 - Apparent first order rate constant for 1200-hr aged Gen2-Stage1 catalyst (logarithmic scale)

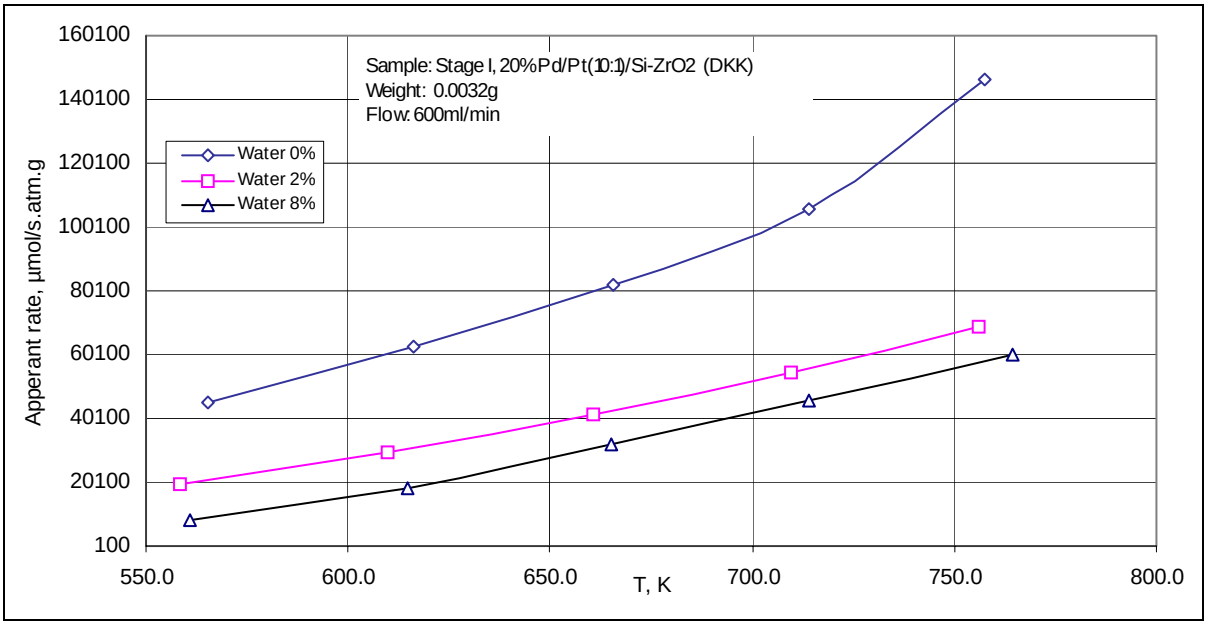

Figure 2-32 - Apparent first order rate constant for fresh COM22 - 20-wt% Pd pre-impregnated high surface area catalyst (linear scale)

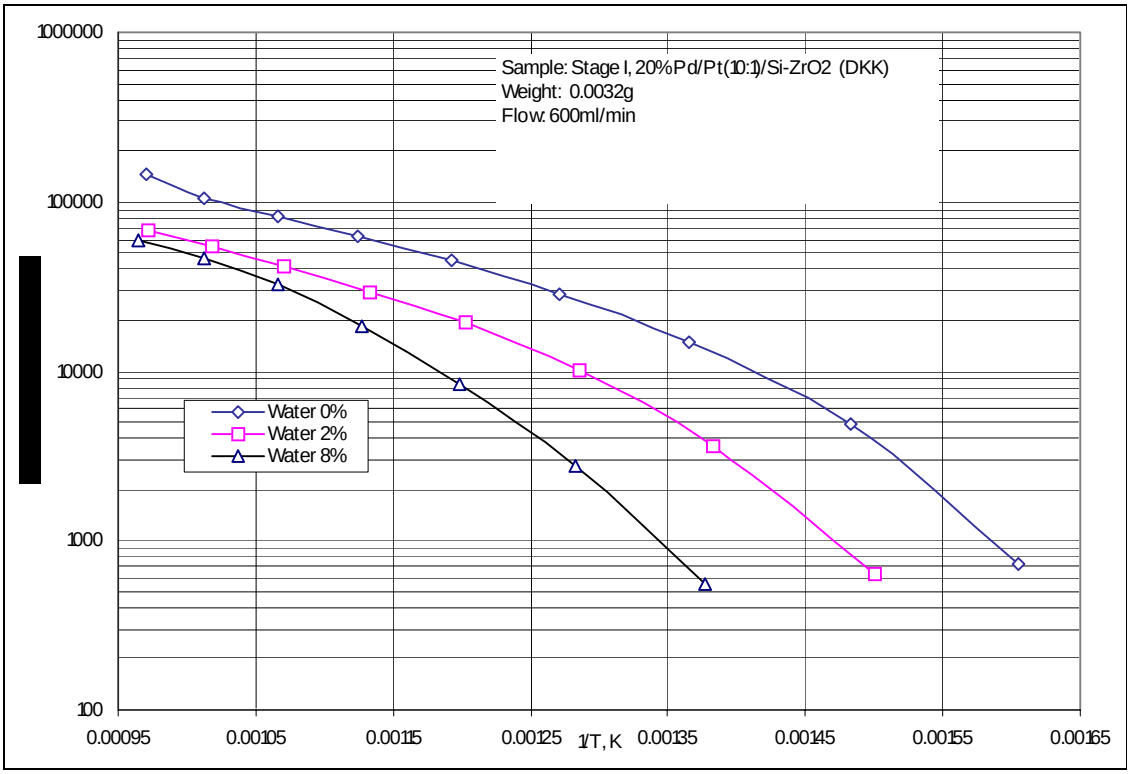

Figure 2-33 - Apparent first order rate constant for fresh COM22 - 20-wt% Pd pre-impregnated high surface area catalyst (logarithmic scale)

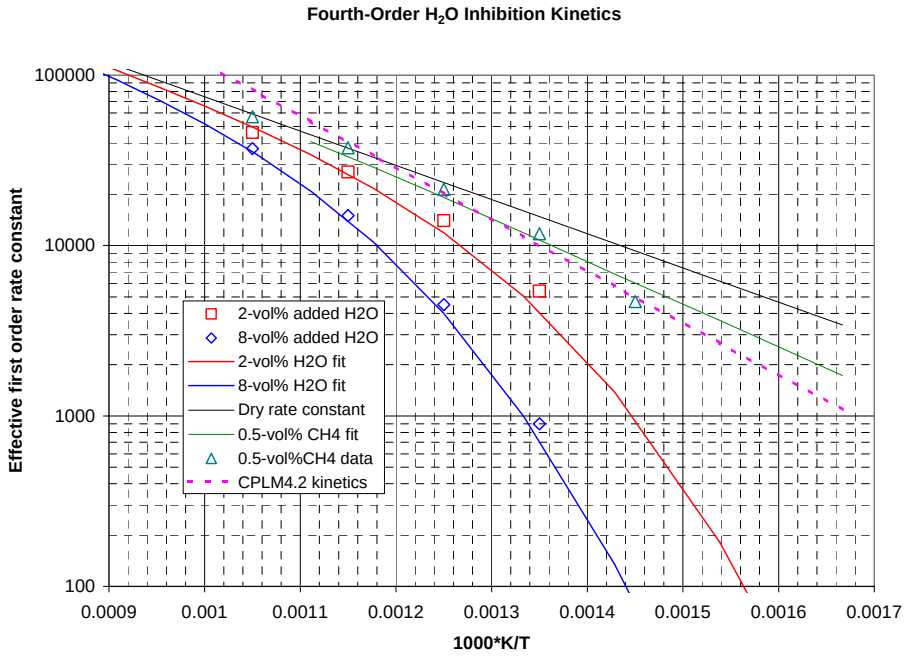

Figure 2-34 - Fourth order water inhibition kinetics for methane oxidation by a supported PdO catalyst

water vapor concentrations. As shown in Figure 2-35, short run experiments (10- to 15-minutes per data point) show a significant inhibition, but extended exposures to high water vapor levels

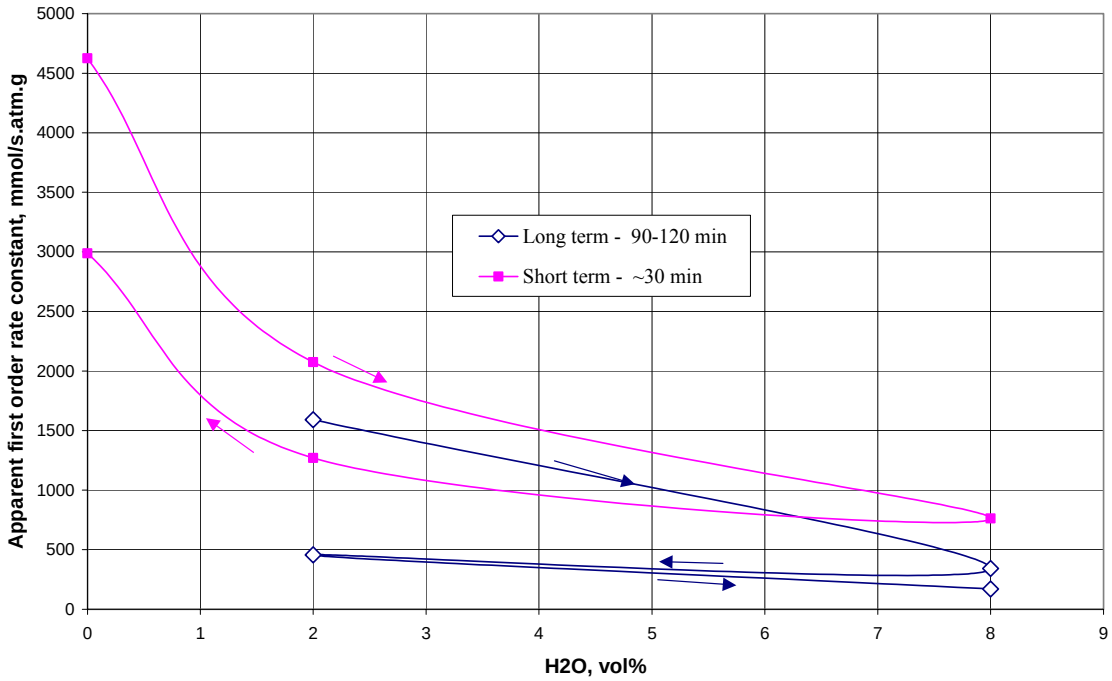

Figure 2-35 - Apparent first order rate constant for methane combustion vs. water concentration at 670°C, 5.5-atm, Gen2.5 catalyst

continued to produce lower combustion activity through period of several hours. This long-term inhibition term was reversible but the inhibition response was slower moving from low to high water vapor levels and from hotter to colder temperatures. The final values for the (short-term) kinetics of methane combustion by water vapor are shown in Table 2-8.

Kinetic Parameter	Value	Units
Water adsorption enthalpy, ΔH	58.6	kJ/mol
Water adsorption enthalpy, ΔS	-96.3	J/mol/K
Water inhibition order, n	4	NA
Rate constant activation energy, E	38.4	kJ/mol
Rate constant pre-exponential factor, A	$7.6*10^6$	AU

Table 2-8 - Kinetics of methane combustion by water vapor

2.5 Conclusions and Recommendations for Future Work

The major objectives of the efforts to increase catalyst life were successfully accomplished under all subtasks of the Task 1.1 – Increased Catalyst Life. Specific conclusions and recommendations for commercialization or future research and development work follow:

2.5.1 Development of Stable Hot Stage Materials – Presintered Palladium-Based Catalysts

- Presintered Pd-based hot stage catalysts were developed that show superior hydrothermal stability relative to the first generation materials.
    - Pre-impregnated low area zirconia supporting oxide powders showed superior resistance to thermal aging compared with physically-mixed fine powders and the first generation catalysts
    - Rates of decrease in exposed (surface) metal for the PI catalyst was about half that of current commercial and PB catalysts under similar thermal aging conditions.
    - Subscale tests show comparable stage conversion as with first generation catalysts.
    - Recommend immediate development and adoption of presintered PI catalysts for application in CESI's commercial combustion modules.
- Development and commercialization of PI hot stage catalysts will require modification of the upstream and hot stage foil-pack structures and manufacturing process development.
    - Subscale tests in two stage catalyst system show good conversion levels – preliminary design work suggests that increasing first stage (and lower hot stage conversion) would compensate for the decreased activity and potential oxide/metal hysteresis of the PI catalyst material.
    - Need to scale-up powder production processes and optimize washcoat slurry formulation in preparation for commercialization.
- Additional aging (HPAR) tests should be conducted to validate the PI-PS catalysts for extension of catalyst life by the indicated factor of two (~8,000- to 12,000-hr).
    - Must examine temperature range from 800 to 850°C to determine sintering rates relevant for the oxide phase.
    - Must examine effect of gas composition and pressure (especially water vapor concentration) on sintering rates.

2.5.2 Development of Stable Hot Stage Materials- Non-Platinum Group Metal Catalysts

- Two non-platinum group metal (NPGM) oxides, ceria and hematite, have been developed and warrant future examination for their application as durable hot (third) stage catalysts.
    - Two different thermochemically compatible supporting (dispersing) refractory oxides were found for both active components and their promoters
    - Different activity-enhancing promoters were found for both active components.
    - Both systems showed superior performance relative to the PI-PS catalyst and aged first-generation Pd-based catalysts

- Small amounts of a candidate promoter, in the 2- to 5-wt% range, were found to be effective in promoting activity of hematite (Fe_2O_3) and this system, with compatible supporting oxide, is chosen for future development.
    - Promoted hematite is inexpensive and potentially has low volatility relative to other transition metal oxides.
    - Promoter may be present as a solid-solution, enhancing the redox potential of Fe_2O_3.
    - Ceria co-catalysts and many transition metal oxide "promoters" were effective only at significantly higher (10-wt%) levels.
- For ceria (CeO_2), an effective promoter was found when added in substantial concentrations (2:1, Ce:promoter).
    - The promoter was also active as a base-component and with ceria promotion (1:2, Ce:promoter) but relative costs favor the ceria-rich formulation.
    - Another promoter chemically similar to the first was also shown effective, thus validating the promoting effect.
    - Many candidate promoters (including the hematite promoter) were not effective with the ceria-based formulations.
- Considerable development effort remains to further optimize and select the most effective NPGM catalyst.
    - This and the success of the PS approach for Pd-based catalysts led to the latter being selected for commercialization at this time.
    - Preliminary design and subscale testing of a three-stage catalyst with candidate NPGM should be conducted and conversion stability examined (~300-hr)
    - Accelerated aging (HPAR) tests should be conducted to determine the potential of these two formulations for extending overall catalyst life to 24,000-hr.

2.5.3 Validation of Catalyst Performance Models – Measurement of Flow Distribution and Mass Transfer in Xonon Modules

- A good correlation friction factor in the form, f = A/Re + B, was found for HbC/HbC modules, with global values of A and B.
    - The accuracy of the friction factor correlation allows its use in the CPLM design tool for determining flow distribution within CESI foil packs.
    - The A parameter is fully compatible with laminar flow and thus can be extrapolated with confidence to flow rates well below those tested in this study.
    - No obvious trend of parameter B, representing the fully-turbulent flow regime, was discernable with respect to catalyst loading, channel height, or foil configuration.
    - Values of friction factor in the HbC/RAD foil pairs were generally lower than in the HbC/HbC pairs as expected for the herringbone/straight channel geometry.

- The Colburn factor for mass transfer 100% IHE HbC/HbC foil pairs was well correlated by a relation of the form, $j_D = A*Re^B$.
    - The measured exponent, B = –0.47, is in good agreement with a reported value of –0.45 for Camet metal monoliths.
    - In all cases, flow IHE was several percent lower than area IHE as expected from differences in channel size.
    - Transport characteristics in the HbC/RAD configuration are different than in the HbC/HbC systems for increasing Reynolds number up to around 5000; methane conversion in the 50% IHE HbC/HbC modules tended to decrease, while conversion in the HbC/RAD module remained fairly constant over these flow conditions.
- Additional work is recommended to further friction factor and transport within foil packs:
    - Conduct experiments with uncoated foils to determine data reproducibility and examine the B parameter in friction factor measurements.
    - Further differentiate friction factor correlations for the HbC/HbC and HbC/RAD packs and quantitatively relate the B values to module specifications, e.g., surface roughness or herringbone segment length and angle.
    - Perform a detailed computational fluid dynamics analysis of a Xonon module in order to gain additional insight into the relevant physical processes.

2.5.4 Validation of Catalyst Performance Models – Measurement of Specific Combustion Rates of Xonon Catalyst Materials

- The new data will allow accurate rate expressions to be used for both the PdO and Pd metal phases and allow a more accurate description of the effect of temperature, pressure and gas composition (especially water vapor content) on combustion rates.
    - The activation energy of supported Pd metal catalysts is significantly higher than that currently used in the CPLM catalyst-life design tool.
    - The effect of water vapor on the apparent first-order methane combustion rate was determined for a range from 0- to 0.45-atm partial pressure H_2O and the rate was found to vary approximately as fourth-order Langmuir-Hinshelwood inhibition. This is a unique and important result of the Task 1 kinetic measurements.
    - The new rate expressions have been incorporated into the CPLM design tool and allow an assessment of ambient humidity and fuel conversion on low temperature combustion rates. This is useful for interpretation of rig test data and for predicting catalyst module performance near the end of catalyst life.
- Additional future kinetic investigations are recommended:
    - Determine the effect of oxygen partial pressure on both metallic (probably negative order) and oxide phases (probably insignificant).
    - Examine in detail the long-term (hours) decay in catalyst activity observed for water vapor levels above 0.1-atm at temperatures below 600°C. This effect warrants further examination but is beyond the scope of the current program.

2.6 References

Bird, R.B., Stewart, W.E., and Lightfoot, E.N. (1960) Transport Phenomena. John Wiley & Sons, New York.

Gulian, F.J., Rieck, J.S., and Pereira, C.J. (1991) "Camet Oxidation Catalyst for Cogeneration Applications." Ind. Eng. Chem. Res. 30, 122-126.

McCarty, J. G. (2000) "Durable Catalysts for Cleaner Air." Nature 403, 35-6.

McCarty, J. G., Quinlan, M. A., and Wise, H. (1988) "Catalytic Combustion of Methane by Complex Oxides." Proceedings of the 9th International Congress on Catalysis, Vol. 4, 1818-1826, Phillips, M. J. and Ternan, M., eds., The Chemical Institute of Canada, Ottawa.

Pereira, C.J., and Plumlee, K.W. (1992) "Grace Camet® Metal Monolith Catalytic Emission Control Technologies." Catal. Today 13, 23-32.

Zarur, A. J. and Ying, J. Y. (2000) "Reverse Microemulsion Synthesis of Nanostructured Complex Oxides for Catalytic Combustion." Nature 403, 65-7.

2.7 Acknowledgements

The catalyst development tasks described in this section were conducted by members of CESI's Materials Development and Process Development teams. The PI-PS catalyst materials were developed by Scott Magno and Dr. Valery Sokolovskii; the PB-PS catalysts were developed by Mike Cooper. The refactory supporting oxides and non-PGM catalyst materials were developed and characterized by Scott Magno and Dr. Xian-dang Wang. All catalyst materials were characterized by Mira Kaczmarek, Dr. Xian-dang Wang, and Ginger DeMars. Scott Magno and Dr. Jon McCarty designed the HPAR and MCSR systems which were developed and operated by Scott Magno. The friction factor and mass transfer testes were conducted and analyzed by Dr. David Ginter with the assistance of Dr. Jeffery Zalc and Jon McCarty. Dr. Gigoriy Malukhin, with Jon McCarty, designed the microreactor test system; kinetic testing and sintering rate measurements were conducted and analyzed by Gigoriy Malukhin.

III. Cost Reduction - Task 1.2 – Module Cost Reduction

3.1 Summary

DOE Components Task 1.2 objectives included the evaluation of design concepts intended to reduce product costs and improve component lives. The overall objective was to improve catalytic combustion system costs to better position the technology for commercialization.

Several design concepts were considered. A life cycle cost model was developed to facilitate conceptual cost comparisons between the various designs. In the end, the "Can-in-Can" container approach was down-selected and taken through Detail Design Review as part of the DOE Components program. Subsequently, the "Can-in-Can" design was taken through fabrication and test as part of the GE10 catalyst module development program.

Included in the Preliminary and Detail Design phases were thermal-stress analyses and subsequent life-cycle and lifetime analyses for the container components and axial supports.

3.2 Background

DOE Components Task 1.2 objectives included the evaluation of design concepts intended to reduce product costs and improve component lives. The overall program considered the catalyst container and catalyst axial supports, but did not address catalyst cost or durability.

The approach was to take design, test, fabrication, and assembly lessons learned from earlier proof-of-concept containers and apply them to new designs. In addition, new and modified concepts were brainstormed and considered along with prior ideas and lessons learned. In addition, manufacturing and durability risk issues were identified. Durability risk mitigation included analyses and testing to sufficiently characterize the durability of the catalyst axial supports and container. Manufacturing process risk mitigation included catalyst axial support welding process development, and weld defect tolerance testing.

3.3 Discussion

3.3.1 Container Design

3.3.1.1 Container Cost Reduction and Commercialization

An effort was initiated in early May 2001 to prepare the Xonon® catalyst module designs for a higher rate of production. The commercialization effort considered the GE10 product line a more likely candidate for volume production than the KHI M1A-13X product line. For that reason, the GE10 was the chosen product line to be the "guinea pig" for further module commercialization considerations.

The initial effort consisted of defining the design goals which would then form a set of criteria by which to measure design concepts' merits. These design goals were listed as:

- Fabrication Cost (initial costs)
- Life Cycle Cost (total costs over useful life period)
- Assembly/Disassembly Time
- Leakage Potential (CDP bypassing catalyst stages, and intra-module)

- Assembly Issues (Tooling Required, Ease, etc.)
- Disassembly/Maintainability
- Reliability
- Producibility
- Flameholding Margin
- Handling/Transportation Considerations
- Technical Risks to development (i.e. how difficult will it be to get it to work? Do we have this experience already?)

Target values were then placed on these goals as follows:

- Fabrication Costs, $22,000 for container items, and $15K for axial supports
- Life Cycle Costs, $8000 per year over ten year period (later studies showed this is probably not achievable without module life extensions out to 16K hours
- Assembly Time, 4 hours at mature production
- Disassembly time, 2 hours at mature production
- Leakage Potential, <1% of CDP total
- Assembly Issues, Goals: 8 on qualitative scale of 10 considering: No restraining fixtures, minimize number of special tools or machines required to build or teardown, maximize use of hand/air tools
- Disassembly/Maintainability issues, Goals: 8 on qualitative scale of 10 considering: No restraining fixtures, minimize number of special tools or machines required to build or teardown, maximize use of hand/air tools
- Reliability, Goals: 10 on qualitative scale of 10, minimize number of prime-reliable components, minimize potentials for any component failure, trap any component that, if broken, may enter flowpath (or otherwise make it prime reliable)
- Producibility, 8 on qualitative scale of 10: maximize the use of inexpensive low variation machining/casting processes, minimize the total number of manufacturing processes/setups, avoid the use of special manufacturing processes such as coatings, heat treatments, etc.
- Flameholding, “digital” scale of yes/no for sustaining flame, use the .125 diameter criteria in flowpath, keep dead volumes to a minimum, keep flowpath steps below .025
- Handling/Transportation Considerations, Goal of 8 on qualitative scale of 10: incorporate handle features for easy handling, design components to withstand pallet drop equivalent to 2.5G

3.3.1.2 Design Concepts Considered

Initial design concept considerations began with the present-day designs and prior design concepts that had been considered in the 1998/1999 timeframe (see Weakley/Barnes report dated January 5, 1999). Since 2.5 years had elapsed from the 1998 cost reduction work, the development container/supports designs for the KHI M1A-13X and GE10 modules had also been advanced beyond their 1998 status. In addition, lessons learned were provided and fed into the design team for the Year 2001 project. These lessons learned included enhanced product cost knowledge as a result of CESI Procurement quotations obtained on the existing GE10 prototype container.

The design team also had to consider the practicalities of the production volumes projected for the Y2002-Y2007 time period. With production volumes in only the 10/year to 30/year range, it seemed unreasonable to commit to production processes where commitments to expensive high-volume MFG tooling (investment cast dies, hydro form tools, etc.) were required. Therefore, an objective was to work within a low-volume environment, but one which could be easily reproduced even in a medium-volume environment.

The initial screening of options included:

(a) Machined casting ring and welded can assembly (same as GE10 prototype but cost reduced on the raw-material end)
(b) A "Can-in-Can" arrangement, with machined cast rings inserted into an outer sleeve
(c) A "Split-Can" arrangement utilizing a machined cast case with inserted slotted machined rings.

Each of these options will be discussed below.

3.3.1.2.1 Machined Casting Rings and Welded Can Assembly

This configuration would be essentially the same as the "Prototype Module A and B" configuration, except incorporates less expensive raw material (see Figure 3-1).

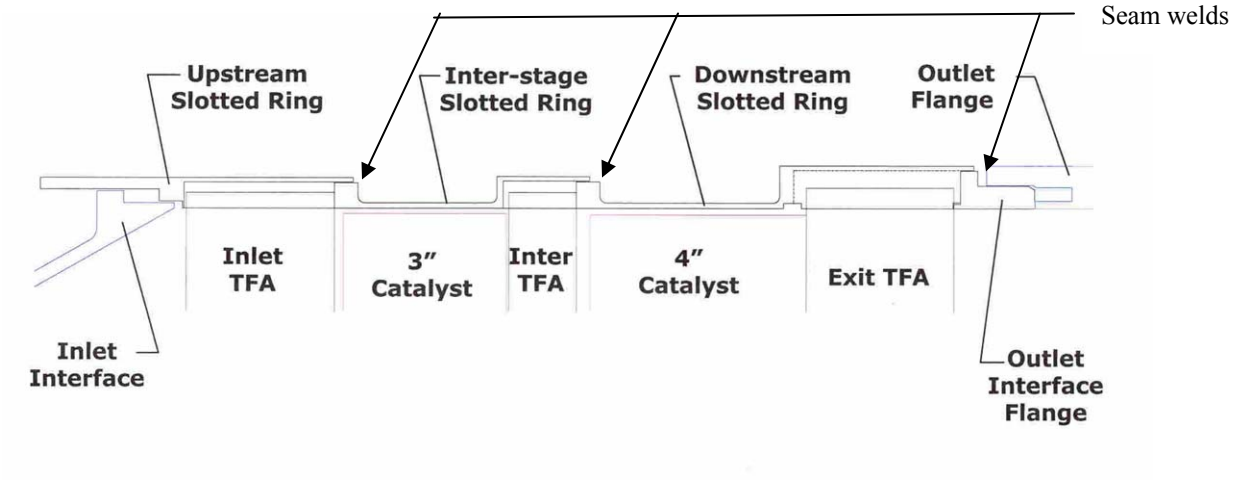

Figure 3-1 - Machined Casting Rings and Welded Can Assembly

In addition, producibility changes such as: rolled tips on TFA's so that there is less material removal required on the slotted rings.

Pros

1. Very low risk of leakages
2. Allows for at least two re-uses of rings
3. Lots of CESI experience with similar configurations
4. Cost basis better understood

Cons

1. Weld distortion of bosses during assembly weld
2. Assembly logistics and time with circumferential welds

3. Challenging ring slots since slotted only through portion of wall, this drives a more expensive material removal process that if the slots were completely through the wall
4. Disassembly time and logistics due to circumferential welds
5. Re-use capability of cans deemed limited to 3-uses due to consumption of land with each re-weld preparation; it may be possible to extend the number of re-uses with weld-repair operations, but this scenario requires further research

3.3.1.2.2 Can-in-Can Assembly

This configuration (see Figure 3-2) was first proposed in 1998 as part of the Barnes/Weakley study as a means of eliminating the assembly weldments, thereby improving assembly cycle time. This also carries the potential for greater dimensional stability during the assembly process, since no assembly weld distortion will occur.

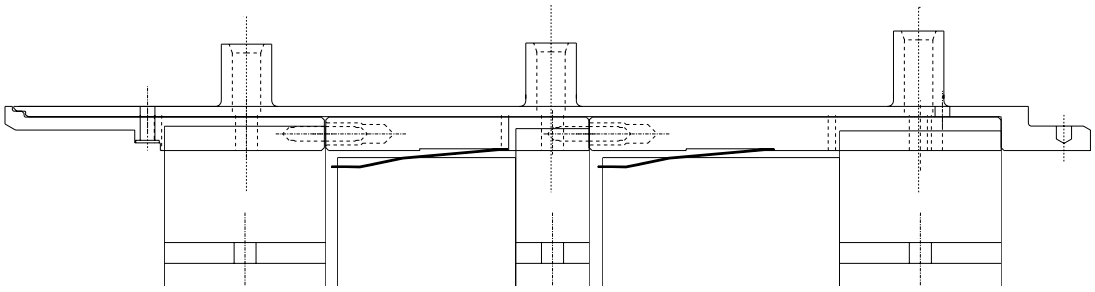

Figure 3-2 - Can-in-Can Assembly

Pros

1. Assembly time expected to be shorter due to elimination of circumferential welds
2. Expected re-use capability extended to an indefinite period, but conservatively assumed to be five re-uses with some "roundness true-up" expected to prepare for re-use
3. Expected greater dimensional control on bosses due to weld elimination
4. Lots of experience with similar configurations for machined rings
5. Cost basis reasonably understood for machined rings

Cons

1. Cost basis of outer can not well understood
2. Can-in-can outer container configuration selected for GE10 was not fully optimized to take advantage of sheet metal construction, but an acceptable configuration with a long cylinder connected to an aft flange could be manufactured from either a casting or from sheet metal welded or brazed to an aft flange
3. Higher mechanical risk at beginning of development program due to uncertain thermal stresses (later to be offset by additional analysis)

3.3.1.2.3 Split-Can Assembly

This configuration borrows design features from gas turbine compressor cases in that it utilizes a machined-casting split into two halves that bolt together along radial flanges (see Figure 3-3).

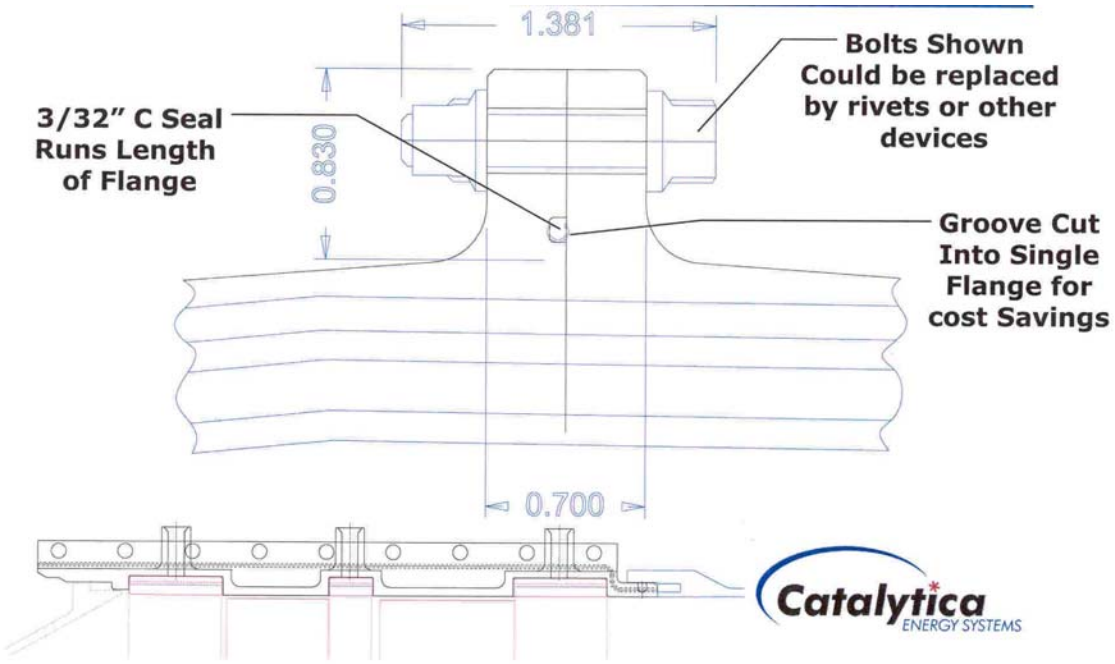

Figure 3-3 - Split-Can Assembly

Pros

1. Assembly time expected to be shorter due to elimination of circumferential welds
2. Expected re-use capability extended to an indefinite period, but conservatively assumed to be five re-uses with some "roundness true-up" expected to prepare for re-use
3. Reduced part count

Cons

1. Higher structural/mechanical risk of success
2. Potential for leakage at flanges
3. Radial thermal gradient a risk for stresses
4. NRE of casting tooling thought inappropriate at this stage of CESI experience base
5. Requires split at finger seals along flange locations
6. Uncertain dimensional stability

3.3.1.3 Life Cycle Cost Model

Since cost reduction was a major objective of this program, it was important to have a method to evaluate comparative expected costs for the various options. In addition, the option to re-use hardware for multiple builds provides the opportunity to offset initial cost with lower re-use cost. Therefore, a life-cycle cost model was created to look at a ten-year time horizon. The model's degrees of freedom include:

(d) Component and quantity per assembly, in this manner, the model BOM can be customized for each unique configuration considered
(e) Component initial fabrication costs (value determined by direct quotation costs or from similarity comparison); Use of costs assumes a comparative accuracy in fabrication costs across the design alternatives
(f) Assembly and disassembly hours; each unique configuration has implications for assembly costs and disassembly costs and needs to be reflected into the "true" costs for comparative purposes
(g) Inflation factor; allows for the year-over-year increase in product costs
(h) Discount Factor; accommodates the "cost of money" and tends to place more value on the nearer term flows of cash; consistent with net-present-value methodology
(i) Component replacement frequency (or component life) in terms of 8000 hour yearly intervals

Outputs from the model include expected initial fabrication and assembly costs, and a yearly average Life Cycle Cost.

The values obtained for each design alternative were fed into the LCC model. The summary is provided in Table 3-1.

Option	Option Description	Container Initial Purchase and Assembly Cost	Container Annualized Life Cycle Cost based on 8000 hr interval	12000 hr interval annualized LCC	16000 hr interval annualized LCC
1	Current As-is, with machined forgings, welded circumferential joints, no design changes	$33,415	$19,702	$13,182	$12,011
2	Conceptual "expendable" sheet metal can with 8000 hr interval	$23,086	$14,949	$13,477	$8,484
3	As-is, with machined cast rings, welded circumferential joints, no other design changes	$26,800	$12,446	$9,953	$8,473
4	Can-in-can, with machined cast outer case, machined cast inner rings	$25,465	$10,558	$8,687	$7,897
5	Longitudinal split-case, with machined cast outer case, machined rolled-ring inner rings	$23,001	$9,871	$7,953	$7,273

Table 3-1 – Container Evaluation Summary

As you can see from the summary table, life cycle costs are strongly driven by the assumed values for:

(a) Maintenance interval,
(b) Initial purchase costs, and
(c) Hardware re-use capability

3.3.1.4 Final Design Down-Selected

The targeted design options are compared using the design goals and objectives. No attempt was made at weighting the parameters, but each factor was given a 1-3-5 scoring. The scoring philosophy is shown in the Table 3-2.

		Normalized Score		
Objective	**Measurement units**	1	3	5
Initial Purchase Costs	Dollars	>$30,000	<$27,500	<$25,000
Annualized Life Cycle Costs	Dollars	<$20,000	<$15,000	<$10,000
Assy Time	equiv hrs	<20 hrs	<10 hrs	<4 hrs
Disassy time	equiv hrs	<20 hrs	<10 hrs	<4 hrs
Leakage potential	Time to 1% Creep	0.50%	0.10%	0
Assy issues	Scaler (1-5) on hassle factors	fair	good	excellent
Maintainability	Scaler (1-5) on hassle factors	fair	good	excellent
Reliability	Scaler (1-5)	fair	good	excellent
Producibility	Scaler (1-5)	experience shows some potential for issues	estimated to be producible but experience not as comparative	excellent experience and solid comparative experience
Flameholding margin	Scaler (1-5)	high risk	med risk	comparative experience, low risk
Handling considerations	Scaler (1-5)	high risk	med risk	comparative experience, low risk
Technical risks	Scaler (1-5)	more than two technical risk items	one or two low risk items which can be mitigated with analysis/testin	little to no technical risks due to similarity with prior designs

Table 3-2 – Container Scoring Philosophy

The option scoring summary is provided in Table 3-3

	Design Option				
Objective	**Can-in-can**	**Current but with cast rings**	**Current**	**Conceptual expendable**	**Split Case**
Initial Purchase Costs	3	3	1	5	5
Annualized Life Cycle Costs	5	3	3	3	5
Assy Time	5	3	1	1	3
Disassy time	5	3	1	1	3
Leakage potential	3	5	5	5	1
Assy issues	5	3	3	1	1
Maintainability	5	3	3	1	3
Reliability	5	3	3	3	1
Producibility	3	3	3	3	1
Flameholding margin	5	5	5	5	3
Handling considerations	5	3	3	3	3
Technical risks	3	5	5	1	1
Total Score:	52	42	36	32	30

Table 3-3 – Container Option Scoring Summary

As can be seen, the can-in-can approach numerically scored the highest total. In addition, a technical review meeting held July 18, 2001 also agreed on the down-select to the can-in-can approach.

3.3.1.5 Can-in-Can Design Features and Benefits

After the configuration down-select, the can-in-can approach was advanced through detail design. Potential manufacturing suppliers were provided preliminary drawings from which to provide CESI with quotations. The outer can was quoted on in both a sheet-metal weldment construction as well as a machined-casting construction. Both options showed great promise but with the machined-casting construction delivering the lowest quotation at the time. In the long run, the sheet metal weldment fabrication approach would most likely provide the lowest-cost solution for the given geometry once the initial costs of tooling were addressed.

The basic configuration of the can-in-can arrangement is provided in Figure 3-4. A three-inch stage 1 catalyst and a four-inch stage 2 catalyst are each supported downstream by thermally free axial supports (TFA's). Axial load is shared from the interstage and outlet TFA's through a reaction at the center shaft, and then back up through the shaft inlet cap to the Inlet TFA. Each TFA reacts a portion of its axial load through the strut contacts against the rings and outer container. All internal axial loads are ultimately reacted out through the outer container and through the forward bosses to the combustor case. Figure 3-5 is the free-body diagram of this arrangement.

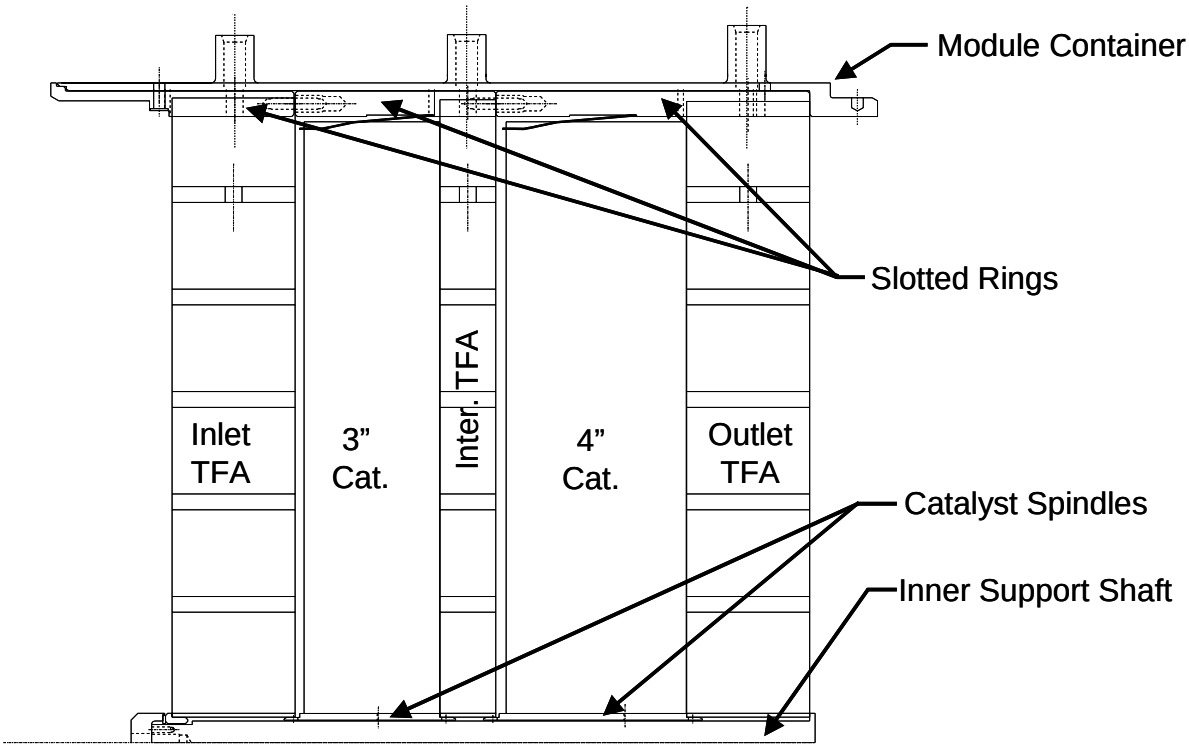

Figure 3-4 – Basic Can-In-Can Configuration

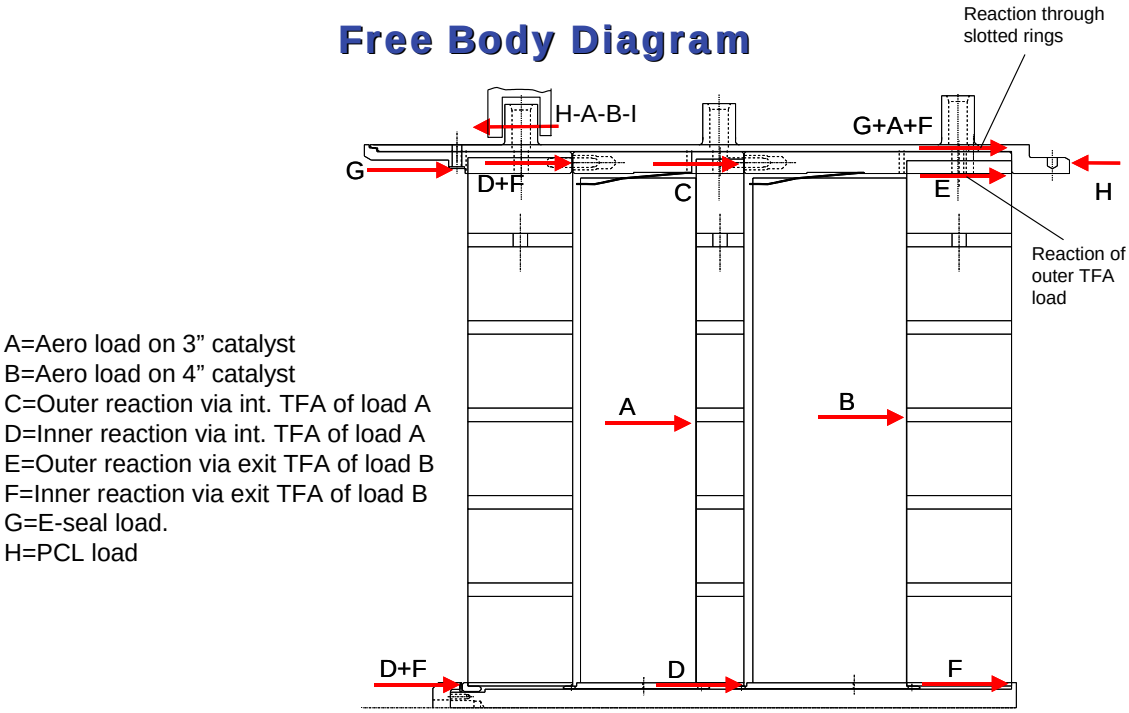

Figure 3-5 – Can-In-Can Arrangement Free Body Diagram

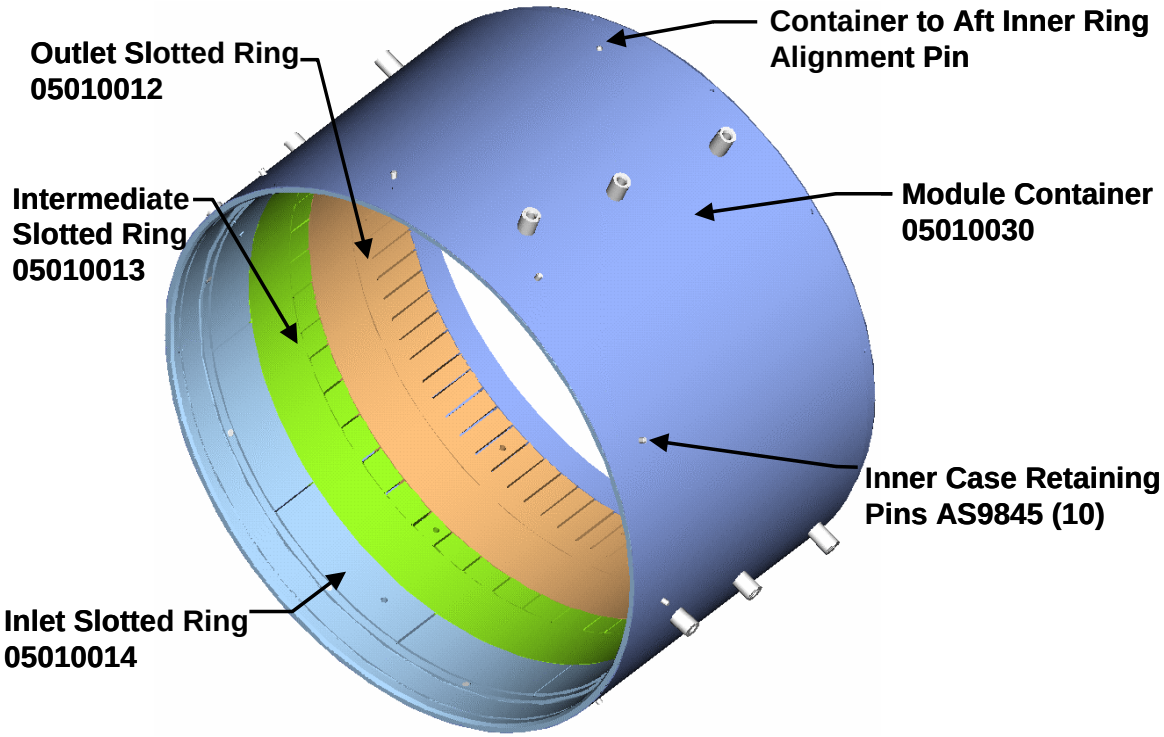

Figure 3-6 – Slotted Ring Location

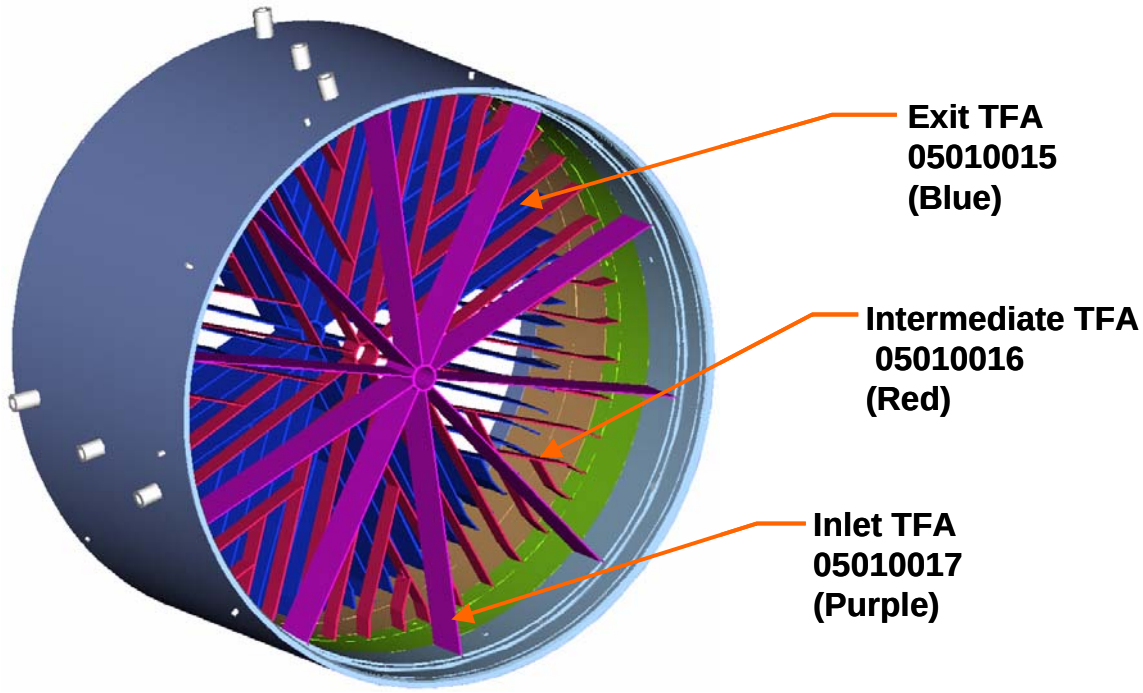

Figure 3-7 – TFA Location

Each slotted ring uses simple turning and drilling operations, followed by milling, slitting saw, or rotary cutter removal of slot material. Through-slots provide more MFG process options and the potential for more cost effective material removal than the prior-design partial-slot, which necessitated either EDM operation or right-angle milling. The TFA's design change which allows each strut to enter the ring perpendicular to the line of tangency (through the axis of rotation) also permits each slot to have the same width and reduces machining setup costs accordingly. This concept is shown in Figure 3-6.

The inlet TFA was simplified by reducing the total number of struts. The prior-art used the same basic design as for the exit-TFA with 80 struts. The new design utilizes 12 radial struts, each strut having on branch for a total of 24 struts. This approach simplified the manufacturing process and will reduce cost of the part from 50% to 65%.

The exit TFA design was simplified by eliminating a T-Bar feature on each of the strut tips (and associated capturing features on the container structure). TFA Locations are shown in Figure 3-7.

3.3.2 Container Durability

3.3.2.1 Transient Thermal Stress Analyses

Thermal and structural evaluation of a concept for the catalyst container has been completed which shows the design is potentially feasible. Initial concerns were the relative thermal expansion of the inner and outer cylinders allowing leakage through the annular gap complicated further by high thermal stresses that could deform the cylinders. Transient thermal stress finite element analyses predict that a reasonably small inner to outer cylinder clearance will close during operation but not cause stresses in excess of yield.

3.3.2.2 Thermal Expansion Gaps

The components of the commercial container were designed to avoid any thermal interference and associated thermal stress. The radial fits for the TFA's are described below. Figure 3-8 shows the ledges and gaps that were examined under cold build, FSNL, start acceleration, and engine trip conditions. FSNL conditions were taken from the thermal analysis.

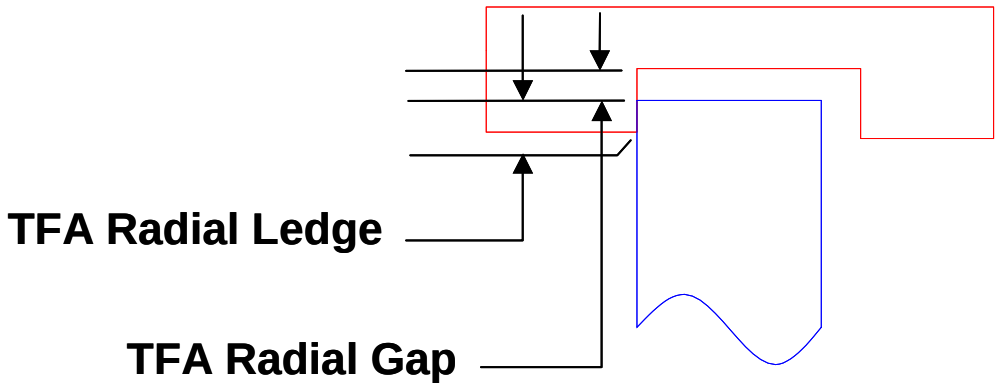

Figure 3-8 - Explanation of TFA Gaps and Ledges

The minimum Radial Gap requirement is a cold-build resultant dimension that ensures there will be no radial binding between the TFA and container in the worst-case operating condition. This is calculated assuming the engine start transient acceleration, with a hot TFA (1600F exit, 1400F interstage, 1200F inlet) inside a cold slotted ring (200F) using the equation [Required Size = l(α*ΔT*R)TFA - (α*ΔT*R)Slot]. Thus, required minimum radial gaps are .204, .175, and .146 inch respectively for the exit, interstage and inlet TFA's.

The minimum Radial Ledge requirement is a cold build resultant dimension that ensures a fully off centered TFA could never become radially disengaged in the worst-case operating condition. This is calculated assuming the trip condition, in which a cool TFA (500F) would reside in a hot slotted ring (1000F exit, 900F interstage, 800F inlet) using the equation [Required Size = l(α*ΔT*R)TFA - (α*ΔT*R)Slot]. Thus, required minimum radial ledges are .060, .048, and .037 inch respectively for the exit, interstage and inlet TFA's.

Actual Radial Gaps and Ledges were calculated using the following equations:

GapR = Rslot – RTFAgap
LedgeR = 2RTFAledge – Rflow – Rslot
Where:
Rslot = (Inner diameter of the outer container)/2
RTFAgap = (Outer diameter of the TFA[no edge bk])/2
RTFAledge = (Outer diameter of the TFA minus edge breaks)/2
Rflow = (Inner diameter of inner flowpath minus edge breaks)/2

Table 3-4 shows the assumptions for temperature, alphas, nominal dimensions and associated tolerances; Table 3-4 also shows the calculated displaced radial locations of these components, at Cold Build, Accelerating, FSFL and trip conditions. Table 3-5 shows the resulting calculated radial gaps, ledges and associated total tolerances. The minimum gap or ledge at any of the operating conditions is equal to the nominal value shown minus the applicable total tolerance.

	Temp @ FSFL (F)	FSFL Alpha in/in/F	Temp @ Accel (F)	Alpha @ Accel (in/in/F)	Temp @ Trip (F)	Alpha @ Trip (in/in/F)	Radial MFG Tol (+/-in)	Edge Break (in)	Radial Edge Bk Tol (+/-in)	Nominal Radius @ Cold Build (in)	Nominal Radius @FSFL	Nominal Radius @ Accel (in)	Nominal Radius @Trip (in)
TFA O.D.													
Inlet	850	7.96E-06	1200	8.60E-06	500	7.50E-06	0.005	0.003	0.003	14.415	14.504	14.555	14.461
Inter	1360	8.92E-06	1400	9.00E-06	500	7.50E-06	0.005	0.003	0.003	14.375	14.540	14.547	14.421
Outlet	1732	1.00E-05	1600	9.60E-06	500	7.50E-06	0.005	0.003	0.003	14.381	14.620	14.592	14.427
Container I.D.													
Intstg Inner Ring	1060	8.46E-06	200	7.70E-06	800	8.23E-06	0.003	0.003	0.003	14.000	14.117	14.014	14.084
Outlet Inner Ring	1260	8.68E-06	200	7.70E-06	900	8.31E-06	0.003	0.003	0.003	14.000	14.145	14.014	14.097
Outer Can aft ID	1422	8.85E-06	200	7.70E-06	1000	8.40E-06	0.003	0.003	0.003	14.000	14.168	14.014	14.109
Slot O.D.													
Outer can ID @ Inlet	850	8.27E-06	200	7.70E-06	800	8.23E-06	0.005	0.003	0.003	14.593	14.687	14.607	14.680
Outer can ID @ Intstg	1060	8.46E-06	200	7.70E-06	900	8.31E-06	0.005	0.003	0.003	14.593	14.715	14.607	14.693
Outer can ID @ Exit	1260	8.68E-06	200	7.70E-06	1000	8.40E-06	0.005	0.003	0.003	14.593	14.743	14.607	14.706

Table 3-4 – Temperatures, Expansion Coefficients, and Tolerances of TFA Gaps and Ledges

		Nominal Cold Build (in)	Nominal FSFL (in)	Nominal Startup Accel (in)	Nominal Trip (in)	Total Tolerance (+/- in)
Calculated Radial Gaps	**Inlet TFA**	0.178	0.182	0.052	0.219	0.010
	Intstg TFA	0.217	0.174	0.060	0.272	0.010
	Outlet TFA	0.211	0.123	0.015	0.279	0.010
Calculated Radial Ledges	**Inlet TFA**	0.232	0.200	0.484	0.154	0.023
	Intstg TFA	0.153	0.216	0.468	0.048	0.023
	Outlet TFA	0.165	0.324	0.558	0.034	0.023

Table 3-5 – Calculated Radial Gaps and Ledges of TFAs at Operating Points

The minimum Axial Thermal Expansion Gap requirement is a cold-build resultant dimension that ensures there will be no axial binding between the TFA and container in the worst-case operating condition. This is calculated assuming the engine start transient acceleration, with a

hot TFA (1600F exit, 1400F interstage, 1200F inlet) inside a cold slotted ring (200F) using the equation [Required Size = I(α*ΔT*L)TFA - (α*ΔT*L)Slot]. Thus, required minimum axial thermal expansion gaps are .039, .015 and .028 inch respectively for the exit, interstage and inlet TFA's.

Figure 3-9 depicts the slot gaps. Table 3-6 shows the assumptions that were made regarding this calculation, and the calculated axial dimensions of the TFA's and the slots at cold build, acceleration, FSFL and trip conditions. Table 3-7 shows the resultant gaps at those conditions; minimum slot gaps equal the nominal minus the associated total tolerances shown.

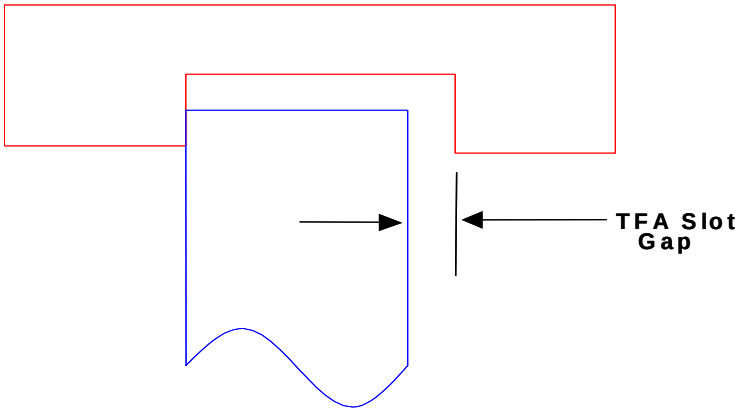

Figure 3-9 - Sketch Detailing The Axial Gap Required Between The TFA and The TFA Slots

	Temp @ FSFL (F)	FSFL Alpha in/in/F	Temp @ Accel (F)	Alpha @ Accel (in/in/F)	Temp @ Trip (F)	Alpha @ Trip (in/in/F)	Axial MFG Tol (+/-in)	Nominal Size @ Cold Build (in)	Additional axial space inside slot full R of slot	Nominal Size @FSFL	Nominal Size @ Accel (in)	Nominal Size @Trip (in)
TFA Length												
Inlet	850	7.96E-06	1200	8.60E-06	500	7.50E-06	0.010	2.750		2.767	2.777	2.759
Inter	1360	8.92E-06	1400	9.00E-06	500	7.50E-06	0.010	1.250		1.264	1.265	1.254
Outlet	1732	1.00E-05	1600	9.60E-06	500	7.50E-06	0.010	2.750		2.796	2.791	2.759
Slot Length												
Inlet	850	8.27E-06	200	7.70E-06	800	8.23E-06	0.015	2.800	0.054	2.818	2.803	2.817
Inter	1060	8.46E-06	200	7.70E-06	900	8.31E-06	0.015	1.300	0.054	1.311	1.301	1.309
Outlet	1260	8.68E-06	200	7.70E-06	1000	8.40E-06	0.015	2.820	0.054	2.849	2.823	2.842

Table 3-6 – Assumptions Regarding the Axial Fits of The TFA Arms Into The TFA Slots

	Calculated Axial Gap between TFA and slot end				
	Cold Build (in)	FSFL (in)	Accel (in)	Trip (in)	Tot. Tol. (+/- in)
Inlet	0.104	0.105	0.080	0.112	0.025
InterStage	0.104	0.101	0.090	0.109	0.025
Outlet	0.124	0.107	0.086	0.137	0.025

Table 3-7 – Calculated Axial Gap Between TFA and End of TFA Slot

The module container, or outer can of the module is expected to operate at slightly lower temperatures than the inner slotted rings since it is bathed in compressor discharge air and is shielded from the catalyst flowpath. As such, a small gap between the inlet and the interstage slotted rings is necessary to allow the inner slotted rings to slightly outgrow the module container. Figure 3-10 shows the location of this gap, and directions of thermal growth that were considered in the calculation.

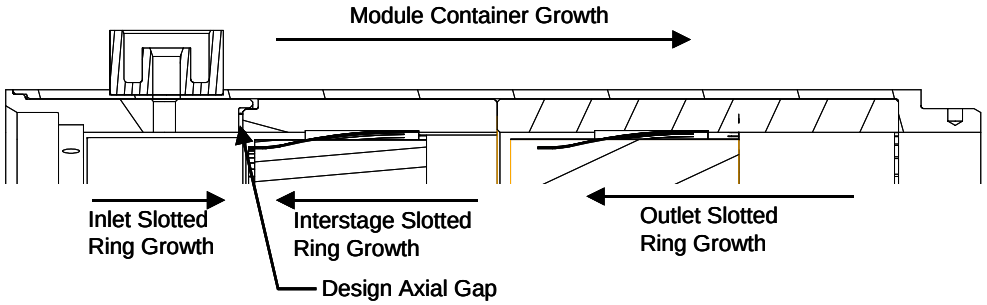

Figure 3-10 - Location of Axial Gap, and the thermal growths considered in its calculation

Description	Temp @ FSFL (F)	Alpha @ FSFL (in/in/F)	Temp @ Accel (F)	Alpha @ Accel (in/in/F)	Temp @ Trip (F)	Alpha @ Trip (in/in/F)	Axial MFG Tol (+/- in)	Cold Build Dimension (in)	FSFL Dimension (in)	Accel Dimension (in)	Trip Dimension (in)
Length from front of Mod. Contnr to aft end	850	7.96E-06	500	8.14E-06	800	8.23E-06	0.005	4.020	4.045	4.034	4.044
Total Axial Length of Interstage slotted ring	1060	8.46E-06	550	8.18E-06	900	8.31E-06	0.002	4.488	4.526	4.506	4.519
Total axial length of outlet slotted ring	1260	8.68E-06	650	8.27E-06	1000	8.40E-06	0.002	7.089	7.162	7.123	7.144
Pin holes to shelf that supports slotted rings	900	8.31E-06	550	8.18E-06	800	8.23E-06	0.005	15.641	15.748	15.702	15.734

Table 3-8 – Assumptions in inner slotted ring gap calculations and calculated dimensions

Table 3-8 shows the conditions assumed to calculate the design axial gap of the inner slotted rings and the dimensions of each component under these conditions. Table 3-7 shows the calculated nominal values of the inner slotted ring gap at the analyzed conditions, and associated total tolerances; minimum gaps are equal to the nominal value shown minus the applicable total tolerance. Thus the Full Speed Full Load gap at this condition is nominally .016" but the minimum gap with a total tolerance of .014" would constitute a .002 gap.

Cold Build Axial Gap	FSFL Axial Gap	Accel Axial Gap	Trip Axial Gap	Total Tolerance
0.043	0.016	0.039	0.027	0.014

Table 3-9 – Inner slotted ring axial gap nominal gaps and associated tolerance

Center Shaft Length and Axial Spacing Considerations:

Refer to Figure 3-11 for the following discussion. Total deflection of the shaft relative to the container is .071 inches, which is a combination of container-to-inner support thermal growth differences and pressure load deflection of the inlet TFA. GapODXA has been set to accommodate this deflection and associated tolerances in the stack loop. Cold build GapODXA opens slightly after creep deflection of the exit TFA.

The catalyst spindle lengths must be designed with sufficient gaps, GapIDU and (First Stage) GapIDI (Second Stage) to freely expand during all transients.

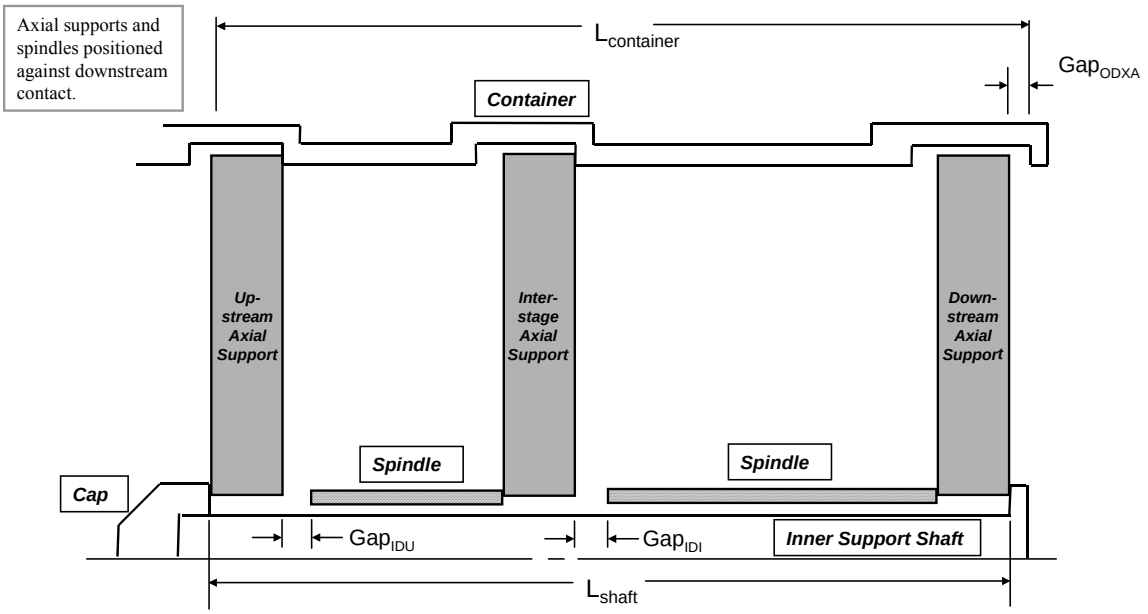

Figure 3-11 - Center Shaft Thermal Expansion Considerations

Table 3-10 shows the temperature, CTE, and actual component dimensions under the cold, FSFL, acceleration, and trip conditions. The manufacturing tolerance of each of these dimensions is also shown to illustrate the impact each dimension has in the stack. The actual gap dimensions, under the described cycle conditions are shown in Table 3-11. The values of displayed gap sizes are nominal; minimum gap sizes are obtained by subtracting the associated total tolerance from the nominal gap.

	Temp @ FSFL (F)	Alpha @ FSFL (in/in/F)	Temp @ Accel (F)	Alpha @ Accel (in/in/F)	Temp @ Trip (F)	Alpha @ Trip (in/in/F)	Axial MFG Tolerance (in)	Cold Length After Outlet TFA Creep Deformation (in)	FSFL Length (in)	Accel Length (in)	Trip Length (in)
Aft Container Length	1000	8.40E-06	200	7.70E-06	950	8.36E-06	0.002	7.089	7.144	7.096	7.141
Interstage Cont. lengt	1000	8.40E-06	200	7.70E-06	950	8.36E-06	0.002	4.488	4.523	4.492	4.521
Inner support shaft	1300	8.80E-06	600	7.70E-06	1300	8.80E-06	0.005	14.256	14.410	14.314	14.410
Exit TFA	1732	1.00E-05	1600	9.60E-06	500	7.50E-06	0.010	2.75	2.796	2.790	2.759
Exit TFA Deflection	1732	1.00E-05	1600	9.60E-06	500	7.50E-06	0.000	0.025	0.025	0.025	0.025
4" spindle	1540	8.90E-06	1300	8.80E-06	600	8.00E-06	0.010	4.195	4.250	4.240	4.213
Inter TFA	1360	8.92E-06	1400	9.00E-06	500	7.50E-06	0.010	1.25	1.264	1.265	1.254
3" spindle	1105	8.50E-06	1300	8.80E-06	600	8.00E-06	0.010	3.136	3.164	3.170	3.149
Inlet TFA	850	7.96E-06	1200	8.60E-06	500	7.40E-06	0.010	2.75	2.767	2.777	2.759

Table 3-10 – Assumptions made in determination of first and second stage spindle gaps

	Cold Gap (in)	FSFL Gap (in)	Accel Gap (in)	Trip Gap (in)	Total MFG Tolerance (in)
Second Stage Spindle Gap	0.098	0.100	0.040	0.184	0.037
First Stage Spindle Gap	0.102	0.095	0.058	0.118	0.022

Table 3-11 – First and second stage spindle gaps at operating conditions

3.3.2.3 Buckling Margin

Hand calculations were conducted to determine margin to buckling in off-design pressure loading conditions. Margins are more than satisfactory and results are shown in Figure 3-12.

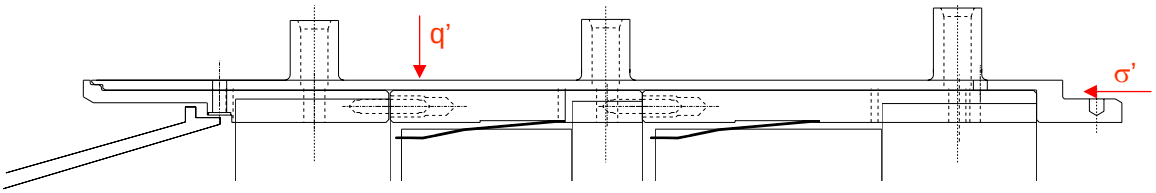

$$q' = .807 \frac{Et^2}{lr} \sqrt[4]{\left(\frac{1}{1-\nu^2}\right)^3 \frac{t^2}{r^2}}$$

q' = 300 psi
Margin = 5.2

Assumes Ends Held Circular

Roark's Formulas for Stress and Strain
6th Edition
Table 35, Case 19A
Thin Tube under Compressing Pressure,
Ends held circular

$$\sigma' = \frac{1}{\sqrt{3}} \frac{E}{\sqrt{1-\nu^2}} \frac{t}{r}$$

σ' = 173 KSI

.4*σ'= 69 KSI
69 KSI equates to 1.1 Million lbs
Margin = 96

Roark's Formulas for Stress and Strain
6th Edition
Table 35, Case 15
Thin Tube Under Axial Compression
Actual value is about 40% Calculated value

Figure 3-12- Container Buckling Margins

3.3.2.4 Mount Boss Load Capability

The mounting bosses on the outer container are subjected to shear and bending loads. Customer design criteria required us to look at capability under two separate conditions (a) 10G load and (b) Trip event. Mount boss capability was acceptable for both conditions and details are provided in Figures 3-13 and 3-14 respectively.

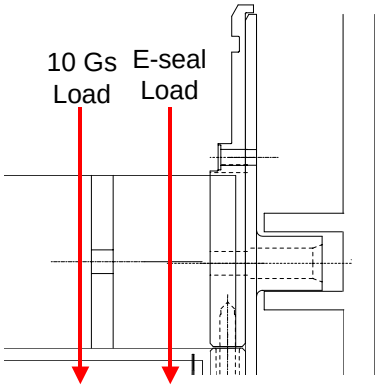

10G Load Requirement

Load Assumptions:
Weight of Cat. Module =600 lbs
Weight of PCL ≈135 lbs
E-Seal Load =2500 lbs

	Bending S	Hoop S	Shear Axial	Shear Lateral	Von Mises Eq S	KT Eq S	Creep	LCF
Load	KSI	KSI	KSI	KSI	KSI	Fillet KT=1.4	Rupture	Cycles
10 Gs Using Cat. Module, Inlet Duct, and PCL	46.4	20	6.2	0	41.7	58.4	N/A	>100,000

No Data Beyond this Point

Figure 3-13 - Mount Boss Steady State Load Capability

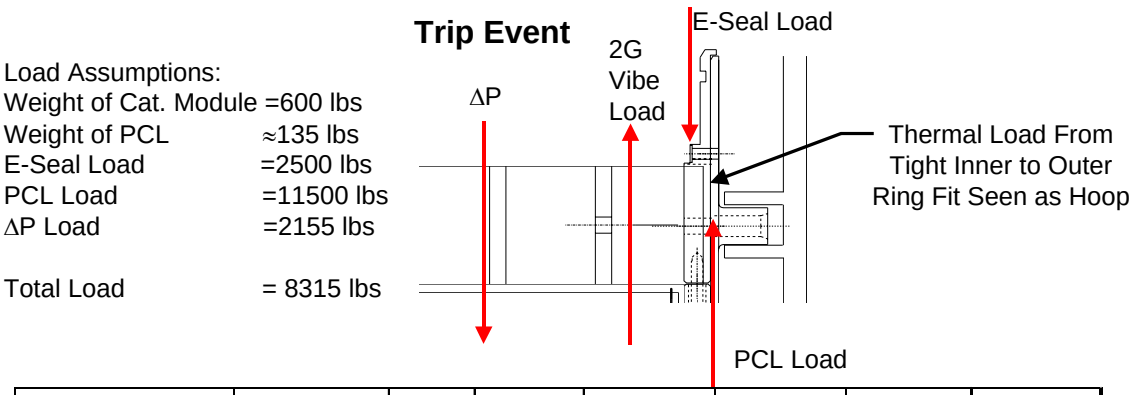

	Bending S	Hoop S	Shear Axial	Von Mises Eq S	KT Eq S	Creep	LCF
Load	KSI	KSI	KSI	KSI	KT=1.4	Rupture	Cycles
Axial Vibe (4 bosses), Axial Pressure	39.1	20	5.2	35.0	49.1	N/A	>100,000

No Data Beyond This Point

Figure 3-14 - Mount Boss Trip Load Capability

3.3.3 Catalyst Axial Support Durability

The function of the axial support is to restrain the catalyst foils from movement due to the force of the combustion gas flow. The contact pressure against the catalyst foils must be sufficiently low to avoid locally deforming the foils. Because the restraint must occur at the exit of the combustion gas from the catalyst, the axial support operates at very high temperature. Also, minimal airflow must be blocked to avoid flow disturbances that could result in flameholding or local over heating within the catalyst foil pack. To accomplish these objectives, a high temperature alloy strut arrangement is employed which distributes the contact to numerous areas while providing very low flow blockage.

Durability issues for the axial support are the typical failure mechanisms considered in gas turbine hot section design. Namely, creep and plastic deformation and low cycle fatigue and fracture due to thermal and mechanical loading. Mechanical vibration and buckling stability will also be considered. Material loss due to oxidation is included in the analyses.

3.3.3.1 Non-Linear Thermal Stress Analyses

Durability of the CESI/ GE10 catalyst axial support has been predicted based on nonlinear finite element analyses combined with available material property test data. The small amount of computed inelastic deformation is predominately caused by stress relaxation into the shape dictated by the displacement of the container relative to the inner shaft from the stack up tolerances, thermal expansion and pressure load. Otherwise, less than .011 inches of deformation was computed. No ratcheting or plasticity is expected to occur. Stress rupture life greatly exceeds 10000 hrs. Fatigue crack initiation is not expected until well beyond 790 cycles (the closest relevant material data point) and the weld joints are shown to be tolerant of a significant lack of weld penetration. Also, a prediction for short-term operation was completed for comparison to prototype testing results.

3.3.3.2 Wear/Fretting

Another potential durability issue is wear and/or fretting at the TFA strut tip to container contact area. This wear/fretting would result from sliding of the two materials due to differential thermal displacements and pressure-driven contact loads. Loads were calculated from the normal baseload pressure drops across the catalysts during baseload. Contact areas were calculated from the geometric areas presented by the TFA/container interface including MFG tolerances. Contact pressures are stated in psi; a 5 ksi upper limit is considered acceptable for this application which experiences low sliding velocities. Engine endurance experience will help verify that there are no long-term issues for wear. Contact pressure calculations for the three TFA's are included in Table 3-12.

	Load (lbs)	Thickness	Number Branches	Contact Area	Contact Pressure
Inlet TFA	732	0.0605	12	0.297	2463
Inter TFA	610	0.0605	48	1.142	534
Outlet TFA	812	0.0605	80	2.178	373

Table 3-12 –Contact pressure of TFA's at FSFL with all geometric constraints considered

3.3.3.3 Material Creep Characterization

The catalyst axial supports are fabricated from Haynes Alloy 214 due to the alloy's superior oxidation resistance, weldability, and high-temperature creep capability. However, the available literature on the alloy's creep capability was insufficient for the strains, temperatures, and durations of an 8000-hour catalyst interval. Accordingly, we instituted a creep-rate characterization test program. This program is discussed in detail section 1.0 of Appendix A.

3.3.3.4 Y-joint weldment fatigue characterization

A component specific test program has been completed to obtain fracture data on Haynes 214. The test is of an actual joint welded by the same process and having a similar stress state as the TFA (Figure 13-15). A notch was machined into the acute side of the weld to have a known and conservative weld defect. The damage tolerance and potential crack growth in the TFA welded joint was then measured by load cycling the specimen at 927°C. Ten specimens were tested without causing crack growth after 2000 load controlled cycles. The final test was stopped after 7221 cycles without indication of crack propagation. It was concluded that the joint is extremely fracture tolerant. This program is discussed in detail section 2.0 of Appendix A.

3.3.4 TFA Manufacturing Process Risk Mitigation

Section cutups of initially fabricated TFAs showed lack of consistent weld penetration at the Y-joints. Since it was not known how critical a quality weld joint was to part durability, this consistency problem was deemed important to solve.

A controlled-process development effort was initiated. The effort consisted of consultations with welding engineers and manufacturing suppliers, weld process trials on Y-joint configurations and

subsequent section-cutups to measure joint penetration. Variables considered in the weld process trials included root opening, back gassing and TIG amperage settings.

Figure 3-15 shows and example of the pre- and post-development weld joint penetration results. A significant improvement was achieved in the average throat thickness (10% increase) and standard deviation (25% reduction) of the process.

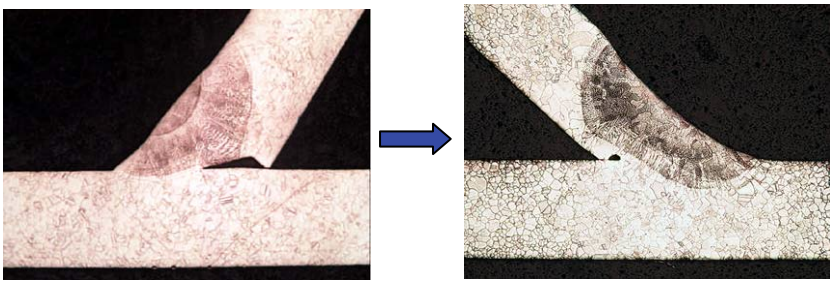

Pre-development Post-development

Figure 3-15 - Y-joint weld penetration improvements

At the conclusion of the process development effort, CESI generated a controlled-process specification that governs the requirements on all TFA welds. Included in the specification are requirements for back-gassing, tensile tests, bend tests, fluorescent penetrant inspection, visual inspection criteria, and 15X-20X visual inspection of periodic cutup samples.

3.4 Assumptions

Assumptions used for the various analyses are indicated in the body of this report at the point where they are relevant.

3.5 Lessons Learned

This design effort resulted in an acceptable solution for the intended goals. There are other design solutions that would also be good solutions. As experience is gained from the follow-on rig and engine test program, and as experience is gained from the prototype fabrication, lessons learned should be applied to continued product improvements.

3.6 Conclusions and Recommendations:

The container and axial support commercialization effort succeeded in providing a configuration reducing projected mature fabrication costs and overall life cycle costs compared to its prior art. Mature fabrication costs are projected to be 20% to 34% lower than the prior art. Life Cycle costs are projected to be on the order of 44% lower than the prior art. Initial purchase costs are projected to be slightly higher than a simplified welded assembly, but re-use capability and dimensional control and ease of assembly are projected to be improved with the can-in-can arrangement. The can-in-can arrangement was, therefore, carried forth through detail design and prepared for subsequent design validation.

A summary of incorporated improvements includes:

- ✓ TFA simplifications and durability improvements including
  - o Elimination of T-bars on exit TFA
  - o Formed strut tips to enter ring slots perpendicular to tangency
  - o Reduced strut count on inlet TFA
  - o Controlled weld process
  - o Material creep rate characterization
  - o Y-joint fatigue capability characterization
  - o Non-linear thermal stress characterization
  - o Vibration characteristics evaluation
- ✓ Container simplifications including
  - o Elimination of T-bar capture features
  - o Assembly weld elimination in can-in-can arrangement
  - o Ring thru-slots for ease of MFG
- ✓ Shafting improvements including
  - o Robustness enhancements to add design load margin
  - o Tooling features added for ease of assembly and disassembly
- ✓ Other Commercialization enhancements including
  - o FPI added to machined hardware for crack detection
  - o Part marking and serialization standardization incorporated
  - o Assembly nameplate convention adopted

IV. Broadened Operating Range - Task 2.1 – Catalytic Secondary Burner

4.1 Summary

This report describes the design of an annular low emission preburner with a catalytic secondary. The size of the preburner is similar to the Catalytica Energy Systems, Inc. (CESI) Xonon 2.0/2.1 design. The 2.0/2.1 DLN secondary stage is replaced with a catalyst requiring extensive redesign of the preburner flow path to provide uniform catalyst inlet temperature at start-up as well as uniform catalyst inlet fuel air ratio from 0 to 100% load. Extensive CFD analysis was used to meet these goals. The preburner catalytic secondary stage is designed to stably operate at inlet temperatures down to 200 °C. This allows for operation at full speed without the primary stage providing the lowest possible emissions. Other than the start transient where the primary burner is lit, the sole contributor to NOx emissions will be the burnout zone. In the KHI M1A-13X cycle this is predicted to amount to less than 0.20 ppmv corrected to 15% O_2. For higher firing temperature turbines this number will be higher, but there will be no NOx contribution from the preburner. Finally, the presence of a catalytic secondary stage in the preburner is expected to favorably affect preburner turndown performance, as it will not display the same non-linear characteristics as a conventional DLN secondary stage due to either a drop in combustion efficiency or the occurrence of combustion instabilities, requiring tuning of control algorithms.

The preburner catalyst replaces the inlet stage catalyst of the Xonon 2.0/2.1 design, but has a larger frontal area resulting in a significant reduction in pressure loss. The predicted reduction in combustor pressure loss is in the order of 15 percent, making this system particularly attractive for the larger frame engines.

4.2 Background

A program was proposed to the DOE in February of 2000 [1] where a catalytic secondary burner would be developed as part of Low-Emissions Preburner Technology. The development is necessary because of the undesirable characteristics of the current staged lean pre-mixed (LPM) technology. One of these undesirable characteristics is instability resulting from operating near the lean blowout limit (LBO) to minimize thermal NOx formation. A solution to the instability problem is to replace a stage of the LPM burner with a catalytic burner. Since a catalyst does not have LBO as long as the inlet temperature is above the catalyst ignition temperature, the instabilities associated with LBO is eliminated.

Another undesirable characteristic is the very non-linear temperature rise vs. fuel flow as observed in the Xonon 2.0 LPM preburner. This requires a unique approach to controlling the entire combustor to avoid large swings in catalyst inlet temperature that could cause the entire turbine operation to become unstable.

4.3 Introduction

A catalytic secondary stage in a preburner offers several potential advantages compared to a lean premix system. For example:

1. With a catalyst that has an extinction temperature above the compressor discharge temperature (CDT), once the preburner catalyst has been lit off, the primary stage may be shut off eliminating the NOx contribution from the preburner.
2. With the primary stage shut off, there is no lean premix combustion to become unstable. Preburner liner pressure drop is often used as a tool to ensure stable combustion. With the primary stage shut off, the preburner liner pressure drop may be relaxed since there is no flame to stabilize.
3. With a slightly higher preburner outlet temperature then the conventional preburner, the preburner secondary stage catalyst can replace the main catalyst inlet stage catalyst making any cost increase relatively small.
4. With the larger annular cross sectional area available in the preburner, the catalyst pressure drop will be smaller than in the typical inlet stage of a two-stage system like the Xonon 2.1.
5. With the preburner feeding fuel air mixture to the preburner secondary stage catalyst and the mixer feeding the fuel to the main catalyst, the system will be more flexible in load variation.

NOx elimination from the preburner may be a significant reduction in overall engine NOx. In the Xonon 2.1 system, predicted NOx will drop to 0.2 ppmv compared to the current ~1.0 ppmv.

4.4 Overview

4.4.1 Preburner System Requirements

The catalytic-secondary pre-burner is intended to meet the requirements given in Table 4-1. The design operating conditions for analysis are shown in Table 4-2.

Parameter	Requirements
Geometric constraints	Pre-burner must be installable into existing KHI M1A-13X XONON combustion system with minimum change to existing hardware and controls logic
NOx emissions, FSNL - 100% load	< 0.1 ppmv NOx emissions, corrected to 15% oxygen
Pressure loss	1.0% of PCD maximum with no bypass flow, measured at ISO-day sea-level base load operation
Velocity uniformity at pre-burner catalyst inlet plane	Maximum variation +/- five percent of mean at FSNL and higher load, 100% speed
Temperature uniformity at pre-burner catalyst inlet plane	Maximum variation +/- one percent of mean at FSNL and higher load, 100% speed
Fuel-air mixture uniformity at pre-burner catalyst inlet plane	Maximum variation +/- five percent of mean at FSNL and higher load, 100% speed
Lean blowout, minimum temperature rise	N/A
Dynamic pressure activity	Quiet operation required for downstream component protection (maximum peak discrete < 0.3 PSI, maximum overall RMS < 3.0 PSI)
Ignition, maximum inlet temperature to pre-burner catalyst	Maximum pre-burner catalyst inlet temperature during light-off < (TBD); reliable ignition and light-around in primary zone
Life	8000 hours / 800 starts (catalyst pack and seal) 24,000 hours / 2,400 starts (pre-burner)

Cost	System cost (includes pre-burner, mixer, main catalyst module, burnout zone, ignition system, and fuel system) should not substantially exceed installed cost of current KHI XONON combustion system
Manufacturability and serviceability	Design shall incorporate features to minimize manufacturing cost. Features shall also be incorporated to facilitate pre-burner catalyst pack replacement in the field.
Catalyst maximum start-up temperature	450 degrees C
Catalyst minimum conversion, fully aged catalyst	Minimum conversion is (TBD) percent at a catalyst minimum inlet temperature of 250 degrees C and a catalyst outlet temperature of 700 degrees C

Table 4-1 – Catalytic-Secondary Pre-Burner Design Requirements

ISO Ambient (60 °F), sea level	**Non-reacting Flow analysis (Base Load)**	**Reacting Flow (low pressure case)**	**Non-reacting Flow (high pressure case).**
Preburner inlet air flow kg/s	0.84	0.84	4.93
Preburner inlet total pressure (atm)	1.24	1.24	9.02
Preburner inlet total temperature (°C)	52	52	335
Primary zone fuel flow kg/s	.0067	.0067	0.0
Catalyst fuel flow kg/s	.0021	.0021	.0379

Table 4-2 – Design Operating Conditions

As the program was developed, a decision was made that the new preburner would look very similar to the existing Xonon 2.1 design, the main difference a catalyst as the secondary stage. The catalytic secondary stage would require a new fuel injection scheme for the catalyst. This is depicted in Figure 4-1.

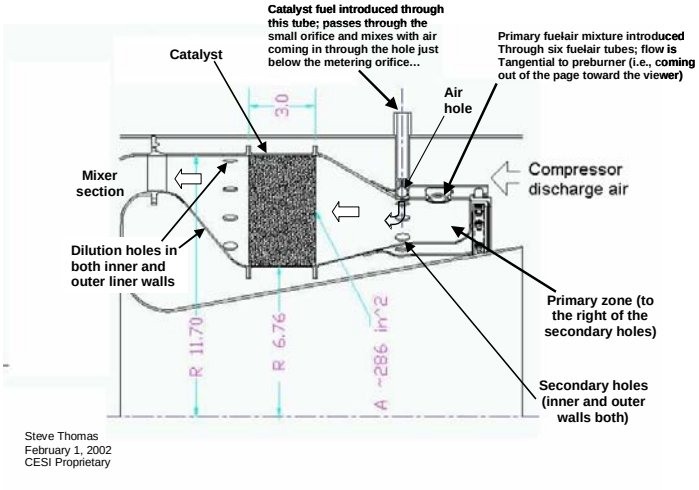

Figure 4-1 - Catalytic Secondary Pre-Burner Concept

The initial concept failed to meet performance objectives in several areas:

- Too high temperature spread at catalyst inletToo large F/A non-uniformity at catalyst inletLarge recirculation zones downstream of secondary dilution air holes
- High wall temperatures in primary zone

It was decided to take a different approach in injecting the secondary fuel/air mixture. One of the concepts that were discussed was the use of lobed mixers in inner and outer annuli, as shown in Figure 4-2.

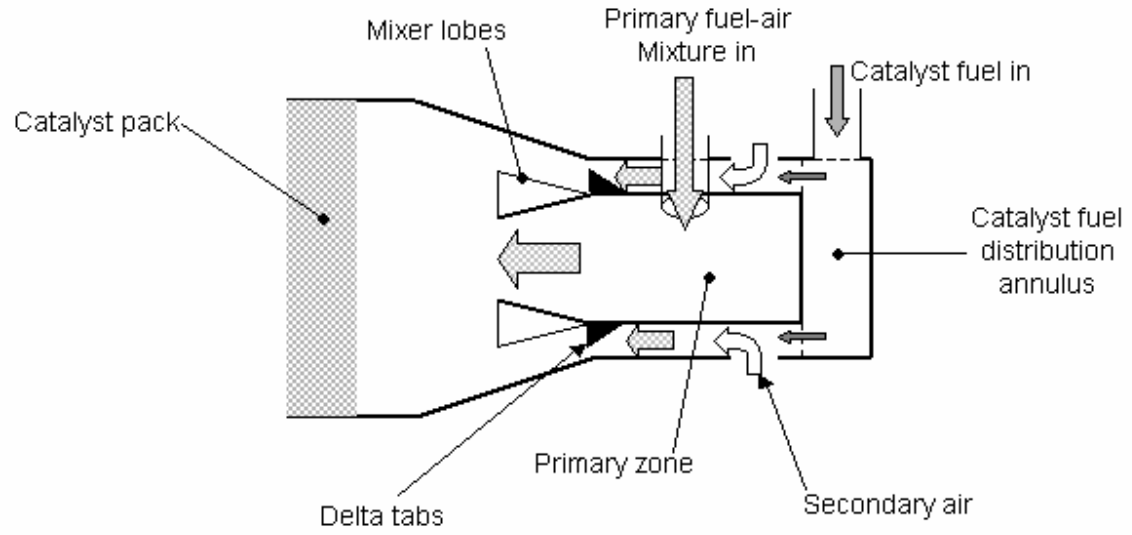

Figure 4-2 - Concept with Lobe Mixers

The primary objective with this design was to achieve better mixing at the 30% speed point that was analyzed in CFD. At this operating condition, the primary stage is running hot and therefore good mixing between the cool secondary air and hot primary exhaust is vital. However, CFD analysis showed that this concept failed to meet the required temperature uniformity by a relatively wide margin. The above figure shows both mixer lobes and delta tabs. The former was not analyzed due to the complexity of the design as well as having an expected performance very similar to the delta tabs. An alternative to the above using swirlers instead of delta tabs was also considered. In all cases, the main problem is how to achieve adequate mixing between the hot exhaust of the primary with the cooler secondary fuel air mixture. By April 15, a relatively larger number of cases had already been run, as shown in the table below.

CATALYTIC-SECONDARY PRE-BURNER CFD ANALYSIS -- SUMMARY TABLE OF CASES RUN

S. Thomas updated 2002-04-15

Case no.	Case run date	Power setting	Reacting flow?	Secondary orifice geometry: Number of OD rows	OD row #1 orifice count x diameter	OD row #2 orifice count x diameter	Number of ID rows	ID row #1 orifice count x diameter	ID row #2 orifice count x diameter	Catalyst fuel injector	Fuel-air uniformity	Velocity uniformity	Plot file name on H: drive	Comments
1	3/29/2002	low power	NO	2	72 x 0.312"	72 x 0.312"	2	72 x 0.265"	72 x 0.265"	baseline	poor	N/A	ch4_base 2002-03-29	Jet penetration and CH4 distribution, subset model of PZ / SZ; poor penetration
2	3/29/2002	low power	NO	2	72 x 0.312"	72 x 0.312"	2	72 x 0.265"	72 x 0.265"	fuel peg "A"	fair	N/A	ch4_peg 2002-03-29	Jet penetration and CH4 distribution, subset model of PZ / SZ; better penetration, but durability and wakes are issues
3	4/3/2002	low power	NO	2	72 x 0.312"	72 x 0.312"	2	72 x 0.265"	72 x 0.265"	reverse-hole	good	N/A	ch4_rev_hole 2002-04-03	Jet penetration and CH4 distribution, subset model of PZ / SZ; good penetration - over-penetrates?
4	4/4/2002	base load	NO	2	72 x 0.312"	72 x 0.312"	2	72 x 0.265"	72 x 0.265"	fuel peg "A"	fair	N/A	ch4_peg_baseload 2002-04-04	Jet penetration and CH4 distribution, subset model of PZ / SZ; better penetration, but durability and wakes are issues
5	4/4/2002	base load	NO	2	72 x 0.312"	72 x 0.312"	2	72 x 0.265"	72 x 0.265"	reverse-hole	good	N/A	ch4_rev_hole_baseload 2002-04-04	Jet penetration and CH4 distribution, subset model of PZ / SZ; good penetration
6	4/5/2002	base load	NO	2	72 x 0.312"	72 x 0.312"	2	72 x 0.265"	72 x 0.265"	baseline	poor	N/A	ch4_base_baseload 2002-04-05	Jet penetration and CH4 distribution, subset model of PZ / SZ; poor penetration
7	4/5/2002	base load	NO	2	72 x 0.312"	72 x 0.312"	2	72 x 0.265"	72 x 0.265"	co-axial jet	good	N/A	ch4_cojet_baseload 2002-04-05	Jet penetration and CH4 distribution, subset model of PZ / SZ; good penetration
8	4/5/2002	low power	NO	2	72 x 0.312"	72 x 0.312"	2	72 x 0.265"	72 x 0.265"	co-axial jet	good	N/A	ch4_cojet_30pct 2002-04-05	Jet penetration and CH4 distribution, subset model of PZ / SZ; good penetration
9	4/8/2002	base load	NO	2	72 x 0.312"	72 x 0.312"	2	72 x 0.265"	72 x 0.265"	reverse-hole	good	poor	(X)_rev_hole_int baseload 2002-04-08; (X)_rev_hole_int baseload 2002-04-08 cat inlet	**Full internal model**, non-reacting flow; plots of CH4, U-velocity, pressure, and velocity vector; catalyst face plots of fuel-air, velocity, temperature
10	4/11/2002	base load	NO	2	72 x 0.410"	72 x 0.410"	0	0	0	reverse-hole	N/A	poor	int_U_hp_3top	**Full internal model**, non-reacting flow; plot U-velocity
11	4/11/2002	base load	NO	2	72 x 0.410"	72 x 0.410"	0	0	0	reverse-hole	N/A	poor	int_U_hp_3top_s	**Full internal model**, non-reacting flow; plot U-velocity

a. Baseline has fuel inject tube flush with OD wall, air inlet feed hole on upstream side of tube to promote fuel-air mixing prior to injection into secondary zone.
b. Fuel peg "A" has five holes on each side, NACA0030 airfoil shape to peg.
c. Reverse-hole concept is similar to baseline, but air inlet feed hole is on downstream side of fuel tube.

Table 4-3 – CFD Cases Run by April 15, 2002

The next design that was proposed may be viewed as the first step towards the final design. This concept is shown in Figure 4-3.

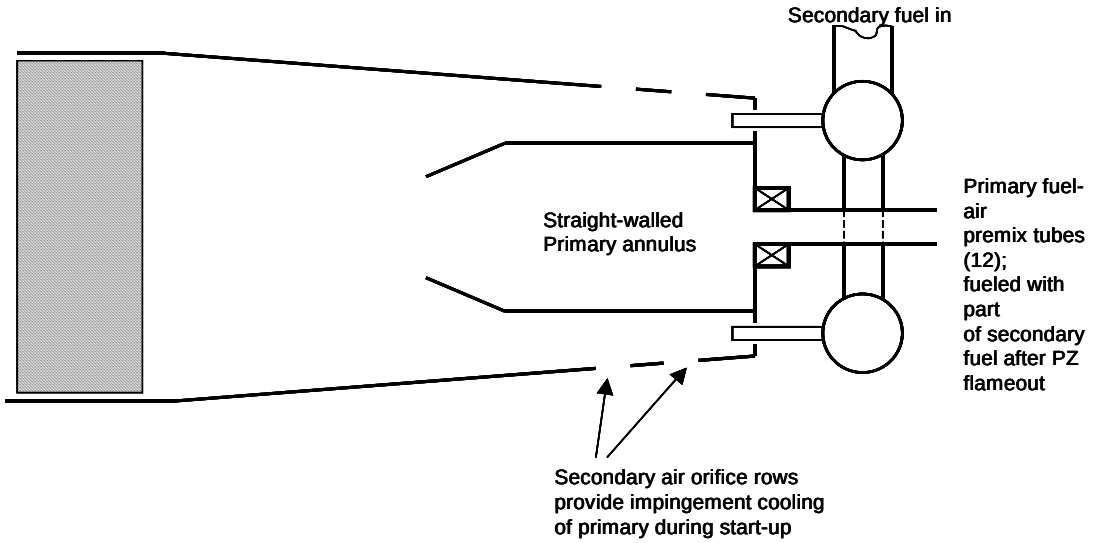

Figure 4-3 - First step Toward Final Design

This concept has the same basic features as the final design, in that the primary stage is in the radial center and fed from the dome side of the preburner.

4.5 Cycle Modeling

A preburner with a catalytic secondary stage has been modeled quite extensively using KHI M1A-13A cycle conditions. The basic cycle conditions are based on the pressure drop and hence flow splits of the standard diffusion flame combustor and the calculations have only been conducted for a 60 °F ambient temperature, assuming a fresh catalyst. The main purpose of the calculations has been to optimize preburner flow splits, gas temperatures and to evaluate how the preburner would be operated through the start transient. It should also be noted that the start transient cycle conditions are not based on actual engine readings, since it by default is impossible to obtain steady-state readings during a transient. Also, at the low flows, both air and fuel flow measurements are not very accurate in this range. The start transient data was therefore obtained from interpolating cycle conditions between 0 and 100% speed. Due to the very inefficient compressor at low speeds, an elliptical rather than linear curve fit was made.

The first part of the cycle analyses consisted of determining how the turbine would be operated through the start transient and load range. This was to a large extent a discussion between catalyst designers and engineering. It was determined that the following cycle conditions should be targeted:

- Preburner catalyst light-off temperature in the start transient: 450 °C (minimum)
- Preburner catalyst outlet temperature: 700 °C (average)
- Preburner catalyst outlet temperature spread: ± 50 °C.
- Mixer inlet temperature (i.e., downstream of preburner dilution air): 650 °C (average)

4.5.1 Flow Splits

To achieve the above temperatures, the following flow splits in Table 4- were chosen.

Primary Stage: Tubes: 6.44% Swirlers: 12.72%	19.16%	Total is fed to secondary stage catalyst
Secondary Catalyst Air:	65.98%	
Dilution:	14.86%	Reduces preburner outlet temperature from 700 to 650 °C
TOTAL:	100%	

Table 4-4 – Flow Splits

4.5.2 Gas Temperatures During Start Transient and Loading

This resulted in gas temperatures during the start transient and load range as shown in Figure 4-4.

The bottom red line shows the rise in CDT as turbine shaft speed increases. At 100% speed this is about 330 °C, depending on load (ISO conditions). The combustor is first lit off in the preburner primary stage. This should occur at just a few percent engine speed.

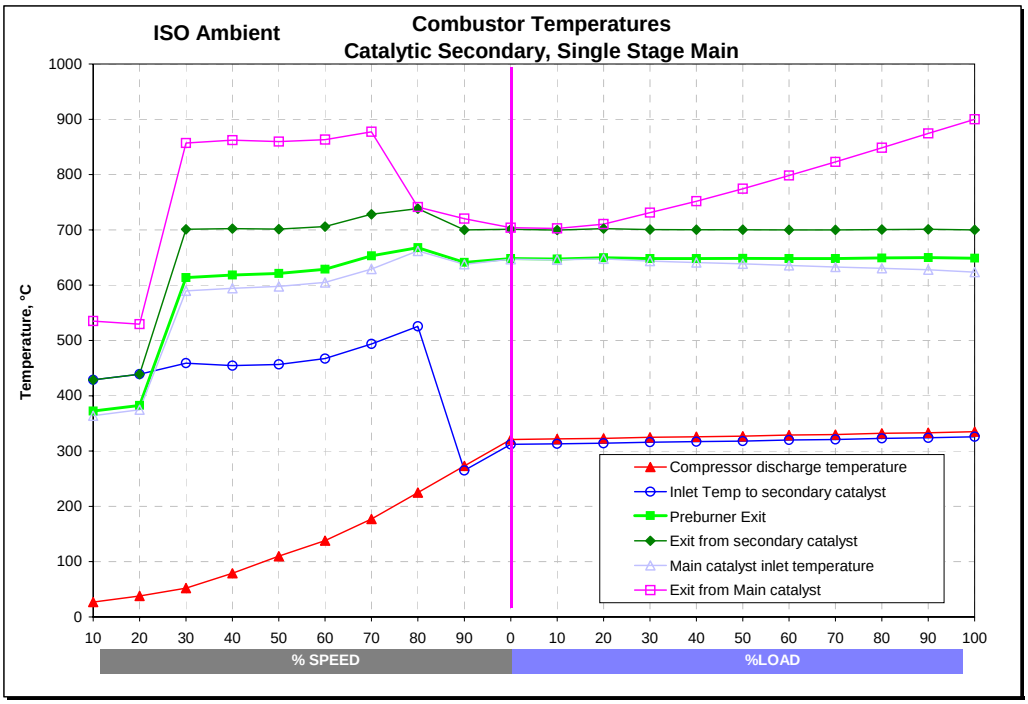

Figure 4-4 - Gas Temperature During Start Transient and Loading

As the starter ramps up speed, inlet temperature to the preburner catalyst will continue to increase due to the heat-up from the primary stage. Thermocouples will be used to monitor preburner catalyst inlet temperature. When this temperature reaches 450 °C, preburner secondary fuel (i.e., catalyst) will be turned on. This will be ramped up to maintain 700 °C average out of the preburner catalyst. In the current design, it is expected that temperature uniformities will cause peaks up to the maximum allowable value, 750 °C. Consistent with the current Xonon 2.1 start transient strategy, fuel will also be fed to the main stage catalyst (which now is only a single stage) to ensure adequate combustor heat release to start the engine. At about 80% speed (at ISO conditions), the combustor inlet temperature will pass beyond the extinction temperature of the preburner catalyst, about 200 °C, and the primary stage will be shut off. A corresponding rise in preburner catalyst fuel flow will take place to account for the drop in inlet temperature as well as the resulting drop in catalyst conversion. This will increase the amount of unburned fuel passing through the preburner catalyst and being fed into the main catalyst mixer. No attempt at this point has been made to quantify the amount of unburned fuel at this operating condition. A comparison between 30% and 100% load local gas temperatures is shown in Table 4-5.

	30% SPEED	FULL LOAD
Preburner inlet:	52 °C	335 °C
Preburner catalyst inlet:	459 °C	326 °C
Preburner catalyst exit:	701 °C	700 °C
Preburner exit:	614 °C	649 °C
Main catalyst inlet:	590 °C	624 °C
Main catalyst exit:	857 °C	900 °C

Table 4-5 – Gas Temperature Comparisons

4.5.3 Pressure Drop

A preburner with a catalytic secondary stage offers lower pressure drop compared to the conventional Xonon 2.1 system. The primary contributing factor is the larger surface area of the preburner catalyst compared to the main stage catalyst, which allows for lower gas velocities. In addition, the preburner catalyst has been designed for low pressure drop. The estimated pressure drop for the catalytic secondary stage is 0.17%. This compares to an estimate of about 0.33% for the inlet stage of the Xonon 2.1 system. In addition, the preburner liner pressure drop has been reduced from a nominal 1.25% to 1.00%. This reduction is justified by eliminating the need to stabilize a lean burning flame during normal operation. Outside of the start transient, the portion of the preburner upstream of the catalyst is only used for fuel/air premixing, and thus the required pressure loss should be less. A comparison of pressure drops in the Xonon 2.1 system with the catalytic secondary system is shown below. Note that the 2.1 pressure drops are based on ISO full load engine measurements, and as such the numbers will deviate slightly from the predicted values. Table 4-6 summarizes measured Xonon 2.1 and predicted catalytic secondary pressure losses.

Pressure Drops (100% load):	CATALYTIC SECONDARY	XONON 2.1
Preburner liner:	1.00%	1.37%
Preburner catalyst (~75% Conv., 239 in² frontal area *)	0.18% **	N/A
Mixer flowpath:	0.14%	0.14%
Main catalyst (41% Conv.*)	0.52%	1.00%
Burnout Zone:	0.37%	0.37%
Other:	1.46%	1.46%
TOTAL (0.67% point gain vs. X2.1):	3.67%	4.34%

* Target for Catalytic Secondary Concept.
** D. Ginter presentation 12/11/01 "Catalytic Secondary Testing"

Table 4-6 – 100% Load Pressure Drop

As a rule of thumb [5], one percent point lower combustor pressure drop improves engine efficiency by 0.5% point and increases power by 1% point. This would offer a significant cost benefit for the larger frame class turbines.

4.5.4 Predicted Engine NOx Emissions

As the preburner primary stage is the main NOx contributor and is shut off at FSNL and above, the only NOx contribution during loading will be from the burnout zone. As reported in a previous Technical Report [4], the estimated NOx at KHI-M1X base load conditions with 1300°C BOZ (Burn Out Zone) T_{AD}, is less than 0.05 ppmv corrected to 15% O_2. This is illustrated in Figure 4-5 which is taken from that report. The reference to "baseline" in that report is the offset error in the analyzer, i.e., the ppmv NOx incorrectly read when no NOx is fed through the analyzer.

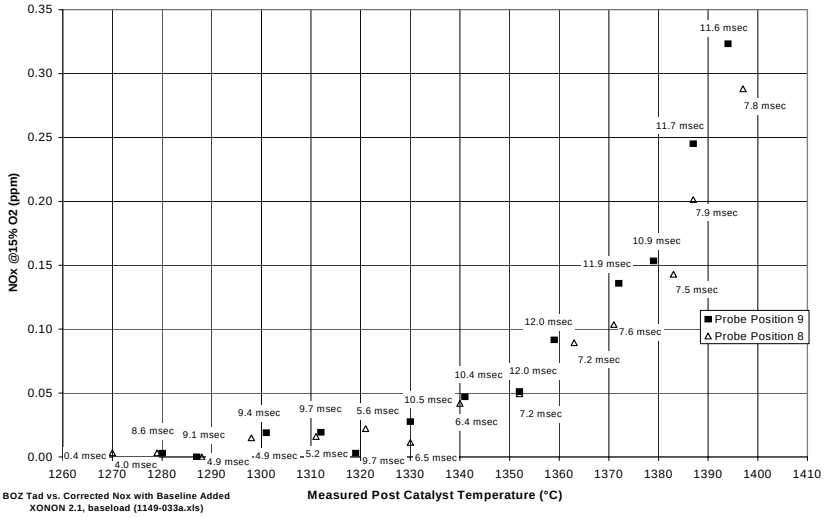

Figure 4-5 - Burnout Zone NOx

4.6 Catalyst Design

The following is a discussion of rig test results for converting preburner secondary fuel [6]. The flow conditions were based on the KHI M1A-13X engine at full load. The goal was to see if a fully catalytic secondary can provide catalyst inlet temperatures up to 650 °C with a low pressure drop, and remain lit at compressor discharge temperatures without fuelling the primary zone. Two separate designs were tested at two velocities. Measured pressure drops met the goals of <0.2% of CDP. Catalyst extinction was 325 °C inlet temperature at 550 °C T_{ad} and 200 °C inlet temperature at 700 °C T_{ad}.

4.6.1 Background

Current Xonon combustor technology requires a preburner to provide high enough catalyst inlet temperatures (450 to 650 °C) for keeping the catalyst lit. The low-NOx preburner on the M1A-13X engine at SVP uses a two-stage LPM preburner, typically generating 1 to 1.5 ppm NO_x (corrected) at baseload. This NO_x is generated in the preburner primary zone, which must remain lit for combustion to occur in the preburner secondary zone. It may be possible to turn off the primary zone combustion when using a catalytic secondary zone if the catalyst can remain lit, making sub-ppm NO_x at baseload a possibility. The issues with a preburner secondary zone

catalyst are whether it can remain lit at inlet temperatures around CDT and whether it can do so without excessive pressure drop. Preliminary evaluations showed specific designs could meet these criteria at velocities that are achievable in the Xonon 2.1 envelope.

4.6.2 Configuration

Rig:
HPR. Base Test Conditions: 123 psig, 3400 and 2420 slpm air (6.3 and 4.9 m/s face velocity), T_{ad} steps at 350 °C inlet, preheat steps at 700 °C and 550 °C T_{ad}
Single stage catalyst tests, 3-in lengthData Collection:
Catalyst inlet and outlet wall and gas temperatures, rig pressure, catalyst dp, post catalyst zone temperatures, fuel concentration at catalyst inlet, fuel flows.

4.6.3 Test Results

Conversion in the fully lit catalyst modules was about 82% at 6.3 m/s face velocity and about 85% at 4.9 m/s face velocity. An inlet temperature of 350 °C was sufficient to keep the catalyst inlet walls active with T_{ad}'s from 700 °C down to about 525°C (see Figure 4-6). There was not a noticeable effect of loading on conversion. Rate of conversion also depends on inlet temperature and catalyst exit temperature. Figure 4-6 shows how conversion changes as a function of inlet and outlet temperatures for a catalyst with a 231 in^2 frontal area.

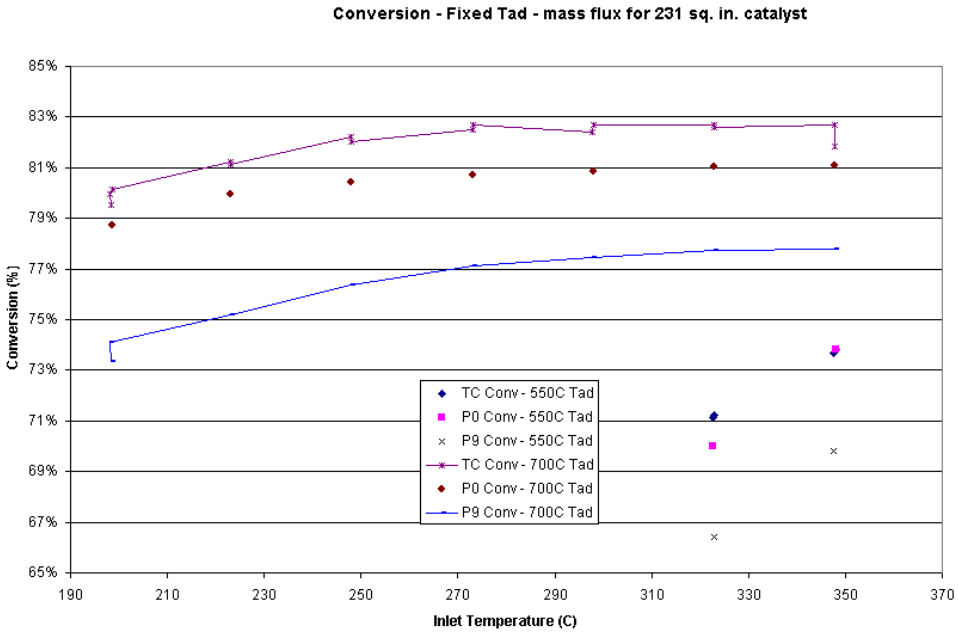

Figure 4-6 - Conversion – Fixed Tad- Mass Flux for 231 Sq. In. Catalyst

In the cycle analysis, the dependence of inlet temperature has been accounted for my making a polynomial curve fit to the Figure 4-7 at 700 °C outlet temperature. The catalyst is run at an almost constant outlet of 700 °C over both the start transient and through the load range.

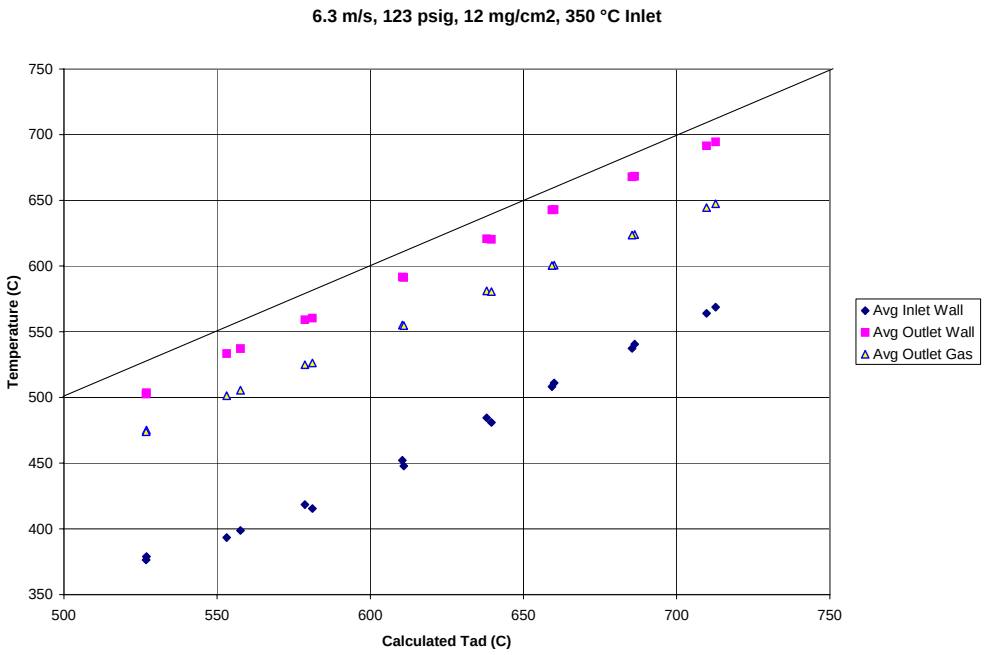

Figure 4-7 - Temperatures in T_{ad} Step Experiment

With 550 °C T_{ad}, the modules extinguished when the inlet temperature fell below 325 °C. With 700 °C T_{ad}, extinction did not occur until 200 °C inlet temperature. (See Figure 4-8.) Velocity and loading had little effect on performance in this test.

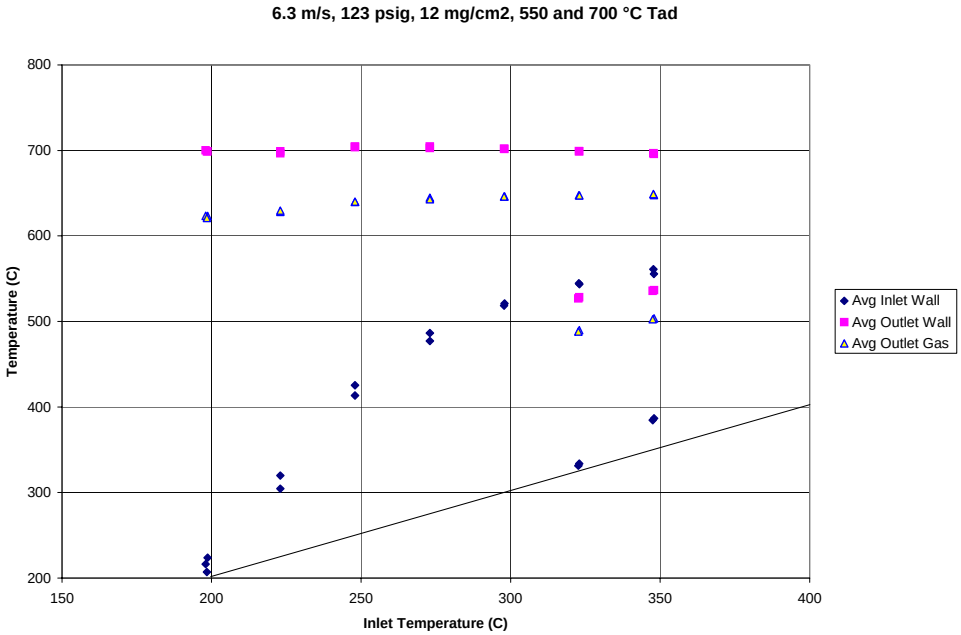

Figure 4-8 - Temperatures in T_{ph} Step Experiment

Pressure drop was very low in these tests. At 6.3 m/s face velocity, pressure drop ranged between 0.13 and 0.17%. At 4.9 m/s, the range was 0.09 to 0.12% (see Figure 4-9). Delta p was slightly lower for the module with lower catalyst loading. The goal of <0.2% of CDP was met.

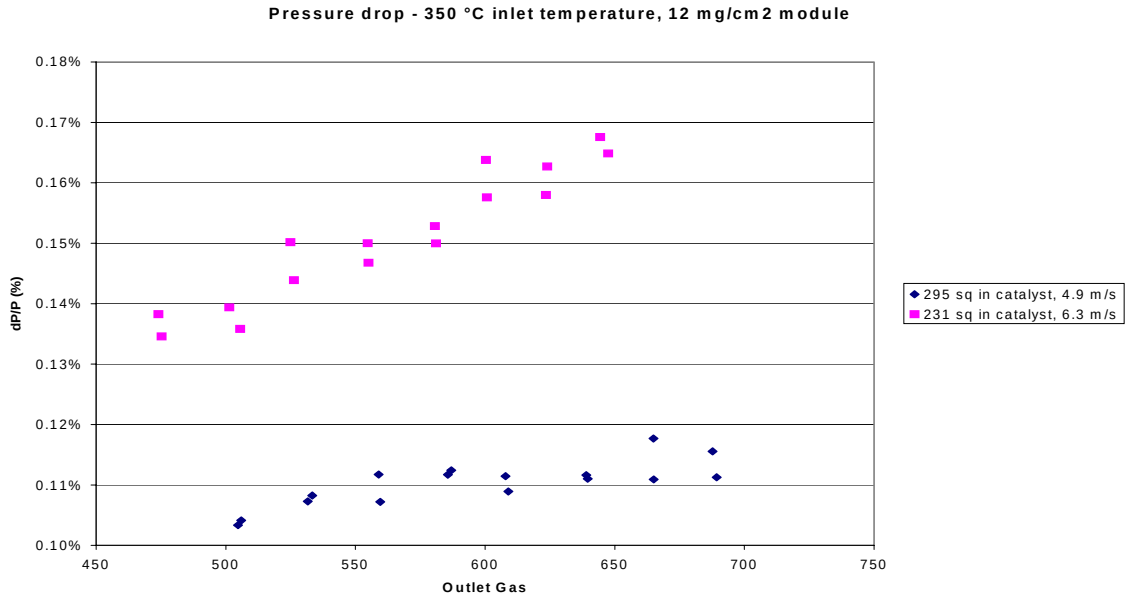

Figure 4-9 - Pressure drop in T_{ad} Step Experiment

4.7 CFD Analysis

CFD has been the focus of this design and concept development effort and has been used extensively to optimize all major components of the preburner that affect aerodynamic and mixing performance. The main areas in which CFD has been used are:

- Primary zone flow recirculation to ensure good lean blowout performance
- Primary zone wall temperature reduction.
- Secondary air jet flow recirculation reduction
- Liner wall shapes optimization to improve manufacturability while simultaneously ensuring no flow separation
- Preburner length tuning to minimize catalyst inlet temperature spread
- Secondary dilution air pattern tuning to minimize catalyst inlet temperature spread
- Secondary fuel manifold orifice pattern tuning to minimize catalyst inlet fuel/air ratio variations
- Primary zone radial height tuning to improve catalyst inlet temperature uniformity

Computational Fluid Dynamics Research Corporation (CFDRC) was contracted to conduct the CFD modeling and design optimization. The latter was done under close cooperation with and supervision of CESI. All analysis was performed using the CFD-ACE+ code. The models used accounted for heat transfer, turbulence, mixing, reaction, swirling flows and pressure drop through the preburner catalyst module. Further details can be found in the report from CFDRC [2].

The overview part of this report described the general approach that was taken and the major steps in the CFD analysis. This section will go into more detail regarding the analysis of the individual components. Over a period of about five months, the concept depicted above was continually refined using CFD. Simulations were performed in a 3D axially symmetric sector for the entire preburner while 2D models were run to optimize the flow field in the primary stage. The final design is shown in Figure 4-10 and highlights areas analyzed through CFD. The CFD analysis that resulted in this design will be discussed in following.

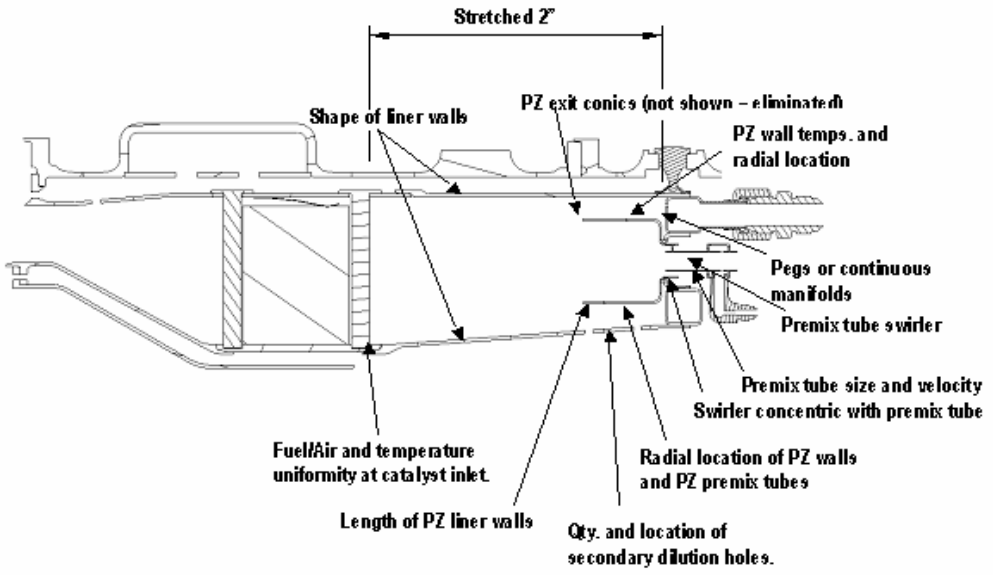

Figure 4-10 – Final Preburner Design

4.7.1 Primary Stage Optimization

Flow analysis of the design utilizing a radially centered primary stage in the front end of the preburner revealed that there was no flow recirculation along the centerline of the primary burner. Also, reactive flow indicated primary zone wall temperatures would be excessive. The course of action to address these two problems was to introduce more swirl in the incoming air, and to carefully balance the air between the premix tube and the concentric swirler to ensure a layer of cool, un-fueled air would shield the walls from the hot combustion gases. It was determined that a matrix of eight cases would be run to study the effect of various parameters that has an influence on flow recirculation as well as fuel/air mixture ratio along the primary walls. The parameters that were varied in the matrix are listed in Table 4-7.

Run number	Internal velocity	Internal swirl angle	Baffle at exit?	External swirler?
1	Low	50 degrees	No	No
2	High	50 degrees	No	Yes
3	Low	60 degrees	No	Yes
4	High	60 degrees	No	No
5	Low	50 degrees	Yes	Yes
6	High	50 degrees	Yes	No
7	Low	60 degrees	Yes	No
8	High	60 degrees	Yes	Yes

Table 4-7 – Effect of Various Parameters on Flow Recirculation

A spreadsheet was used to score the results from the CFD analysis, and the numbers normalized to allow for a simple comparison of performance between the different variations. The variables that were rated were:

- Fuel/air uniformity at primary exit plane. This would have an effect of the fuel/air uniformity at catalyst inlet with the primary stage being a part of the premixer.
- Velocity uniformity at primary stage exit plane.
- Recirculation zone strength.
- Near-wall temperatures (reacting flow)

Conclusions from the Design of Experiment (DOE) matrix provided the following insight into the primary stage performance:

- External swirler is required to keep primary zone liners cool. Tradeoff: F/A uniformity deteriorates with cooler walls.
- Recirculation zone strength shows weak dependence on fuel/air tube internal swirl
- Exit velocity uniformity correlates to external swirler, internal fuel/air tube swirl and velocity.
- External swirler is favored.

DOE case 2 has best overall scores**.** The geometry for this case is:

- 50 degree average internal swirl angle in fuel/air premixing tube
- High velocity fuel/air mixture flow inside the tube
- No conic at fuel/air premix tube exit
- External swirler.

Case 2 performance scores were :

- Best recirculation zone strength
- Second best velocity uniformity
- Third best wall temperature score
- Lowest fuel/air uniformity score, but still within one percent

Based on the promising results of the initial analysis, additional analysis was performed on case 2. The results showed:

- Lower internal velocity in fuel/air premixing tube. The target is to reduce wall temperatures further, but may trade off for weaker core recirculation.
- Increased airflow through external swirler. For same total airflow, results in a richer core fuel/air ratio which might improve light-around performance at start-up. May also improve combustion efficiency. Increased outer swirler airflow would also probably lower wall temperatures.

Four additional cases were run, referred to as cases 9 to 12, although all of these were derivatives of the original case 2. Of these, case 10 was considered the best concept. This design utilized a 50 degree premix tube swirler, a low premix tube velocity, no cone at exit of premix tube and a 25 degree swirler concentric with the premix tube exit. The findings from the 2D analysis revealed the following:

- Reducing premix tube internal velocity shortens the recirculation zone
- Eliminating the premix tube exit cone dramatically increases centerline recirculation and slightly improves exit velocity uniformity, albeit at the expense of exit fuel/air uniformity.
- Increased swirler airflow dramatically reduces near-wall gas temperatures.

An additional performance improvement was observed by simply shortening the primary zone walls. The benefits can be summarized as:

- Short walls easier to cool by requiring less cooling air
- Lowering peak temperature at catalyst inlet
- Improved mixing with secondary stage fuel/air mixture

Figure 4-11 shows one-half of an axial symmetric 2D model of a vector plot of the flow-field in the primary stage of concept 10 where the flow splits and swirler angles have been optimized:

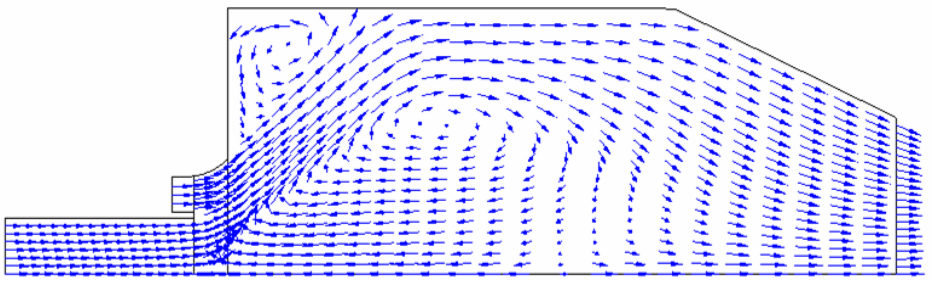

Figure 4-11 – Concept 10 Vector Plot

As mentioned elsewhere, the exit conics have been removed without significantly altering the flow pattern. The Figure 4-11 flow distribution, when analyzing the primary stage using reactive flow, showed much lower wall temperatures as depicted Figure 4-12.

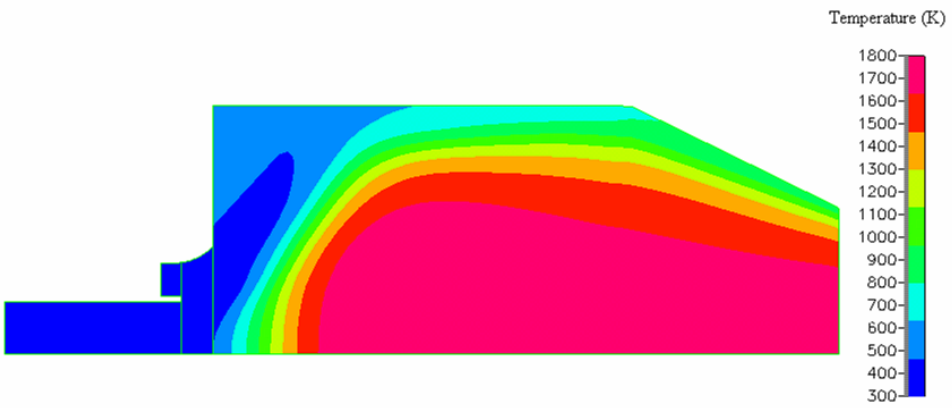

Figure 4-12 – Concept 10 temperature distribution

Notice the gas temperatures along the hot side of the liner wall in Figure 4-12 approach the 750°C (1000-K) range.

4.7.2 Catalyst inlet temperature uniformity

The System Requirement for the preburner is for a catalyst exit temperature of 700 °C average with maximum and minimum temperatures at ± 50 °C of the average. This criterion has been used to define an identical catalyst inlet temperature uniformity, namely ± 50 °C of the average. The final design, optimized through CFD, meets this criterion. Figure 4-13 shows the inlet face temperature uniformity in the sector of the catalyst that was part of the 3D CFD model:

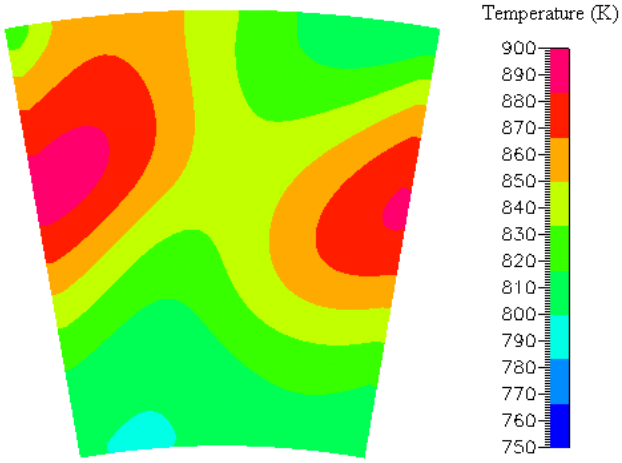

Figure 4-13 – Final Design Inlet Face Temperature Uniformity

Temperature contours at the catalyst inlet for the case with three rows of secondary holes and a 2 in. stretched combustor. Range is ~790 to ~890 K (~ 520 – 620 °C).The two pink spots represent the hot streams from two adjacent primary premixing tubes, while the cool spot in the lower portion is contributed to secondary stage air. This plot is indicative of the degree of thermal mixing that one should expect to occur at the 30% speed point where the primary stage runs hot to support light-off of the preburner catalyst.

4.7.3 Axial velocity contours

Figure 4-14 is a plot showing the axial velocity magnitude for the final design. As one would expect, high velocities are observed in the primary stage premix tube and swirler while almost stagnant regions exits near the secondary fuel manifolds and in the forward corners of the primary stage.

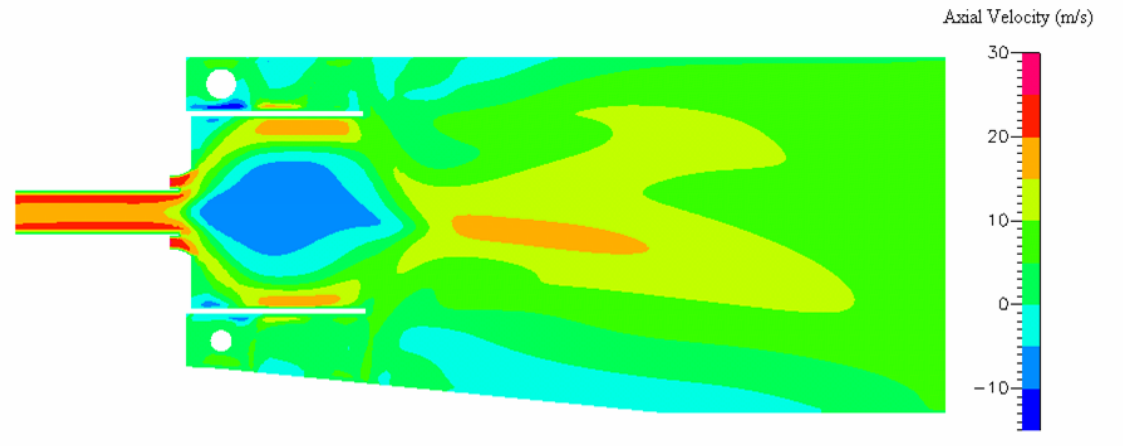

Figure 4-14 – Final Design Axial Velocity Magnitude

The two white rings in the front end of secondary annuli are the fuel manifolds. The geometry does not represent the final fuel manifold design, but the effect on the aerodynamics should be minimal and it was therefore deemed not worthwhile do update the CFD to reflect the final fuel manifold design.

4.7.4 Axial Temperature Contours

Temperature contours are of importance during the start transient, when the primary stage is lit. The objective is to improve thermal mixing between the hot gases emanating from the primary

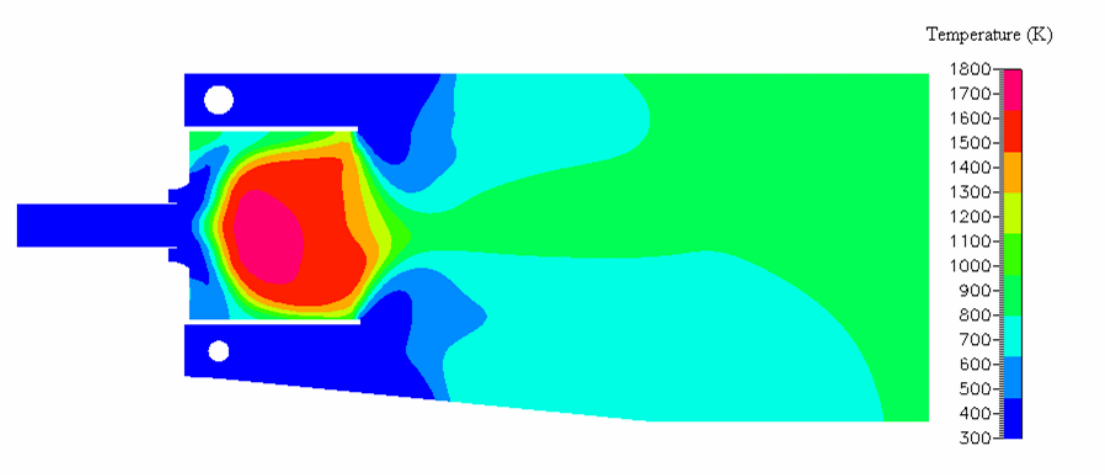

Figure 4-15 – Final Design Start Transient Temperature

stage and the significantly cooler secondary fuel air mixture, to achieve the most uniform possible temperature at the catalyst inlet. Figure 4-15 shows axial gas temperature contours at the 30% speed point. This plot does not include the effects of wall heat transfer in any part of the preburner.

4.7.5 Primary Zone Liner Wall Heat Transfer

Additional analysis was done with heat transfer on the primary zone liner walls included. ***T***his heat transfer assumed INCO 625 wall material and no hot side TBC. The effect on gas temperatures can be seen in the plot below. The analysis indicates peak temperature is reduced by about 100 K and also reduces the catalyst inlet temperature in the outer band.

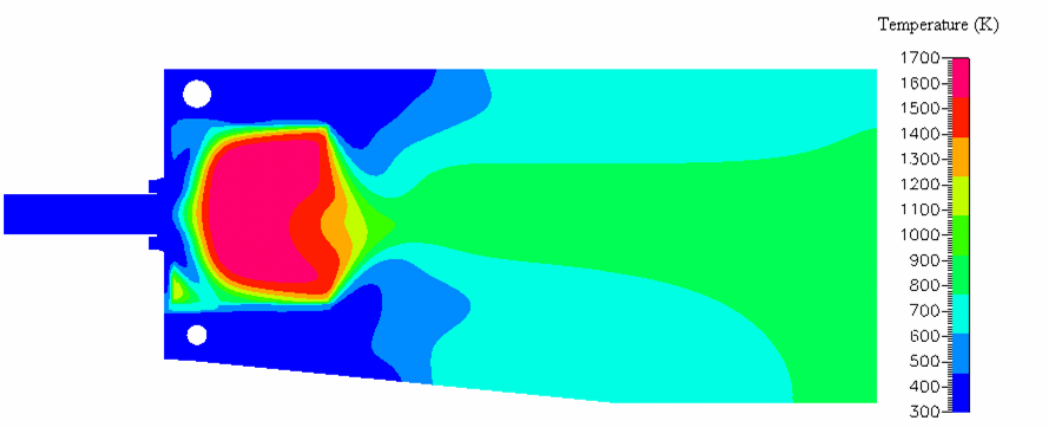

Figure 4-16 – Primary Zone Temperature Analysis

The effect of including primary zone liner wall heat transfer on catalyst inlet temperature uniformity can be more clearly seen in the Figure 4-17. Again, the hot spot results from one of the 18 primary premix tubes which causes a circumferential thermal gradient at the radial mid-span. The temperature range in the plot above is from about 740 to about 820 K, i.e., an 80 K temperature spread, which is a 20 K improvement over the same conditions without heat transfer analysis.

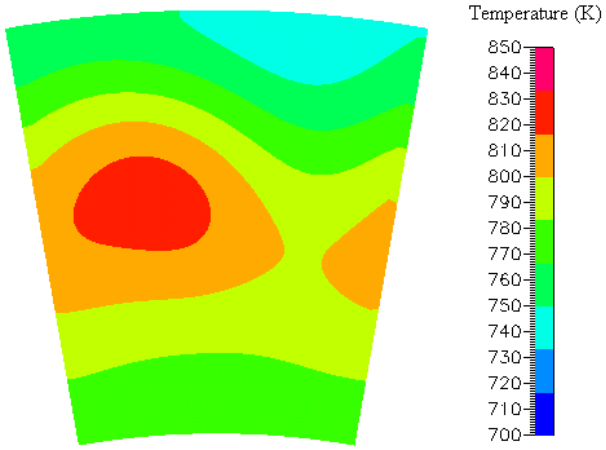

Figure 4-17 – Catalyst Inlet Temperature Uniformity

The last plot, Figure 4-18, depicts temperatures on the hot side of the primary zone liner walls. The most striking characteristic is the very large temperature gradients on the inner wall. Again, no TBC was modeled, which probably would have reduced these gradients. An empirical

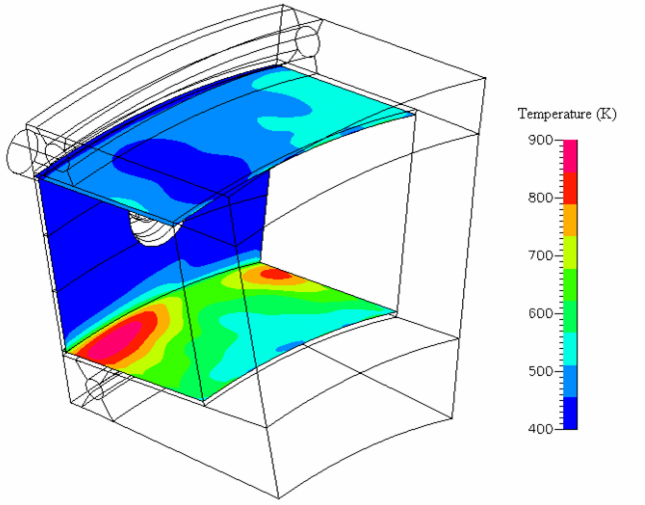

structural

Figure 4-18 – Primary Zone Liner Hot Side Wall Temperatures

assessment was made of these results and the liner walls were deemed as "not having any life at all". One of the actions in a potential follow-on program would therefore have to be to reduce temperature gradients either by improved cooling, incorporating hot side TBC, reducing hot side heat transfer or by other means.

4.7.6 Secondary zone optimization

Some optimization of the secondary zone also took place once the final concept had been developed. The inner and outer secondary premixing annuli are expected to perform in a very similar manner, and their main features are described below. Some of these features were tuned as part of the CFD analysis.

- Means of introducing fuel into the manifold; discrete pegs or continuous manifold.

  The first design used a circular manifold external to the preburner, with discrete peg penetration evenly spaced around the head end of the secondary annulus. The pegs used orifices to inject the fuel perpendicular to the peg centerline and upstream of the first air dilution holes. CFD analyses showed that with any reasonable amount of fuel pegs, it was very difficult to achieve the required fuel air uniformity. This led to the second and current fuel manifold configuration. In this case, the circular manifold is brought inside the fuel air premixing annulus, and allows incorporation of a very large number of small orifices to ensure adequate fuel/air uniformity at the catalyst inlet. This approach also allows for simple modifying orifice sizes and location in case geometry changes or operating conditions require a change in the fuel injection profile.
- Secondary air introduction.

Secondary air is introduced through rows of holes in the preburner liner. Rapid mixing with the secondary fuel is required in order to meet the fuel air uniformity target as well as quickly diluting the fuel to minimize the flame holding risk. The secondary annulus height is relatively small, which aids in the secondary air jets penetration. The small channel height allows for up to three rows of secondary air dilution holes. By staggering these holes, excellent mixing between the secondary air and fuel can be achieved over a short distance. It was found that the optimum configuration was three rows of staggered holes where the third most downstream row would be inline with the primary stage exit.

- Preburner length.

Three different lengths of the preburner have been tried. Two and four inch extensions of the preburner section upstream of the catalyst were modeled. The purpose was to see if a longer mixing channel would improve the thermal mixing between the hot gases from the primary stage and the cool secondary fuel air mixture during the start transient. This mixing has to take place over a very short distance due to the space limitations of the preburner combined with the length of the primary zone liner walls. The elongation of the preburner aimed at increasing the distance between the downstream end of the primary stage and the catalyst inlet. A decrease in catalyst inlet temperature of 100-150 K was observed at the 30% speed point when the preburner was stretched two inches. The additional benefit of increasing the stretch to four inches was relatively small. It was determined the compromise between preburner length, catalyst inlet temperature uniformity and conflicts with other combustor components would be with a two inch stretch.

4.7.7 Key conclusion and highlights from CFD analysis

Final geometry is characterized by:

- Primary zone liner walls 1.5” long
- Preburner stretched 2” upstream of catalyst
- 3rd row of secondary dilution holes added at aft end of PZ liner walls

Performance:

- Less than 100 °C temperature spread at catalyst inlet at 30% speed (Target ± 50 °C)
- About ± 12% velocity variation at catalyst inlet (Target ± 5%)
- PZ liner walls excessive temperature gradients, results in “no life”
- CH4 variation at catalyst inlet at base load less than ± 3% (Target ± 5%)

4.8 Mechanical Design

4.8.1 Summary

18 fuel-air mixing tubes feed the primary zone, while the secondary annuli are each fed by a ring manifold. Each secondary manifold has 0.050 diameter holes spaced every one degree. The catalyst module itself is designed to be field serviceable, requiring minimal work to remove and replace in the field. An outer flange secures the module, and the other end rests in slip-joints at the secondary. This provides sealing and allows for easy replacement of the catalyst module.

A complete detailed layout, drawing number SK29010005, has been released. This detailed layout provides sufficient information for combustor fabrication and inspection.

4.8.2 Discussion

The final design can be broken down into five separate components: Design Requirements, Overview/Design Approach, Primary/Secondary Zone, the Catalyst Module, and the Dilution Zone. Each of these will be covered individually.

4.8.3 Design Requirements

The approach for this design task was to integrate a catalyst module into a pre-burner unit, using the current Xonon 2.1 to base the design. The main requirement was to create a pre-burner that would allow easy and quick access to the catalyst for replacement. This requirement included the need for minimal bolts to remove, no welds to have to break, and a protected catalyst, which would prevent the mechanics from actually having to handle the catalytic foil pack during replacement. It was also desired to be able to replace the catalyst during a single work shift, thereby minimizing the down time of the engine. Since the possibility existed for this design to be tested in the KHI engine at SVP, the design would have to be incorporated within the Xonon 2.1 combustion system envelope.

Performance requirements, from the aero-thermal side, were a large driver for the current design, as the design went through a number of revisions while trying to meet goals. Figure 4-19 is an over/under image, showing how the catalytic preburner compares with the current pre-burner installation in the Xonon 2.1. Figure 4-20 is another view of the catalytic pre-burner.

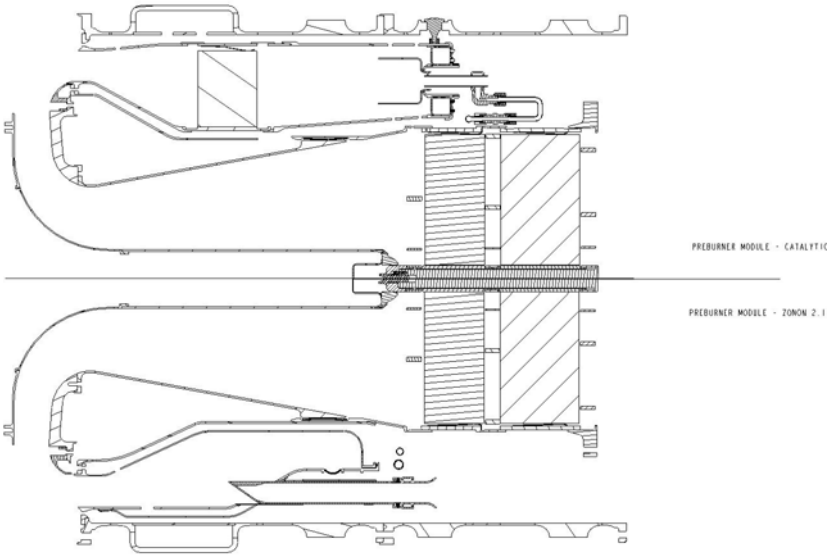

Figure 4-19 – Preburner Comparisons

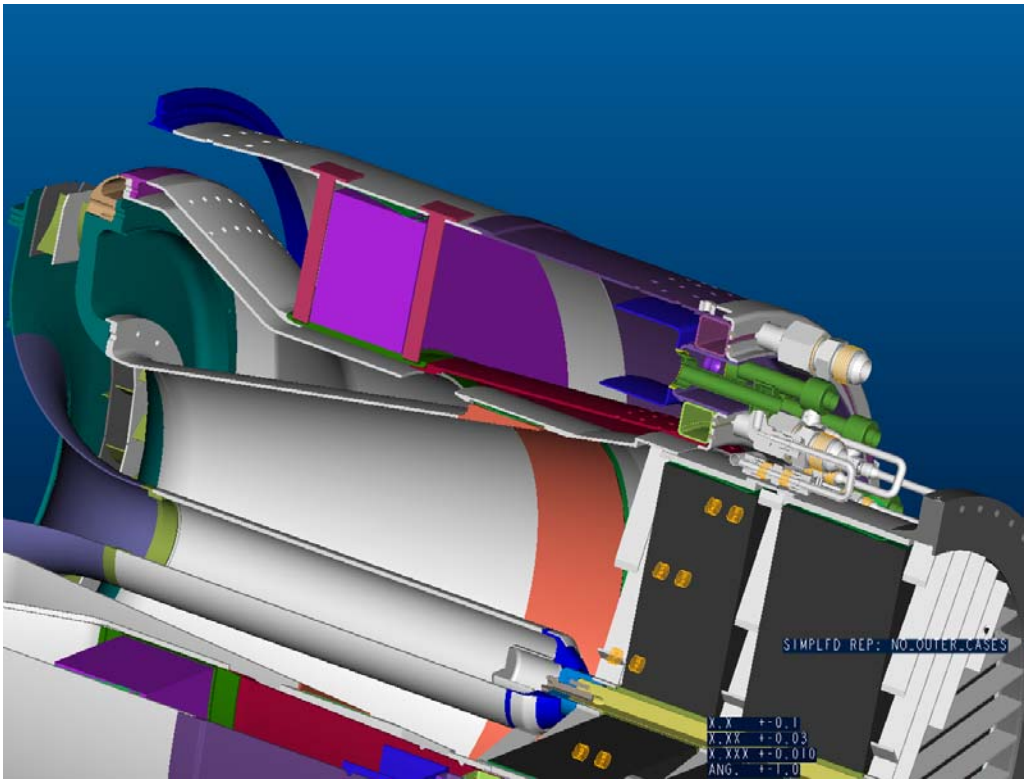

Figure 4-20 – Catalytic Preburner

4.8.3.1 Overview / Design Approach

In order to create a design that allowed the easy removal of the catalyst pack, the preburner had to basically be created in two parts. Among other things, this created the need for separate structural support systems. Figure 4-21 shows the support, and load paths that each carries.

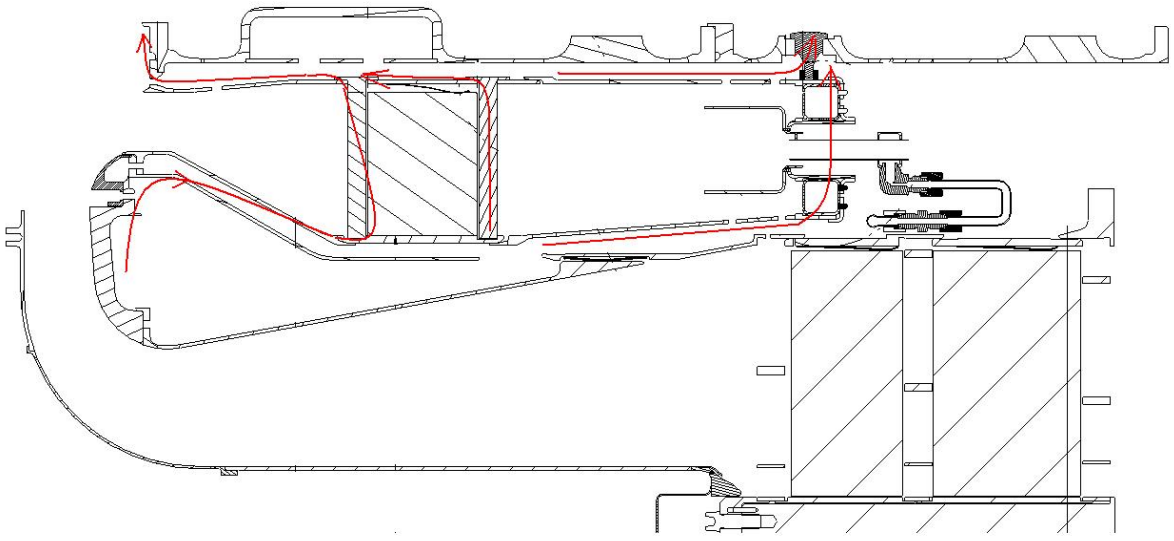

Figure 4-21 – Preburner Mechanical Support and Load Paths

The primary objective of the three support pins going through the case is to support the Primary / Secondary zones and fuel systems. The slip-joints in the liners upstream allow thermal growth of different liners, as well as allow removal of the catalyst module, but are not intended to transfer load across. The OD flange, downstream of the catalyst, is the primary support for the catalyst module, the flowpath, and part of the vane pack load. The flowpath and vane pack load are transmitted into the catalyst spindle, and that is carried by the radial supports. The ends of the supports are fitted into slots in the spindle. The design is sized such that the supports can not become disengaged from the spindle, due to either relative motion or thermal growth. This ensures the structural integrity of the flowpath, as well as support for the catalyst foils.

4.8.3.2 Primary/Secondary Zone

This part of the design involves the handling and distribution of the pre-burner fuel, as well as the primary flame, used to heat the catalyst during start-up. It is comprised of an annular Primary Zone, surrounded by two Secondary Zone annuli. The Primary Zone (PZ) is supplied fuel by 18 separate fuel / air tubes, each with a fuel supply connection and air swirler. The two Secondary Zone (SZ) annuli are supplied fuel by internal fuel manifolds, which act as support for the PZ. These fuel manifolds have 360 fuel ports (every 1 degree), and are allowed to 'float' within the liners, allowing for thermal growth. Secondary air is supplied by holes in the liners just downstream of the fuel manifolds. (See Figure 4-22)

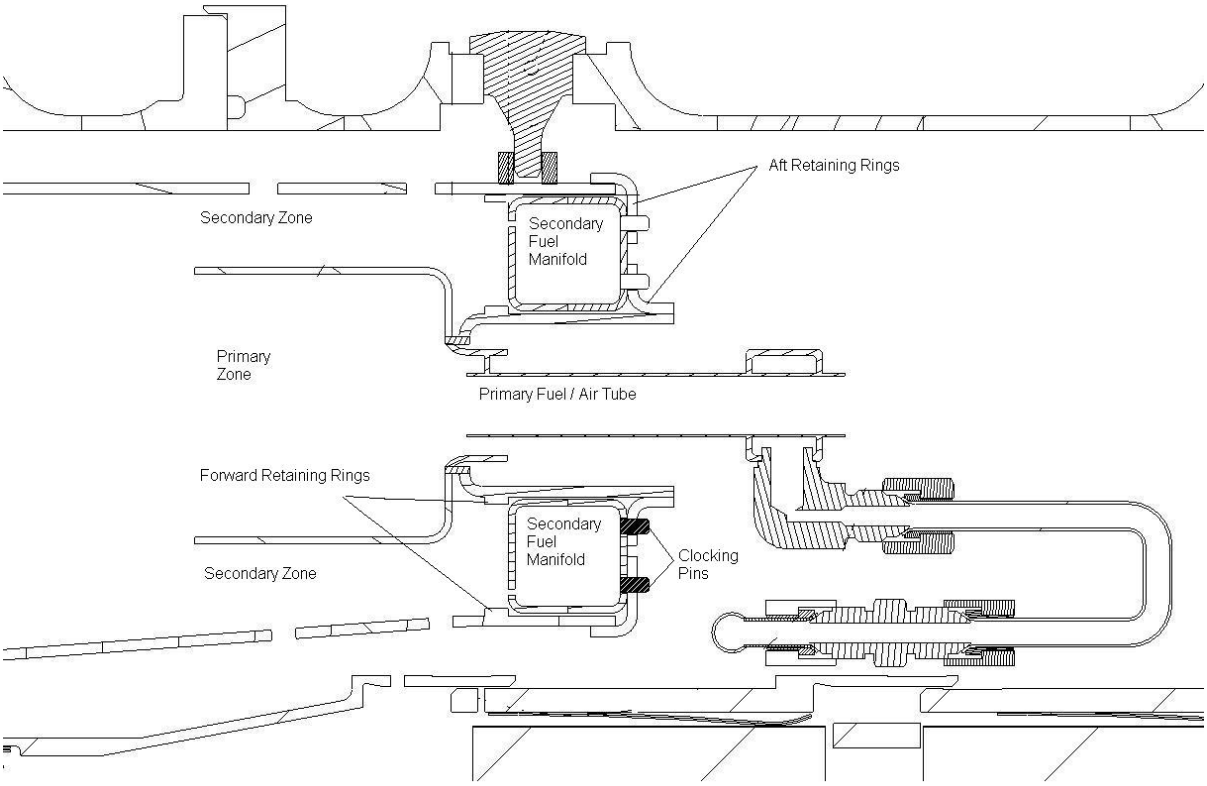

Figure 4-22 – Preburner Secondary Flow Passages

The short time of the PZ activation creates the need to have the secondary fuel manifolds float, as they will see a thermal gradient along the PZ bulkhead that supports them. For this preliminary design, the actual metal temperatures and gradients for the PZ bulkhead are unknown; estimates were made for the metal temperatures. Clocking pins are included in the manifold design, to ensure correct orientation of the assembly. This correctly locates the manifolds to the fuel supply lines & bulkhead fittings that take the fuel lines through the pressure case. Both the inner and outer fuel manifolds will be supplied by three (3) fuel lines each. This ensures that there will not be a significant pressure loss along the manifold, and that there will be adequate pressure and flow-rate for the fuel injection.

The supports that hold the fuel manifolds in place are welded on the liners, and brace the manifolds. This will allow air leakage around the manifold and into the secondary annuli. With more accurate metal temperatures, the actual operational gaps will be known, and can be accounted for, by reducing the amount of air that is introduced just downstream.

The outer liner is supported by three pins that are secured to the outer case. These pins support the Primary / Secondary zone, but allow relative movement for thermal growth. Control of tolerances will dictate the amount of movement allowed for the Primary / Secondary.

4.8.3.3 Replaceable Catalyst Module

The next segment of the design is the catalyst module, shown in Figure 4-23. The requirement for this was that it had to be field replaceable within a short amount of time ('single-shift change'). To facilitate that, the catalyst module is a 'floating' design, where it will only be captured at one area, the outer flange where it meets up with the outer case. The opposite end of the module will create slip-joints with the secondary liners, allowing relative motion to avoid thermal stress. This joint will allow the catalyst module to be replaced without needing to remove any fuel lines and connections, or requiring any difficult disassembly procedures.

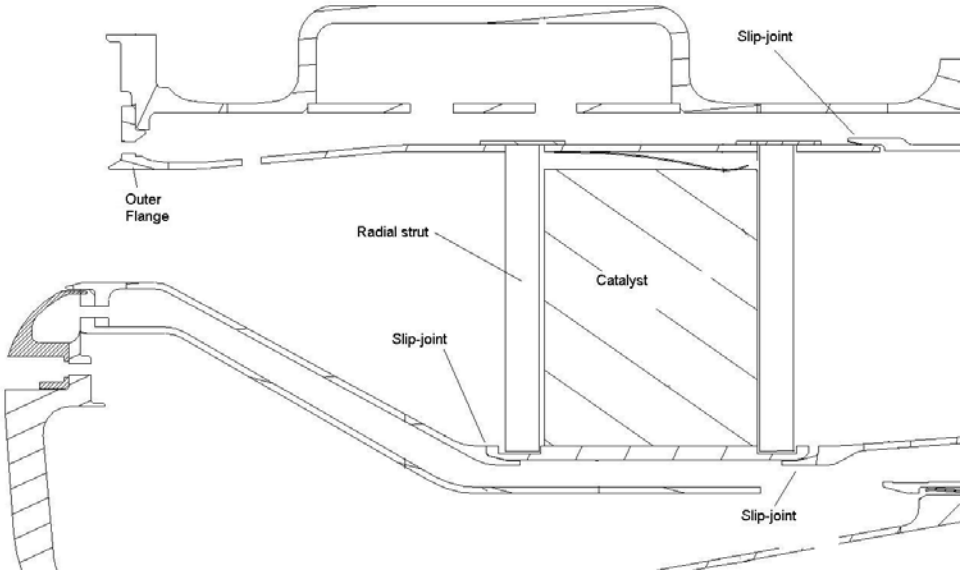

Figure 4-23 – Replaceable Catalyst Module

With better metal temperatures (follow-on program), the liners can be sized to minimize the leakage area through the slip-joints. Also, more detailed CFD analysis can show the affect on the flow and fuel distribution. If this is deemed to be an issue, a more leak-tight slip-joint can be designed for the area, such as a piston-seal or 'C' seal (albeit at a higher cost). A spring seal is installed within the catalyst module, to seal between the catalyst and the outer liner.

The inner flow-path, including the vane-pack, is supported by the catalyst module. The load from the inner spindle is carried through the radial struts and out to the outer liner (and then the outer case). The radial struts are welded to the outer liner, and rest in a slot in the catalyst spindle. They are sized to allow for thermal expansion during operation, but will not bind up and create thermal stress. They are also designed to ensure that they will always be engaged, and never come out of the slot (doing so would not allow them to support either the flowpath assembly or the catalyst).

The radial strut count was determined by estimating the worst-case loads the catalyst module would see during handling and shipping. In this case, a 10g load was assumed.
Normal operational loads were not used, since the ΔP across the catalyst is so low (~ .08%) that it would not impart a significant load to the struts. So the larger concern becomes the possibility of damaging the foil during transportation or installation of the module (bumping or dropping the module). An estimated limit pressure on the foil of 600psi was used in the calculations, and a count of 43 struts per side was calculated.

Another aspect of the catalyst module design was the required gap at the slip joints, so that the liners didn't grow to an interference fit as they heated up. This would impart stresses into the parts, reducing the life of the parts. For the preliminary design, liner temperatures were estimated at 625°F (compressor discharge temperature), while the outer case was assumed to be 200°F for transient, and 500°F for steady-state calculations. The minimum needed gap was calculated to be 0.030", and was doubled in the design to account for tolerance stack-ups.

4.8.3.4 Dilution Zone

This area is comprised of the volume just downstream of the catalyst, enclosed by the liners. Here, the rest of the air is introduced through holes in the liners (Figure 4-24). The inner liner rests on the catalyst spindle, and supports the vane-pack load, as well as the flowpath sheet metal. The inner liner is captured by the vane pack and the dome, which limits the axial movement allowed by the liner. This ensures that the slip joint will not become disengaged. The dilution zone also includes a cooling shroud, which will accelerate air underneath the catalyst spindle, aiding in the cooling of the spindle. This air is then directed into the dilution zone.

In the dilution zone, the inner liner and cooling shroud will be re-used in a catalyst replacement. The outer liner is part of the catalyst assembly, so it cannot be reused. The slip-joint part of the inner liner will be machined from a forging and welded onto the sheet metal, so it should have minimal deformation from the thermal cycles of the engine, and be able to mate up to a new catalyst spindle. There will also be clocking features from the catalyst spindle to the inner liner. This is needed so that the mixer assembly lines up with the support bolts, as well as the fuel pegs that protrude into the assembly. The outer flange also has clocking features on it, so that it will ensure that the entire assembly is correctly oriented.

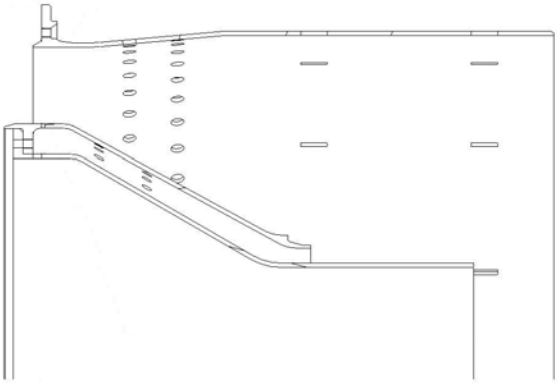

Figure 4-24 – Preburner Dilution Zone

4.8.3.5 Risk Elements & Mitigation

The following issues are seen as risks to the design which need to be addressed before rig hardware and testing are initiated. Each issue is followed by plans to examine them in depth, and a relative priority for the investigation; basically how severe an issue it is to the testing phase. Also included are some mitigation ideas that could be incorporated into the design. These would be in addition to 'fine tuning' the current design, which more than likely would be the result of CFD work.

Risk Elements & Mitigation:	Priority	Potential Mitigation
Flashback at Secondary Fuel Manifold: • More extensive CFD, Rig Testing	High	-Mechanical Shield
Structural risk of manifold design: • Fretting calculations, Stress Calcs, Rig Testing	High	-Hard coating, -Design optimization
Primary Zone Liner life (thermals): • Design Optimization with CFD, Rig Testing	High	-Liner Cooling Optimization
Air Leakage affects on Performance: • CFD, Rig Testing	Med	-Better sealing (mechanical seals)
Igniter Placement: • Rig Testing	Low	

4.9 Recommendations

The last purpose of this TDR is to capture design issues that came up, but were not addressed in the current design. These issues would have to be resolved before taking the design to an engine development status. These issues are:

- 3-D CFD on current design details
- Simplification of Fuel System Design

- Comprehensive Structural Analysis
- Igniter / Outer Case Design
- Metal Temperatures
- Thermal Stress for design
- Part Review with Manufacturing / Suppliers
- Catalyst Module Simplification

4.10 Donald Bahr Commentary

Donald Bahr is a member of the CESI Technical Review Board. It was determined that a third party opinion from someone highly experienced in the area of gas turbine combustion was desirable in reviewing the final catalytic secondary preburner design. His commentary [3] is included in full below.

Mr. Bahr was Manager - Combustion Technology at GE Aircraft Engines (GEAE) for more than twenty years prior to his retirement in 1994. He joined GEAE in 1956 as a combustion research engineer. As Manager - Combustion Technology, he was responsible for leading a variety of design analysis, development and qualification efforts to provide combustion systems for use in both commercial and military aircraft turbine engines, and in industrial turbine engines. A major aspect of these responsibilities was the evolution of low pollutant emission combustors.

Mr. Bahr has issued six patents. He is a Fellow of the American Society of Mechanical Engineers (ASME) and of the American Institute of Aeronautics and Astronautics (AIAA). He was the 1982 recipient of the GEAE Perry T. Egbert Engineering Achievement Award, the 1983 recipient of the AIAA Air Breathing Propulsion Award and the 1998 recipient of the ASME R. Tom Sawyer Award. He was elected to the National Academy of Engineering in 1991 and, in 1995, to the General Electric Propulsion Hall of Fame.

COMMENTARY

Subject: Preburner Design with Catalytic Secondary Stage – for CESI XONON Combustion System

Introduction

As a means of eliminating many of the performance and NOx emission penalties associated with the existing lean-premix secondary stage of the preburner, the replacement of this secondary stage with a catalytic secondary stage is being studied by CESI. This design approach appears to offer several important advantages.

A specific preburner configuration which features the use of a catalytic secondary stage has been defined by CESI. Additional studies to refine and develop this design are underway.

At the request of CESI, a brief assessment of this design was conducted. The following are comments on several specific design issues.

Attainment of Secondary Stage Inlet Gas Velocity Uniformity

Obtaining thorough mixing of the primary stage gases with the two secondary stage flows is likely to be difficult, even with the maximized mixing length that has been incorporated into the preburner design. As such, attaining secondary stage catalyst inlet gas flow uniformity is a difficult challenge. Some provisions that might be considered to provide enhanced mixing are:

- The incorporation of some swirl flow into the secondary stage inner annulus stream (possibly by the use of dilution air holes with some type of a partial tangential feed). Such a swirl flow element would provide some centrifuging of this secondary stream outboard and into the primary stage stream.
- The introduction of some stream mixing enhancement at the trailing edge of the primary stage outer-side liner: One possible approach is the incorporation of circumferential convolutions (lobes) into the downstream end of the liner (probably an 18-lobe array to line up with the 18 primary stage fuel injectors). Such a convoluted configuration, like a daisy mixer, would promote considerable mixing between the two streams, by bringing some of the primary stage flow outboard and some of the secondary stage flow inboard. Such mixing arrays are commonly used in mixed-flow aircraft engines to mix the core and fan streams. The effectiveness of mixing provisions of this kind can be evaluated with CFD analyses.

Attainment of Secondary Stage Inlet Gas Temperature Uniformity

At operating conditions above about 80% speed, fuel-air ratio uniformity at the secondary catalyst inlet face can be maintained by properly regulating the fuel flows to each of the three preburner streams (primary, inner secondary, outer secondary). However, at engine speeds below about 80%, the primary stage fuel-air ratios will be higher and, as a result, the mid-span catalyst inlet temperatures will be higher. To mitigate this concern, enhanced mixing of the primary and secondary stage streams may be needed. The above-mentioned mixing enhancement provisions are some possible means of obtaining any needed improvements.

Thorough fuel-air premixing within the two secondary stage annuli is also an important need. To ensure good premixing, the secondary stage air admission (dilution) holes should be configured so that there are no circumferential gaps where fuel jets can penetrate and pass through the premixer without being impacted by one or more dilution air jets. To meet this need, the dilution air holes should be appropriately clocked, rather than being in an axial alignment – so that some dilution air is admitted at every circumferential position. Even with such clocking, it may not be possible to have adequate circumferential coverage in the inner annulus, because its dilution holes must be smaller in diameter than those of the outer annulus. If so, oval (racetrack) shaped holes may be considered.

In addition,, to ensure good secondary stage fuel-air premixing, uniform fuel flows from each of the 360 ports is a requisite. The proposed use of three lines to feed each of the two manifolds is an excellent provision for meeting this need. However, at the lowest secondary stage fuel flows, ideal fueling may still not be obtained because of the likelihood of low fuel injection pressures.

Primary Stage Liner Cooling/Durability

Obtaining sufficiently low liner temperature levels and gradients to ensure adequate liner life is likely to be a difficult challenge. In particular, in the currently defined preburner design, cooling of the two corner regions, where the liner turns from a radial to an axial direction, appears especially challenging. Added backside baffles or other features to provide better convective and/or impingement cooling in these areas are definitely needed. In addition, the use of a thermal barrier coating of the entire liner should be considered. The use of such a coating would result in generally lower temperatures throughout the liner and decreases in the magnitudes of any thermal gradients in the structure.

Use of Ferrules in Primary Stage

To accommodate the effects of thermal growth of the liner the use of, a ferrule around each of the 18 swirlers is probably required., Since the radial location of the premixer tube/swirler assembly will remain fixed, such a sliding slip joint of this kind is a likely requisite to permit the liner to move radially as needed, For the same reasons, if the igniter tip is to be positioned (as currently shown) in a hole in the outer side of the preburner liner, a ferrule will probably also be needed in this location.

Primary Stage Premixing Tube Air Entry Provisions

To improve the uniformity of the airflows of the 18 tubes, each tube should be provided with a bell mouth inlet. Preferably, a low pressure loss restriction, such as a venturi nozzle, should be incorporated downstream of the bell mouth. Such a restriction would greatly minimize the possibility of fuel escapement out of the inlet, due to flow separations and other flow anomalies.

Summary and Conclusions

The presently defined preburner design with a catalytic secondary stage is definitely a well-conceived design with considerable promise. This design offers the potential of eliminating many of the performance, operational and NOx emission concerns associated with the lean-premix secondary stage of the existing XONON combustion system preburner. In addition to these important benefits, the predicted combustion system pressure losses with this new preburner are reduced – by about 0.65%.

Further analysis and development efforts are needed to address the above-described design issues. Also, one other key design issue – an increased propensity for flashback occurrences in the main stage fuel-air premixer – must be addressed.

Donald W. Bahr

October 21, 2002

4.11 Conclusions

A preburner with a catalytic secondary stage has been developed and refined through extensive use of CFD. Mechanical design features have been incorporated and some simple hand calculations performed to evaluate the life of the most critical components.

4.12 Recommendations for Further Work

A Detailed Design Review meeting was held October 8, 2002. The purpose of the meeting was to go through the main features of the final design, the CFD analysis that had lead to this design and the mechanical design features that were built into to make it technically feasible as well as incorporating features for ease of manufacture, assembly and disassembly. Below are the meeting notes taken from the meeting. These are comments to the work completed and will also serve as recommendations for further work, in addition to the comments above from Donald Bahr.

1. Evaluation of 8,000 hrs catalyst life cycle. Update cycle analysis spreadsheet for new catalyst with high conversion, aged catalyst with reduced conversion. Effect on main stage inlet temperature/performance.
2. Evaluate need for combustor bypass air vs. ambient and catalyst main stage age. How will it compare to Xonon 2.1?
3. Slide 6 in "overview" presentation: Revisit calculated temperatures between preburner exit and main catalyst inlet. Action: KL
4. Slide 7 in “overview” presentation : Revisit Xonon 2.1 pressure drops. Action: KL
5. HPR testing of optimized catalytic secondary stage and main stage in Go-Forward program.
6. Slide 9 in "overview" presentation: Change main stage catalyst conversion to get 900 °C catalyst outlet temperature at ISO base load. Action: KL
7. Slide 9 in "overview" presentation : What is expected turndown before hitting 10 ppm CO (w/o bypass)?
8. Slide 10 in "overview" presentation : Acceptable velocity non-uniformity at catalyst inlet should be +/- 10%. Preburner catalyst pressure drop should be higher than 0.08% based on current frontal area. Action: KL
9. Slide 3 in "CFD" presentation: Compare calculated Tad to integrated primary zone gas temperature across primary zone height. Action: KL
10. Fuel manifold, liner, bulkhead thermal growth analysis required.
11. Slide 8 in mechanical design presentation: Estimate seal leakage between preburner front end and catalyst module, thermal growth analysis.
12. Slide 18 mechanical design presentation : May be able to use stainless steel for fuel manifolds. Stainless considered equivalent to nickel alloys (incl. erosion resistance) at temperatures up to 800 °F, according to boiler code.
13. Preburner interference with main stage inlet T/C's:
14. Determine need for main catalyst inlet T/C's in the first place. Calculate catalyst inlet T from preburner exit.
15. Move T/C's to aft end of mixer centerbody
16. Design T/C's to not be field replaceable
17. Additional CFD: Investigate possible reduction of fuel orifice quantity in secondary manifolds from 360 to something less. Note: clogging not much of a concern due to current orifice size; mainly cost reduction, simplification.
18. Stress analysis required to determine number of segments (if any) in secondary fuel manifolds.
19. Include Tim C's memo about high gas temperature flameholding/flashback in final report.
20. Get D. Ginter rig data from catalytic secondary test (2" foil).

21. Catalyst:
22. "Mechanical design" presentation: Elevated temperatures in mixer need to be looked at(vane stresses, LCF, creep, etc.)
23. Life vs. catalytic secondary performance using predictive tools.
24. Is catalytic secondary outlet temperature < 650 °C possible? May eliminate need for bypass system.
25. Main stage catalyst must be better matched to preburner catalyst.
26. High H2O testing. Include effect of water vapor on predicting catalyst conversion.
27. Baseline preburner catalyst exit temperature may be 650 °C to allow room for T exit to grow as main catalyst ages.
28. Use 650 °C preburner catalyst T exit as starting point for fresh main catalyst, 750 °C with aged catalyst.
29. Analyze effect of up to 50% drop in preburner catalyst conversion. What will F/A ratio and temperature be downstream of catalyst?
30. Generic comments.
31. This design may be favorable in a multi-can application, like GE 7FA.
32. Estimate benefit (for power, efficiency) of reduced combustor DP to an F-class engine.
28. Present $\Delta P/P$ benefit to management.
29. Consider fueling the primary stage on the rich side ($\phi > 1$) so as to provide both temperature rise and an unburnt F/A mixture to the secondary stage catalyst.

4.13 References

[1] CCSI document "Solicitation DE-SC02-00CH11000".

[2] CFDRC Report 8473/1 by David L. Black: "DOE Catalytic Secondary Preburner CFD Analysis", September 2002.

[3] Donald Bahr, email (donbahr@msn.com) titled "Comments on Preburner", dated 10/20/2002.

[4] Philip Tuet, "Xonon 2.1 Burnout Zone NOx Formation at Baseload Conditions", CESI Technical Report, May 11, 2001.

[5] Per communication with Jere Osmer at Agilis, 1996/1997, FT-4 program.

[6] David Ginter: "Catalytic Secondary Rig Testing", preliminary Technical Data Report, 01/31/02.

V. Broadened Operating Range - Task 2.2 – Catalytic Pilot for Lean Premix Burner

5.1 Summary

This report describes design, analysis and testing conducted in a DOE sponsored program called "Catalytic Pilot". The program has consisted of three stages; conceptual design, rig testing at the University of California at Irvine (UCI) and rig testing at Solar Turbines. UCI and Solar acted as subcontractors of CESI in this program. Different hardware was used for the two test sites, and the UCI rig testing was atmospheric while the Solar testing at full pressure. The results have been encouraging in that NOx emissions have been measured as low as 4.4 ppmv corrected to 15% O_2 at simulated full load conditions. Combustion dynamics have also been very low in both test rigs, although rig test results can usually not be translated to engine conditions. An 8-atm intermediate pressure rig test was scheduled at UCI, but was repeatedly delayed and eventually failed to deliver any useful test data.

5.2 Background

A program was proposed to the DOE in February of 2000 [1] where a catalytic pilot burner would be developed as part of Low-Emissions Preburner Technology. . In CESI's proposal [1], task 2.2 describes the scope of work for a "Catalytic pilot for lean premix burner". A typical concept is one in which the catalytic pilot is installed in the center of a fuel injector encircled by a main stage burner, thereby acting in a way very similar to existing piloted lean injectors. When the combustor inlet temperature has reached the light-off temperature of the catalyst, the pilot will be fed a fraction of the fuel flow adequate to ensure stable operation of the main stage while simultaneously achieving ultra low NOx emissions, hopefully in the sub 10 ppmv range. One serious obstacle in achieving this with existing DLN technology, has been combustion-driven pressure dynamics. Increasing the amount of fuel fed to the pilot injector can reduce this, but unfortunately this also raises the NOx emissions. As opposed to the conventional diffusion flame pilot injector where thermally generated NOx plays an important role, a catalytically stabilized pilot burner would actually reduce NOx with the higher percentage of fuel fed to it, under normal gas turbine operating conditions. At part load conditions where the combustor inlet temperature would be below the light-off temperature for the catalyst, the pilot could be fed whatever amount of fuel that would provide stable operation of the main stage and not compromise combustor performance in any other way. Since no fuel conversion is taking place in the catalyst, it will be insensitive to the amount of fuel fed through it. In this mode, the catalytic pilot could function similar to a diffusion flame pilot, although the pilot fuel air mixture would likely be leaner and more uniform. When approaching the catalyst light-off temperature as turbine load increases, the pilot fuel flow would have to be kept below a certain threshold to avoid overheating the catalyst as light-off occurs.

5.3 Introduction

The combination of a highly competitive marketplace as well as ever tightening emissions regulations is forcing the major gas turbine manufacturers to improve their low emissions combustion technology beyond the current 15 ppmv (@ 15% O_2) guarantee on natural gas fuel which now has become an industry standard met by several OEMs. One of the major problems

in decreasing NOx emissions by leaning out the fuel mixture is the associated increase in combustion driven pressure dynamics. Several means of addressing this issue have been used, but many of them have one thing in common, namely to create a stratified fuel/air mixture where a fuel rich pocket (often in the center of the recirculation zone) enables the surrounding area to operate much leaner and thus overall reducing NOx emissions. The problem with this approach is that the required fuel/air richness of this pocket is almost always a function of combustor design and operating conditions, and it can become a significant NOx contributor, which often negates the benefit of operating the surrounding fuel air mixture significantly leaner. Diffusion flame pilots in particular, are at a particular disadvantage since diffusion style combustion leads to near stoichiometric reaction temperatures where thermal NOx has a huge impact on NOx generation. The very small fuel fraction to the pilot relative to the main stage has a substantial mitigating effect, however, and is what makes this approach a viable concept. The use of a catalytic pilot would not only eliminate the thermal NOx produced by a diffusion flame pilot, it would actually decrease the overall combustor NOx the higher the fuel fraction to the pilot. This is because the pilot produces temperature rise totally without NOx production, provided there is no NOx produced downstream due to homogenous combustion or a significant increase in the main stage flame temperature. The effect of a catalytic pilot vs. a diffusion flame pilot can be seen in Figure 5-1, which is based on actual test data:

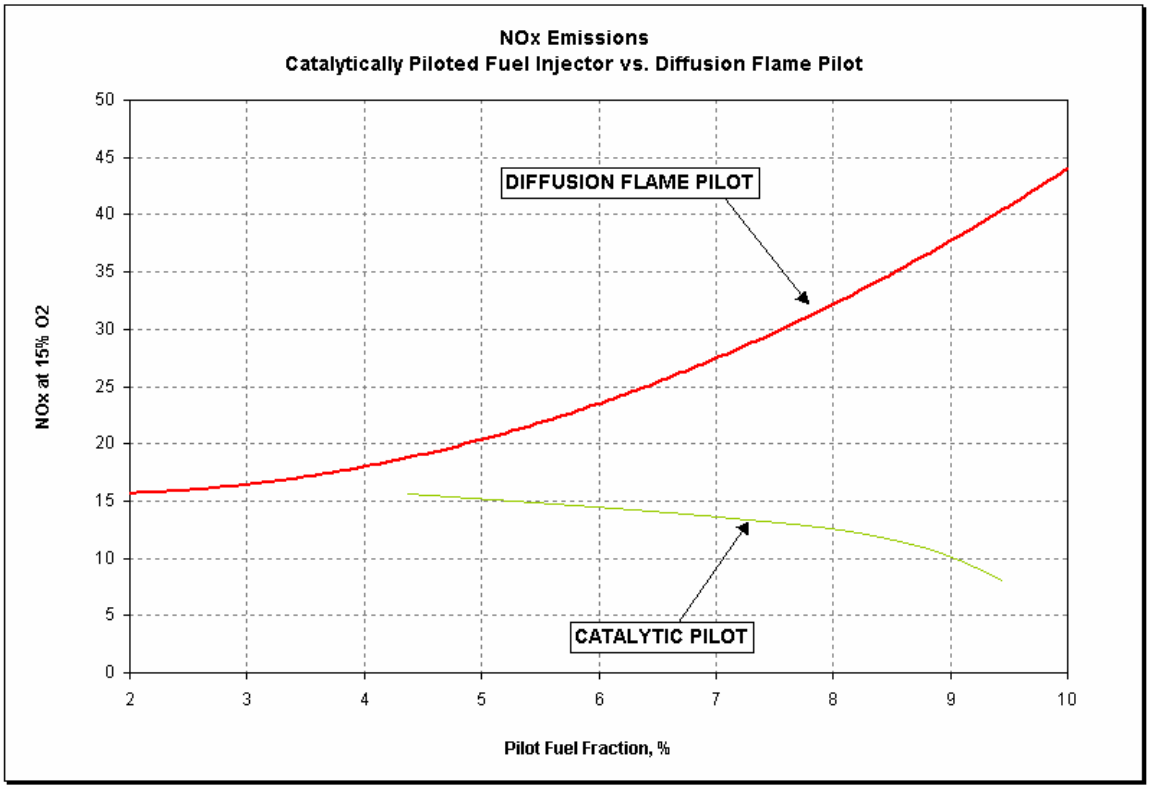

Figure 5-1 - Comparison of NOx production between a diffusion flame pilot and a catalytic pilot with a constant main stage flame temperature

5.4 Catalytic Pilot Concepts

Below follow several catalytic pilot concepts that were evaluated under Task 2.2. Some of these concepts show two catalyst stages, and some show only one. In all cases, the catalyst length is the same as the diameter, 1.54". In an engine installation, each catalyst would most likely be longer, typically 3 or 4" long. This will eliminate some of the concepts merely from space limitations. Further, the choice of using one or two catalyst stages, depends on several factors. For example, the desirable rate of fuel conversion in the pilot can determine the number of catalyst stages. A very low conversion design could be accomplished with only one stage, while a high rate of conversion more likely will require two stages. The velocity trough the catalyst foil channels also affects the rate of conversion and thus catalyst length. If pilot airflow is reduced by restriction at the inlet, it could affect the catalyst design. As will be described later, a low conversion pilot seems to be the most attractive concept when judging emissions and combustion stability. Other factors that may influence a commercial design are the mechanical complexity of the design, cost (driving towards a single-stage catalyst design), and the desire to get a uniform airflow entering both the pilot burner and the main stage.

In the early phase of the concept evaluation, several concepts were evaluated. The catalytic pilot would comprise three main sections: (1) Fuel injection, (2) Fuel/air premixing and (3) the catalytic foil(s).

Concept 1 utilizes a venturi which also manifolds the fuel prior to injection into the pilot tube. This design assumes a single stage catalyst with a very short mixing length. The main advantage is a very short injector that lends itself to compact installation requirements. One might imagine a derivative of this concept where the pilot tube is stretched forward to maximize the space available. A slightly longer inlet section of the pilot tube could allow for improved fuel/air mixing upstream the catalyst.

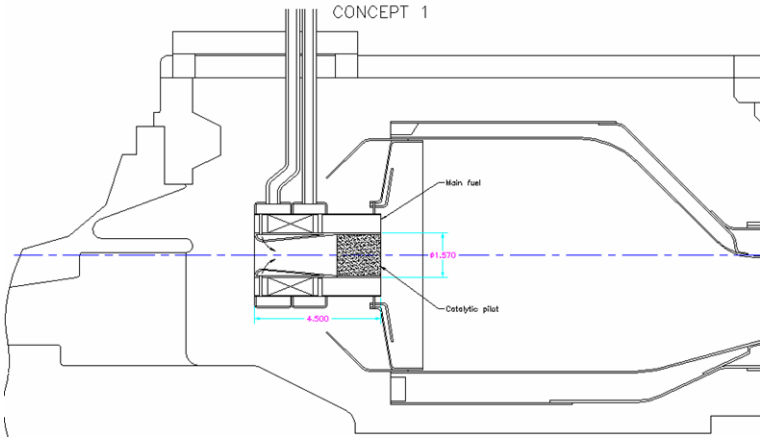

Concept 2 incorporates two catalyst stages. The pilot inlet is directed radially from the centerline, feeding through a full circle radial swirler. Fuel could be fed through the wall (as shown) or through spokes inserted into the flow path. This design takes advantage of the space available in the plenum upstream the preburner to ensure somewhat uniform airflow into the pilot. One disadvantage with this system is the blockage created for the fuel injector main stage inlet.

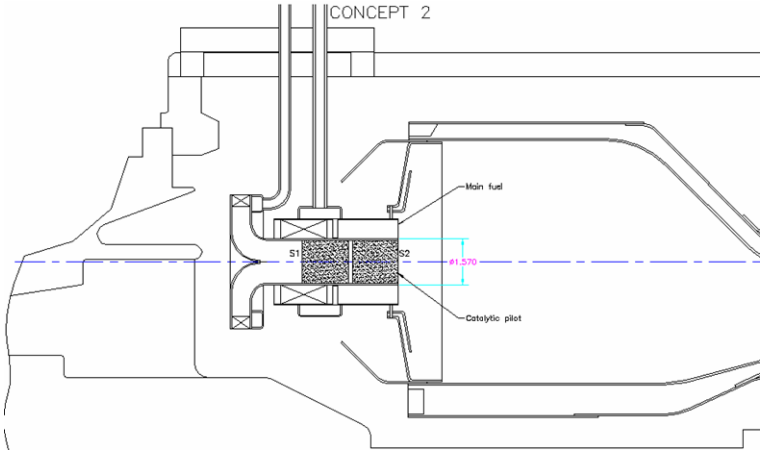

Concept 3 is similar to concept 2, but turns the pilot inlet aft to create a U-shaped flowpath. An axial swirler sits at the inlet. The first stage catalyst sits in the radial flow section of like a slice of pineapple. This configuration reduces the velocity through the inlet stage and should enable a slightly higher pilot air flow. The outlet stage is moved upstream to where the inlet stage sits in configuration 2. This leaves enough room downstream of the outlet stage to allow for a small burnout zone within the pilot.

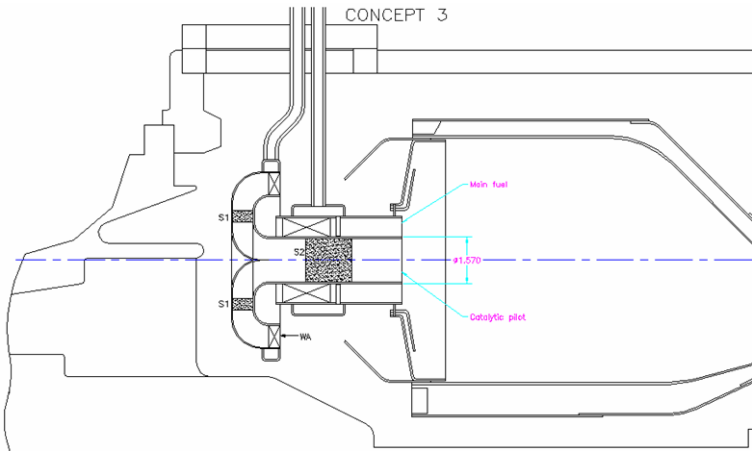

Concept 4 directs the pilot inlet radially outboard and maintains a tubular cross section geometry as opposed to concepts 2 and 3. The inlet stage sits in the radial portion of the tube, while the exit sits in the axial part, also leaving enough room for a burnout zone. Manifolding the pilot fuel around the OD of the tube inlet also creates a potential conflict with the neighboring combustor case. A non-uniform velocity profile going into the outlet catalyst stage may also become an issue due to the 90° turn of the flow.

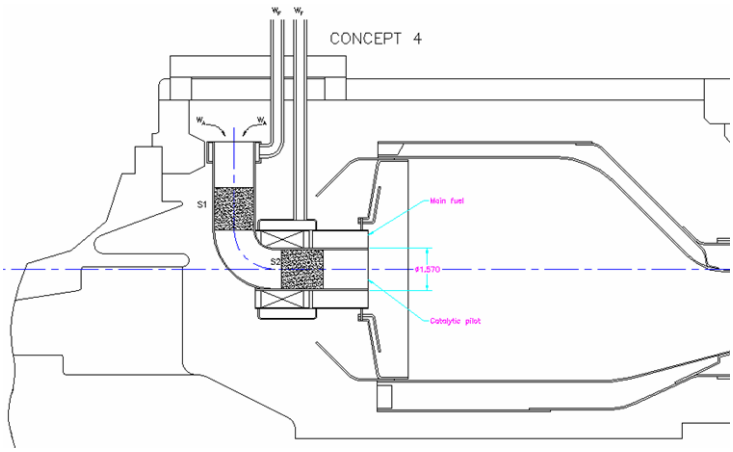

Concept 5 is an attempt to eliminate the blockage of the injector main stage as pointed out in the concepts above. At the same time, enough room for two catalyst stages have been incorporated into the tube. In this concept, the pilot tube is envisioned as a two-part assembly, split between the two catalyst stages, and assembled inside the combustor. The last stage would be to install the pilot fuel injector through the aft compressor diffuser case.

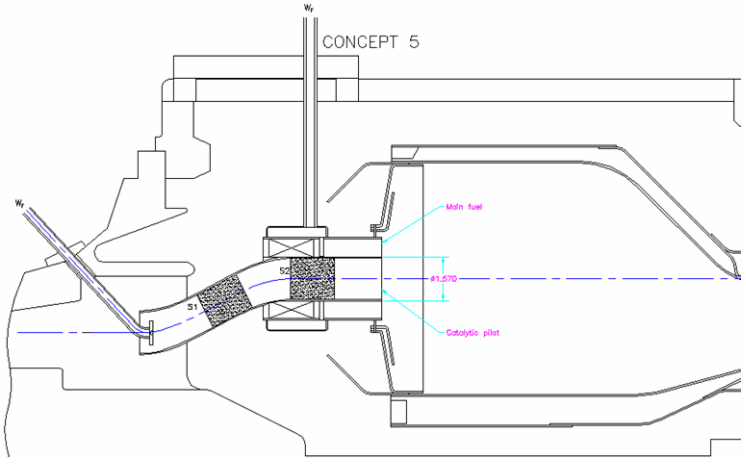

Concept 6 shows another way of incorporating two catalyst stages while maintaining a straight inlet section to the pilot. The flared inlet will lower the inlet velocity and should make the pilot less sensitive to the blockage at the aft diffuser section. This concept also greatly reduces the blockage of the injector main stage.

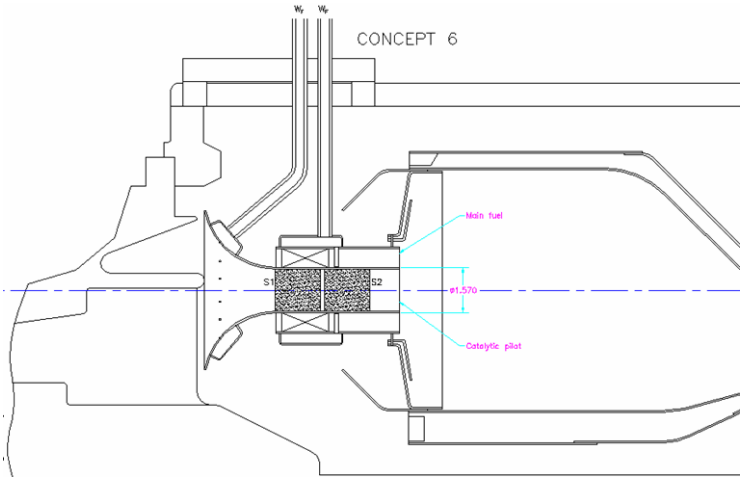

Concept 7 is similar to concept 5, but much more compact. The pilot tube inlet barely clears the aft end of the compressor diffuser, and the two catalyst stages are again short (1.57" long) and installed close together. The advantage is that the catalyst fuel system can likely be integrated into the main fuel flange like in most other concepts, and there is little aerodynamic blockage between the pilot inlet and the main stage inlet. Given the traditional design of catalyst stages being 3" long or more, this concept would be more viable for a single stage catalyst design.

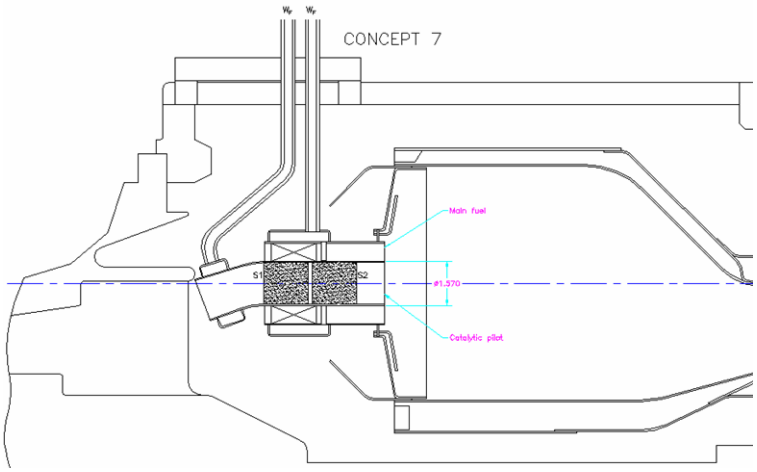

Concept 8 is a hybrid between the single tube inlet and the radial inflow inlet, in that the tube splits in two sections, diverting the inlet to left and right. The advantage with this concept is a better utilization of the volume upstream the combustor and in particular the space available between adjacent fuel injectors. Interference with the aft diffuser case should not be an issue, and pilot fuel can be supplied from the same flange as the main stage fuel.

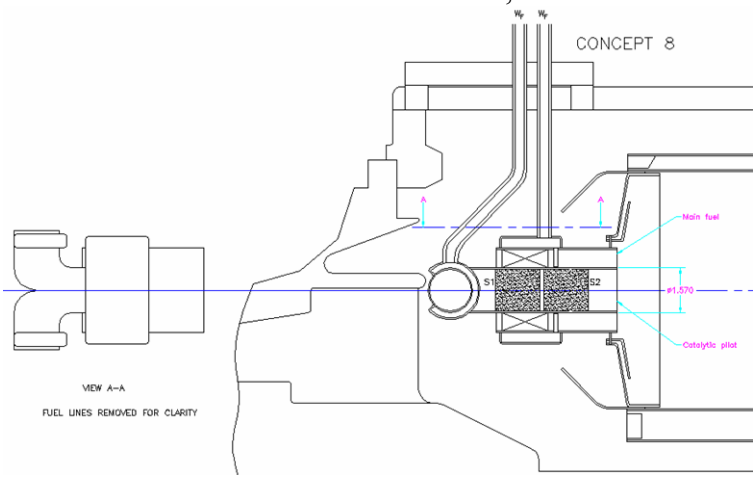

Concept 8B is similar to concept 8, with the inlet section of the pilot tube stretched, giving enough room for the inlet stage catalyst to be installed into this section of the tube. Two alternatives are shown; Alt. 2 is a symmetric design just like concept 8, which will require two inlet stages, one for each side, and alt. 1 showing an asymmetric design requiring only one inlet stage and thus being simpler and a lower cost alternative. Moving the inlet stage catalyst upstream now gives more room for the outlet stage catalyst, making this a more attractive alternative if a two stage catalyst is required.

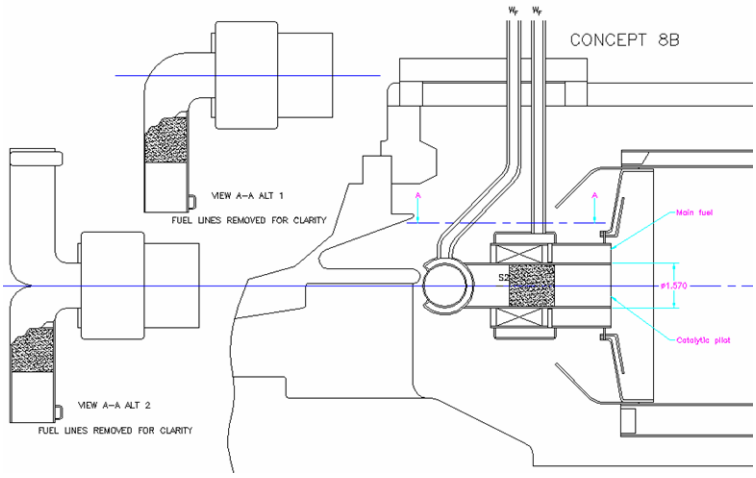

Concept 10 is almost identical to concept 4. The difference is that to avoid partially blocking the injector main stage inlet, the main swirler has been stretched around the inner radius of the pilot tube to allow for a larger opening on that side. This complicates the swirler design, but with appropriate use of CFD and rig testing, a uniform inlet air flow to the main stage could be achieved.

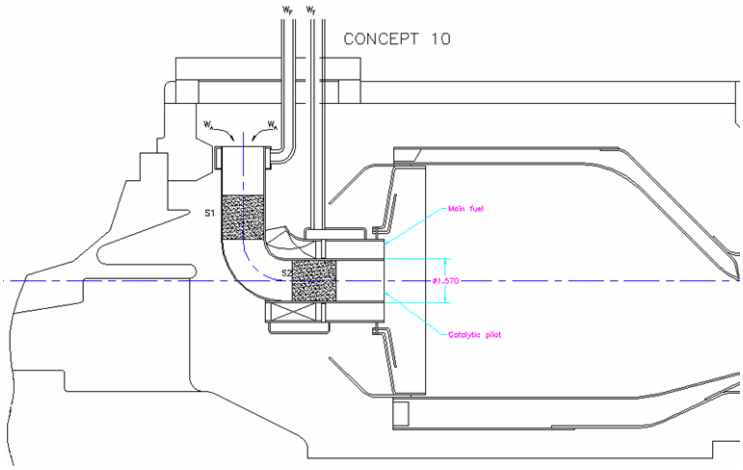

Concept 11 is a variation of concept 4, but in this case the inlet to the pilot tube has been turned further, to now pointing aft. An advantage with this concept is the substantially longer flowpath within the pilot tube, allowing more room for the catalysts, fuel/air mixing and a short burnout zone. Another advantage is that the partial blocking of the main stage is less pronounced than in concept 4 due to the large radius of the pilot tube.

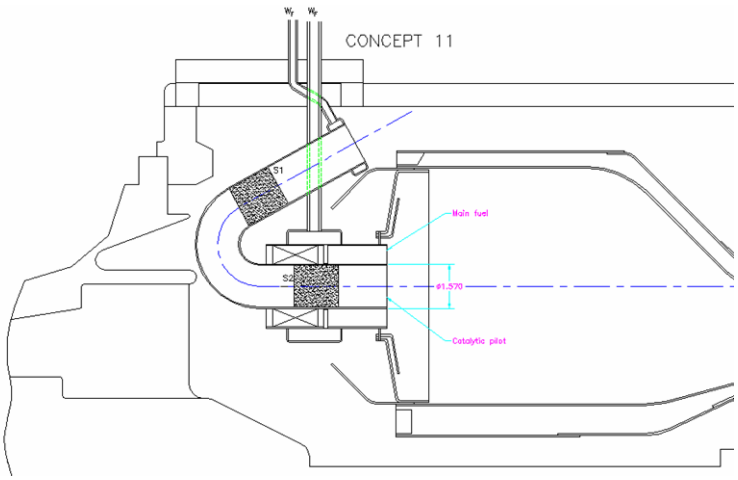

5.4.1 Down Selection

The above concepts were internally reviewed at Catalytica by peer combustion engineers. The most important factors when incorporating a design were discussed, in particular allowing enough room for the difference components within the pilot injector, simplicity of the design, aerodynamic interference, ease of installation and removal. The two winning candidates were concepts 2 and 11, but minor improvements were suggested to the proposed concepts.

Concept 2B. This is an improved version of concept 2 where the aerodynamic blockage of the injector main stage has been addressed. The pilot inlet section has been stretched forward to the extent possible. Also, the area ratio between two sections of the radial pilot inlet compared to the catalyst frontal area (A_{REF}) has been calculated. This shows that for the chosen radial channel height, the ratio goes from 4.6x A_{REF} at the radial inlet to 1.4x A_{REF} just upstream the throat, which should provide a smooth acceleration of the flow as it approaches the catalyst inlet.

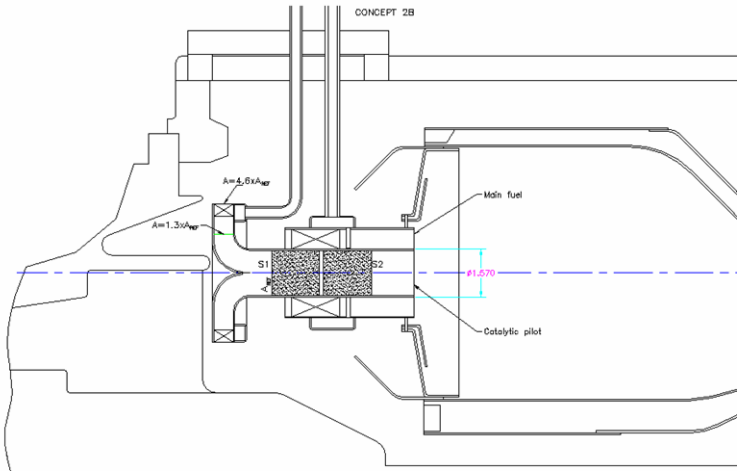

Concept 11B merges the best features of concepts 11 and 4. It maintains much of the simplicity of concept 4 in that the pilot tube is pointing more radially outboard, while incorporating the larger tube radius from concept 11 that greatly reduces the partial blockage leading into the main stage swirler. As in concept 4, there should be adequate room for a two-stage catalyst design.

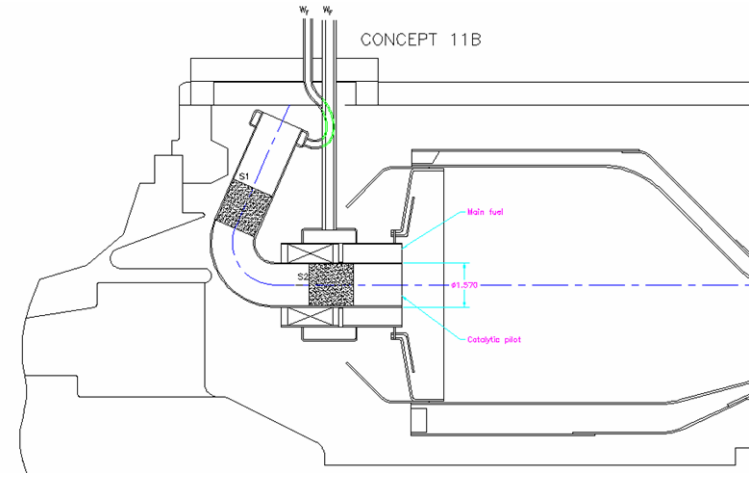

5.5 Catalyst Testing.

5.5.1 CESI Testing to Support UCI

A significant amount of catalyst mapping was conducted at CESI's 2" reactor rigs in support of testing at UCI. For the atmospheric testing conducted at UCI during fall of 2001, three different catalyst assemblies were tested and shipped to UCI. An assembly can consist of one or two stages, where each stage is a foil pack of predetermined length and a diameter 0.93". Each foil pack was then numbered consecutively as "element 1", "element 2" and so on. The assemblies can be characterized in several different ways, as shown in Table 5-1.

Config.:	Design #:	Inlet stage:	Outlet stage	Conversion/ϕ/Tad
A		Element 1	N/A	Blank
B	21	Element 2, GE10 inlet stage 1, P00-5-026	Element 3, GE10 outlet stage 2, P00-5-027	High conv./low ϕ/Tad Shipped 4/01
C	22	Element 4, GE 7FA single stage, P01-5-009	N/A	Low conv./high ϕ/Tad Shipped 4/01
D	23	Element 5, 3" inlet stage 0, P00-4-022	Element 6, 4" outlet stage 2, P00-4-026	Very high conv./very low ϕ/Tad Shipped 4/02

Table 5-1 – Catalyst Foil Nomenclature

The blank catalyst foil and designs 21 and 22 were available to UCI for their atmospheric rig test in fall of 2001. Results reported from UCI and shown in the next chapter were all on the blank and design 21. In a meeting 11/07/2001 where the majority of the testing had been completed, it was determined to delay testing of design 22 [2, 3], consequently it was never tested in their atmospheric rig under this program.

The purpose of this mapping was to characterize the several types of foil to be tested at UCI and thus create a broad map of catalyst performance that would help determine what would be the optimum catalyst design in a pilot application. For example, would the optimum design be one of low conversion that could be fueled relatively rich to provide both high gas temperature and a large amount of unburned fuel, or would a design with a very high level of conversion perform better. Also, how would the large combustor pressure drop that the catalyst would be exposed to affect conversion. Variation of catalyst pressure drop as function of catalyst ΔT was mapped.

Tests at Catalytica in 2001 were conducted to characterize the catalysts to be used in UCI's atmospheric rig testing later that year. Additional tests at Catalytica in late winter and spring of 2002 were conducted at 8-atm, the same pressure as what would be used in UCI's high pressure test rig. During the course of atmospheric rig testing at UCI, it became apparent that catalyst

conversion in general was much lower than measured in Catalytica's reactor rigs. Although not determined conclusively, this was thought of being associated with the large difference in pressure for the two test sites.

5.5.1.1 Pressure Drop

The issue of pressure drop is different from most other catalyst applications, as the pressure drop across the combustor liner has already been determined. Since the pilot flow area is so small, it will not affect the liner ΔP to any notable extent. The question then becomes, for a given ΔP what airflow can one expect through the pilot. Other than the fixed ΔP, the airflow also depends on the temperature rise across the pilot. Tests in the reactor rig were run to determine this effect, and results are shown in Figure 5-2.

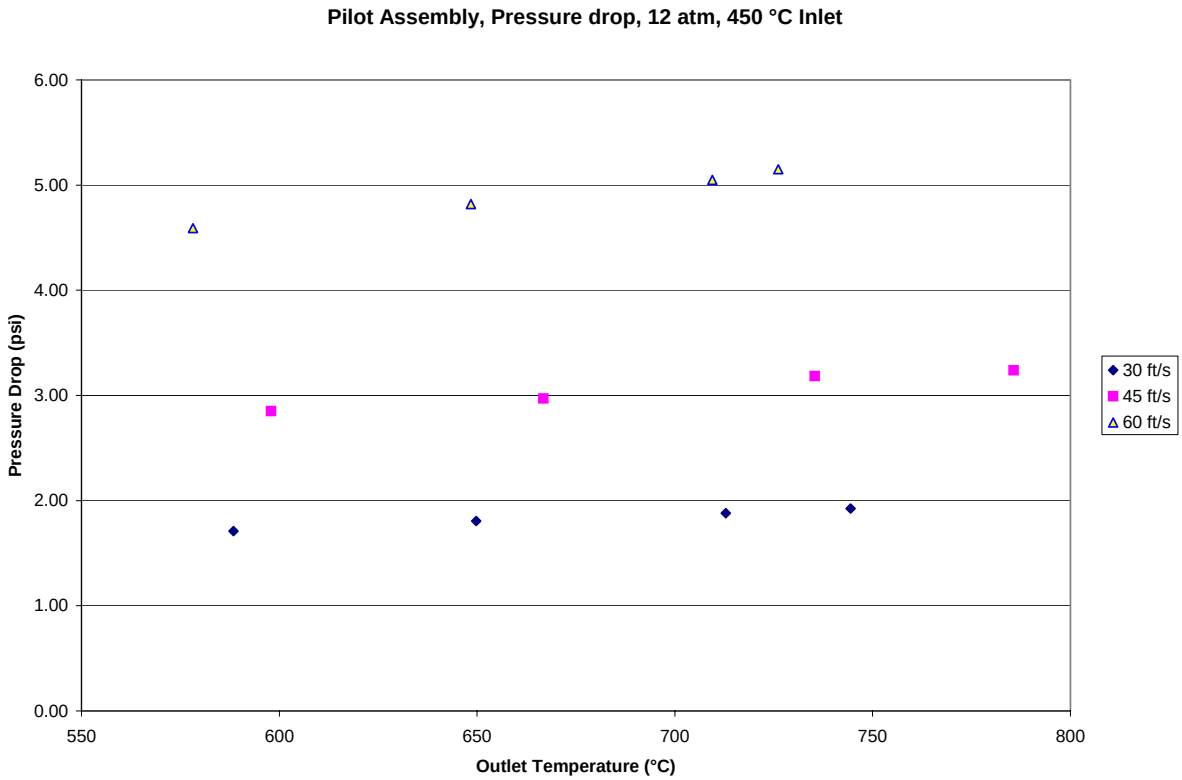

Figure 5-2 - Pressure Drop vs. Velocity and Temperature Rise

5.5.1.2 Mapping of Catalyst Foils

Table 5-2 shows test conditions under which several different catalyst foils were tested in Catalytica's reactor rigs in preparation for the 8-atm rig test at UCI. The intention was to select three different catalyst configurations that would cover a relatively large variation in conversion rates and thus enable us to distinctly determine the advantages and drawbacks of each design in different areas.

Figure 5-3 shows the CESI HPR measured operating characteristics for the four catalyst designs. The objective was to cover a range of catalyst outlet temperatures with a variety of

Test Conditions:	*8-atm*
Target catalyst pressure drop:	*2.5% and 3.5%*
4 modules tested:	
Single stage	*Very high ϕ/Tad (very low conversion)*
Single stage	*High ϕ/Tad (low conversion)*
Two stage	*Low ϕ/Tad (High conversion)*
Two stage	*Very low ϕ/Tad (Very high conversion)*

Table 5-2 – Catalyst foils tested for UCI

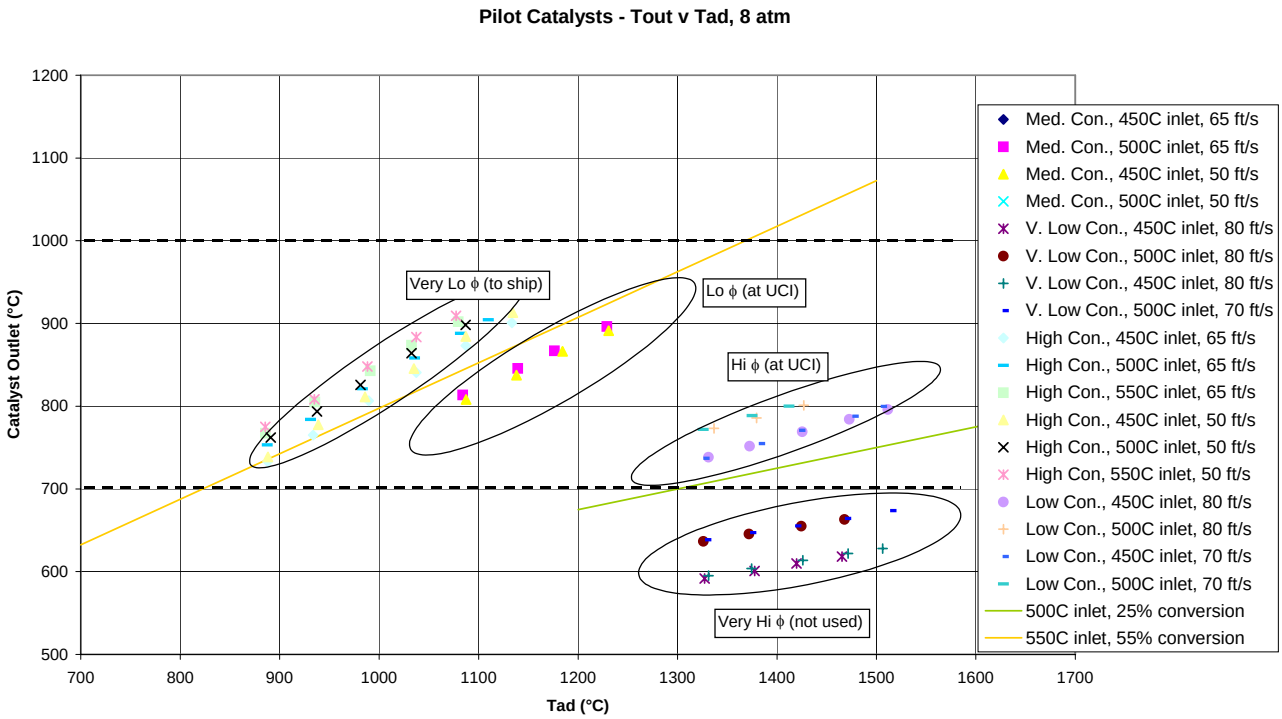

Figure 5-3 - Operating Temperature Characteristics of Test Catalysts

adiabatic temperatures in the burnout zones downstream from the catalyst. Based on this test information, the "Lo ϕ" catalyst was selected for the first catalyst test at UCI. Results marked "Lo ϕ" were with catalyst design 21 and "Hi ϕ" design 22 as described in table 5-1.

5.5.2 Low Pressure Rig Testing at UCI

A catalytic pilot was tested at UCI in the fall of 2001 in their generic atmospheric test rig. The test results were presented to CESI in a report/presentation dated 11/07/2001 [3]. The catalyst testing during this period was referred to as a "Gen. II" test series, as a catalytic pilot concept had been tested at UCI in 2000/2001 under a different program. The catalyst used in the Gen II testing was a 0.93" diameter, two-stage module of the GE10 design, design 21 in table 5-1.

In addition to testing a CESI designed catalyst, UCI also tested, at same operating conditions, a diffusion flame pilot, a blank catalyst foil pilot, a fully premixed pilot and a partially premixed fuel and air pilot. Other parameters examined were the air split between main stage and pilot and for fuel split. In addition to measuring temperatures, flows and other rig operation related parameters, emissions and combustion dynamics were measured. Figure 5-3 is a schematic of the UCI atmospheric rig.

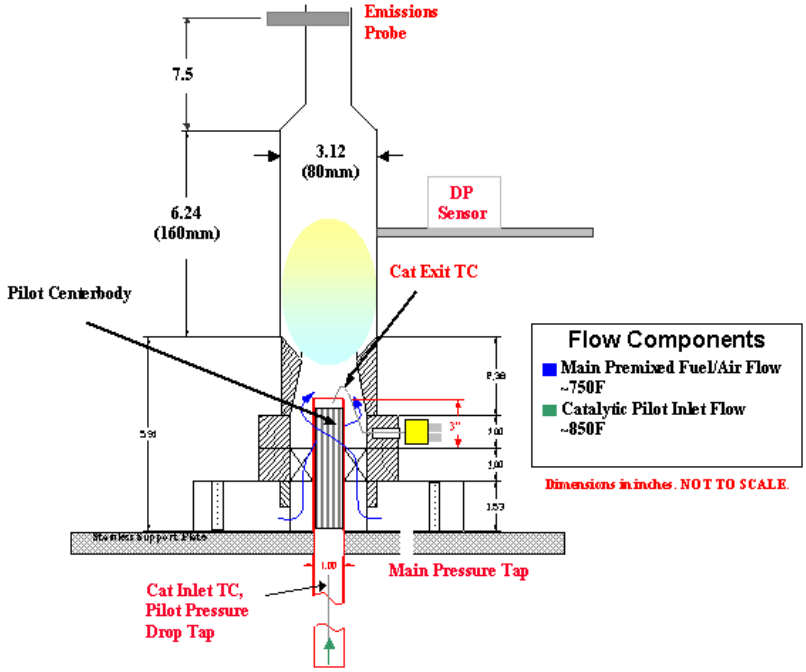

Figure 5-4 - Combustor Cross Section

Pilot fuel air mixture temperature as well as pilot airflow could be controlled independently from the main stage through separate flow circuits, so no modifications of the burner hardware was necessary. The combustor liner was fabricated from a piece of quarts pipe, allowing full visual access to the flame zone. Test conditions are shown in Table 5-3.

- **TEST CONDITIONS:**
  - **Atmospheric Pressure**
  - **~30kW Firing Rate**
  - **Natural Gas Fired**
  - **Main Combustion is Fully Premixed**
  - **Constant Airflow Splits: Main / Pilot (pph)**
    - **Diffusion: 158 @ 800F Main Only**
    - **Premixed & Catalytic Pilot: 140 @ 800F / 14 @ 880F**
    - **Solar: 147@ 800F / 4.5 @ 800F**
  - **Variables:**
    - **Pilot Type**
    - **Pilot Fuel**
    - **Main Fuel**

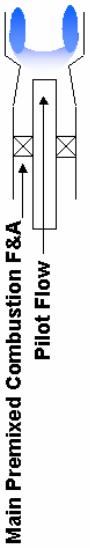

Table 5-3 – Test Conditions

Table 5-4 shows the range for which data was acquired for each variable. Note that a total of five pilot configurations were tested, the four shown below plus the "blank" (uncoated) catalyst foil.

Test Description	Variables	Ranges	Diagnostics
I. Catalyst Characterization	Pilot Fuel	$0<\phi_{pilot}<0.50$	Thermocouple
II. Pilot Emissions	Pilot Type	Diffusion, Premixed, Catalytic	Emissions
	Pilot Fuel	$0<\phi_{pilot}<0.50$	
III. Pilot Stability Effect	Pilot Type, Fuel	ϕ_{pilot}=0.08, 0.24, 0.48;	Emissions
	Main Fuel	$LBO<\phi_{main}<0.55$	Acoustics

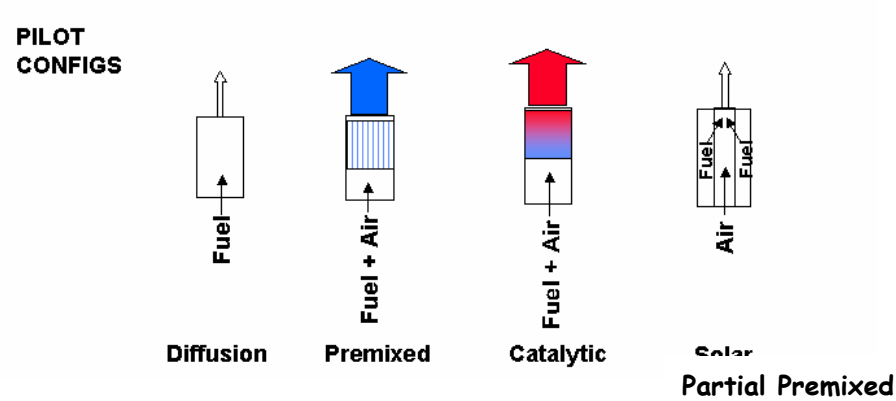

Table 5-4 – Ranges of Data

5.5.2.1 Test Results

Below follows a brief description of test results with emphasis on emissions, lean blowout characteristics and combustion dynamics.

5.5.2.1.1 Emissions

Figure 5-5 shows NOx emissions vs. pilot equivalence ratio for a constant main stage fuel/air ratio.

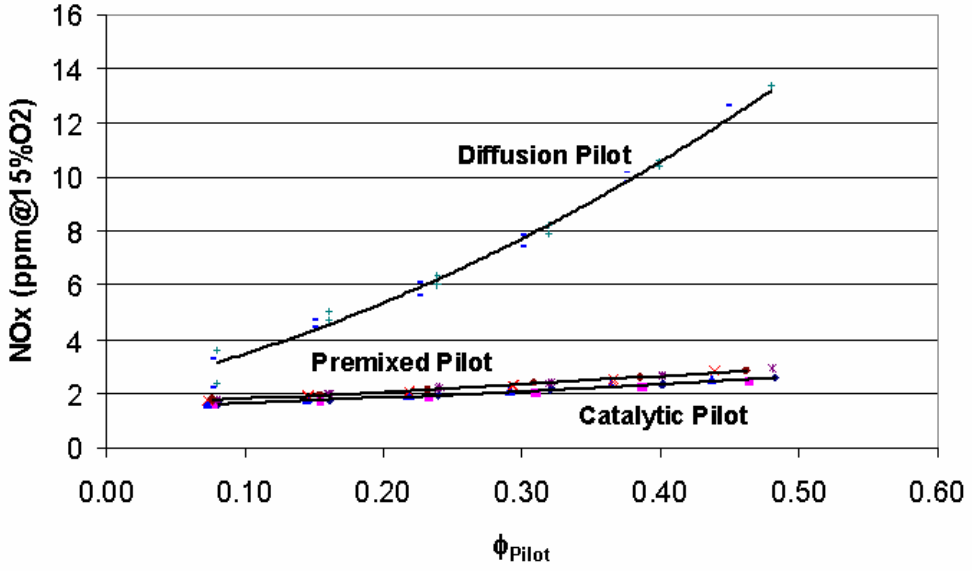

Figure 5-5 - NOx vs. pilot equivalence ratio for three pilot configurations. ϕ_{MAIN} = 0.50

The steep rise with the diffusion pilot is consistent with Catalytica's test experience in the Solar Turbines high pressure rig. However, during test at Solar the overall fuel air ratio was kept constant, which would decrease the main stage fuel as pilot fuel (equivalence ratio) was increased. This would lead to lower NOx as pilot fuel flow increased while in the case above it was almost constant. The small difference between the catalytic pilot and premixed pilot is probably due to the low pilot equivalence ratio (< 0.50), which will result in very little thermal NOx being generated. Figure 5-6 compares CO produced under same test conditions as in Figure 5-5. Again the main stage equivalence ratio is fixed at 0.050. This number is the fuel split ratio between the main and pilot.

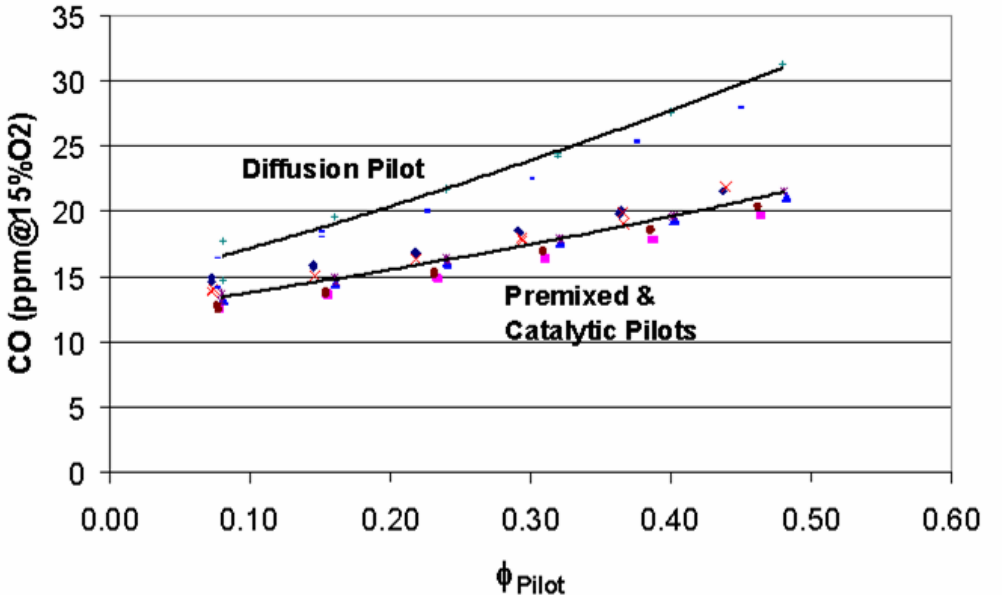

Figure 5-6 - CO emissions for three pilot configurations and a main stage ϕ of 0.50

Additional UCI testing was done where the fuel split between the main stage and pilot was varied. Figures 5-7 and 5-8 show entries in the legend followed by a number (0.08 to 0.60). NOx for the catalytic pilot is much less sensitive to main vs. pilot fuel splits for pilot equivalence ratios in the range of 0.08 to 0.60.

Figure 5-8 shows CO at the same operating conditions. The higher CO with increasing gas temperatures (or equivalence ratio), is contrary to what one would expect as combustion efficiency has a tendency of improving with higher flame temperatures. The explanation is likely that this phenomenon is equilibrium CO, and therefore not so much related to the relative performance of the different concepts tested.

5.5.2.1.2 Lean Blowout Performance

A lean blowout summary follows in Table 5-5 for the four concepts tested. For each concept, lean blowout for the main stage is recorded for various equivalence ratios of the pilot. In theory, the higher equivalence ratio to the pilot, the better its ability to stabilize, therefore the main should blow out at a lower equivalence ratio. Equivalence ratio is based on time-averaged measured fuel- and airflow, using calibrated instruments.

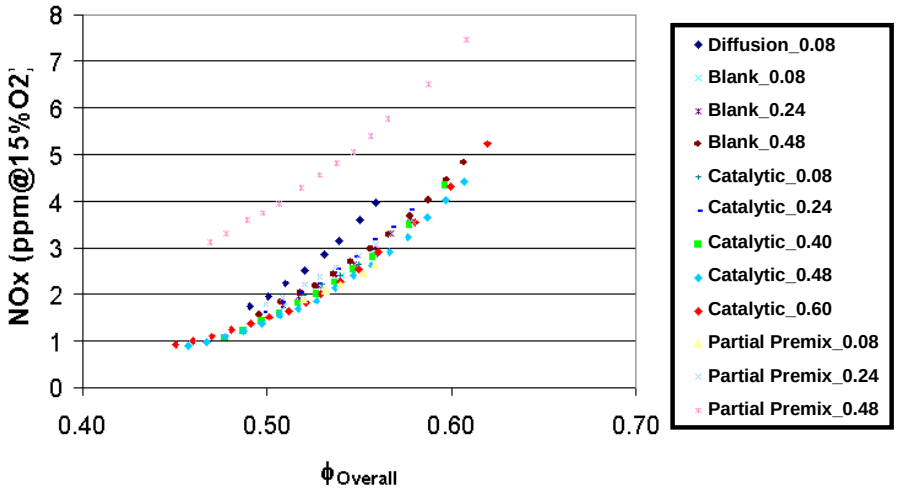

Figure 5-7 - NOx vs. Combustor Equivalence Ratio

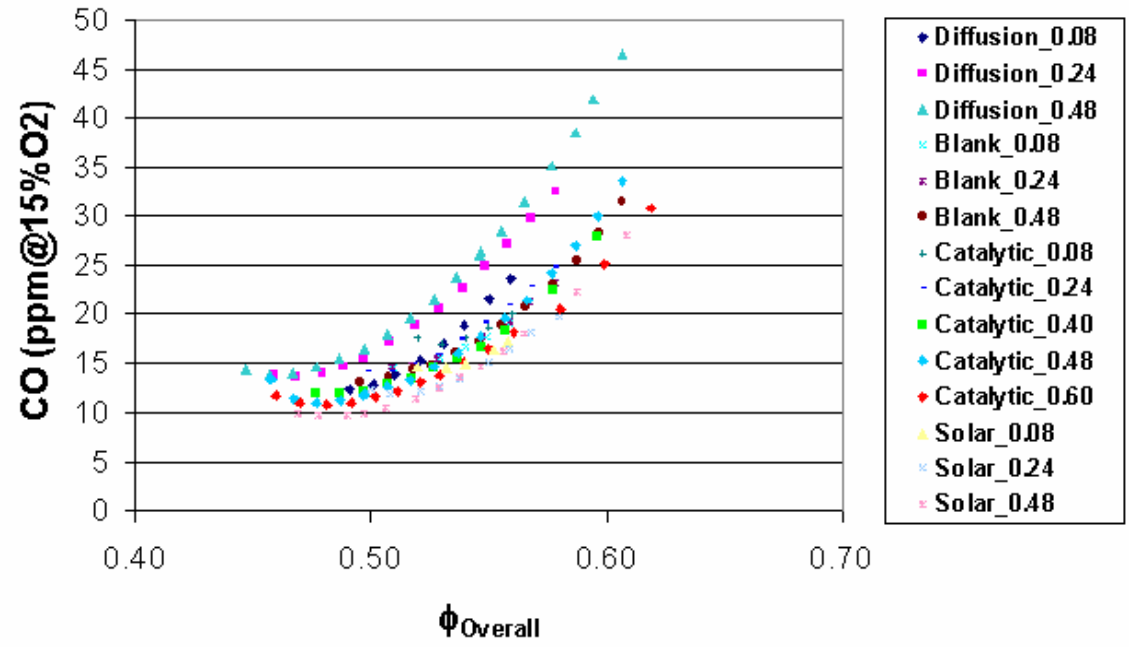

Figure 5-8 - *CO vs. Combustor Equivalence Ratio*

Pilot Configuration	ϕ_{Pilot}	ϕ_{LBO}
Premixed	0.08	0.51
	0.24	0.51
	0.48	0.50
Catalytic	0.08	0.52
	0.24	0.50
	0.40	0.48
	0.48	0.46
	0.60	0.45
Diffusion	0.08	0.49
	0.24	0.46
	0.48	0.45
Solar	0.08	0.52
	0.24	0.50
	0.48	0.47

Table 5-5 – Lean Blowout Summary

5.5.2.1.3 Combustion Dynamics

Four distinctly different modes of combustion were observed during testing of the different concepts. These differences relate to flame appearance such as its shape, relative location and magnitude and frequency at which it was moving around, and also the acoustic characteristics. The four different modes are summarized in Table 5-6.

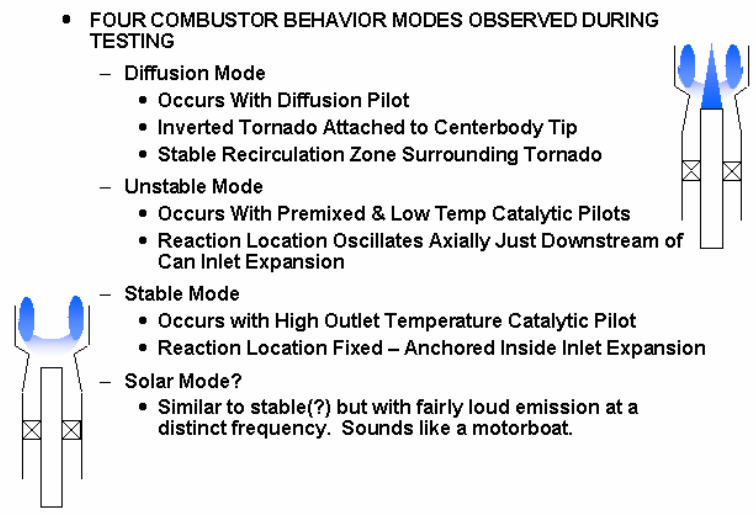

Table 5-6 – A description of the different combustion modes

Spectra for the different configurations are shown in Figures 5-9 and 5-10. Combustion acoustics was measured with a microphone in the combustor exhaust. Figure 5-9 shows the RMS amplitude for the different configurations.

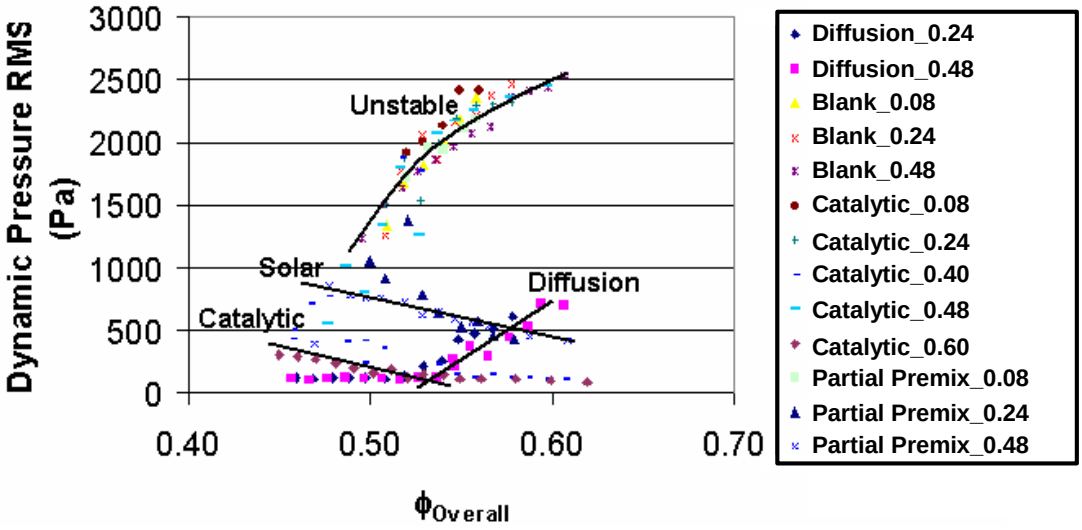

Figure 5-9 - Dynamic Pressure (RMS, Pa) vs. Overall Equivalence Ratio

Figure 5-10 shows the power spectrum of these combustion dynamics. For many DLN combustion systems, these types of dynamics are often observed in the 50-300 Hz range, although dynamics at a higher frequency are not unusual. The two graphs show dynamics for two different overall equivalence ratios, 0.6 and 0.5 respectively.

The spectra in Figure 5-10 show the highest amplitudes were recorded with the "premixed" centerbody, at peaks around 50 and 60 dB normalized and frequencies at about 400 and 750 Hz in the top graph and 250-300 Hz in the bottom graph. It is also noteworthy in the bottom graph that with the catalytic centerbody, the amplitude dropped when the pilot equivalence ratio was increased from 0.48 (pink line) to 0.60 (burgundy line), demonstrating the ability of a catalytic pilot to lower dynamics.

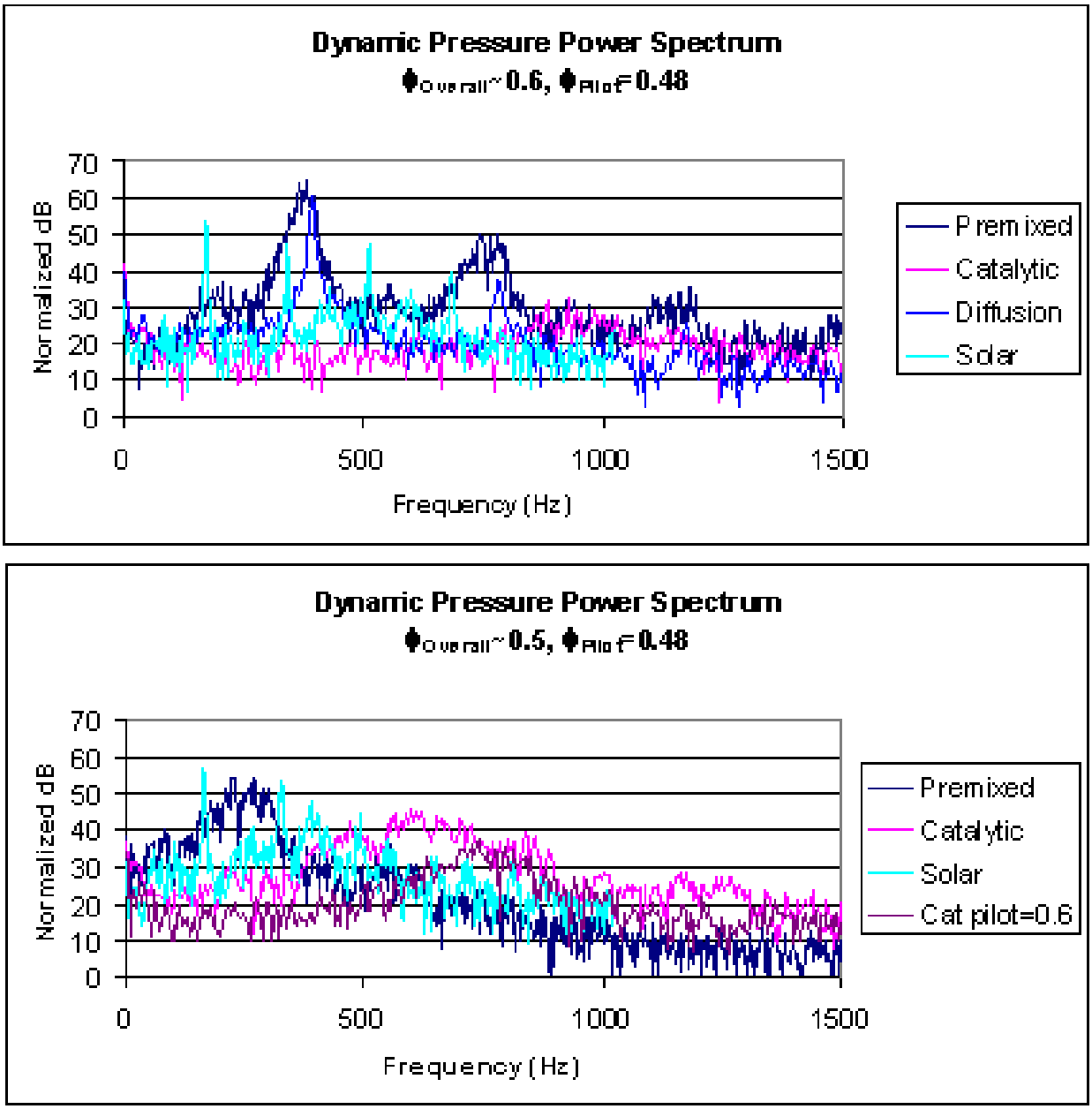

Figure 5-10 - Combustion Dynamics

5.5.2.1.4 Summary from UCI Atmospheric Rig Tests

Table 5-7 summarizes the observations made during the rig testing at UCI.

SUMMARY

- IMPACT OF CATALYTIC PILOT DEPENDENT UPON EXIT TEMPERATURE
- AT HIGHER TEMPERATURES CATALYTIC PILOT
  - Lowest Achieved NOx
  - Comparable CO
  - Extended System LBO
  - Low Acoustic Emissions
- CATALYTIC PILOT APPEARS VIABLE BASED ON GENERIC COMBUSTOR TEST BED RESULTS OBTAINED TO DATE
  - Vs Solar Pilot
  - Vs Diffusion Pilot

Table 5-7 – Summary from UCI rig testing

5.5.3 UCI High Pressure Test

Based on successful atmospheric rig testing at UCI and full pressure T60 conditions at Solar, it was determined in late January 2002 that a more generic test matrix for this technology was desirable. The objective was to eliminate the constraints of testing to Solar T60-like conditions imposed on the characterization of the pilot system. This would enable us to create a much broader map of the interdependence between the pilot and what particular features of the pilot needed to be optimized. Examples of the latter would be pilot conversion rate, pilot and main stage emissions performance at inlet temperature much higher than the T60, ideal pilot to main stage air split and so on. From an intellectual property standpoint, it was also desirable to disconnect any links between the pilot technology and a particular OEM's hardware or turbine operating conditions, or any IP ownership an OEM or other third-party could claim in co-developing this technology. To meet these objectives, CESI renegotiated a new confidentiality and IP agreement with UCI and we started preparing for a high pressure rig test at UCI. this test would be conducted at 8 atmospheres and test several catalyst conversion rates and pilot to main stage air splits among other things. In parallel with the above, a patent application was filed on 02/22/2002. High pressure testing was scheduled at UCI for about three weeks in May 2002. As we progressed closer to the test window, start-up was delayed numerous times due to delays in hardware delivery or modifications required to the test rig. First light-off did not occur until July 2002, and then only to be followed by additional delays due to malfunctioning instrumentation and repairs required to instrumentation ports in the combustor liner. Eventually, in early August 2002 UCI was able to fire the combustor. After several days of rig shakedown testing and limited amount of data acquisition, an overheat occurred on 8/12/02 where the combustor liner was damaged. A recovery plan was quickly put together, which entailed fabricating and installing replacement rig parts. Early September, the rig was once again ready. On September 13, a similar yet more serious meltdown of the combustor liner occurred. Although not firm conclusions were drawn, it seemed the overheat was due to a combination of the cooling scheme employed and the material used in the liner. The cooling consisted of a 1/4" diameter stainless

steel tube coiled around a stainless steel liner. Water being fed through the coil would provide the cooling. In retrospect, it seems this was an inadequate cooling scheme given the high hot side gas temperatures. CESI determined that this cooling scheme, choice of materials together with numerous igniter and instrumentation port failures, would require a significant amount of engineering to achieve satisfactory performance. At this point (September 2002), it was therefore determined to cancel any further testing at UCI while at the same time try to negotiate a new agreement with Solar to allow for a more generic style test in their full pressure combustor rig. This testing would follow as an independent program, and not an extension of the DOE funded program. This testing will therefore be covered in a separate report. The unfortunate conclusion from the high pressure testing is that numerous hardware delays, rig problems and inadequately design components resulted in that no valuable data was acquired at UCI in their 8 atm test rig.

5.5.4 Solar Full Pressure Rig Test

A custom-made catalytic pilot fuel injector assembly was fabricated for testing in Solar's high pressure combustor rig. This rig can run under full engine conditions. It has a single can emulating the annular DLN combustor. In addition, it has significantly more space available upstream the combustor can, providing more design flexibility for rig hardware. Figure 5-11 is the Solar turbines high pressure rig used for the catalyst pilot characterization tests.

The fuel injector is installed horizontally through a port on the left side of the rig to the lower right in the picture. Next to the fuel injector is a camera port that allows a side-view of the fuel injector exit. A torch igniter is mounted on the top to ignite the main stage. To install the fuel injector, the injector without the pilot tube is first inserted through the port on the left side of the right and bolted down. The end flange to the far right in the picture is removed to install the catalytic pilot tube into the fuel injector, hook up the fuel supply tube to the pilot and finally connect the instrumentation. With the flange bolted back on, the rig is ready to go.

Figure 5-12 shows the catalytic pilot centerbody1. It shows the 3" inlet stage and the 4" long outlet stage. Two of the four fuel orifices in the pilot fuel injector are shown; alluding to how the pilot fuel jets provide the premixing with the incoming air upstream of the catalyst.

Fuel is injected in a similar fashion to the Xonon 2 preburner fuel injectors and the concept relies on turbulent mixing between fuel and air in the path down to the first stage catalyst. The fuel injector is made of stainless steel while the catalyst tube (from the bolted flange down) is made of Hastelloy-X due to the high temperature exposure when the catalyst is fueled. There is a 1/2" axial space in-between and also downstream of the two catalyst stages, where a 0.40" wide and 0.063" thick strut of Haynes 214 is installed. This is the axial support for the catalyst foil pack. The drawing also shows the routing of the two thermocouples measuring catalyst exit gas temperature. They are fed through a 1/4" stainless steel tube through the center of the exit catalyst. Finally, ceramic cement is used to plug up the inlet to this tube to avoid any un-reacted fuel/air leaking through it.

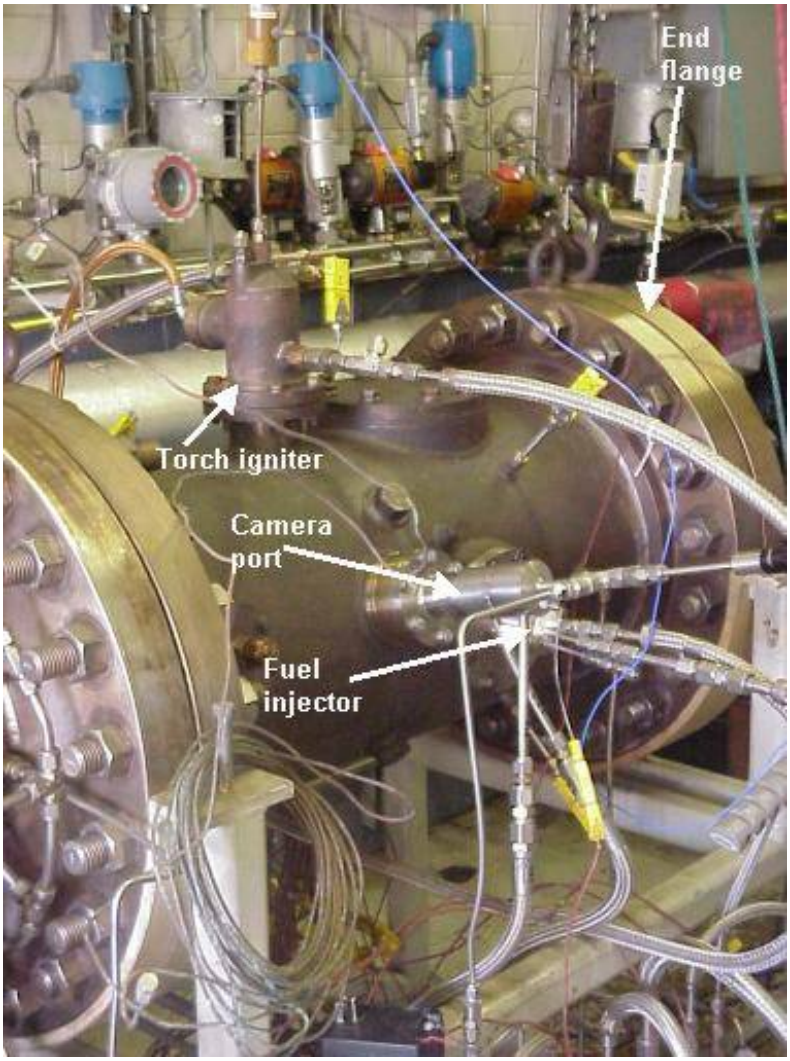

Figure 5-11 - Solar high pressure combustor rig

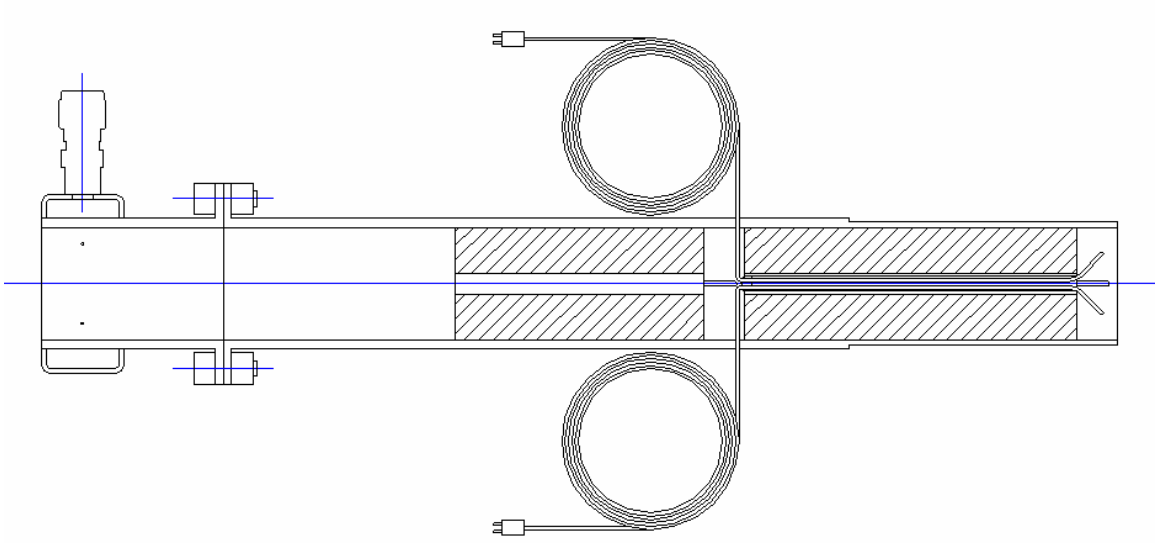

Figure 5-12 - Internal details of pilot fuel injector

5.5.4.1 Test Results

A total of 33 test points were completed in the January 16 '02 test. The test were run by setting the combustor inlet temperature and pressure to the right conditions and adjusting airflow until the desired pressure drop reading was observed. Under these conditions, the ratio of pilot to main stage fuel flow was varied while trying to keep the total fuel flow constant. Due to the high exit gas temperature from the combustor and the non-uniform exit gas temperature, setting test points based on exit temperature was not deemed to be a reliable independent parameter. The agreement is quite good, although most test points were run at 5-10% below selected engine cycle front end flame temperature. The graph in 5-13 shows the agreement between the rig test points and the engine conditions. In general, flame temperature was between 0 to 8% lower for the test than in the engine. Figure 5-14 shows calculated front end flame temperature for all

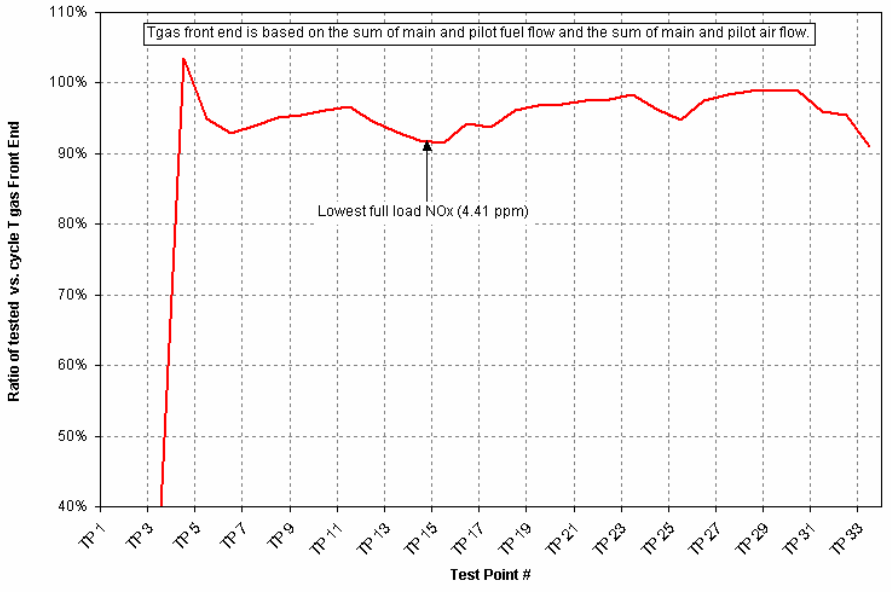

Figure 5-13 - Rig Test Combustor Front End Gas Temperature vs. Cycle Deck

the test points. The dependent parameter is calculated based on fuel flows, air flow, measured air splits, assumed combustion efficiency and fuel heating value.

The combustion efficiency was in general very high, and should not affect the results to a significant degree. The actual front end gas temperature was between 26-2800 °F for most of the test points. The optimum flame temperature range for low emissions combustors are often referred to as the 1700-1900 K range [5], which, in a very well premixed system, can provide both low emissions and stable combustion. The 26-2800 °F range corresponds to 1700 to 1810 K, thus being where minimum emissions should be achieved. The catalyst used in this test was referred to as a medium conversion design. In this test, a rate of conversion was calculated to give the best agreement between inlet temperature, pilot exit gas temperature, pilot fuel flows and heating value. The best fit was achieved with a conversion rate of 32.15% (Figure 5-15). At pressure, in CESI high pressure reactor rig (HPR), a conversion rate of over 50% was achieved with the same foil, see Figure 5-16.

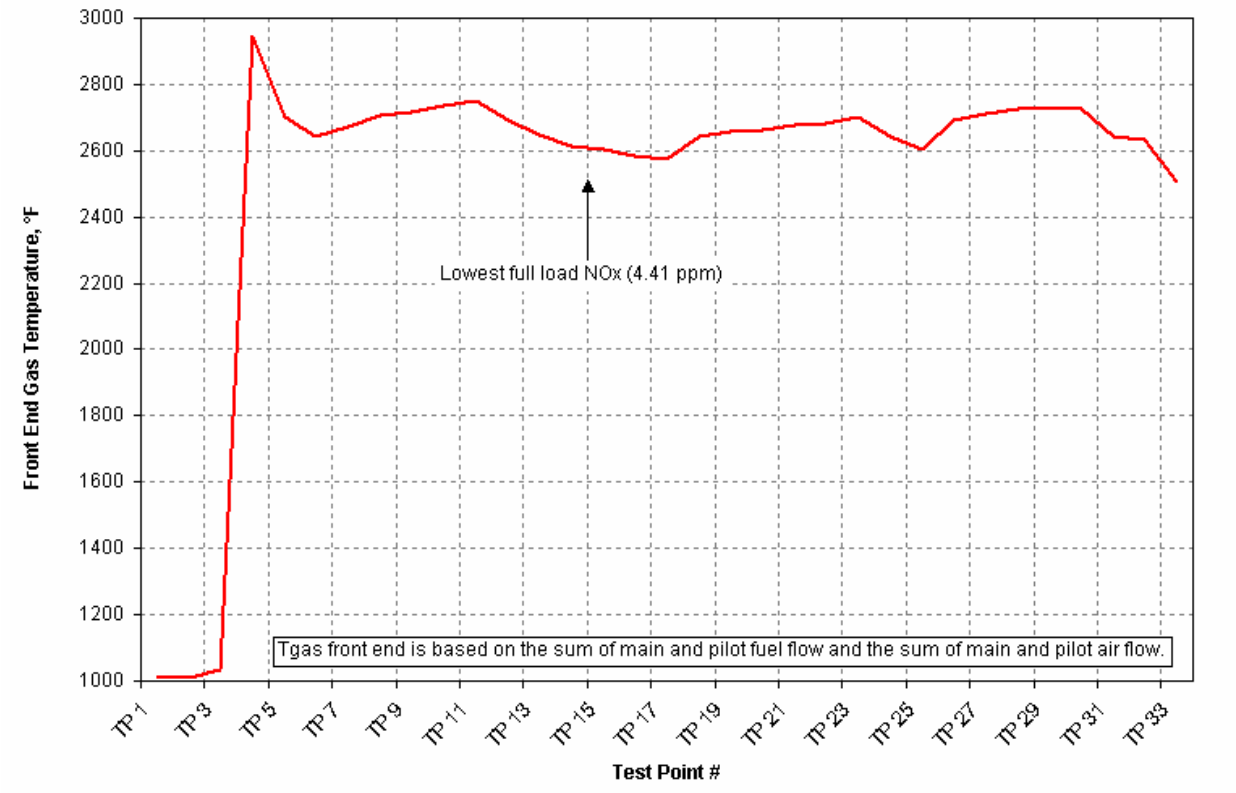

Figure 5-14 - Front End Gas Temperature vs. Test Point

Combustor flow areas and fuel heating value is shown in Table 5-8.

Liner:	in^2	1.440
Main swirler:	in^2	1.783
Total combustor:	in^2	3.358
Fuel LHV:	*Btu/lb*	20,538
Stoichiometric F/A		0.0609

Table 5-8 – Flow areas and fuel heating value. Main swirler is total of main stage and pilot and takes 55.3% of total flow.

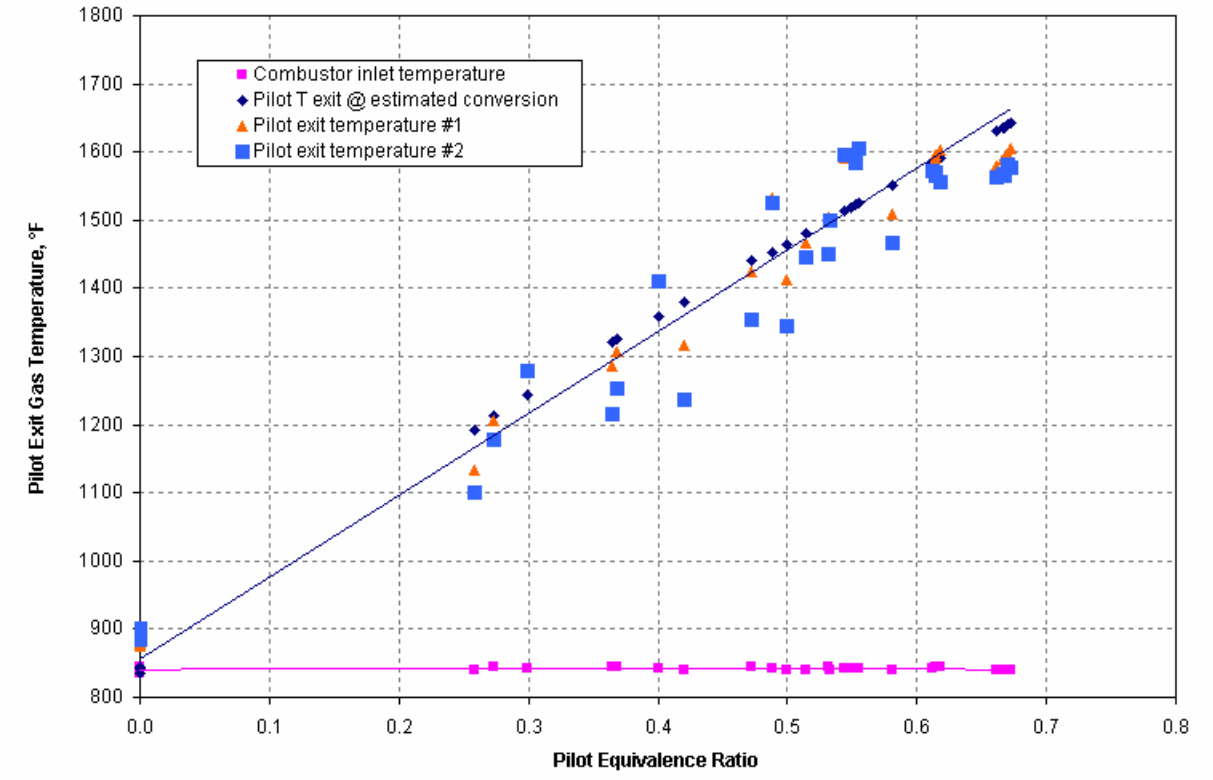

Figure 5-15 - Pilot Exit Gas Temperature at 32.15% Conversion

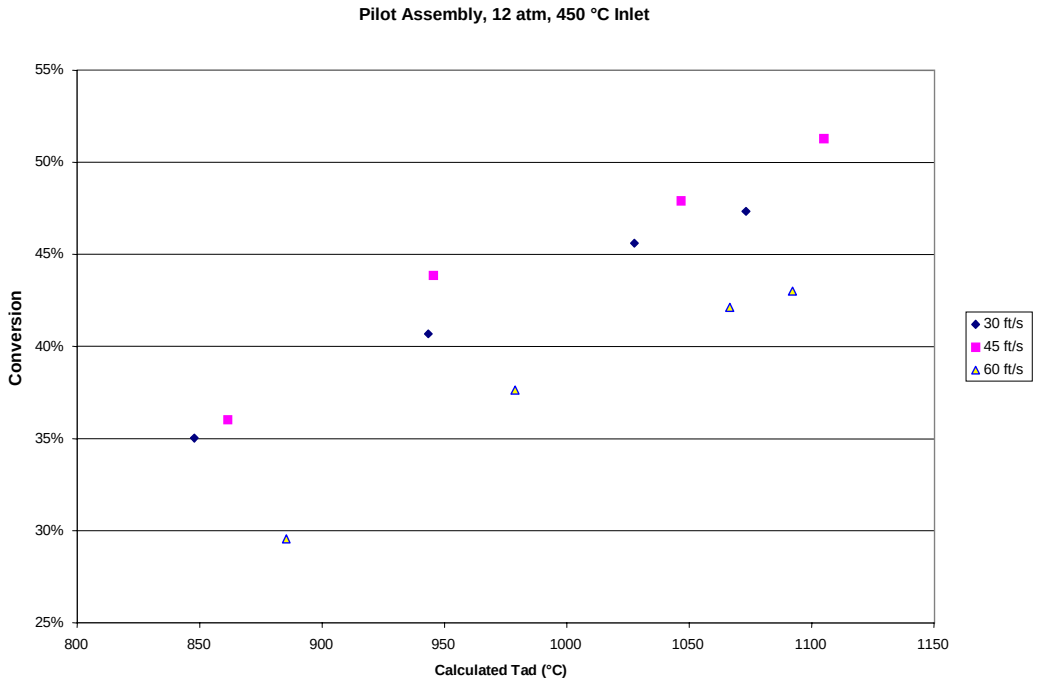

Figure 5-16 - Catalytic Pilot Test in CESI's HPR

5.5.4.2 Emissions

5.5.4.2.1 NOx.

As was shown in Figure 5-5, NOx emissions exhibit an inverse trend using a catalytic pilot as compared to a standard diffusion flame or partially premixed pilot. The explanation is simple. In a diffusion flame burner, thermal NOx is a large contributor due to the diffusion of raw fuel towards the flame front and thus very high flame temperature. In a partial premix system this problem is only alleviated to the extent fuel and air has had a chance to mix prior to combustion, thus reducing the flame temperature. This reduction may be local or global in the flame, depending on the degree of premixing and of course the equivalence ratio of the fuel air mixture. In a catalytic system, two effects contribute to the lower NOx. First, the catalyst itself contributes to a temperature rise without creating NOx. This can be compared to operating a small part of the combustor at a higher inlet temperature, thus requiring less fuel in this region to reach the final flame temperature. In this context, it is interesting to know the upper limit of pilot airflow available for any given configuration. This is determined by three factors: (1) Catalyst diameter (i.e., fuel injector centerbody diameter), (2) Catalyst design (i.e., pressure drop caused by friction losses in the catalyst and (3) The temperature rise across the catalyst. Factors (1) and (2) are determined in a cold flow ACd test of the entire combustor assembly, blocking off all parts of the available flowpaths but the one in question. This results in a table like Table 5-5, except pilot ACd will also be known. Next, based on reactor rig testing at CESI, the increased pressure drop due to pilot temperature rise can be found. This data can be reduced to produce a graph like the one shown in Figure 5-17, where the drop in flow vs. catalyst ΔT is curve fitted to a second order polynomial. This is used in the spreadsheet where pilot airflow and thus fuel/air ratio and % conversion is calculated.

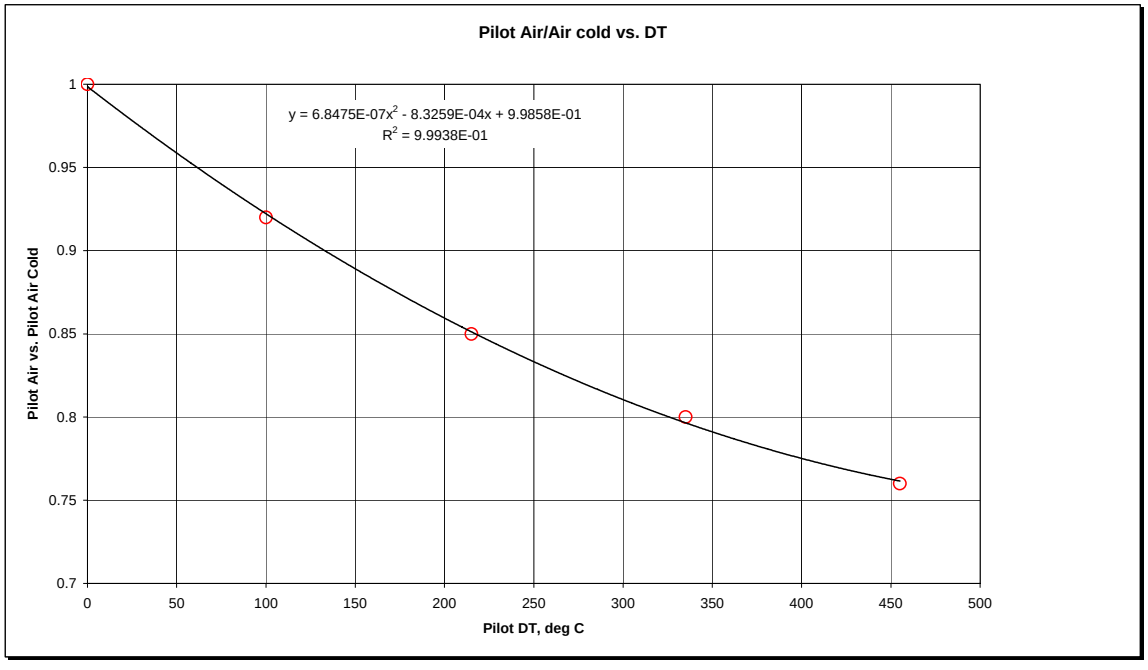

Figure 5-17 - Drop in catalytic pilot air flow as DT rises from 0 to 450 °C

The reduction in combustor NOx as fuel to the catalytic pilot is increased, is interesting and contrary to some existing test data, but also easy to explain. For a fixed total fuel flow, reducing the fraction to the main stage results in lower exhaust NOx produced by the main stage. This is why as the portion of the total fuel to the pilot increases, the NOx emissions drop. Since the pilot only converts part of the fuel in the catalyst, the rest is fed into the main stage recirculation zone as an extremely well premixed, lean mixture. Figure 5-18 shows this trend including the Jan 16 data points.

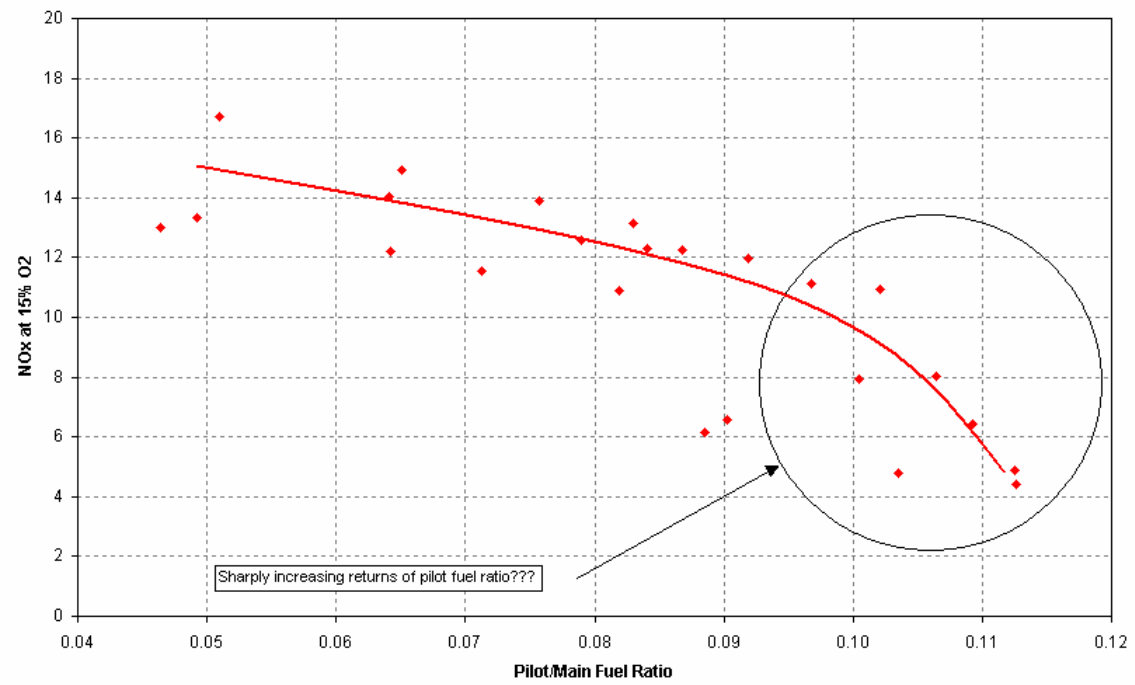

Figure 5-18 - NOx emissions vs. pilot/main stage fuel ratio

5.5.4.2.2 Carbon Monoxide (CO)

CO emissions were in general very low for all test points. Figure 5-19 shows CO emissions where the majority is clustered below 2 ppm in the 2600-2800 °F flame temperature range. The outliers at 1000 °F are test points with pilot fuel only. The high point at 11.1 ppmv is the only test point without pilot fuel.

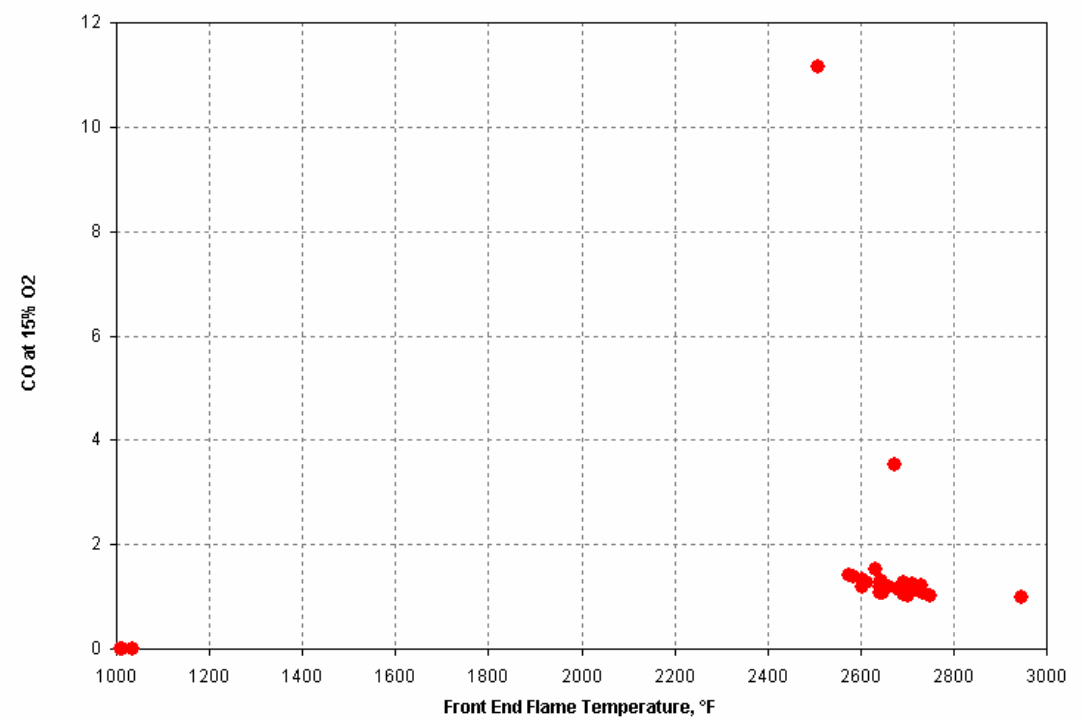

Figure 5-19 - CO Emissions vs. Calculated Front End Flame Temperature, °F.

The graph in Figure 5-19, is replicated in Figure 5-20, but with NOx emissions included.

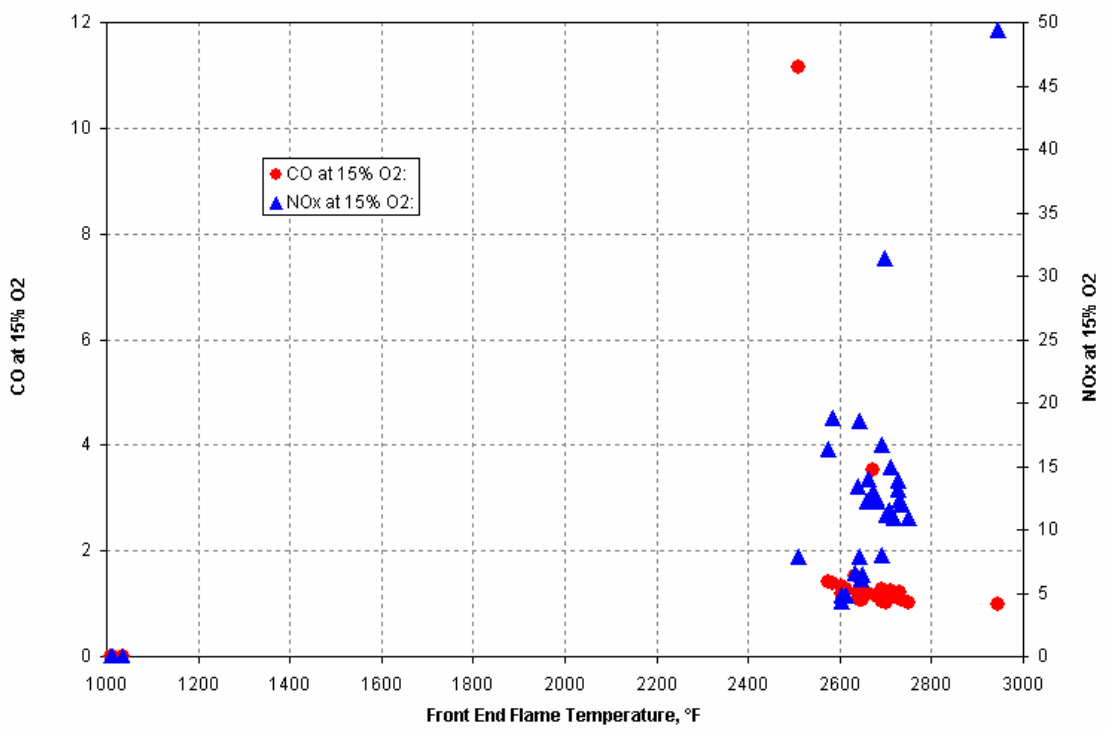

Figure 5-20 - CO and NOx Emissions vs. Calculated Front End Flame Temperature, °F

Finally, Figure 5-21 shows both NOx and CO emissions as function of pilot to main stage fuel split.

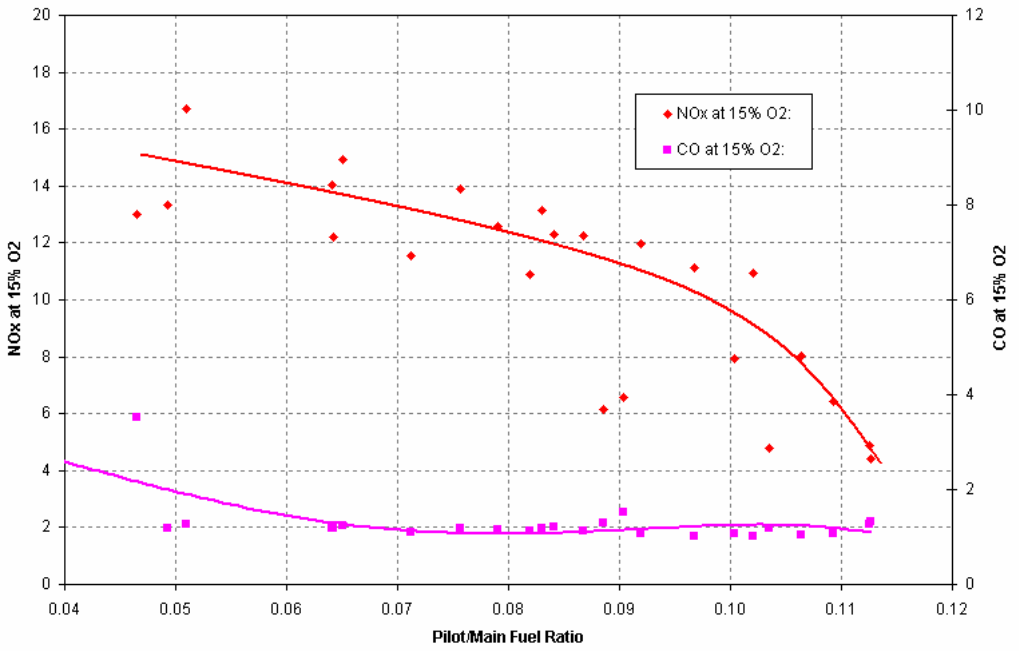

Figure 5-21 - CO and NOx Emissions vs. Pilot to Main Fuel Ratio

As the graph shows, CO emissions show no clear dependence on fuel split as NOx does. CO stays quite consistently around 2 ppm for most test points, and there is no sharp increase, as the pilot fuel flow gets closer to 0. The only significant dependence is evidenced after the pilot has been shut off entirely.

5.5.4.3 Combustion Dynamics

Combustion dynamics were measured during the full pressure rig test at Solar. However, the usefulness of this data is very limited for two reasons. First, combustion acoustics are highly dependent on combustor geometry and not only the liner itself, but also the combustor case and the up- and downstream hardware. Secondly, acoustics is dependent on the uniformity of the inlet airflow. The many discrepancies between rig conditions and actual engine conditions will in most cases render acoustics measurements questionable. It has also been observed that injectors producing large amplitudes ("noisy") in the engine, are often quiet in the test rigs. And, obviously, if injectors are quiet in the engine, no firm conclusions can be drawn no matter how they behave in the test rigs. The only acoustics data that has been acquired so far, therefore, is that from the atmospheric rig test at UCI.

5.6 Conclusions

Through catalyst mapping in Catalytica's reactor rig, atmospheric rig testing at UCI and full pressure testing at Solar Turbines, an extensive investigation into the performance of a catalytic pilot in a DLN combustion system has been completed. The results, since all of them are on test rigs and not on an engine, can only be deemed indicative and assessed based on the limits inherent in using test rigs. Nevertheless, the following conclusions can be drawn:

- Use of a catalytic pilot will reduce combustor NOx emissions as the portion of the combustor fuel flow diverted to the pilot increases. This will be true up to the point where the adiabatic temperature created by the pilot reaches that of the main stage.
- Use of a catalytic pilot has demonstrated lower acoustic noise under atmospheric conditions compared to a partially premixed diffusion style pilot burner.
- Use of a catalytic pilot has the potential of reducing NOx emissions to the 4 ppm level in the rig. This will translate to less than 9 ppm in an engine.
- Use of a catalytic pilot in a DLN combustion system does not appear to have any detrimental effect on combustor CO emissions, in fact, most of the tests with a pilot had lower CO, which may be attributed to higher equilibrium CO produced by the temperatures observed in a diffusion style pilot burner.

5.7 Recommendations for Further Work

As this report is completed, a follow-on program is in progress. The purpose with this program is to generate a more generic map of the interaction between a catalytic pilot and DLN main stage in a gas turbine combustor. This will be accomplished by varying key operating conditions such as inlet temperature, inlet pressure, pilot temperature rise, pilot rate of conversion through the use of different characteristic catalytic foils and finally through varying the overall fuel air ratio of the combustor.

Two other key performance criteria that will need to be addressed prior to a commercial launch of this product are:

- Lowering the catalyst light-off temperature to enable the use of catalytic pilot support at combustor inlet temperatures far below full load only. A desirable target would be down to 50% load.
- Demonstrate a NOx reduction potential to about 4 ppm in the test rig at full load conditions. This will be required in order to meet an OEM guarantee of maximum 9 ppm NOx in a commercially installed unit.

5.8 References

[1] CCSI document "Solicitation DE-SC02-00CH11000".

[2] K. Lundberg: "11_7_01.doc", a Word file containing meeting notes from 11/07/2001 meeting at UCI.

[3] Steve Hill, Rich Hack, Vince McDonell: "Catalytic Pilot Status Meeting", UCI Combustion Laboratory, 11/07/2001.

[4] David Ginter, "CatPilot0502.ppt", a PowerPoint presentation of reactor rig test results of different catalyst foil designs, presented internally at CESI 05/02/2002.

[5] A. H. Lefebvre: "Gas Turbine Combustion".

VI. Extension to Back-up Diesel Fuel

6.1 Background

In certain situations, generally for favorable pricing of local fuel supply contracts, a gas turbine user needs to have the capability to operate on at least an occasional basis with a liquid fuel rather than the natural gas used for normal operations. Prior DOE-supported work at Catalytica investigated the use of propane, hexane and diesel as a backup fuel. This work showed that liquid petroleum gas (LPG, primarily propane) could be a workable back-up fuel for a Xonon catalyst system. But the prior work also showed that other heavier liquid fuels could not be workable back-up fuels without substantial re-design of the combustion module. Because of the desirability of using widely available and lower cost diesel oil as the back-up fuel, the current program included investigation of a novel approach to this market demand, the upstream, on-site conversion of diesel fuel into a pressurized substitute gaseous fuel suitable for direct use in catalytic combustion modules.

The task 3 work under the current program addresses both technical and economic features of a process whereby diesel fuel can be converted into gaseous products before being directed into the turbine fuel handling system. As originally envisioned, if preliminary process economic evaluations showed that overall life cycle costs of a conceptual system were reasonably economical and practical, then the program would have conducted an experimental proof of feasibility via a subscale rig test demonstration using commercial product gas. This was to have been the ultimate deliverable for Task 3. For this work, the Solar Mercury 50 ATS was selected as the primary engine cycle data to be used for the cost analysis and for subscale rig demonstration.

Instead, preliminary economic analysis of investment costs for on-stream processing diesel to combustion gases were significantly above an economically viable target. As a result, further economic evaluation was initiated (Task 3.1) and focused on greatly reducing capital investment costs using modifications of commercial processes, including lower-temperature higher-pressure processing of diesel fuels into substitute natural gas SNG. Because the initial vendor and subsequent in-house capital cost estimates remained well above target levels, and because conversion of the product gases into SNG added little additional capital costs, the decision was made to forego rig simulation of the gas processed from diesel fuel. Instead novel technical processing concepts were initiated (Task 3.2) with the potential to greatly reduced fuel conversion investment costs.

Adiabatic catalytic high-pressure hydrothermal reaction was considered as a promising fuel processing approach because a large air compressor would not be required, heat exchanger size would be significantly reduced, and reactor temperatures significantly lowered (although at significantly increased pressure). From May through July 2002, SRI International conducted preliminary high-pressure hydrothermal reaction tests with simulated diesel (dodecane)/water mixtures over a variety conditions using catalysts and materials supplied by CESI.

6.2 Summary of Results

Task 3.1 – Diesel to Gas Process Economic Evaluation:

Initial evaluation of the fuel processing process by a well-know international engineering firm showed capital costs at $250/kW, a level well above our target of about $40/kW. Therefore, an in-house effort to analyze capital costs for a base-case diesel fuel conversion process was launched at the end of November 2001. Process specifications were defined and the preliminary equipment sizing and cost estimates were concluded in January 2002. The baseline direct fixed costs (DFC) at a 40-MW scale at $110/kW were again above target values, but well below the vendor's estimates. It was clear from the in-house investigation that the original vendor's estimates included on-site preparation and battery costs not appropriate for the smaller-scale and established siting of an auxiliary processing system for gas turbine power generation. Also modular fabrication instead of on-site construct ion of many such fuel processing systems can greatly reduce unit investment costs.

The capital costs of the in-house process equipment were almost evenly distributed among the air compressor, reactors, and heat exchangers. The final summary report for the series of process economics analyses conducted by Mike Cook or Aurora Engineering is included as Appendix C. Several modifications, such as bleeding the small amount of process air from the gas turbine compressor, were made to reduce investment costs and an optimized case showed reduced DFC at $79/kW. Further reductions in temperature and pressure for the steam-assisted auto-thermal reforming (ATR) fuel processing were then assumed and an optimized best case showed direct fixed cost (DFC) approaching $60/kW. Because it was desirable to convert the ATR product gas (containing carbon monoxide and hydrogen at elevated pressure) into SNG, a final "polishing" step was added bumping DFC up to $63/kW (see Appendix C).

Although these latter "optimized" reactor processing conditions are probably not viable for long-term operation (>1000-hr) because they may lead to coking and catalyst deactivation, they are likely to leave the process effective over the shorter periods (~100-hr) needed to insure power generation when gas supplies are interrupted. Catalyst regeneration and conditioning could be conducted during the long periods of time when the fuel processing system was not needed for turbine operation.

Although the final fuel processing system was considered technically feasible, capable of producing gas compatible with the combustion catalyst modules, and had investment costs greatly reduced below the original vendor estimates, those final costs remained about 60% higher than our cost target which was deemed economically viable. A novel processing approach was conceived during the course of the process analysis that, while suitable for the reduced scale of the gas turbine application, would not be economical for very large scale production of SNG. The technical feasibility of this approach was examined during the summer of 2002. The report describing the short-term experimental investigation is attached as Appendix D.

Task 3.2 – Hydrothermal Diesel to Gas Process Evaluation:

Three catalyst powders representing a variety of possible catalytic materials were prepared at CESI and tested in a pressurized autoclave reactor under the direction of Dr. Indira Jayaweera at SRI International (Appendix D). In the test system, separate streams of dodecane (representing

diesel fuel) and water were pumped into a high-pressure tube reactor. The tube reactor was filled with a heat conducting diluent (graded 80-mesh silicon carbide powder) and contained a section of physically mixed diluent and catalyst powder within a furnace-heated reaction zone. The liquid products were condensed and collected in flasks downstream of the back-pressure regulator and the gaseous products were collected batch-wise in gas sampling bags. Both streams were analyzed, but semi-quantitatively given the short term and limited scope of Task 3.2.

A blank reactor (filled with diluent) and an inexpensive catalyst material proved ineffective, but two catalysts showed promise with one (previously tested at CESI for autothermal reforming of fuel oils) showing high conversion (90%) at a reasonable temperature, 550°C, and 100-atm pressure with a 3:1 steam:carbon molar feed ratio. Primary products (using dodecane as simulated diesel fuel feedstock) were methane and carbon dioxide as expected with <5-vol% light alkanes. Hydrogen was detected (but not quantified) and as little as 5-wt% by-product liquids relative to dodecane feed were collected. The overall carbon balance was ~85% in this preliminary feasibility test reaction.

Very rough cost estimates showed DFC between $45 to $55/kW based on elimination of the booster air compressor required for low-steam ATR processing, reduction of the reactor volume, and reduction in the size and units of heat exchanger equipment required. Materials costs would increase given the higher pressures. Many technical challenges remain to be investigated before this promising fuel processing approach can be deemed viable, as discussed below.

6.3 Recommendations for Future Work

Further economic analysis of modified commercial diesel fuel processing is not recommended for follow-up work. The processing modifications adopted for the best case scenario are deemed technically feasible and the final product contains primarily methane as a fuel although diluted to ~44-vol% with nitrogen (~29-vol%) and by-product carbon dioxide (21-vol%). Some hydrogen is produced (~4-vol%) but this represents a very low fraction (~5%) of the medium heat content fuel gas (Appendix C). Although this degree of dilution would require an increase in the size of the gas manifold and control valves, and may impact upstream burner operation, it is very unlikely to significantly impact catalyst performance. This approach to extending fuel flexibility to include diesel fuel is consider ready for engineering development in those (perhaps exceptional) cases were the need can justify the substantial investment costs for the fuel processor ($1,575,000 for a 25-MW gas turbine, presuming a modular fabrication basis).

The hydrothermal fuel processing approach shows enough promise to warrant further investigation of technical feasibility. Key technical questions include the following:

- Catalyst coking – Semi-quantitative analysis suggested an approximate carbon balance, but clearly additional tests using diesel fuel should be conducted over a 100-hr period to detect coking and catalyst deactivation. Ideally the high partial pressure of water vapor nad the presence of alkaline earth oxides should suppress coking at these modest (550°C) temperatures.
- Sulfur contaminants – ATR catalysts containing PGM active components can tolerate sulfur contaminants but only for temperatures well above those envisaged for

hydrothermal conversion (>750°C vs. 550°C). Catalyst deactivation by fuel sulfur and residual fuel ash must be ruled out over total catalyst life (many 1000s hours).

- Conversion rates – The cost of the hydrothermal reactor (i.e., its volume) varies significantly with residence time of the fuel steam mixture. Catalysts must be found with high sustainable activity to hold reactor costs within the preliminary overall system DFC of $45/kW.
- Materials – Superheated high-pressure steam is notoriously corrosive. The presence of strong reducing agents in the fuel and its products may well protect corrosion-resistant alloys, but sulfur and carbon deposition could impact high-strength (nickel or cobalt-based alloy) materials

These considerations must be addressed if the hydrothermal route to dilute SNG is to be shown as a technical and an economical viable process for making diesel fuel a suitable back-up replacement for natural gas.

Appendix A

Haynes 214 Material Creep Characterization for TFA Durability Prediction

by
John Barnes

Catalytica Energy Systems, Inc.
430 Ferguson Drive
Mountain View, CA, 94043

January 3, 2003

Executive Summary

Haynes 214 alloy has been material tested to characterize creep behavior and thereby improve the accuracy of long-term durability predictions of the TFA catalyst support structure. Five tests were run at temperatures of 1650, 1750 and 1800°F and stress of 400, 800 and 1200 psi in order to closely approximate the TFA operating environment. Testing duration has reached 6000 hours on two specimens. Results show creep rates different than published by Haynes International.

Background

The catalyst support structure known as the TFA must restrain the catalyst foil against pressure loading in the axial direction at temperatures up to 1750°F. Haynes 214, a nickel-chromium-aluminum-iron superalloy was selected for the TFA construction due to its outstanding high temperature oxidation resistance and creep strength. Unfortunately, no creep data is available in the literature so only the manufacturers published data could be used for mechanical design. The manufacturers data tended to be at higher stress and shorter time than required for predicting the TFA behavior. Also, this data was extrapolated for times beyond 1000 hours and represents unknown statistical significance so further testing was considered necessary.

Discussion

The test specimens conform to ASTM E8 Figure 1 (sheet type) and all testing was per ASTM E139. Displacement was recorded approximately every .5 hours early in the test while primary creep was underway but at intervals of up to 70 hours later when the secondary creep rate was more constant.

The material testing conditions completed are summarized in Table 1. The intention is to eventually complete all the table cells to fully characterize Haynes 214 over the stress and temperature range. The 1750°F test time durations are run longest because this is closest to the highest temperature of interest. Also, a Larson Miller time temperature correlation will be used to extrapolate the higher temperature data to longer, lower temperature conditions thus extending the 1650°F data duration.

Stress (psi)	Test Temperature °F (°C)		
	1650 (900)	1750 (954)	1800 (980)
400	2012 hrs (P2001-003-1) [faster than Haynes]	>6000 hrs (P2001-003-2) [faster than Haynes]	2012 hrs (P2001-003-3) [slower than Haynes]
800		>6000 hrs (P2001-003-6) [faster than Haynes]	
1200	2012 hrs (P2001-003-9) [slower than Haynes]		

Table 1. Creep Testing Summary- Total Hours and Specimen ID

The creep data is plotted in Figure 1 along with the closest Haynes curve. In general, the creep behavior trends are correct. Higher stress and temperature each cause increased creep strain. Comparison to Haynes data is not exactly analogous but requires interpretation. The Haynes stress (1300 psi) is higher than the nearest test (800 psi) but the temperature (1700°F) is lower than the test (1750°F). These differences should be similar in significance so the similarity of the data curves is then as expected.

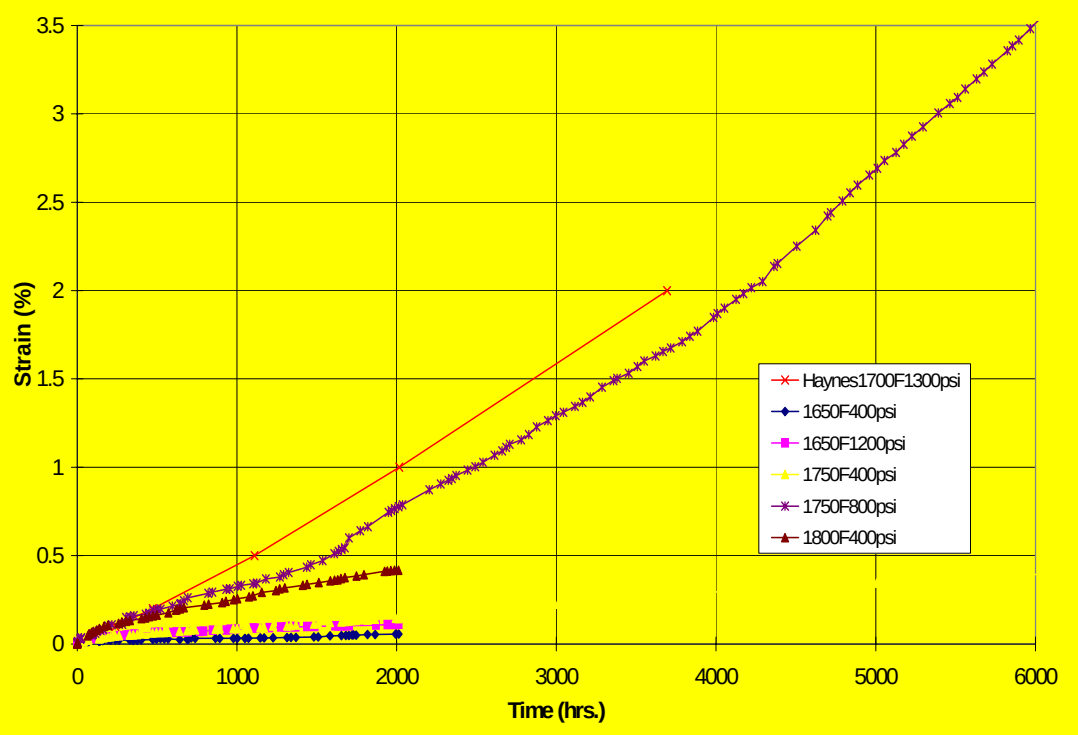

Figure 1. Haynes 214 Sheet Creep Testing Compared to Haynes Data

Conclusions and Recommendations

Creep characterization of Haynes 214 has been completed at numerous stress and temperatures out to 6000 hours. The data is following expected trends and compares qualitatively with Haynes literature. Additional testing is required to fully characterize over the stress and temperature range of importance to the catalyst axial support structure. Also, the material must be tested for longer time to find the maximum replacement limit.

Appendix B

TFA Y Joint Low Cycle Fatigue Testing

by
John Barnes

Catalytica Energy Systems, Inc.
430 Ferguson Drive
Mountain View, CA, 94043

January 28, 2003

Executive Summary

Low cycle fatigue testing of TFA welded Y joint specimen has been completed that measured up to 7221 loading cycles without failure under conservative conditions. The test specimens were produced with welds identical to an actual TFA. The strain state for the specimen closely matched the TFA and amplified stress levels were tested. Testing temperature was 1700°F. Notches were included on the weld backside to initiate cracking and represent worst-case weld quality. Load controlled cycling was conservatively used to simplify testing though the actual TFA strain is predominately caused by displacement. Improvements to the test were implemented as results were obtained. Although crack growth and fracture did not occur, the durability of the TFA weld joints has clearly been demonstrated.

Background

The test program described was needed to improve the ability to predict the TFA long-term durability. Due to limited materials data relevant to this application, predictions of low cycle fatigue life are lower in accuracy than is possible. No Haynes 214 fatigue data has been found in the literature. By testing a welded joint similar to the actual TFA, the fatigue and fracture strength of the TFA was determined.

Discussion

Test Strategy

Haynes 214 fatigue and fracture testing is needed to assess cyclic life of the TFA. By using a geometry specific specimen rather than a standard fatigue specimen, the test will evaluate the actual joint weld. The weld joints are obviously the life limiting location since the stress is highest due to the stress concentration and the welding weakens the material properties. Specimen geometry has been developed which closely represents the stress state in the TFA while maintaining a simple specimen and loading technique Load cycling of the specimen will also cause realistic crack propagation thus assessing joint fracture. Two minute hold time at load was used to also include some creep damage effect.

Specimen Design

Finite element stress analysis was used to develop a specimen geometry, support and loading conditions that has a similar strain distribution as the actual TFA. A material testing laboratory was consulted to design a workable arrangement and fixture. The specimen geometry is shown in Figure 1.

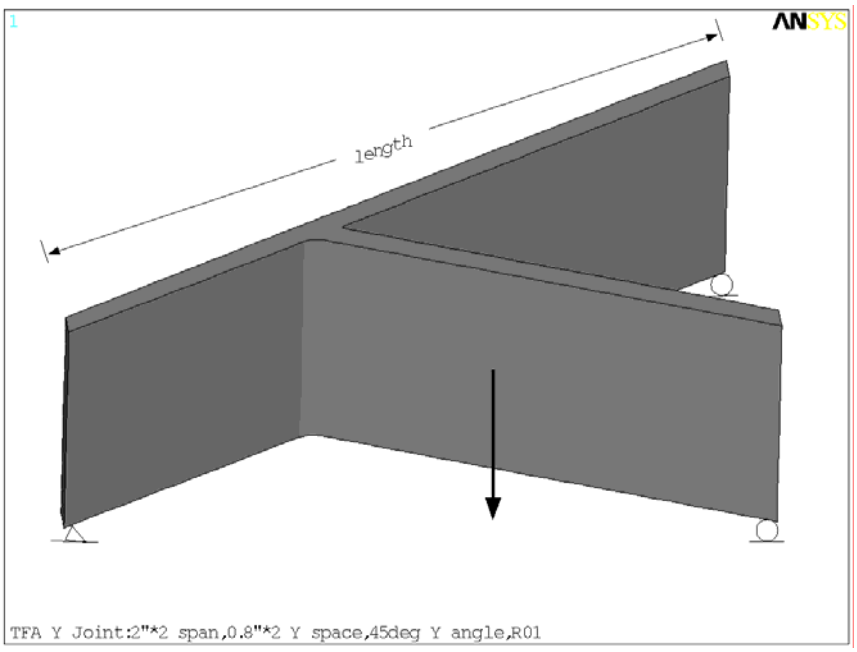

Figure 2. Test Specimen General Arrangement

The concept is similar to a 3-point bend specimen. As depicted in Figures 2 and 3, the length is 2 inches, thickness of material is 0.062 inches, height is .75 inches and the angle of the Y connection is 45° and 60° corresponding to the GE10 and KHI M1A, respectively. The Y is 0.8 inches from the left end support. The ends are simply supported and the load is applied to the shorter strut via contact at the top.

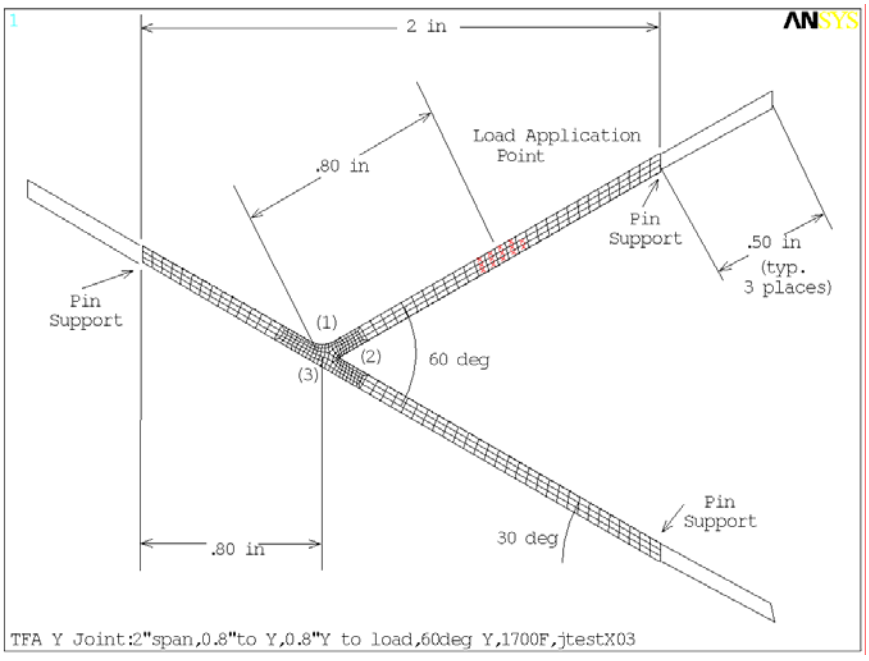

Figure 3. Specimen geometry for KHI M1A TFA

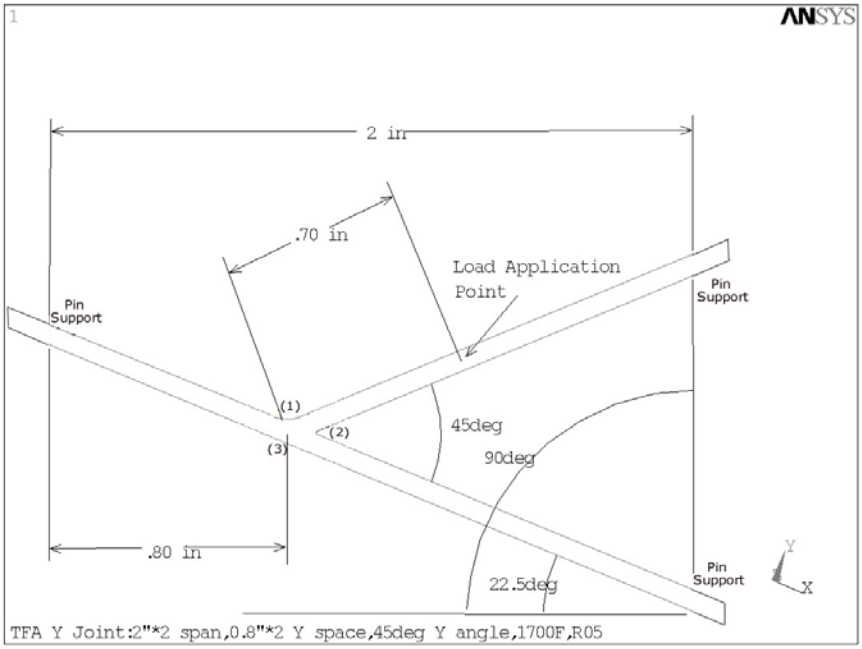

Figure 4. Test Specimen for GE10 TFA

The geometry shown closely replicates the tensile strain at the backside of the weld and nearby maximum equivalent strain of the actual TFA. Detail FEA stress analysis of the TFA's was used as the basis. This comparison is to the joint closest to the center which has been shown to be fatigue limiting. Three locations marked (1), (2) and (3) in the previous two figures are compared in Table 1.

Table 1. Comparison of Specimen to TFA Strain

	Eqv Strain at (1)	'Y' Strain at (2)	Eqv Strain at (2)	Eqv Strain at (3)
	(%)	(%)	(%)	(%)
X2.1 TFA	.0119	.0036	.0085	.009
Specimen w/ 38 lbs	.0112	.0036	.015	.013
GE10 TFA	.052	.012	.052	.052
Specimen w/ 217 lbs	.059	.020	.068	.064

Test Fixture and Conditions

The tests were performed at 1700°F under strain distributions related to the actual TFA. A fixture supported the specimen in the tensile testing machine as shown in Figure 4. The simple support condition is provided by the 0.250 inch diameter cylinders as shown. Also, lateral support occurs at the vertical cylinders. Load is applied by a blunt contact at the specified location on the shorter strut.

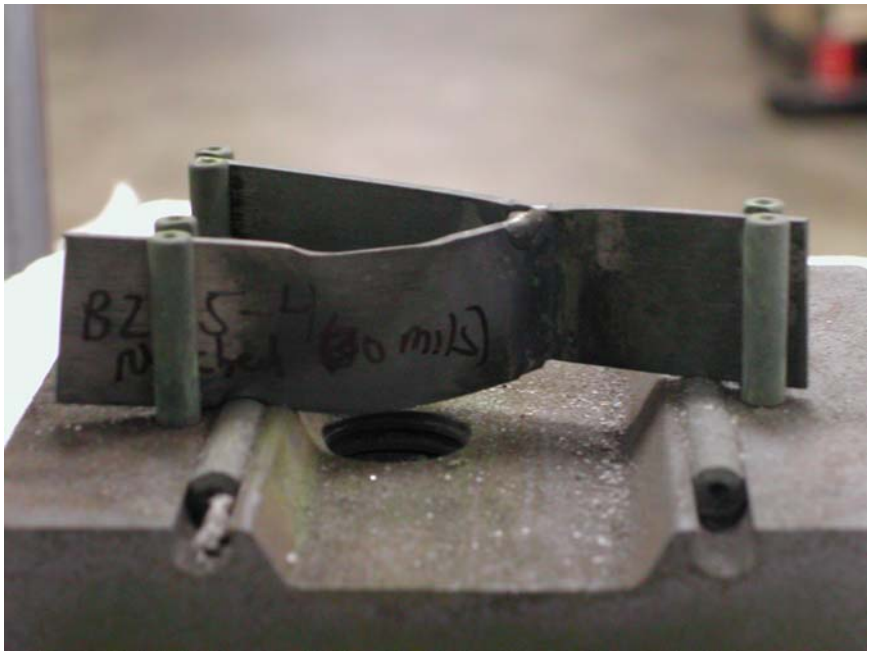

Figure 5. Test Fixture

Note that the fixture was modified part way through the test program as will be discussed further with the results. Pictured is the final fixture. Initially, there were fewer lateral supports and the base plate was not recessed between the simple supports. On some of the higher load tests, the specimen eventually contacted the base plate and wthout lateral support the struts twisted.

Notice also that the specimen shown in Figure 4 has deformed due to the testing. This particular specimen was overloaded with 279 lbs, has an 0.030 inch notch and endured over 6000 cycles for 200 hours under load. This causes significantly more creep than will occur in the actual TFA but the joint is still intact.

Load controlled cycling was used to simplify the fixture while causing a conservative loading compared to the actual TFA. The GE10 specimen and TFA have a total equivalent stress of 13.1 ksi. However, from the TFA stress analysis, only 1.2 ksi is due to mechanical load while the remainder is caused by displacement changes from thermal expansion. Load control testing will cause rupture whereas the actual TFA, having predominately displacement controlled load would have strain limited by the enforced displacement. For perspective, the 100-hour rupture strength at 1,700°F is 6.5 ksi. The test time for 2,500 cycles with 2-minute hold time is 83 hours so it is possible that rupture will over contribute to cracking. In order to test is strain control, reverse loading capability would be needed greatly complicating the fixture and possibly accuracy of the test.

Notches were added to the back of the weld joint as depicted in Figure 5 to create a worse case weld with a known defect and to hopefully initiate crack growth. This EDM cut extended through the entire height of the specimen.

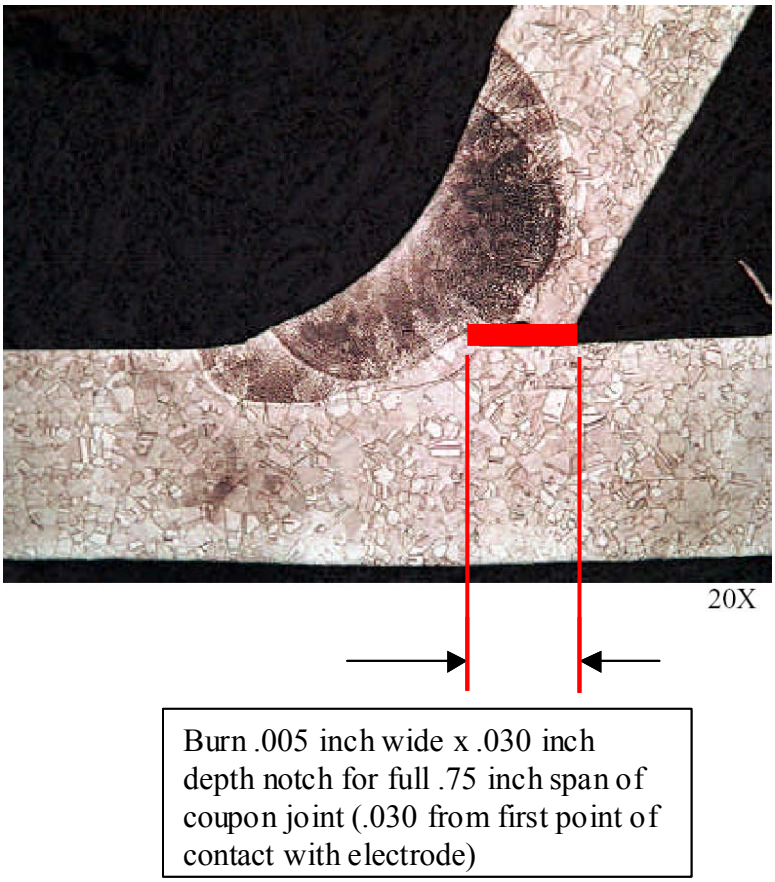

Figure 6. Notch in Weld

Test Results

Table 2 summarizes the testing. Given are the specimen identification information, notch description, loading, number of cycles reached without failure, the cycle when contact with the fixture occurred and the equivalent stress at the weld.

The contact with the fixture was related to the initial base plate previously mentioned. After reviewing the early test data, an increase in response stiffness was observed that was most likely due to contact between the specimen and the fixture. Other changes in the test such as cracking at the joint or lateral deformation of the struts would cause decreases in stiffness. Also, it was seen that less creep deflection occurred during the 2-minute hold time period after the stiffness increase that again indicates the specimen has bottomed out against the fixture. Unfortunately, detailed load deflection was only recorded for selected cycles so it was not possible to pin point when the contact occurred.

The stress given in the table includes the amplification due to the overload and the effect of the notch. For the notch specimen, the stress is estimated based on area reduction.

Table 2. Y Joint LCF Testing Result Summary

batch	angle	part no.	notch	load	N_f (cycles)	cycles at stiffness increase	S_{eqv} at Y
1	60	.004 s3	no	190	>2500	>2500	10
1	60	.004 s2	no	76	>2500	>1000- data missing	4
1	60	.004 s1	no	38	>2500		2
2	45	.001 s3	no	326	>2500	after 500	21
2	45	.001 s2	no	279	>2500	after 500	17
2	45	.001 s1	no	217	>2500	no hyster data	13
3	60	.004 s2	0.055	190	>2500	>2000	27
3	60	.004 s1	0.055	38	>2500	>2500	5
4	45	.001 s1	0.055	326	1955	after 100	55
4	45	.001 s2	0.055	217	>2500	after 500	35
New fixture- no contact expected							
4	45	.001 s3	0.055	326	82	should not happen	55
4	45	.001 s4	0.030	217	7221	"	23
4	45	.001 s5	0.030	279	>6280	"	30

The first test with the improved fixture resulted in separation of the weld joint in 82 cycles. However, this does not indicate a durability concern for the TFA because of the extreme conservatism in the test. The test method had evolved based on initial testing not causing any structural degradation. In an attempt to find the amount of margin to failure, the load had been increased from 217 to 326 lbs and a 0.055 inch depth notch had been cut into the weld causing the stress to increase from 13 to 55 ksi. Visual inspection at 3X magnification did not show striations that would indicate fatigue crack growth. It is more likely that the failure was caused by creep rupture considering the high local stress.

The next test reached 7221 cycles without failure by having the load decreased to produce similar stress as the actual TFA and the notch size reduced. Following that, the load was increased to 279 lbs and over 6280 cycles were run before stopping the test. These final two tests show the Y joints have exceptional durability. Even the tests prior to the fixture modification show the Y joints have acceptable fatigue life based only on the number of cycles before fixture contact occurred. Unfortunately, the conditions to cause failure or crack propagation were not quantified since it was impossible to cause either of these two events in the test.

None of the 60 degree KHI M1A specimen were tested in the new fixture because the initial tests had reached adequate number of cycles to demonstrate durability. This TFA has lower stress than the GE10.

Lessons Learned

The TFA welded Y joints have exceptional durability. It was not possible to propagate cracks from the flaw at the backside of the weld or fail the joint except with a severe overload that ruptured the joint.

A fatigue test method has been developed specific to the critical Y joints of the TFA. This test will be valuable for future TFA development.

Creep interaction could have an effect on the Y joint life though good durability could be expected based on some of the results. One test at excessive load did rupture the joint so it may be possible that lower load for longer time may have the same effect. However, another test at slightly lower Y joint stress and longer time had significant creep deformation without severing the weld.

Conclusions and Recommendations

The TFA welded Y joints have exceptional durability based on 12 tests of Y joint specimen with very similar welds, temperature and strains as the actual TFA. It was not possible to quantify crack propagation or cycles to failure since neither event could be produced due to the robustness of the Y joint. To cycle the joint until cracks propagate would require displacement controlled testing to avoid specimen deformation prior to crack growth. This complication was not deemed worthwhile considering the extremely large number of cycle endured in harsher load control.

The possibility of creep crack growth and/or rupture was seen in one test point that is not relevant to the TFA life due to excessive loading. However, additional testing should be performed to quantify the effect of longer time at lower stress.

Appendix C

Diesel to Gas Project Economic Evaluations

by
Mike Cook

for
Catalytica Energy Systems, Inc.
430 Ferguson Drive
Mountain View, CA, 94043

September 12, 2002

Memo

To: Jon McCarty

From: Mike Cook

Date: 9/12/2002

Re: 5445-30: Diesel to Gas Project Economic Evaluations

Summary

Further preliminary process economic evaluations have been completed for Project 5445-30: Diesel to Gas. Earlier reported work by V. Gurevich titled "Diesel to Gas: Feasibility Study, Intermediate Report" issued on 02/02/2002, presented a base case process that was compared to the commercial process by Haldor Topsoe to produce 110 MW of energy. In that report, the "Basecase" process was estimated to have a direct fixed cost per kW (DFC $/kW) of 110$/kW compared to the TOPSOE process having a DFC of $250/kW. In addition to the Basecase, an "optimized" base case was presented that utilized plate heat exchangers (Packinox) in place of standard shell and tube and used 316 stainless steel materials for the reactors in place of Incoloy. This optimized case had an estimated DFC of $78/kW. The process was based on operating the ATR and Reforming reactors at a pressure of 30 atm, a steam:carbon ratio of 3.5:1, a carbon:O_2 ratio of 2.6:1, and an inlet temperature of 650 °C for the ATR. The reactors were estimated as a single Gibb's reactor, operating adiabatically, resulting in an effluent temperature of 844°C. Total thermal energy production was 109 MW.

Picking up where V. Gurevich left off, further evaluations were performed for this analysis by first reconfirming the earlier work. This was done to establish consistent methods and then the following process changes were made and evaluated for this work:

1. ATR/Reformer effluent temperature controlled to 650 °C by reduction of the air feed rate and inlet temperatures. (Resulted in Carbon/O_2 ratio = 4.5, Steam/Carbon kept at 3.5)
2. ATR/Reformer effluent pressure reduced to 22.4 atm from 30 atm.

Results of these changes were simulated using PRO/II and evaluated using Est$Pro for the impact on equipment costs. For this analysis, the direct fixed costs (DFC) were estimated at $80.1/kW for a process using standard shell and tube heat exchangers and incoloy material for the ATR and reforming reactor (case 3). For the same process but substituting the conventional shell and tube heat exchangers for those made by PACKINOX (plate frame units) produced an estimated DFC of

$68.3/kW (case 4). These two cases were then further optimized by assuming that the reformer reactor and ATR could utilize 316 series stainless steel in place of the Incoloy. The understanding that proper insulation will reduced the reactor's skin temperature to <1100°C drives this assumption. For the case utilizing conventional shell and tube heat exchangers, a DFC of $71.5/kW was estimated (case 5) and for the PACKINOX case, a DFC of $59.6/kW was estimated (case 6). All of these cases are shown in Table 1.0 along with the reformer reactor's temperature, pressure and effluent compositions.

TABLE 1.0

ID	DFC ($/Kw)	Reactor Outlet Temp. (°C)	Pressure (atm)	Type Heat Exchangers	Reactor Mat'l
Case 1 * (Basecase)	110.2	844	30.0	Shell/Tube	Incoloy
Case 2 * (Optimized case)	78.9	844	30.0	PACKINOX	316SS
Case 3	80.1	650	22.4	Shell/Tube	Incoloy
Case 4	68.3	650	22.4	PACKINOX	Incoloy
Case 5	71.5	650	22.4	Shell/Tube	316 SS
Case 6	59.6	650	22.4	PACKINOX	316 SS
Case 7 **	63.1	650	22.4	PACKINOX	316 SS

*Confirming earlier work by V. Gurevich

** Methanation reactor added, see comments below.

As depicted in Table 2.0, the ATR/Reformer effluent streams shows high levels of hydrogen and carbon monoxide in cases 1 thru 6. Carbon monoxide levels greater than 5 mole% are problematic for the downstream gas turbine and needs to be reduced to have a viable Diesel to Gas process. Reduction of the high CO levels was obtained by the addition of a fixed bed methanation reactor. For this case (7), the increase in capital for the methanation reactor increased the previous estimated DFC of $59.6/kW (case 6) to $63.1/kW. Again this is for a process operating at 22.4 atm, a reactor effluent temperature of 650°C and utilizing PACKINOX heat exchangers and 316 SS reactor material.

TABLE 2.0 Simulated Gas Turbine Feed: Dry, Nitrogen Free Basis

Case ID	H2 (mole%)	CO (mole%)	CO2 (mole%)	CH4 (mole%)
Cases 1 - 2	63.1	14.9	20.9	1.1
Cases 3 - 6	52.6	5.6	26.1	15.7
Case 7 **	5.7	0.1	30.4	63.7

** Methanation reactor added.

Process Descriptions:

30 Atm Basecase and Optimized Cases 1&2 :

The process simulation flow sheet for the Basecase (case 1) and Optimized case (case 2) is shown in Figure 1. The design basis for both were as follows:

- Thermal energy production 109 MW
- Diesel consumption 10 metric ton/hr
- Air:
  - Flow rate 37.4 metric ton/hr
  - Pressure 16 atm
- Water to Reactor 45 metric ton/hr
- Steam : Carbon molar ratio 3.5:1
- Carbon : O_2 molar ratio 2.6:1
- Steam cracking inlet 450°C
- ATR / Reformer Effluent 844°C, 30 atm
- Gas to Gas Turbine (battery limits):
  - Pressure 30 atm

This simulation calculated that the total makeup water consumption was approximately 12 metric ton/hr and the feed gas stream to the gas turbine would contain the following composition shown in Table 3.0.

Table 3.0: Basecase Case Gas Turbine Feed Composition

Compound	% mole – total stream basis	% mole – Dry, N2 free basis
Water	1.6	--
CO	9.6	14.9
CO2	13.4	20.9
H2	40.6	63.1
N2	34.1	--
CH4	0.72	1.1

Figure 1

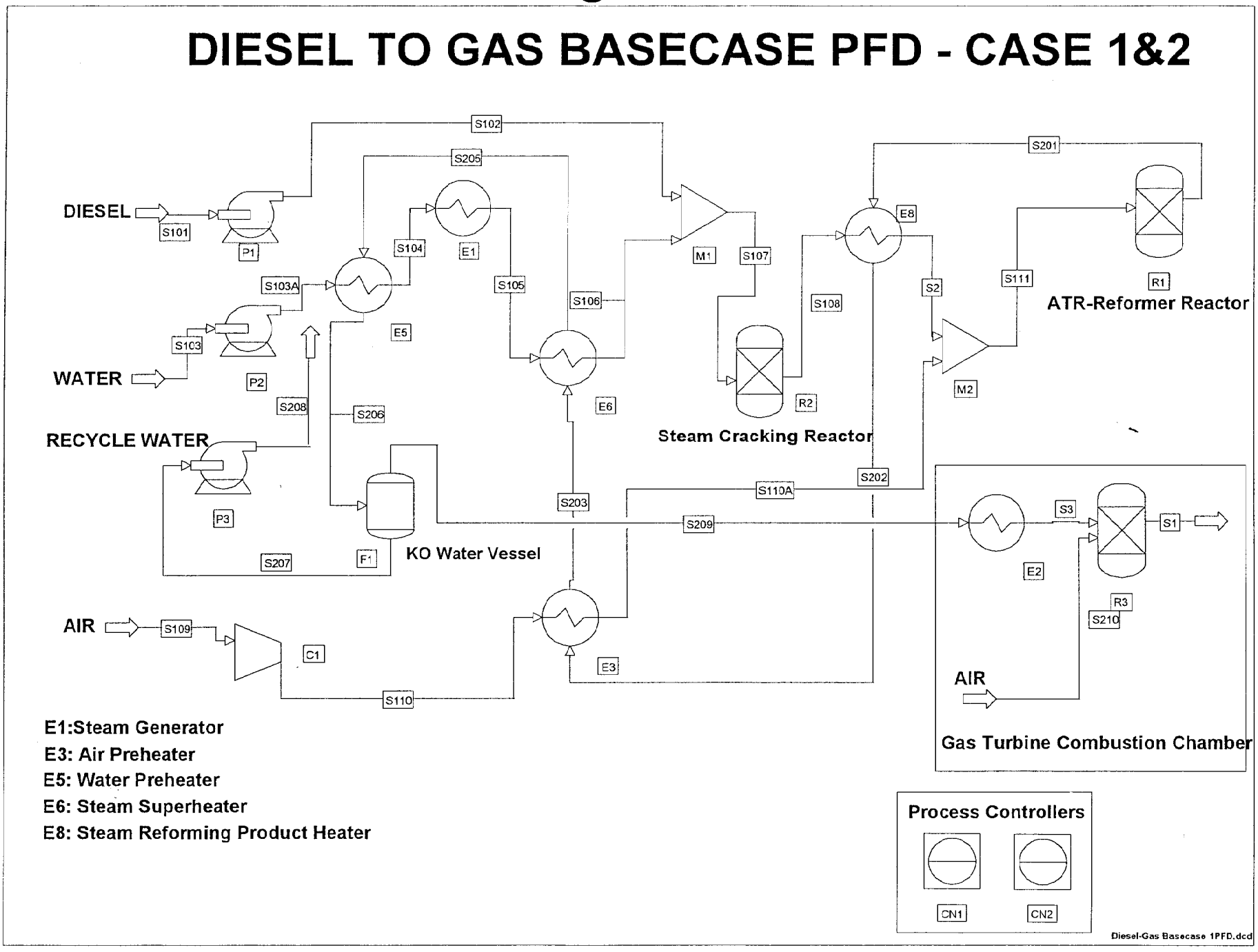
DIESEL TO GAS BASECASE PFD - CASE 1&2
DIESEL
WATER
RECYCLE WATER
AIR
S101
S102
S103
S103A
S104
S105
S106
S107
S108
S109
S110
S110A
S111
S201
S202
S203
S205
S206
S207
S208
S209
S210
S1
S2
S3
P1
P2
P3
E1
E2
E3
E5
E6
E8
M1
M2
C1
R1
R2
R3
F1
KO Water Vessel
Steam Cracking Reactor
ATR-Reformer Reactor
AIR
Gas Turbine Combustion Chamber
E1:Steam Generator
E3: Air Preheater
E5: Water Preheater
E6: Steam Superheater
E8: Steam Reforming Product Heater
Process Controllers
CN1
CN2
Diesel-Gas Basecase 1PFD.dcd

22.4 Atm Cases 3 thru 6:

The process simulation flow sheet for the 22.4 Atm cases 3 through 6 is shown in Figure 2. The design basis for was as follows:

- Thermal energy production 112 MW
- Diesel consumption 10 metric ton/hr
- Air:
  - Flow rate 22.4 metric ton/hr
  - Pressure 16 atm
- Water to Reactor 45 metric ton/hr
- Steam : Carbon ratio 3.5:1
- Carbon : O_2 molar ratio 4.5:1
- Steam cracking inlet 450°C
- ATR / Reformer Effluent 650°C, 22.4 atm
- Gas to Gas Turbine (battery limits):
  - Pressure 20 atm

This simulation calculated that the total makeup water consumption was approximately 10.4 metric ton/hr and the feed gas stream to the gas turbine would contain the following compositions shown in Table 4.0.

Table 4.0 22.4 Atm Cases 3 thru 6: Gas Turbine Feed Composition

Compound	% mole – total stream basis	% mole – Dry, N2 free basis
Water	1.2	--
CO	3.9	5.6
CO2	18.5	26.1
H2	37.2	52.6
N2	28.2	--
CH4	11.1	15.7

Figure 2

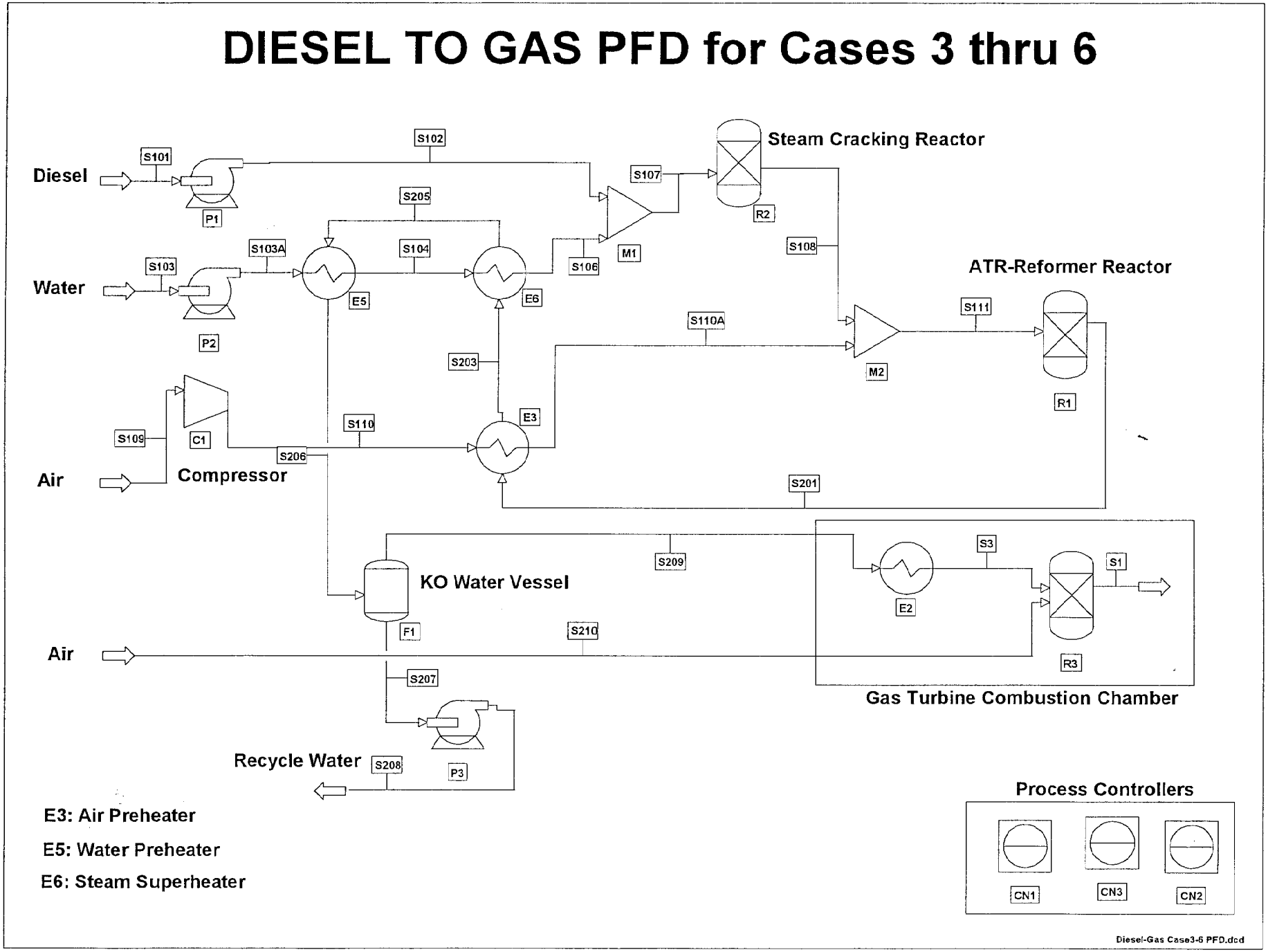
DIESEL TO GAS PFD for Cases 3 thru 6
Diesel
Water
Air
Air
Recycle Water
Steam Cracking Reactor
ATR-Reformer Reactor
Compressor
KO Water Vessel
Gas Turbine Combustion Chamber
Process Controllers
S101
S102
S103
S103A
S104
S106
S107
S108
S109
S110
S110A
S111
S201
S203
S205
S206
S207
S208
S209
S210
S1
S3
P1
P2
P3
E2
E3
E5
E6
M1
M2
R1
R2
R3
C1
F1
CN1
CN3
CN2
E3: Air Preheater
E5: Water Preheater
E6: Steam Superheater
Diesel-Gas Case3-6 PFD.dcd

22.4 Atm Case 7 with Methanation:

The process simulation flow sheet for the 22.4 Atm cases 3 through 6 is shown in Figure 3. The design basis for was as follows:

- Thermal energy production:
  - Methanation 9 MW
  - Gas Turbine 102 MW
- Diesel consumption 10 metric ton/hr
- Air:
  - Flow rate 22.5 metric ton/hr
  - Pressure 16 atm
- Water to Reactor 45 metric ton/hr
- Steam : Carbon ratio 3.5:1
- Carbon : O_2 molar ratio 4.4:1
- Steam cracking inlet 450°C
- ATR / Reformer Effluent 650°C, 22.4 atm
- Methanation:
  - Inlet Temperature 371°C, 19.9 atm
  - Outlet Temperature 401°C, 19.4 atm
- Gas to Gas Turbine (battery limits):
  - Pressure 19 atm

This simulation calculated that the total makeup water consumption was approximately 5.2 metric ton/hr and the feed gas stream to the gas turbine would contain the following compositions shown in Table 5.0.

Table 5.0 22.4 Atm Case 7 w/Methanation: Gas Turbine Feed Composition

Compound	% mole – total stream basis	% mole – Dry, N2 free basis
Water	2.5	--
CO	0.08	0.1
CO2	21.0	30.4
H2	4.0	5.7
N2	28.5	--
CH4	43.9	63.7

Figure 3

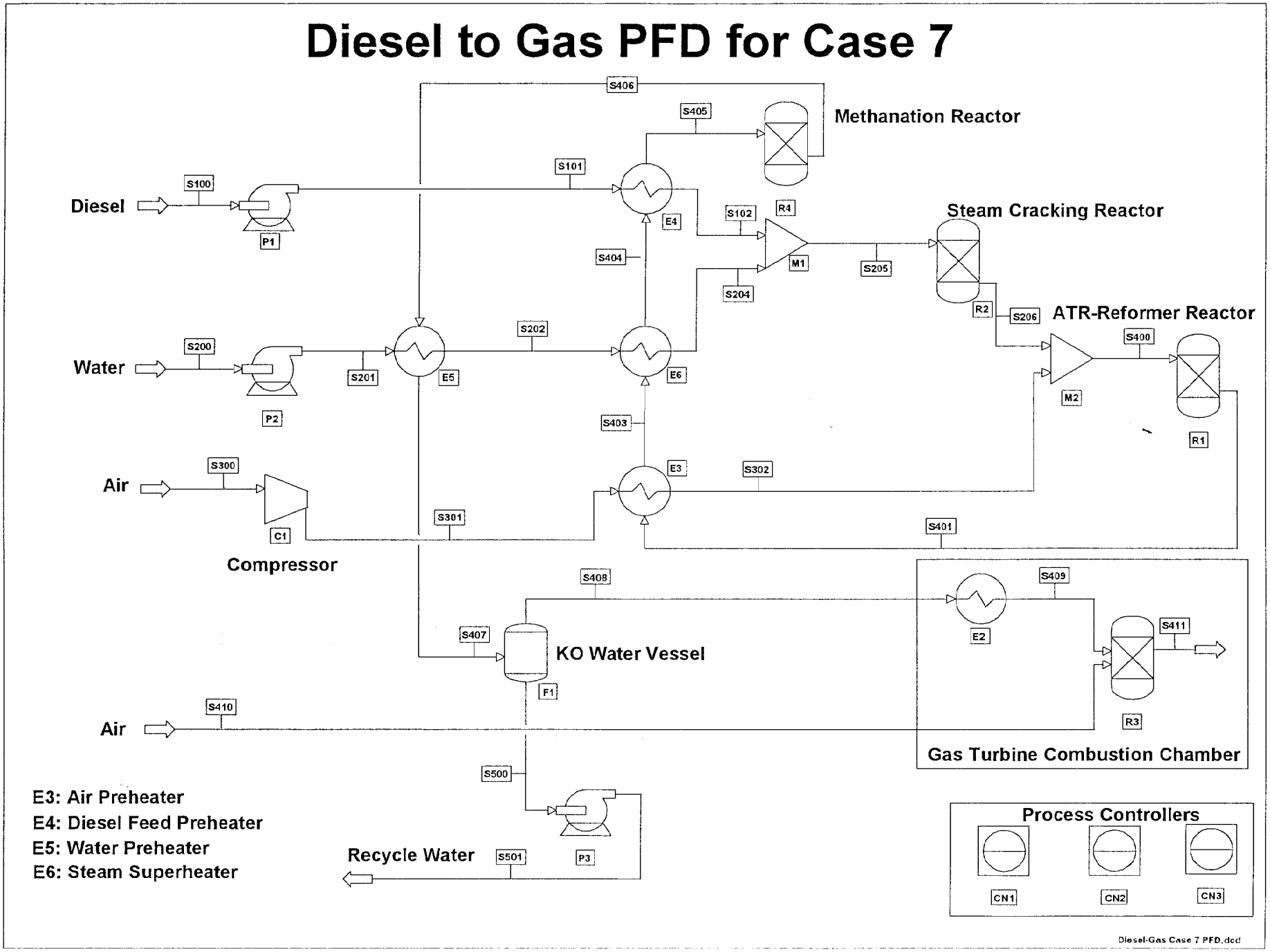
Diesel to Gas PFD for Case 7
S406
S405
Methanation Reactor
S101
S100
Diesel
P1
E4
S102
R4
Steam Cracking Reactor
S404
M1
S205
S204
R2
S206
ATR-Reformer Reactor
S200
Water
P2
S201
E5
S202
E6
S400
M2
R1
S403
E3
S302
S300
Air
C1
S301
S401
Compressor
S408
S409
E2
S407
KO Water Vessel
S411
F1
R3
S410
Air
Gas Turbine Combustion Chamber
S500
E3: Air Preheater
E4: Diesel Feed Preheater
E5: Water Preheater
E6: Steam Superheater
Recycle Water
S501
P3
Process Controllers
CN1
CN2
CN3
Diesel-Gas Case 7 PFD.dcd

Economic Evaluation:

The equipment sizing and costing methodology used was based on the following approach:

- Obtain heat and material balances from simulation and apply these to the sizing of the heat exchangers using Est$Pro software.
- Perform pressure drop calculations for sizing the ATR and Reformer reactors based on reactor conditions per simulation.
- Estimate bare equipment costs for all the major equipment using Est$Pro software.
- The equipment was assembled into skids to make a more mobile product. The total skid price was then estimated using Est$Pro costing software.
- Having both the bare equipment and skidded equipment costs then allowed for calculations of the total direct fixed costs by estimation of the various installed costs per standard engineering factors. These factors are displayed in each DFC worksheet.

All of the worksheets showing the detailed costing methods for each case is attached for reference in Appendix A. Located in Appendix B are the PRO/II output files for the three cases evaluated.

Appendix D

Conversion of Dodecane under Supercritical Water Conditions

By Indira S. Jayaweera and Montserrat Marti-Perez

SRI International

July 18, 2002

July 18, 2002

Conversion of Dodecane under Supercritical Water Conditions

Final Report
Prepared by:

Indira S. Jayaweera and Montserrat Marti-Perez
SRI International
333 Ravenswood Avenue
Menlo Park, CA 94025

Prepared for:

Catalytica Energy Systems, Inc.
430 Ferguson Drive, Building 3 Room 312
Mountain View, CA 94043-5272
650/940-6381 - office; 650/965-4345 - fax
jmccarty@catalyticaenergy.com - email

Attn: Dr. Jon G. McCarty,
Manager of Materials Development

INTRODUCTION

Interested in converting diesel fuel to gasoline range or lighter hydrocarbons, Catalytica Energy Systems, Inc. (CESI) contracted SRI to conduct a feasibility study to evaluate the efficiencies of several catalysts under supercritical water (SCW) conditions. The SRI study involved testing of five selected catalyst materials provided by CESI for decomposition of a model compound (e.g., dodecane). SRI's letter proposal for the work is attached below as Appendix A1. This report is prepared as requested by CESI to provide the data obtained from this study.

EXPERIMENTAL INFORMATION AND RESULTS

CESI provided five catalyst samples for testing; Table 1 lists their identifications. CESI also provided inert silicon carbide (SiC) fine powder as diluent material.

Table 1. Catalyst identification

CESI Catalyst ID	SRI ID
ATR-10c (1% PGM)	Catalyst #1
1% PGM/Calcia	Catalyst #2
Calcia	Catalyst #3
ATR-10c (1% PGM)	Catalyst #4
ATR-36d (Ni/Al2O3)	Catalyst #5

A simplified schematic of the process flow diagram of the test reactor system is given in Figure 1. Experimental conditions related to the catalyst testing are given in Table 2 (Table 2a provides information on catalyst loading corresponding to each run). The initial runs (1 and 2) were conducted at higher organic flow rates than the later ones to increase the contact time (reactor residence time). In Run #2 (Catalyst #1), the total flow rate (organic and water) was changed from 2.7 cc/min to 1.35 cc/min to accommodate the increase in gas release. Note that Run #7 (Catalyst #4) was not completed because an increase in system pressure caused the system to fail. It was later found that quartz wool used at the end of the reactor had disintegrated under SCW conditions and caused the reactor plugging (e.g., frits).

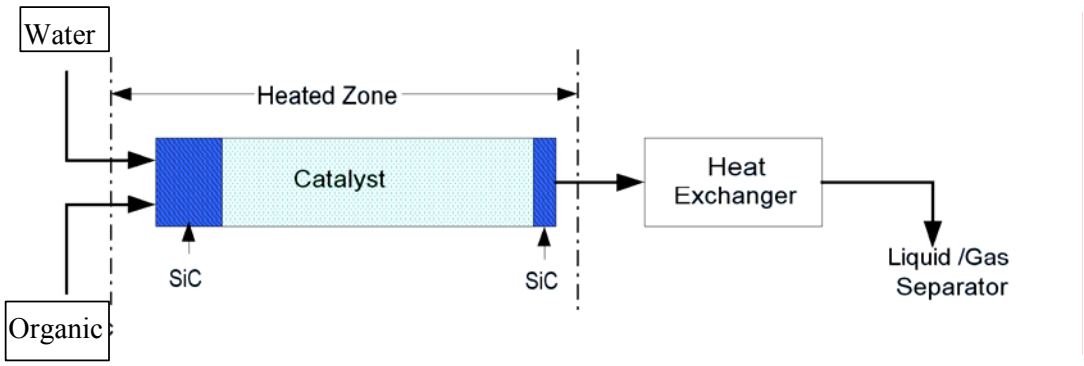

Figure 1. Simplified process flow diagram for the SCW test reactor.

Table 2. Experimental conditions for catalyst testing.

	Catalyst Loading (g)	Temperature (C)	Pressure (psi)	Water Flow (cc/min)	Organic Flow (cc/min)	Gas Collection Time (min)	Liquid Collection Time (min)
Run #1 SiC (0,5)	0	300	1500	1	0.35	4	10
		350	1500	1	0.35	4	10
		400	1500	1	0.35	4	10
		500	1500	1	0.35	4	10
		600	1500	1	0.35	4	10
Run #2 Catalyst #1	1	300	1500	2	0.7	10	10
		400	1500	2	0.7	10	10
		450	1500	2	0.7	10	10
		500	1500	2	0.7	3.7	10
		550	1500	1	0.35	3.7	10
Run #3 Catalyst #2	1	550	1500	0.5	0.167	13	25
		600	1500	0.5	0.167	6.4	25
Run #4 Catalyst #2	1	500	1500-1700	0.5	0.167	25	25
Run #5 SiC (0, 10.5)	0	400	1500-1700	0.5	0.167	8	25
		500	1500-1700	0.5	0.167	12	25
		600	1500-1700	0.5	0.167	18	25
Run #6 Catalyst #3	2	400	2400	0.5	0.167	25	25
		450	3200	0.5	0.167	25	25
Run#7 Catalyst #4	2	400	>3000				
Run#8 Catalyst #5	2	450	1600-1700	0.5	0.167	25	25
		500	1600-1740	0.5	0.167	12.25	35
		550	1700-1830	0.5	0.167	43	55
Run #9 Catalyst #5	3	400	1720	0.5	0.167	no gas	25
		450	1720-1840	0.5	0.167	no gas	26
		500	1940-2050	0.5	0.167	24	37
		550	1870-1890	0.5	0.167	22	25
Run#10 Catalyst #1	3	400	2000-2200	0.5	0.167	34	39
		450	2100-2200	0.5	0.167	17	31
		500	2200-2300	0.5	0.167	8	25
Run#11 Catalyst #3	1	400	1630	0.5	0.167	no gas	25
		450	1720	0.5	0.167	no gas	26
		500	1630-1720	0.5	0.167	27	37
		550	1730-1790	0.5	0.167	23	25

Table 2a. Supplemental Information for Table 2

Run	Information on catalyst loading
#1	0g catalyst; 5g neat filling material
#2	1g catalyst; 4g filling material; mixed
#3	1g catalyst; 4g filling material; mixed
#4	1g catalyst; 4g filling material; mixed
#5	1g catalyst; 4g filling material; mixed
#6	0g catalyst; 5g neat filling material
#7	2g catalyst; 4g filling material; mixed
#8	2g catalyst; 3g filling material; mixed
#9	3 g neat catalyst; 1g filling material inlet; 0.5g filling material outlet; not mixed
#10	3g neat catalyst;1.5g filling material inlet;0.5g filling material outlet; not mixed
#11	1g catalyst; 4g filling material; mixed

The data in Table 3 are compiled to indicate absolute values. As an example, the data for Run #2, Catalyst #1 at 550°C indicates that 0.0154 moles of dodecane (which contains 0.185 moles of carbon) decomposed at 550°C with 1 g of catalyst would generate 0.001 moles of CO, 0.029 moles of CH_2, and 0.017 CO_2. The conversion of dodecane at 550°C is 78% at 0.35 cc/min organic flow rate. In this run, the amount of dodecane recovered (unreacted) is 0.0034 moles. Therefore, the total amount recovered is $C_1 = CO_2+CO+CH_4 = 0.047$ moles or 25% of the initial carbon present in the dodecane.

The last column of the table, "other liquid products," was calculated from the FID response and percentage relative to the total area. For example, the GC (FID) trace for Run #10 (Catalyst #3 at 550°C) given in Figure 2 shows corresponding peak areas for dodecane and "other liquid products" to be 25% and 75% of the total area, respectively. A calibration curve for dodecane is given in Appendix A-2. Dichloromethane is used for extracting the organic fraction from the collected effluent mixed with both organics and water.

Figure 3 shows the corresponding gas analysis for Run #10 (Catalyst #1, 500°C).

Table 3. Results for dodecane.		Catalyst Loading (g)	Temperature (C)	CO (mol)	CH4 (mole)	CO2 (mole)	H2 (mole)	Other Gas Products >C1 (mole)	Dodecane-t=0 (mole)	$[C_1]$ initial (mol)	Dodecane-Recovered (mole)	Other Liqid Products (%)
Run #1	**SiC (0,5)**	0	300	NCL	NCL	NCL	NCL	NCL	0.0154	0.185	NA	no
			350	NCL	NCL	NCL	NCL	NCL	0.0154	0.185	NA	no
			400	NCL	NCL	NCL	NCL	NCL	0.0154	0.185	NA	no
			500	NCL	NCL	NCL	NCL	NCL	0.0154	0.185	NA	no
			600	ND	0.007	ND	ND	ND	0.0154	0.185	0.00033	29
Run #2	**Catalyst #1**	1										
			300	NCL	NCL	NCL	NCL	NCL	0.0308	NA	0.007	0.5
			400	0.001	0.001	0.002	ND	ND	0.0308	0.370	0.0105	0.3
			450	0.001	0.002	0.006	ND	ND	0.0308	0.370	0.0105	2
			500	0.001	0.009	0.015	ND	ND	0.0308	0.370	0.013	13
			550	0.001	0.029	0.017	DET	DET	0.0154	0.185	0.0034	30
Run #3	**Catalyst #2**	1										
			550	0.002	0.002	0.008	ND	ND	0.0184	0.221	0.0105	0.4
			600	0.007	0.013	0.016	ND	ND	0.0184	0.221	0.000383	49
Run #4	**Catalyst #2**	1										
			500	0.003	0.002	0.004	ND	ND	0.0184	0.221	0.0083	0.2
Run #5	**SiC (0, 10.5)**	0										
			400	NCL	NCL	NCL	NCL	NCL	0.0184	0.221	0.00001	no
			500	NCL	NCL	NCL	NCL	NCL	0.0184	0.221	0.00002	no
			600	0.003	0.017	ND	ND	ND	0.0184	0.221	0.0008	59
Run #6	**Catalyst #3**	2										
			400	0	0	NCL	NCL	NCL	0.0184	0.221		no
			450	0	0	NCL	NCL	NCL	0.0184	0.221	0.008	1.5
Run#7	**Catalyst #4**	2										
			NA	NA	NA	NA	NA	NA	NA	NA	NA	NA
Run#8	**Catalyst #5**	2										
			450	0	0	0	NCL	0	0.0184	0.221	ND	no
			500	0.0043	0	0		0	0.0184	0.221	0.00314	7.3
			550	0	0.0018	0.0045	DET	0.00045	0.184	0.221	0.00136	23
Run #9	**Catalyst #5**	3										
			400	NCL	NCL	NCL	NCL	0	0.0184	0.221	0.0176	no
			450	NCL	NCL	NCL	NCL	0	0.0184	0.221	0.01596	0.7
			500	0.00236	0.00027	0	ND	0.000676	0.0184	0.22	0.0108	6.5
			550	0.0002	0.0036	0.0004	ND	0.0038	0.0184	0.221	0.00225	38
Run#10	**Catalyst #1**	3										
			400	0.00064	0.0038	0.0058	DET	0	0.0184	0.221	0.0092	23
			450	0	0.0105	0.0137	DET	0.00806	0.0184	0.221	0.0052	43
			500	0	0.033	0.026	DET	0.002	0.0184	0.221	0.000813	75
Run #11	**Catalyst #3**	1										
			400	NCL	NCL	NCL	NCL	NCL	0.0184	0.221		0.07
			450	NCL	NCL	NCL	NCL	NCL	0.0191	0.232		0.5
			500	ND	0.0027	ND	ND	ND	0.0184	0.221	0.00168	3.8
			550	0.002	0.002	ND	ND	ND	0.0184	0.221	0.0072	25

NCL- no gas evolution , ND- not detected in the collected gas, DET- detected in the collected gas. $[c_1]$ initial = [dodecane]*12

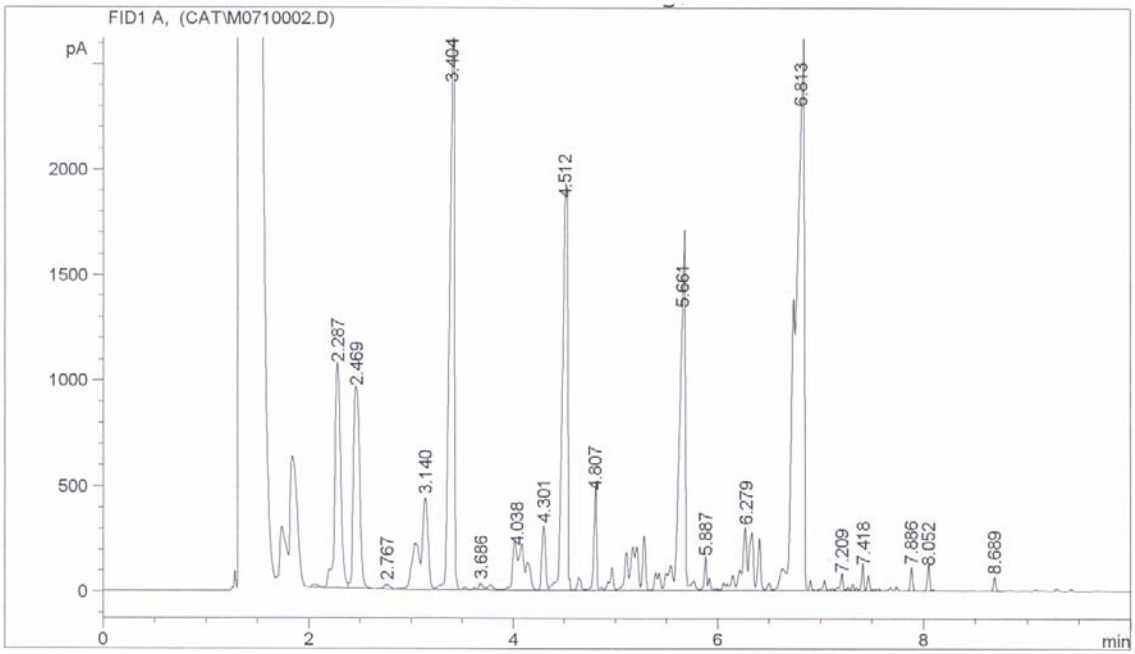

Figure 2. Gas chromatogram (FID) from Run #10 (Catalyst #1, 500°C). Dodecane elute at 6.813 min (the peak at 1.5 min corresponds to dichloromethane).

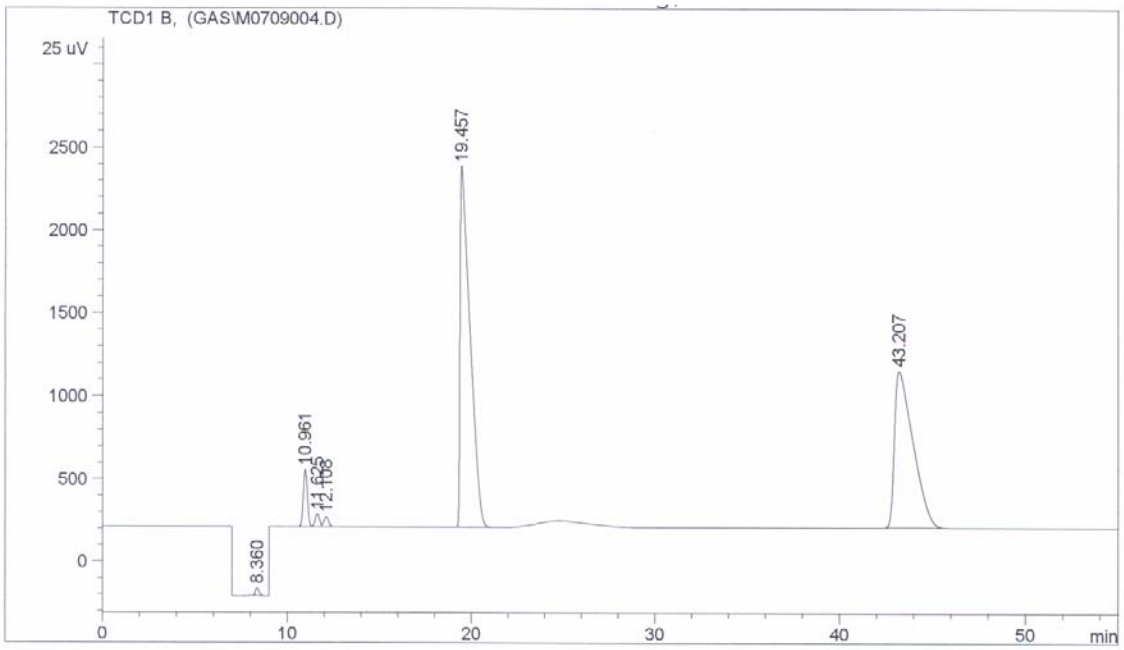

Figure 3. Gas chromatogram (TCD) for Run #10 (Catalyst #1, 500°C). Retention times for N_2, O_2, CO, CH_4, and CO_2 are 10.9, 11.6, 12.1, 19.4, and 43.2 min, respectively.

The run shown in Figure 3 clearly indicates the presence of hydrogen. The hump at 25 min could be ethane (this needs to be verified in future tests).

Comparison of Catalysts

The difference between Catalyst #1 and #3 is striking, and here we selected data from Runs #10 and #11 for these two catalysts for comparison. Since the GC FID trace data for run #10 at 500°C is given above, the same temperature data for Catalyst #3 at 500°C can be used for comparison. The GC (FID) trace for catalyst #3 from Run #11 is shown in Figure 4. A quick investigation of these two runs indicates that numerous liquid products are generated at 500°C with Catalyst #1. In addition, more gas products were also produced from this run in comparison with Catalyst #3. The presence of hydrogen was detected in Run #10 at 500°C, but no hydrogen was detected in the gas analysis for Run #1.

We have analyzed the liquid product from these runs using GC-MS to identify the components indicated from the GC (FID) analysis. The CG-MS traces are depicted in Figures 5 and 6. As can be noted from these figures, alkanes (heptane, octane, nonane, decane, undecane, and dodecane) are formed from Catalyst #1, and mostly alkenes are formed from Catalyst #3.

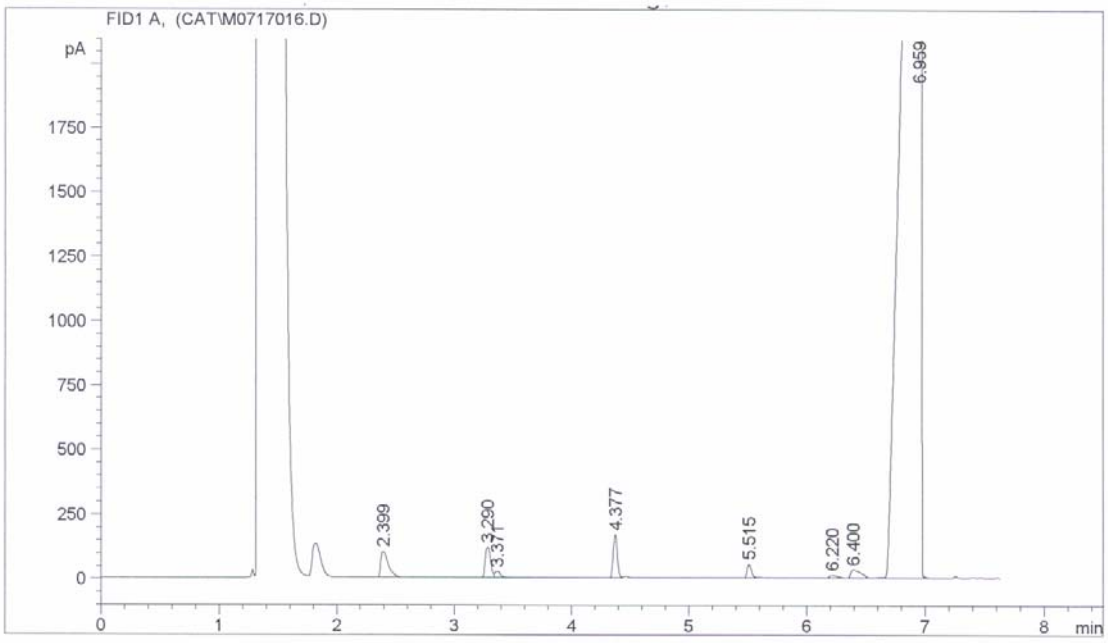

Figure 4. Gas Chromatogram (FID) for Catalyst #3, Run #11, 500°C. Dodecane elute at 6.813 min and Dichloromethane at 1.5 min.

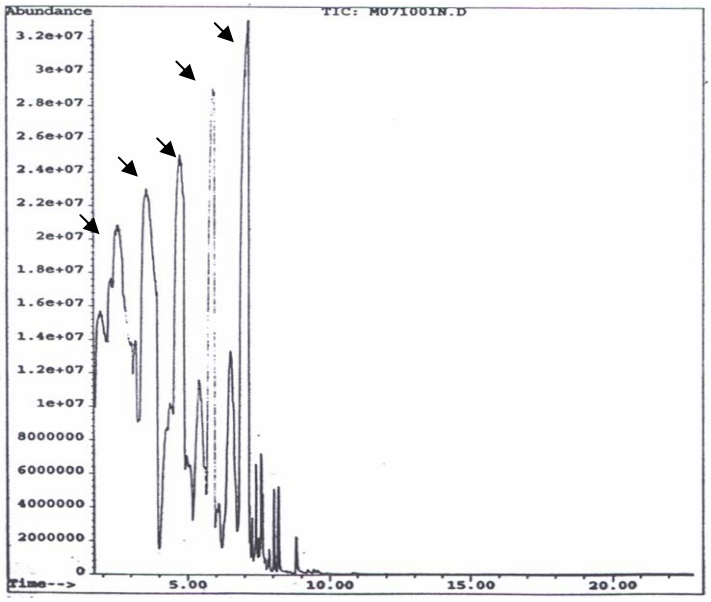

Figure 5. GC/MS trace for Run #10 (Catalyst #1, 500°C). The five major peaks, starting from left, are heptane, octane, nonane, decane, undecane, and dodecane .

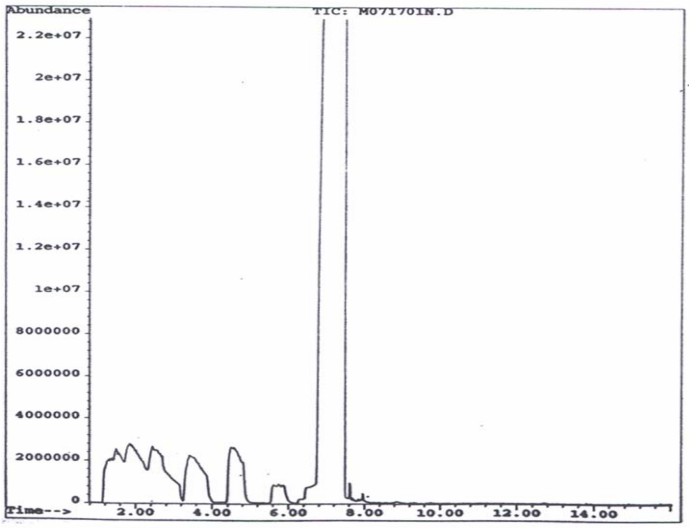

Figure 6. GC/MS for Run #11 (Catalyst #3, 500°C). The peaks starting from left are 1-hexene, 1-heptene, 1-octene, 1-nonene, 1-decene, 1-undecene, and dodecane.

Graphical Interpretation of Dodecane Conversion for Selected Runs

The comparison of data from Runs #10 and #11 are shown in Figures 7 and 8. These results show that while both calcia (Catalyst #3) and the catalyst with noble metal content

(Catalyst #1) are capable of converting dodecane to similar levels between 400°C and 550°C, the noble-metal catalyst greatly increases the yield of methane and carbon dioxide.

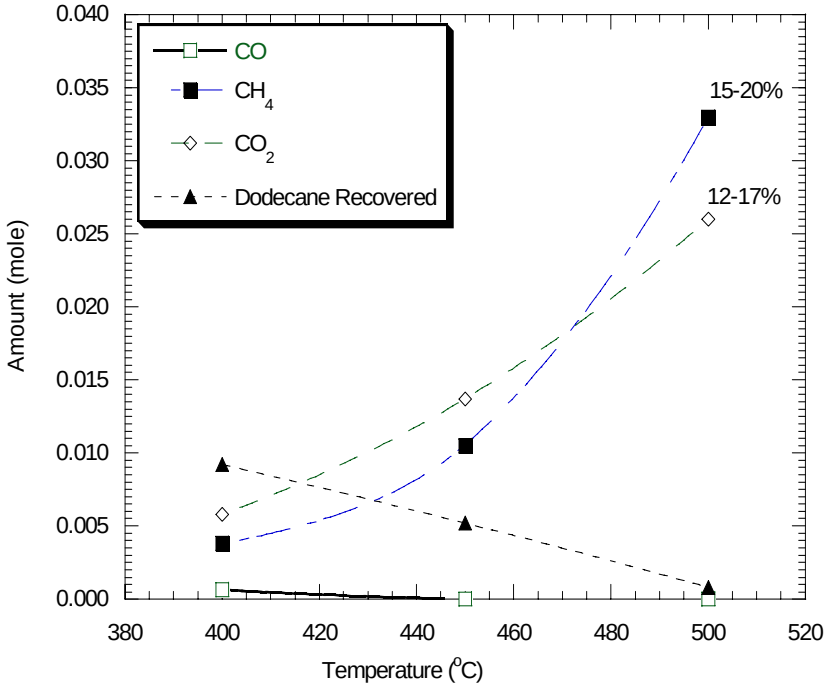

Figure 7. Data from Run #10 (Catalyst #1, 400°C - 500°C).

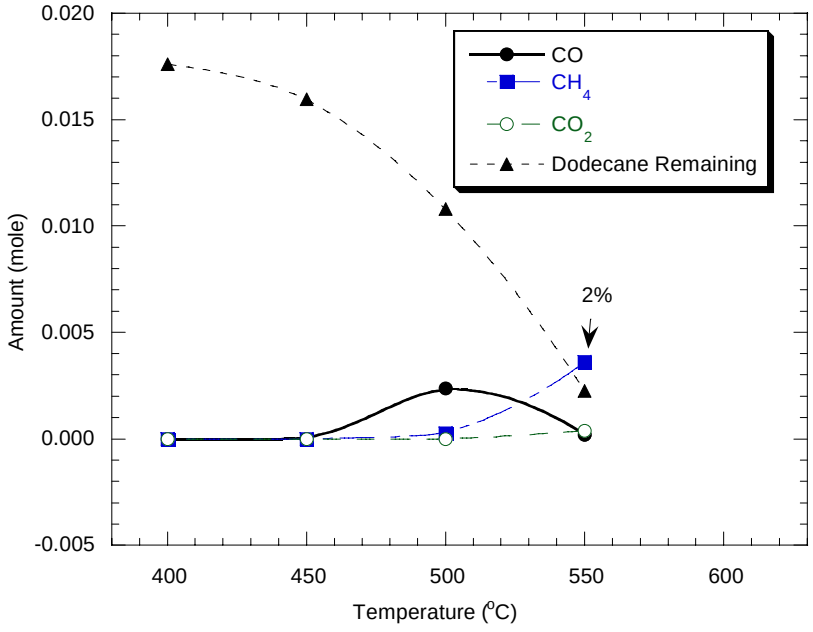

Figure 8. Data from Run #11 (Catalyst #3 at 400°C - 550°C).

APPENDIX D-1

April 25, 2002

Catalytica Energy Systems, Inc.
430 Ferguson Drive, Building 3 Room 312
Mountain View, CA 94043-5272
650/940-6381 - office; 650/965-4345 - fax
jmccarty@catalyticaenergy.com - email

Attn: Jon G. McCarty, Manager of Materials Development

Subject: SRI Proposal No. PYC 02- 066
Conversion of Dodecane Under Supercritical Water Conditions

Dear Dr. McCarty,

In response to your request, SRI International proposes to conduct selected number of experiments to determine the decomposition of a single model organic compound (e.g., dodecane) under supercritical water conditions.

Proposed Experimental Conditions:

- Pressure: 100-atm
- Water/carbon molar ratio: 3:1
- Liquid water flow rate: 2.00-mL/min
- Liquid dodecane flow rate: 0.70-mL/min
- Temperature range: 600 decreasing to 350°C in 50°C increments
- Hold time: 30-min minimum for very low (<5%) or very high (>95%) dodecane conversion to 120-minute maximum (three analytical samples of reactor product per temperature) GC analysis: CH4, CO, CO2, dodecane (calibrated, quantitative); other HCs qualitative via retention time and FID peak area only
- Reactors: 0.25-in OD (0.049-in wall thickness) by 8-in length
- Catalysts and diluent materials: All materials and reactor loading instructions provided by the client
- Number of experiments: 12 (experimental data will be delivered to the client in the form of a data table via e-mail)

An estimate of SRI's fees for the proposed work is given in the attached Agreement, and the fees for any additional work other than the work described in this proposal will be provided upon request.

This proposal is SRI confidential and may contain proprietary information, provided only for your consideration in funding the described work, and is not to be disclosed to third parties without SRI's permission. This service project can be authorized by signing and returning two copies of the attached Agreement. A fully executed copy of the Agreement will be returned to you. Work can begin on receipt of the advance payment and the test catalysts.

This proposal will be effective until [June 28, 2002]; however, SRI will be pleased to consider an extension.

We look forward to a favorable response and to a mutually successful working relationship. Please address any technical questions to Indira Jayaweera, (650) 859-[4042], and address contractual or administrative questions to Mary Bastida at (650) 859-5508.

Sincerely,

Indira Jayaweera
Hydrothermal Program Leader

Attachments: Agreement (2 copies)

APPENDIX D-2

Figure B1. Dodecane calibration curve.